Sede Amministrativa: Università degli Studi di Padova

Dipartimento di Scienze Chimiche

SCUOLA DI DOTTORATO DI RICERCA IN SCIENZE MOLECOLARI

INDIRIZZO SCIENZE CHIMICHE

CICLO XXVI

Gold-based anticancer derivatives of oligopeptides: synthesis, characterization, delivery strategies and biological activity

Direttore della Scuola: Ch.mo Prof. Antonino Polimeno

Supervisore: Ch.mo Prof. Dolores Fregona

Dottorando: Giulia Boscutti

A special acknowledgment goes to Fondazione CARIPARO,
for funding this three-year PhD project

Index

Abstract

At present, cisplatin (*cis*-diamminodichloroplatinum(II)) is one of the most largely employed anticancer drugs, used especially for the treatment of testicular cancer and, in combination with other drugs, of ovarian, small cell lung, bladder, brain, and breast tumors. Anyway, despite its high effectiveness, it exhibits severe drawbacks, as normal tissue toxicity (in particular, nephrotoxicity) and intrinsic or acquired resistance to the treatment. To overcome these problems, new Pt- and other metal-based complexes were designed and tested as anticancer drugs. In particular, since gold-based complexes were linked for centuries to the treatment of rheumatoid arthritis (due to their antiinflammatory and immunosuppressive properties), they were also tested for their antiproliferative properties..

In the last decade in our research group, some Au(III)-dithiocarbamato derivatives were synthesized, characterized and tested, showing outstanding antiproliferative activity on human cancer cells.

Starting from the promising results obtained both *in vitro* and *in vivo* for the “first generation" compounds of formula $[Au^{III}X_2(dtc\text{-}L)]$ (X= Cl, Br; dtc=dithiocarbamato; L= dimethylamine, pyrrolidine, N-methyl glycine (Sar) esters), a "second generation" of complexes was designed to improve bioavailability, selectivity and cellular uptake. In particular, the dithiocarbamato moiety was functionalized with different oligopeptides of general formula $[Au^{III}X_2(dtc\text{-}Sar/Aib\text{-}(AA)_n)]$ (AA= different aminoacids), to be recognized and uptaken by specific peptide transporters called PEPTs (PEPT1 and PEPT2), predominantly present in epithelial cells of small intestine, mammary glands, lung, choroid plexus and kidney, and overexpressed in some tumor types. A unique feature of these transporters is their capability for sequence-independent transport of most possible di- and tripeptides, thus representing excellent targets for the delivery of pharmacologically-active peptidomimetics such as β-lactam antibiotics and some angiotensin converting enzyme (ACE) inhibitors. Interestingly, these complexes demonstrate high capability to strongly inhibit tumor cells growth by exploiting a mechanism of action different from the clinically-established platinum drugs, overcoming drawbacks without any observed cross-resistance.

In this PhD thesis work, new Au(III)-peptidodithiocarbamato complexes were synthesized and fully characterized, mainly by means of elemental and X-ray analysis, mono- and bidimensional NMR, FT-IR and UV-Vis spectroscopy.

The water-insoluble compounds, previously dissolved in DMSO, showed high reactivity in aqueous conditions, generally undergoing hydrolysis of the bromido ligands which leads to the formation of the water insoluble dihydroxo derivative. Nevertheless, when analyzing more complex environments, as cell culture medium, a stabilizing effect seemed to be exerted by the components of the medium

itself (e.g., proteins, organic molecules), as confirmed by interaction studies with the serum carrier protein BSA (Bovine Serum Albumin).

The antiproliferative activity of the complexes was tested on different human cancer cell lines, representative of different cancer types (e.g. lung, ovary, breast), showing promising cytotoxicproperties. Furthermore, their antitumor activity was confirmed *in vivo* on breast MDA-MB-231 human xenografts, while their toxicological profile, preliminary evaluated *ex vivo*, was similar to the "first generation" compounds.

To overcome the solubility problem in aqueous conditions and to avoid the intrinsic toxicity of DMSO (normally used as primary solvent), new solubilizing methods were explored. In particular, micelles based on Pluronic F127 and liposomes based on DPPC phospholipids were prepared, characterized and tested *in vitro*. These systems were proved to stabilize the compounds in physiological conditions, without affecting their antiproliferative activities. Moreover, micelles functionalized with CCK8 octapeptide were tested as targeting moieties to be selectively delivered to cancerous cells overexpressing the CCK-receptors. In this case, the GI_{50} values of the encapsulated compounds were improved of one order of magnitude.

To achieve more information about their mechanism of action, the interaction *in vitro* with some purified enzymes was performed, confirming that the complexes inhibit all the three enzymatic functions of the proteasome, together with the activity of PARP-1 enzyme.

More detailed studies, taking into account the kinetics of gold uptake by cells and the real-time inhibition of cell growth and adhesion, suggested that the complexes probably exert their cytotoxic effect on cells in the 4-5 h after administration, acting probably at the membrane level.

All together these results highlight the promising properties of the complexes as anticancer agents, and put the basis for the pursuance of the preclinical characterization, including deeper studies of their pharmacological properties and biological activity.

Riassunto

Il cisplatino (*cis*-diamminodicloroplatino(II)) è tuttora uno dei farmaci antitumorali più utilizzati, impiegato in particolare per il trattamento del tumore al testicolo e, in combinazione con altri chemoterapici, per la cura del cancro all'ovaio, al polmone a cellule piccole, alla vescica, al cervello e alla mammella. Nonstante la sua efficacia, il suo utilizzo viene fortemente limitato dall'insorgenza nei pazienti di effetti collaterali molto gravi, come l'elevata tossicità verso i tessuti sani (in particulare nefrotossicità) oltre che da meccanismi di resistenza al trattamento o acquisiti dopo alcuni cicli di terapia.

Per superare questi inconvenienti, sono stati sintetizzzati e testati come potenziali farmaci antitumorali nuovi complessi sia a base di platino che di altri metalli di transizione.

In particolare, alcuni composti di oro, già utilizzati da molti anni per la cura dell'artrite reumatoide (grazie alle loro proprietà anti-infiammatorie e immunosuppressive) sono stati testati per le loro proprietà antiproliferative, aprendo la strada a una nuova classe di potenziali composti antitumorali.

Da circa un decennio nel nostro gruppo di ricerca sono stati sintetizzati, caratterizzati e testati nuovi complessi ditiocarbammici di oro(III), che hanno dimostrato promettenti proprietà antiproliferative su diverse linee cellulari tumorali umane. I promettenti risultati ottenuti sia *in vitro* che *in vivo* per alcuni composti di “prima generazione” del tipo $[Au^{III}X_2(dtc\text{-}L)]$ (X= Cl, Br; dtc=ditiocarbammato; L= dimetilammina, pirrolidina, esteri della N-metilglicina (Sar)), hanno portato al *design* di una nuova serie di complessi di "seconda generazione", al fine di aumentarne la biodisponibilità, la selettività e l'*uptake* cellulare.

A questo scopo, sono stati preparati complessi ditiocarbammici funzionalizzati con diversi oligopeptidi, aventi formula generale $[Au^{III}X_2(dtc\text{-}Sar/Aib\text{-}(AA)_n)]$ (AA = diversi amminoacidi), affinchè potessero essere riconosciuti e trasportati da specifici trasportatori di membrana denominati PEPT (PEPT1 and PEPT2). Queste proteine risultano prevalentemente espresse nelle cellule epiteliali dell'intestino tenue, nella mammella, nel polmone, nel plesso coroideo e nei reni, e vengono in particolare sovraespresse in alcuni tipi di cellule tumorali. La principale caratteristica di queste biomolecole è la loro capacità di trasportare la maggior parte dei di- e tri-peptidi naturali, indipendentemente dalla loro sequenza, dimostrandosi quindi degli eccellenti *target* per il riconoscimento ed il trasporto selettivo di composti peptido-mimetici farmacologicamente attivi, quali ad esempio antibiotici β-lattamici ed alcuni inibitori di enzimi convertitori dell'angiotensina (ACE).

I complessi sintetizzati hanno mostrato ottime proprietà antiproliferative, esercitando un meccanismo d'inibizione della crescita tumorale diverso da quello normalmente descritto per i farmaci a base di

platino comunemente utilizzati in chemoterapia clinica, superandone anche i tipici effetti collaterali e i problemi di resistenza crociata al trattamento.

In questo lavoro di tesi sono stati sintetizzati nuovi complessi di Au(III) con leganti peptidoditiocarbammici, i quali sono stati ampiamente caratterizzati attraverso analisi elementare e di diffrazione a raggi-X su monocristallo, NMR mono- e bidimensionale, FT-IR e spettroscopia Uv-Vis. I complessi non-idrosolubili (previa dissoluzione nella minima quantità di DMSO) si sono dimostrati molto reattivi in soluzioni acquose caratterizzate da diverse condizioni di pH o di composizione salina. Generalmente essi tendono ad idrolizzare, scambiando con l'acqua un legante bromuro e portando alla formazione del di-idrosso derivato, insolubile in acqua. Andando però ad analizzare ambienti più complessi, come ad esempio il mezzo di coltura cellulare, è stato notato un effetto stabilizzante derivante probabilmente dalla presenza di particolari componenti del mezzo stesso (e.g. proteine, molecole organiche), come confermato anche da studi di interazione con la proteina del siero BSA (Bovine Serum Albumin).

L'attività antiproliferativa dei complessi è stata testata su diverse linee cellulari di tumori umani, rappresentative di diversi tipi tumorali (e.g. polmone, ovaio, mammella), mostrando promettenti attività citotossiche. La loro attività antitumorale è stata ulteriormente confermata *in vivo* sul tumore xenografico umano alla mammella MDA-MB-231, mentre una valutazione preliminare del profilo tossicologico effettuata *ex vivo* ha messo in luce un'analogia con i risultati ottenuti per uno degli analoghi composti di "prima generazione".

Per superare il problema della scarsa solubilità in soluzioni acquose, oltre che per evitare la tossicità intrinseca del DMSO (normalmente utilizzato per sciogliere i complessi), sono stati valutati nuovi metodi di dispersione. In particolare, sono state preparate, caratterizzate e testate *in vitro* sia micelle a base di Pluronico F127 che liposomi costituiti da fosfolipidi DPPC. Questi sistemi si sono dimostrati in grado di solubilizzare e stabilizzare i complesi in condizioni fisiologiche, senza tuttavia alterarne le proprietà antiproliferative. Inoltre, micelle funzionalizzate con l'octapeptide CCK8 sono state testate come nanosistemi per il trasporto selettivo verso le cellule tumorali che sovraesprimono il recettore specifico CCK-R. In questo caso i valori di GI_{50} registrati sono risultati di un ordine di grandezza inferiori rispetto allo stesso sistema non funzionalizzato.

Per ottenere maggiori informazioni sul meccanismo d'azione dei complessi, ne è stata in seguito valuatata la capacità di inibire *in vitro* alcuni enzimi selezionati per la loro rilevanza nell'attivazione della risposta apoptotica nelle cellule tumorali. I composti si sono dimostrati in grado di inbire tutte e tre le funzioni del proteasoma, inibiendo contemporaneamente anche l'attività dell'enzima PARP-1.

Studi più dettagliati hanno in seguito riguardato la cinetica di *uptake* dei complessi di oro da parte delle cellule tumorali, e la valutazione in tempo reale del profilo dell'inibizione della crescita

cellulare. I risultati ottenuti hanno suggerito che i complessi esplicano la loro attività citotossica nelle prime 4-5 h dalla somministrazione, agendo probabilmente a livello della membrana cellulare.

Questi risultati sottolineano le promettenti proprietà dei composti come potenziali agenti antitumorali, e gettano le basi per il proseguimento della loro caratterizzazione preclinica, la quale prevede una più approfondita valutazione delle loro proprietà farmacologiche e della loro attività biologica.

Aim of the work

The present work is mainly focused on the synthesis of new gold(III)-oligopeptide-dithiocarbamato derivatives for anticancer therapy, with the evaluation of their biological activity and stability in physiological conditions. In addition, we tried to gain insights in the understanding of their mechanism of action.

The rationale of this research project springs from previous results obtained in our research group on analogous gold(III)-dithiocarbamato aminoacid derivatives. Indeed, "first generation" compounds of type $[Au^{III}X_2(dtc)]$ (X=Cl, Br; dtc= various dithiocarbamates) were previously analyzed, showing promising antiproliferative activity both *in vitro* on a large panel of cancer cell lines, and *in vivo* on xenograft tumors[1,2]. Moreover, the toxicity profiles detected *in vivo* for these compounds resulted very promising if compared with cisplatin reference drug[3].

To improve their selectivity and their therapeutic effectiveness, a new "second generation" series of complexes was designed to specifically target membrane receptors overexpressed in cancerous cells.

In particular, the dithiocarbamato ligand was specifically functionalized with di/tripeptides in order to target PEPT receptors, which are present in humans in two isoforms (PEPT1 and PEPT2). They are proton-coupled integral membrane proteins that cotransport H^+ and substrates (as di- and tripeptides) across cell membranes. The driving force for the accumulation of the substrate in the cell against its concentration gradient is provided by an inwardly directed proton gradient. They are expressed in different tissues like small intestine, kidney, pancreas, bile duct, liver, mammary glands, lung and choroid plexus and are overexpressed in tumor cells, so they can be targeted for specific delivery of the therapeutic agents into the tumor site.

In addition to their physiological substrates, PEPTs are also responsible for membrane transport of many pharmacologically active peptidomimetic drugs and prodrugs, such as β-lactam antibiotics, angiotensin-converting-enzyme (ACE) inhibitors, renin inhibitors, thrombin inhibitors, or the anticancer drug bestatin, owing to their structural resemblance to di- and tri-peptides[4,5].

Starting from this rational, the experimental work mainly focused on the synthesis and the evaluation of the biological behavior of some new gold(III) dithiocarbamato derivatives of dipeptide ligands, for the selective targeting of PEPT receptors (**IT01-05**, **Figure I**), in comparison with a platinum-based reference drug and some "first generation" gold compounds (**cisplatin**, **AuL12**, **Figure I**).

Considering the possible application as anticancer compounds, their stability was analysed in different aqueous conditions (after dissolving the compounds in DMSO), starting from distilled water to saline solution NaCl 0.9%, and from PBS buffer pH=7.4 to cell culture medium.

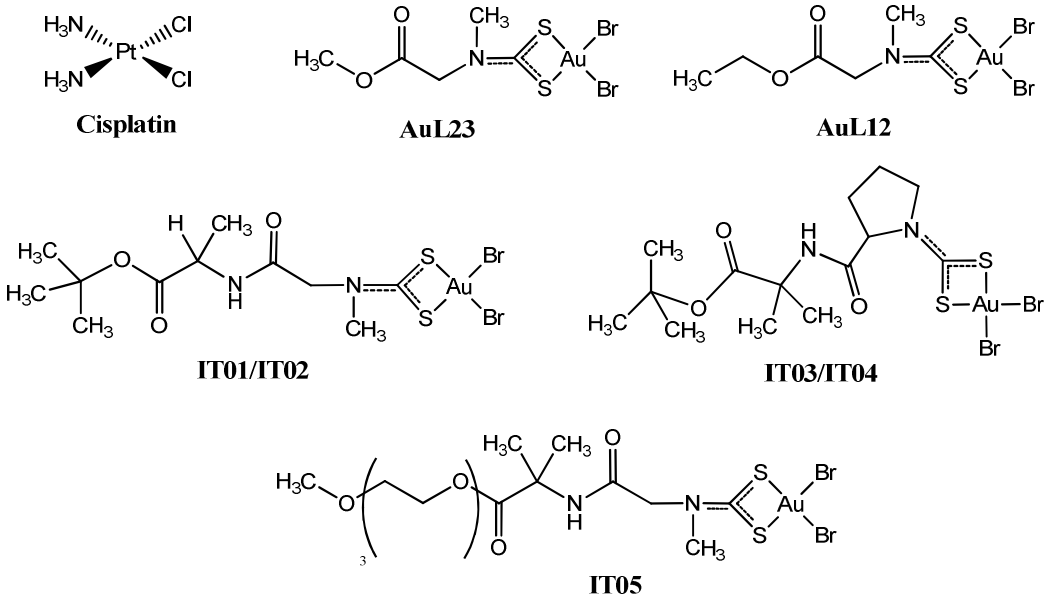

Figure I: molecular structures of cisplatin and gold(III)-dithiocarbamato derivatives analyzed in this project.

The ability of the compounds to interact with blood transport proteins was further evaluated, choosing the BSA (Bovine Serum Albumin, homologous of the human isoform) as a model for the studies. The interaction was analyzed by means of different spectroscopic techniques, in order to assess the presence of a stabilizing interactions between the protein and our compounds, which can eventually account for an enhanced stability of the complexes in the blood stream, accompanied by an increased bioavailability.

The *in vitro* antiproliferative activity of the compounds was screened on a large panel of human cancer cell lines, representative of different tumor types. In addition, toxicological studies were performed through an *ex vivo* set of experiments, to evaluate the toxicity on healthy rat tissues from liver, kidney and colon, along with preliminary *in vivo* experiments on human xenografts.

Because of the very poor solubility of the dithiocarbamato gold(III) complexes in physiological conditions, all the experiments were carried out pre-dissolving the compounds in DMSO, as above mentioned. This procedure is normally adopted also for the *in vitro* testing, keeping the DMSO concentration down below the 1% v/v to avoid effects deriving from the intrinsic toxicity of the organic solvent. However, for the forthcoming *in vivo* tests, a more biocompatible system to solubilize our compounds has been studied.

To overcome the complexes solubiliy problems, micellar and vesicular systems based on non- or low-toxic amphiphilic components were prepared and tested on cancer cell lines, allowing the exclusion of possible drawbacks deriving from the use of organic solvents.

In particular, micelles based on Pluronic F127 ($EO_{98}PO_{57}EO_{98}$; EO= ethylene oxide; PO=propylene oxide) were prepared and tested in comparison with vesicular systems derived from DPPC (dipalmitoylphosphatidylcholine) phospholipids.

After preparation and characterization of the different dipersant systems, the stability of the loaded compounds and their cytotoxic activity were tested. Furthermore, targeted delivery of a "first generation" gold(III) dithiocarbamato complex was exploited through the functionalization of micelles with the CCK8 peptide, specifically recognized by CCK receptors overexpressed in cancerous cells.

Moreover the reactivity towards the selected biomolecules PARP-1 and proteasome was investigated in order to obtain more insights into the mechanism of action of the gold compounds.

Finally, we performed some kinetic studies to determine the time-dependance of the cell growth inhibition by our compounds and their cellular uptake.

Abbreviations and acronyms

ACE	angiotensin-converting-enzyme
BER/SSB	Base Excision Repair/Single Strand Break
BSA	Bovine serum albumin
DCM	dichloromethane
DEDT	diethyldithiocarbamato
DIPEA	*N*,*N*-Diisopropylethylamine
DLS	Dynamic Light Scattering
DMAP	4-dimethylaminopyridine
DMEM	Dulbecco's Modified Eagle Medium
DMDT	*N*,*N*-dimethyldithiocarbamate
DMF	Dimethylformamide
DMSO	dimethysulfoxide
DPPC	dipalmitoylphosphatidylcholine
dtc	dithiocarbamato
EDCl	1-ethyl-3-(3-dimethylamminopropyl)-carbodiimide hydrochloride
EO	Ethylene oxide
ES	Ethylsarcosine
ESDT	Ethylsarcosine dithiocarbamato
FCS	Fetal Calf Serum
Fmoc	Fluorenylmethyloxycarbonyl
GI_{50}	Growth Inhibition concentration
HMBC	Heteronuclear multiple bond correlation
HMQC	Heteronuclear multiple quantum correlation
HSA	Human Serum Albumin
HSQC	Heteronuclear single quantum correlation
HoBt	1-hydroxy-1H-benzotriazole
ICP-AES	Inductive Coupled Plasma - Atomic Emission Spectroscopy
MTT	3-(4,5-dimethylthiazol-2-yl)-2,5-diphenyltetrazolium bromide
NMM	*N*-methylmorpholine
NMR	Nuclear Magnetic Resonance
PF127	Pluronic F127
PARP	Poly (ADP ribose) polymerase
PEG	Polyethylene glycol
PO	Propylene oxide
PyBOP	benzotriazol-1-yl-oxytripyrrolidinophosphonium hexafluorophosphate
RPMI	Roswell Park Memorial Institute
TDM	4,4'-tetramethyldiaminodiphenylmethane
TEA	trietilamine
TEG-OH	Triethylene glycol monomethyl ether
TFA	Trifluoroacetic acid
TIS	Triisopropylsilane
TMS	tetramethylsilane
WME	Williams Medium E
Z	carboxybenzyl

ZOSu	*N*-(benzyloxicarbonyloxy)succinimide

Introduction

Cancer is today considered a leading cause of mortality worldwide since it accounted for 7.6 million deaths (13% of all deaths; WHO, World Health Organization) in 2008, projected to continue rising with an estimated 13.1 million deaths in 2030 (**Figure 1**)[6].

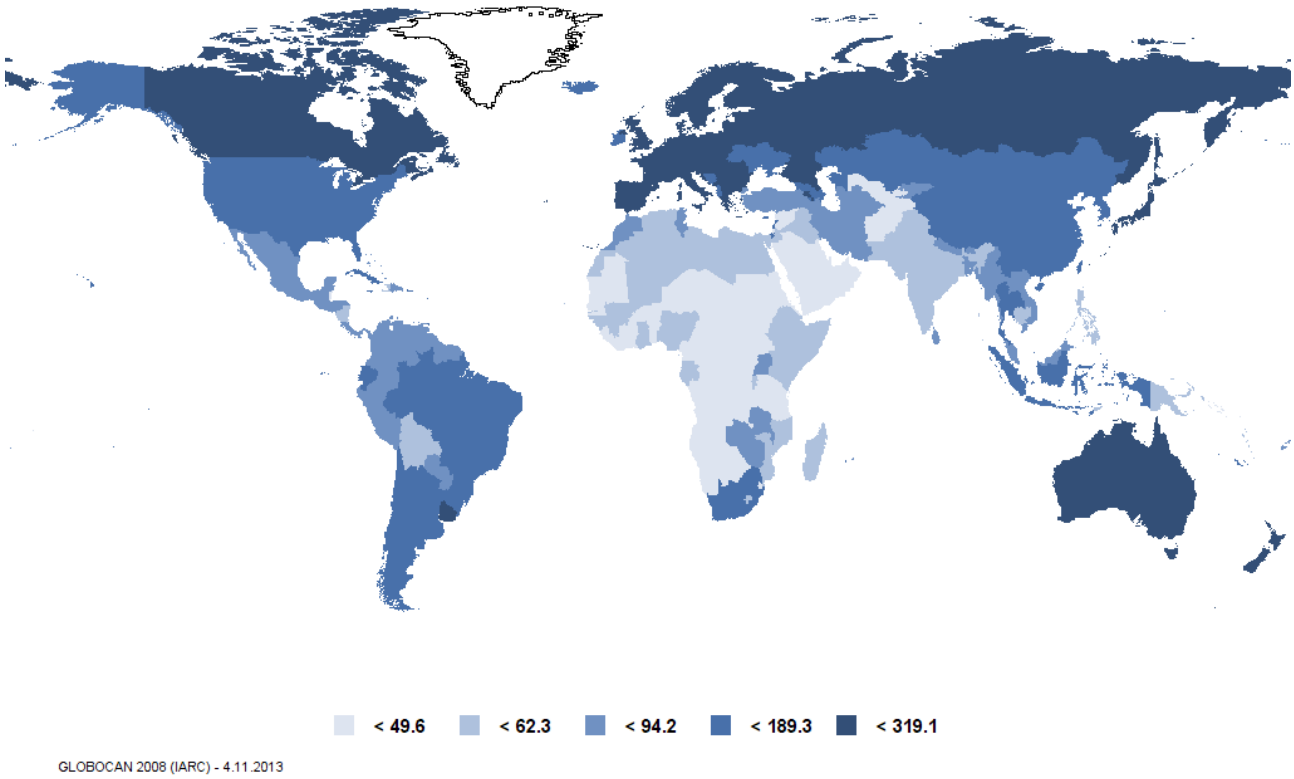

Figure 1: estimated crude mortality rate over 100000 people in 5 years (both sexes, all cancer types except melanoma)

The most diffuse cancer types are currently lung (1.37 million deaths), stomach (736 000 deaths), liver (695 000 deaths), colon (608 000 deaths), breast (458 000 deaths) and cervical cancer (275 000 deaths), with incidences that differ between men and women (word projection in 5 years, **Figure 2**)[7]. The main risks (nearly 30%) of developing a malignancy is connected to wrong behavioral and dietary habits: high body mass index, low fruit and vegetable consumption, lack of physical activity, tobacco use, alcohol use. In particular, it was proved that tobacco use is the most important risk factor for cancer causing 22% of global cancer deaths and 71% of global lung cancer deaths. In the low-income countries, chronic infections from hepatitis B (HBV), hepatitis C virus (HCV) and some types of Human Papilloma Virus (HPV) are leading risk factors for cancer.

Knowledge about the causes of cancer, and interventions to prevent and manage the disease is extensive, and cancer cases can be reduced and controlled by implementing evidence-based strategies for cancer prevention and early detection of cancer, since many tumors have a high chance of cure if detected early and treated adequately.

Cancer treatment requires a careful selection of one or more intervention, such as surgery, radiotherapy, and chemotherapy with the aim to cure the disease or considerably prolong life, while improving the patient's quality of life, usually with the help of psychological support.

Some cancer types, even though disseminated, such as leukemias and lymphomas in children, and testicular seminoma, have high cure rates if appropriate treatment is provided. In other cases, the same outcome can be achieved if treatment is combined to screening programs and early detection, as in the case of breast cancer, cervical cancer, oral cancer and colorectal cancer.

Palliative care is treatment to relieve, rather than cure, symptoms caused by cancer, helping people to live more comfortably.

Cancer cases wordwide in adults (5-year projection over 28803266 people)

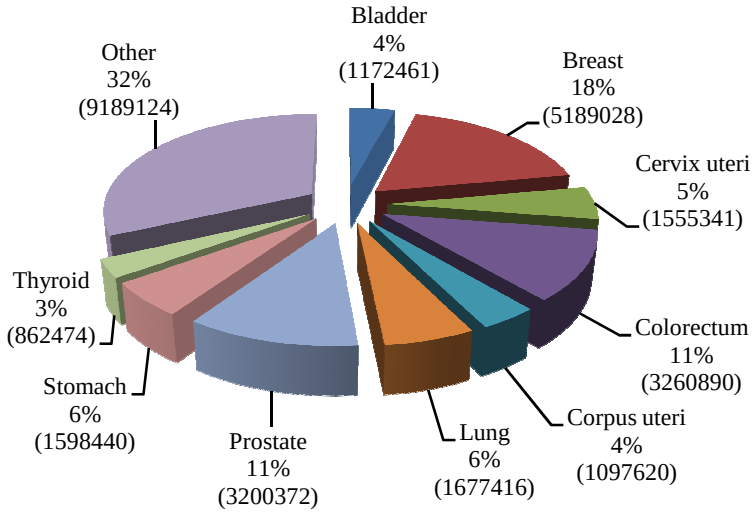

Figure 2: cancer cases in adults over 28,803,266 people (both sexes).

At a molecular level, the occurrence of cancer is due to modifications that take place in single cells. It is known that the transformation from a normal cell into a tumour cell is a multistage process, typically characterized by a progression from a pre-cancerous lesion to malignant tumours. These mutations are the result of the interaction between a person's genetic factors and three categories of external agents, including: physical carcinogens (such as ultraviolet and ionizing radiation), chemical carcinogens (such as asbestos, components of tobacco smoke, aflatoxin, arsenic, etc.) and biological carcinogens (such as infections from certain viruses, bacteria or parasites)[6].

Ageing is another fundamental factor for the development of cancer, and the incidence of cancer rises dramatically with age, combined with the tendency for cellular repair mechanisms to be less effective when a person grows older.

Hallmarks of cancer

The progression of a normal cell into a cancer cell can be described as a multi-step process. New achievements in anticancer research recently led to the definition of six hallmarks characteristic of all cancer types, as summarized in **Figure 3**.

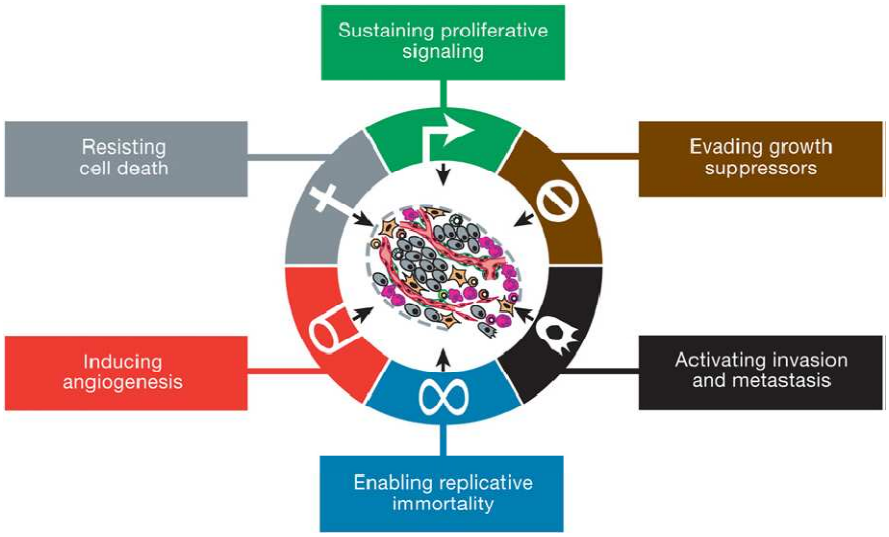

Figure 3: of six hallmarks characteristic of all cancer types.

1. Sustaining proliferative signaling

The most fundamental trait of cancer cells is their ability to sustain chronic proliferation. Contrarily to normal cells, the malignant counterparts lose the control on the production and release of growth-promoting signals, thus entering into and progressing through the cell life cycle in an unregulated way. The unbalanced homeostasis is largely due to the release of mitogenic signals and the conveyance of growth factors to neighboring cells. In the extracellular matrix, growth factors bind to cell-surface receptors, which trigger intracellular signaling pathways involved in cell growth and function. Likewise, this stimuli may be sent to normal cells within the supporting cancer-associated stroma, which reciprocate by supplying the neoplastic cells with several growth factors. Interestingly, some somatic mutations are known to enhance receptor signaling by either up-regulating the receptor proteins at the cancer cell surface or structurally changing the receptor molecule, thus making such cells hyper-responsive to growth factors[8,9].

2. Evading growth suppressors

To induce and sustain positive growth-stimulatory signals, tumor cells must also circumvent programs that negatively regulate cell proliferation. Dozens of tumor suppressors which operate in various systems to limit cell growth and proliferation have been discovered in different cancers, regulated by the expression of specific genes. Two prototypical oncosuppressor genes encode in particular for TP53 (tumor protein 53) and RB (retinoblastoma-associated).

RB protein is involved in the regulation of the cell growth-and-division cycle, and it is known in to in particular inhibit the cell from replicating damaged DNA, by preventing its progression along the cell cycle through G_1 (first gap phase) into S (synthesis phase). When the genes encoding for these protein are mutated, the protein is dysfunctional, causing a persistent cell proliferation[10].

TP53 is, similarly, a tumor suppressor protein that plays a crucial role in regulating cell cycle, and has been also described as "the guardian of the genome" because of its role in conserving stability by preventing genome mutation functioning, thus acting as a tumor suppressor.

3. Resisting cell death

Functional studies conducted over the last decades proved apoptosis to be a natural barrier to cancer development in normal cells[11]. Various physiological stresses that cancer cells experience during their tumorigenesis or as a result of anticancer therapy, trigger apoptosis. The main apoptosis-inducing stresses derive from signals imbalances as result of high levels of oncogene signaling and DNA damage associated with hyperproliferation. The apoptotic machinery is composed by both upstream and downstream effector components, whilst the regulators can be divided in those receiving and processing extracellular death-inducing signals (extrinsic apoptotic pathway, involving for example Fas ligand/receptor) and those sensing and integrating a variety of signals of intracellular origin (the intrinsic program)[10].

4. Enabling replicative immortality

Normal cells are able to pass only through a defined number of subsequent cell growth and division cycles. Then, the cell enters into a phase of senescence, characterized by the entrance in a non-proliferative but viable state, and ultimately passes to a crisis condition, which results in cell death. Nonetheless, it is possible that cells, when in the crisis phase, revert to a proliferating state with an unlimited replicative potential. This transition is called immortalization[10] and depends strictly from the action of telomeres, hexanucleotide repeats protecting the ends of chromosomes[12,13]. In normal cells they serve as "clocking" device, since are progressively shorten during duplication until leaving chromosomal DNA unprotected from end-to-end fusions, thus triggering apoptosis. In neoplastic cells this control is lost, since they are able to maintain telomeric DNA long enough to

avoid the induction of senescence or of apoptosis, usually upregulating the expression of telomerase. This enzyme is almost absent in normal cells, but was found expressed at functionally significant levels in cancer cells. By lengthening telomeric DNA, the tumor cell will not experience the progressive telomere erosion.

5. Inducing angiogenesis

The sprouting of new blood vessels from existing ones is normally associated with the need of cancer cells to absorb more oxygen and nutrients, as well as discharging metabolic wastes and carbon dioxide. In normal adult cells, angiogenesis is activated transiently only for wound healing and female reproductive function cycle. Instead, during malignancy the angiogenesis is always activated and consists in the continuous developing of new vessels from the existing vasculature[14].

6. activating invasion and metastasis

The process of invasion and metastasis comprehends a series of discrete biological changes, starting with local invasion, intravasation of malignant cells into neighboring blood and lymphatic vessels and transit of neoplastic cells through the lymphatic and circulatory systems. These processes are followed by escape of cells from the lumina of such vessels into the parenchyma of distant tissues (extravasation), formation of small nodules of cancer cells (micrometastases) and ultimately by growth of micrometastatic lesions to yield macroscopic tumors (colonization)[10].

Anticancer metallodrugs

From the historical point of view, a large number of metal compounds have been used in medicine, even if their toxicity has often prompted alternative options. Some of these compounds have been developed and used for specific diseases, including lithium compounds to treat hyperactivity, gold compounds in arthritis treatment, barium sulfate in gastrointestinal diagnostic strategies as imaging agent or contrast medium; some other have been used for more common applications such as antacids, fluoride as tooth decay preventative and zinc oxide for protection against sunburn[15,16].

The use of metal-based drugs can be dated in prehistoric times and through the age of alchemists, since empirical and, more often, pseudoscientific preparations were used for the treatment of a wide variety of diseases. For instance, gold salts were used in the late 19th century to treat alcoholism, opium addiction and neurasthenia, although modern medicine finds no value for such treatments. In some cases, metal ions were combined with other substances, including herbal extracts such as gentian or cinchona, organic medicines such as quinine, strychnine and opium, cod liver oil and even

red wine[17]. The German physicians Paul Ehrlichmann and Robert Koch made pioneering contributions to modern medicine, including scientific approaches to the development of arsenicals and gold compounds, respectively, for the treatment of various diseases. In particular, Robert Koch's research on the antibacterial activity of $K[Au(CN)_2]$ for the treatment of tuberculosis led to the successful use of gold thiolates for treating rheumatoid arthritis.

Until the 1960s, research on metal ions in biochemistry and medicine attracted the attention mostly of clinical medicine, nutritional science and toxicology. Notably, in the 1960s, more powerful physicochemical methods of characterization became available to study the role of metal ions in biological systems, allowing a well-aware use of metal ions in biochemistry and medicine. The enhanced knowledge of metal ion biological activity, as well as the progressive unraveling of their structure/activity relationships, has led in the last decades to the development of a wide variety of new metal-based drugs suitable for the treatment of specific pathological diseases[18-20]. The design and development of new and more effective metal complexes has been further boosted by the recent identification and characterization of a huge number of proteins (*e.g.* serum albumin, metallothionein and transferrin), able to modify oxidation state and bioavailability of metal ions, as well as by the discovery of crucial details on the metabolism of small molecules, such as ligands or redox active species.

Despite the scientific progress, few compounds achieved the approval by national drug agencies; in addition, the mechanisms of activity and of toxicity of most of these complexes still remains ambiguous, as in the case of cisplatin introduced in therapy by FDA (Food and Drug Administration) in 1970s[21].

Cisplatin: the archetype of metal-based anticancer drugs

Cisplatin was firstly synthesized by Michele Peyrone in 1845[22] and only 50 years later Alfred Werner proposed a square planar geometry for this compound and distinguished between the *cis*- and *trans*-isomers, namely cisplatin {*cis*-$[PtCl_2(NH_3)_2]$} and transplatin {*trans*-$[PtCl_2(NH_3)_2]$} (**Figure 4**)[21,23,24]. The capability of cisplatin, but not its *trans*-isomer, to inhibit cellular division was serendipitously discovered only in 1960s by Barnett Rosenberg, during an experiment on the effects of electric fields on bacterial cell division. Nowadays cisplatin is one of the best drugs for the treatment of testicular cancer, resulting very effective also against melanoma, non-small-cell lung carcinoma and, in combination with other anticancer drugs such as paclitaxel, against ovarian cancer[25].

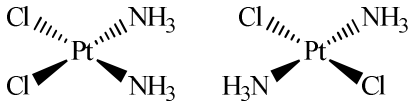

Figure 4: Cisplatin and transplatin chemical structures.

Although its mechanism of action remains still elusive, it is generally believed that cisplatin carries out its anticancer activity by forming adducts with DNA, which induce programmed cell death (apoptosis)[26]. In these adducts, the two chlorido ligands are lost (by hydrolysis), whereas the two ammonia groups remain coordinated to the metal center. Upon endovenous administration, the relatively high extracellular chloride concentration (approximately 100 mM) reduces the possibility for cisplatin to undergo hydrolysis of the metal-bound halogen before entering the cells. Early studies suggested that cisplatin passes intact through the cell membrane mainly by passive diffusion[27]. More recently, experimental evidences have pointed out the existence of active transport mechanisms which exploit Cu-transporting proteins[28]. Once inside the cell, the lower intracellular chloride concentration (~4-20 mM), induces a partial solvolysis of the drug which replaces one of the chlorine-ligands with a water molecule. The mono-aquo species is responsible for at least 98% of the platinum binding to DNA within the cell nucleus[29].

Mono-aquo cisplatin forms a monofunctional adduct with nucleobases[30], followed by ring closure to give a bifunctional adduct, usually guanine-guanine[31], either directly or subsequently to the solvolysis of the second *cis*-chlorido-ligand (**Figure 5**)[32]. The final adduct induces significant distortion to the DNA structure, leading some DNA-binding proteins to initiate signal pathways of apoptosis. The biological ineffectiveness of transplatin can be explained by the inability of the *trans* isomer to form similar adducts with DNA[33].

In spite of its efficacy, it has been estimated that only about 1% of intracellular cisplatin is able to reach the nucleus and explicate its cytotoxic activity, because of the presence of many extracellular (serum albumin and other proteins containing cysteine and methionine amino acids) and intracellular S-donor molecules (mainly glutathione and metallothionein). In fact, the soft metal center Pt(II) shows high affinity towards soft S-donor ligands, this resulting in displacement of harder ligands (Cl^-), cisplatin sequestration and deactivation[34].

In addition, the effectiveness of cisplatin treatment is strongly limited by the development of tumor resistance. This phenomenon includes a decreased intracellular drug accumulation, an increased capability of cells to repair or tolerate the DNA damage caused by cisplatin and higher levels of cytoplasmic thiols able to scavenge the DNA adducts by coordinating the metal center[32].

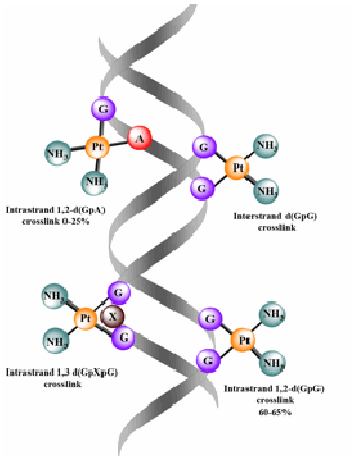

Figure 5: main adducts form upon interaction of cisplatin with DNA.

For these reasons, the research has been focusing its efforts on the design of new and more effective Pt-based drugs (*second generation drugs*) with improved clinical performances, aimed at reducing side-effects associated with cisplatin treatment (*i.e.* toxicity to kidneys and nervous system, hearing difficulties, nausea, vomiting)[35]. Rosenberg and coworkers developed carboplatin (**Figure 6**), less active than cisplatin but with less severe side-effects[36]. In fact, in carboplatin bidentate dicarboxylate leaving group determines a higher ligand-metal bond stability than the chlorido groups in cisplatin, due to the chelate effect; this results in a slower reactivity and, hence, a reduced toxicity with respect to cisplatin[37]. Another second-generation Pt-based drug, oxaliplatin, has a broader activity spectrum and a better safety profile than cisplatin (**Figure 6**)[38]. It has also shown lack of cross-resistance with cisplatin or carboplatin, likely resulting from the chemical and steric features of its DNA-adducts[38]. From 1970s onwards, several cisplatin analogues, more tumor-specific or less prone to resistance development, have been reported in literature. In addition, other biologically active platinum complexes with *trans*-geometry or containing multiple platinum centers have been recently under extensive investigation[39],[40].

The issue to overcome cisplatin limitations, to enlarge the activity spectrum of the drug and, in this context, the failure of several Pt-based candidates, has led many researchers to focus on non-Pt coordination compounds for cancer treatment[41]. Among the most promising drug candidates, Ru-, Cu- and Au-based complexes have shown interesting cytotoxic activity against some solid tumors and constitute a subject of intensive studies aimed at clarifying their mechanism of action and toxicological profiles[42].

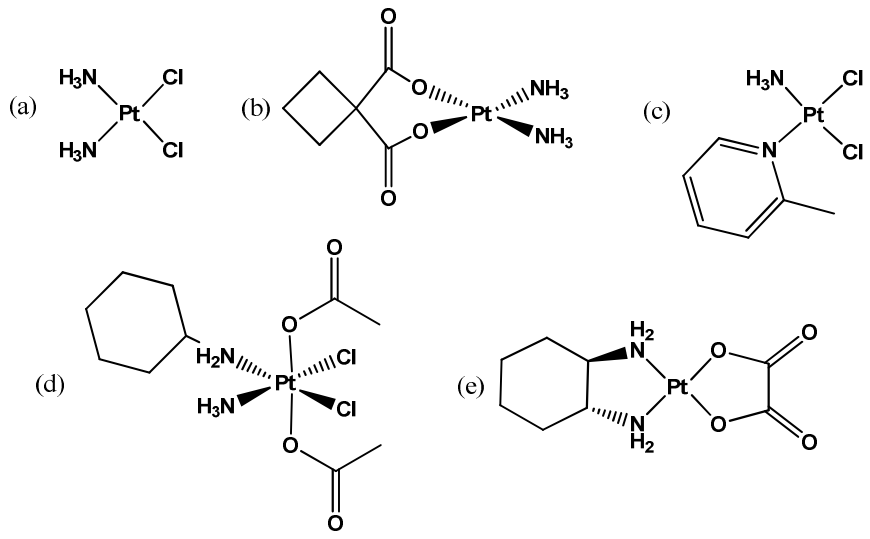

Figure 6: most popular platinum-based anticancer agents**:** (a) cisplatin, (b) carboplatin, (c) picoplatin, (d) satraplatin, (e) oxaliplatin.

Gold and its history

Gold was the first pure element known to early man; since early ages it was found in stream beds and other geological formations and was visually attractive and easily workable. Medical uses from ancient civilizations in Egypt, China and Greece included this metal for the treatment of a wide variety of diseases[43]. These ancient civilizations attributed magical and healing powers to items fashioned from gold or to preparations containing the powdered metal[44].

The modern use of gold in medicine, known as chrysotherapy (χρυσός, gold), traces its scientific origins to the above-mentioned pioneering work of Dr. Robert Koch, who studied the antibacterial properties of potassium aurocyanide, $K[Au(CN)_2]$, while screening potential metal-based drugs against *tubercle bacilli*. This led to the clinical, but ultimately unsuccessful, use of other gold compounds to treat tuberculosis in the late 19th and early 20th centuries[40]. In 1930s, the physician Jacque Forestier observed beneficial effects of gold compounds on the rheumatoid arthritis of some patients, thus prompting their use for the cure of the disease. Since the early 1970s, an oral gold preparation, Auranofin (2,3,4,6-tetraacetyl-β-1-D-thioglucopyranosato-*S*-(triethyl-phosphine) gold(I)), was developed and finally approved in the late 1980s[45]. In modern medicine, gold compounds are clinically used to treat rheumatoid arthrite and, at present, are studied for their antitumor, antiparasitic and antiviral activities.

Gold and its chemistry

Gold is most "noble" metal and has peculiar features due to its position in the periodic table. The physical properties conferred by its crystal structure (cubic close packed), such as ductility, high melting point (1064°C) and density (specific gravity 19.32 $g \cdot cm^{-3}$ with respect to water), are easily matched by other metals as silver. Nevertheless, the bright and yellow color of gold represents a rare exception in the bright silvery appearance of many other metals, where only copper and a small number of alloys (*e.g.* common brass) show a different color[16].

The chemical behavior of gold contributes to make this element unique as well[46]. Because of its "noble" character, gold at the elemental state (electron configuration $[Xe]4f^{14}5d^{10}6s^{1}$) is not easily combined or mixed with other elements, even after long exposure to extremely aggressive conditions, making possible the existence of pure gold veins in the earth's superficial layers.

Most of the applications of gold and its compounds, until the early 1980s[47], exploited the inertness of the metal to give lasting protection of materials against degradation by chemicals or light (for example, astronauts' gold mirrored visors or non-corrodible electrical conductors at very small dimensions). The durability and ductility of the metal allowed the production of extremely thin films (gold foils, gold leaves) and wires for technological applications by simple mechanical procedures, even though deposition techniques from gaseous precursors (including gold vapors) or from solutions of gold chemicals (by electrolysis, electroplating or electroless methods) are also available and easy to carry out[48].

Until the last century, gold-based coordination compounds have played a minor role if compared with gold at metal state. In fact, these compounds were used as intermediates in the recovery process of gold from ores. The most important species are the gold cyanide complexes formed in the cyanide leaching and extraction processes, in which finely crushed ores are treated with sodium cyanide in the presence of oxygen. Typically, the resulting sodium gold cyanides ($Na[Au(CN)_2]$) are then adsorbed on high affinity carbon-in-pulp coal and, after re-extraction, depleted of gold by various reductive processes to yield gold metal[49]. For further conversion, gold metal can be taken up again in cyanide or in aqua regia (nitric and hydrochloric acids in a volume ratio 1:3) that is the only acidic medium able to dissolve it. In this process, one among the very few thermodynamically stable gold compounds, tetrachloroauric acid, is formed; this acid and its derivative salts are used for the preparation of other gold-based chemicals, whose the overwhelming majority is thermodynamically labile and has been proved to decompose into metallic gold and side-products.

Therefore, it is not surprising that gold chemistry, which is clearly dominated by the metallic state, has remained undeveloped for so long as it was merely regarded as an art aimed at recovering and converting the metal into possible forms for decorative, monetary, anticorrosive or electrical usages.

Since the 1980s, gold chemistry has been characterized by innovative approaches and by unprecedented branches of research interests. New ways of recovering the metal were explored in view of the environmental hazard deriving from the traditional amalgam and cyanide-based processes, as for the use of non-toxic and biologically degradable thiourea to recover gold from electronic scrap[48]. Biomass, prepared from algal cells, constitutes an efficient binding medium for gold salts in aqueous solution; this bio-absorption process may provide a lucrative alternative for gold recovery from mining effluents[50].

Studies on stereochemistry[51-53], bioinorganic and medicinal chemistry[54] application of gold coordination compounds[55,56] are very attractive, in particular for gold compounds in unusual oxidation states as well as for gold clusters or complexes with exceptional gold-gold or gold-metal bonds[57]. Since the last decade, many researches have been focusing on the use of gold nanoparticles in different application fields (*e. g.* drug delivery, catalysis, photovoltaics, sensors).

Au(I) and Au(III) are the most common and stable oxidation states that dominate the aqueous chemistry of gold. The aquated ions are unstable and rapidly undergo reduction, even though many complexes are stabilized by a large variety of "soft" ligands.

Gold(I) is characterized by the electronical configuration $[Xe]4f^{14}5d^{10}$ and it can form linear, trigonal-planar or tetrahedral complexes. Gold(I) is a very "soft" metal ion and the stability constants for some of its complexes (determined in acetonitrile solutions, where disproportion of gold(I) does not basically occur) follow the reported series[58]:

1. anionic complexes $[AuX_2]^-$: $CNO^- < CNS^- \sim Cl^- < Br^- < I^- << CN^-$;
2. cationic complexes $[AuL_2]^+$: $Ph_3PO < Me_2S < Py < Ph_3As < NH_3 << Ph_3P \sim ArNC < MeNC < Ph_2PMe < PhPMe_2$;
3. neutral complexes [AuXL]: $Me_2O << Me_2S < Me_2Se < Ph_3Sb < ArNC \sim Ph_3As < Me_2Te < MeNC \sim Ph_3P < Ph_2PMe < PhPMe_2$.

In case of complexes with potentially bidentate ligands, gold(I) binds almost invariably the softer end of the ligand; for example, the ligands NCO^-, $S_2O_3^{2-}$ and SO_3^{2-} will be bound through *N* or *S* rather than *O* atoms. Similarly, SCN^- is normally bound through *S* rather than *N* atom, although the equilibrium between *N*- and *S*-bonded species in [AuL(SCN)] complexes depends on the nature of the ligand *L*[59]. An example of a trigonal-planar complex is $[Au(SCN)(PPh_3)_2]$ with *S*-bonded thiocyanate[60].

The electron configuration of the "less soft" gold(III) ion, is [Xe]4f^{14}5d^{8}. All the gold(III) complexes are diamagnetic with a low-spin configuration. Although it forms a larger number of complexes with "hard" ligands with respect to gold(I), it has been argued that gold(III) displays a higher selectivity for "soft" ligands such as sulfur[61]. The wide majority of these complexes are square-planar, but penta- or hexa- coordinated derivatives with distorted square-pyramidal and tetragonally distorted octahedral structures, respectively, are also reported in literature[62]. Gold(III) can readily form square-planar complexes with a variety of bidentate sulfur-donor ligands such as toluene-1,2-dithiolate, maleonitriledithiolate and dithiocarbamate.

In their most common stereochemistry, gold(I) and gold(III) centers have 14 and 16 valence electrons, respectively. Thus, most gold complexes are coordinatively unsaturated and can undergo ligand addition, usually proceeding through five-coordinated intermediates. However, the number of characterized 5-coordinate complexes reported is limited, and typically show a chelating bidentate ligand with the first donor atom coordinated on the plane and the second, more distant, in apical position.

The "noble" character of gold is originated by its high reduction potential, which makes it inert by nature. Indeed, gold is the most electronegative among all the metals (2.54 on Pauling scale going from 0.7 estimated for francium to 3.98 of fluorine) and can easily be reduced. The value of its standard electrochemical potential (E_0) is the highest of any other metal:

$$Au^{3+} \xrightarrow{1.29\,V} Au^{+} \xrightarrow{1.68\,V} Au$$

$$Au^{3+} \xrightarrow{1.42\,V} Au$$

According to these values, any Au cationic form will virtually undergo reduction by accepting electrons from any reducing agent, to form neutral gold atoms and, consequently, metal gold aggregates in bulk. As a rule, the values of reduction potentials for Au ions may be lowered by ligand coordination[53].

Gold and its use in medicine: antiarthritic therapy

In 1922, Landé was the first to report on the use of gold(I) compounds, in particular aurothioglucose (Solganol), to treat various diseases, including rheumatic fever[63]. In 1935, Forestier proposed the use of aurothiopropanolsulfonate (allocrysin), aurothiomalate (myocrysin) and aurothiosulfate (sanocrysin) (**Figure 7**) for the treatment of rheumatoid arthritis, an autoimmune disease in which the synovial tissues that line and lubricate the joints are under attack by the immune system[64].

All of these gold(I) compounds are characterized by linear -S-Au-S- geometries and appear to be polymeric. A full trial started only in 1957 and, few years later, the reports showed myocrysin

effectiveness against rheumatoid arthritis[65]. These gold drugs are referred to as "disease modifying anti-rheumatic drugs", able to retard and sometimes to cause remission of the disease stage[66]. However, the use of these compounds has some adverse effects, such as skin rashes, diarrhea and kidney inflammation; in addition, patients widely differ in their tolerance. For this reason, its use is usually postponed until failure of safer alternative methods[67].

Among second-generation gold-based drugs, auranofin (2,3,4,6-tetraacetyl-β-1-D-thiogluco-pyranosato-*S*-(triethylphosphine)gold(I)) (**Figure 7**) is the only one approved for use against arthritis by oral administration. This compound is a monomeric species with a linear geometry, able to cross the cell membrane due to the lipophilic phosphine ligand. *In vivo*, the tetraacetylthioglucose ligand is rapidly displaced by ligand-exchange reactions, whereas the phosphine is removed more slowly by the same process after 24 hours, causing fewer toxic side effects than its conventional forerunner agents. Nevertheless the slow reactivity also influences the efficacy of the drug, which results generally reduced with respect to the other compounds, i.v. administered[68].

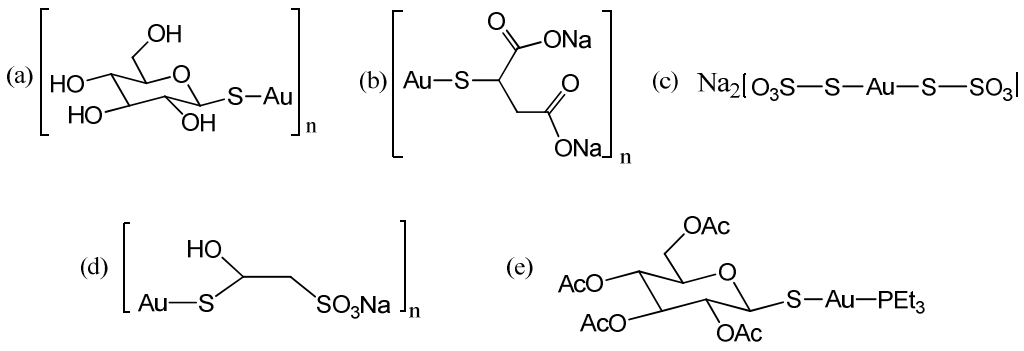

Figure 7: most popular gold(I)-based anticancer agents: (a) solganal, (b) miocrisin, (c) sanocrisin, (d) allocrisin, (e) auranofin.

The most important recognized effect of chrysotherapy is the anti-inflammatory activity; additional effects have been reported on the inhibition of various enzymes (thiol-containing proteins), antimicrobial activity, reduction of antibody-mediated system, effects on lymphocytes, monocytes or neutrophils (especially inhibition of T-cell proliferation and of polymorphonuclear monocyte activation). Multiple concerted mechanisms of action have been hypothesized for chrysotherapy, but for any of them there is a wide acceptance of one particular as primary biological action[46,69].

Gold and its use in medicine: anticancer chemotherapy

Gold compounds have been extensively tested to assess their antitumor activity in cell cultures and, in the case of the more promising species, also in animal models[70].

Some antiarthritic gold-based drugs (*e.g.*, the *6*-mercaptopurine and cyclophosphamide) have been initially tested as anticancer agents, due to their well-known immune-suppressive and anti-inflammatory actions[71]. In addition, two rationales have been accounted for the investigation of gold compounds as antitumor agents: similarities between gold(III) square-planar complexes and their platinum(II) analogues and the possibility to synthesize gold(I) and gold(III) complexes with active organic chemotherapy agents as ligands, in order to modulate or confer new properties to the metal ion. However, as gold(III) compounds may be expected to be reduced *in vivo* to gold(I) or metallic gold, due to the generally reducing physiological environment, a proper selection of the right type of ligand enhances the stabilization of the metal center, by lowering its reduction potential.

Early investigations of gold-based Auranofin analogues for antitumor activity were not fruitful. The first attempts suggested that a less toxic action and an enhanced delivery of gold would have been achieved with less labile ligands than the currently used monodentate thiolates provided with antiarthritic action. Successively, the screening of numerous Auranofin analogues with variations on the phosphine and thiolate ligands has led to the development of a promising antitumor agent. $[Au(DPPE)_2]Cl$ (DPPE = bis(diphenylphosphino)ethane) was identified as a stable metabolite of the dinuclear gold compound $(\mu\text{-DPPE})(AuCl)_2[Au(DPPE)_2]^+$ by Berners-Price[72]. However, the development of a treatment based on this compound was prevented by the discovery of significant cardiovascular toxicity caused by inhibition of mitochondrial functions. In contrast, the complexes (dimethylaminomethylphenyl)-dichloro-gold(III) and its acetato- analogue showed interesting properties. From a chemical point of view, these compounds are strongly stabilized by the chelating *C,N* donor ligand that generates a neutral complex and stabilizes the gold(III) against reduction *in vivo*. The two complexes showed promising activity, with a different mechanism of action compared to cisplatin, but clinical trials have not been undertaken, because of their low solubility[55].

In last decades, various classes of cytotoxic gold(III) compounds were developed in few laboratories worldwide and were found to exhibit very attractive biological profiles[73,74]. Other than chlorides, these complexes exhibit *N*-, *O*- and *P*- donor ligands coordinated. The most representative ones have *N*-donor ligands, such as complexes with aldiminate derivatives, porphyrins, aliphatic amines and heteroaromatic rings.

Recently, a group of thirteen structurally different gold(III) complexes, including the dithiocarbamato complex AuL12 (see following Section), has been tested *in vitro* at the German Biotech Company Oncotest GmbH, according to a specific comparative strategy for the development of new anticancer agents. Among all, AuL12 turned out to be the second best performer with GI_{50} (concentration which leads to 50% Growth Inhibition of cancer cells) values in the low micromolar range on all the screened 36 human tumor cell lines, in particular against ovary and brain cancers, and showed an

excellent degree of selectivity (17%). Intriguingly, from a comparative analysis by 110 reference substances with known modes of action, AuL12 proved to be the only gold(III) complex whose mechanism of action did not resemble that of any other reference compound[75].

Research on gold(III)-based anticancer compounds

In principle, gold(III) shows more chemico-physical similarities with platinum(II) than the gold(I) counterpart. Gold(III) shares with platinum(II) the same d^8 configuration, forming complexes with square-planar geometry and similar chemico-physical properties. These properties suggested that gold(III) could be a better candidate in replacing platinum(II) in anticancer compounds, to achieve similar mechanisms of action but with reduced toxicity[55,76]. Anyway, the high redox potentials of gold in the oxidation state +3, limit their utilization in physiological conditions.

In the last decades, a series of gold(III) complexes were synthesized owing to the suitable choice of stabilizing ligands presenting in particular sulfur- and nitrogen-donating groups.

The compounds developed by different scientists can be divided in four groups, differing substantially for the nature of coordinating ligands[77]:

i) *mononuclear gold(III) complexes:* belong to this class gold(III) complexes with square-planar geometry characterized by nitrogen-donating and halogens ligands (**Figure 8**). The nitrogen-donating ligands act as stabilizers with respect to gold(III) reduction, whist the halogen ligands can be, almost in principle, exchanged in physiological conditions with water molecules, rendering the metal center available to interact with target biomolecules, as for cisplatin[41].

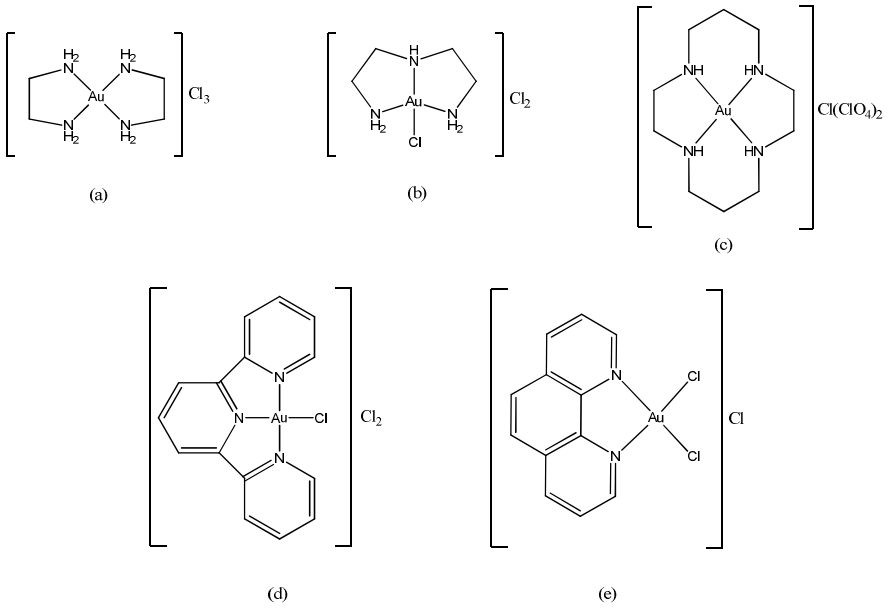

Figure 8: Principal gold(III) complexes with *N*-donating ligands: (a) $[Au(en)_2]Cl_3$, (b) [AuCl(dien)]Cl, (c) $[Au(cyclam)]Cl(ClO_4)_2$, (d) $[AuCl(terpy)]Cl_2$, (e) $[AuCl_2(phen)]Cl$.

ii) *porphyrinic gold(III) derivatives*: these complexes (**Figure 9**) result particularly stable with respect both to the reduction to gold(I) and to the de-metallation of the ligand. Their antiproliferative activity seems to be connected to the intercalation of the porphyrine to DNA but also to the alteration of normal mithocondrial functions[78].

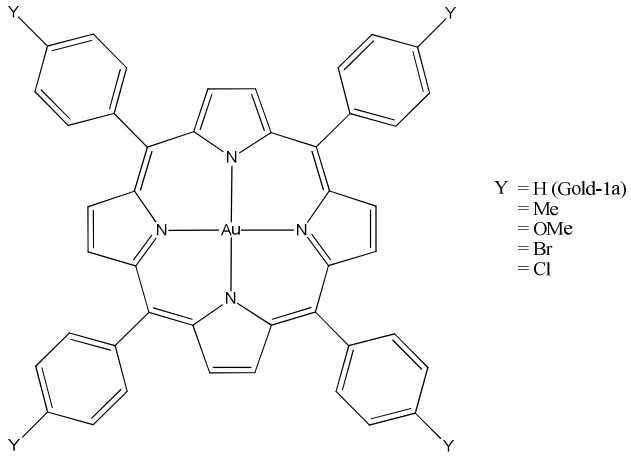

Figur e 9: porphyrinic derivatives of gold(III).

iii) *gold(III) organometallic compounds*: in this promising class of gold(III) complexes the presence of one or more direct metal-carbon bonds owns an high stabilization of the metal center towards reduction in physiological conditions (**Figure 10**)[76,79].

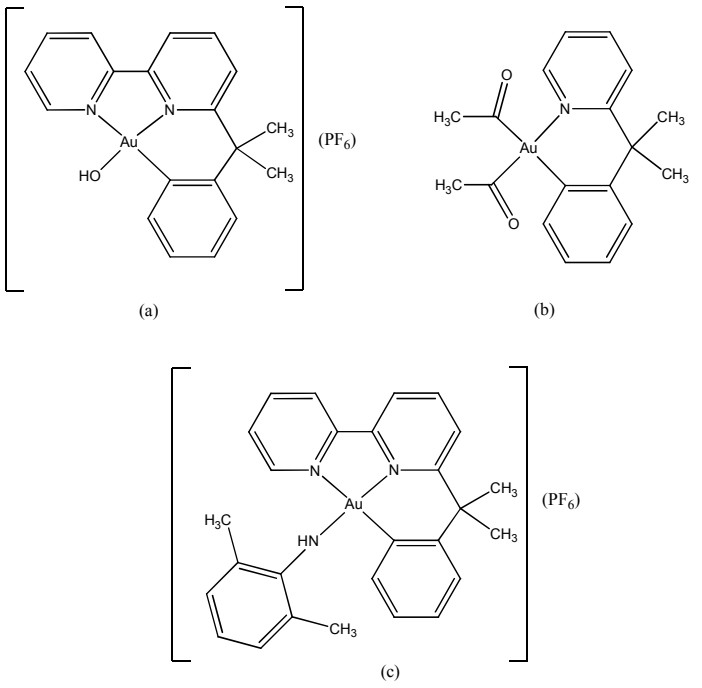

Figure 10: organometallic derivatives of gold(III): (a) [Au(OH)(bipy^{c}-H)](PF_6), (b) [Au$(AcO)_2$(py^{dmb}-H)], (c) [Au(bipy^{dmb}-H)(2,6-xylidinyl-H)](PF_6).

iv) dinuclear complexes of gold(III): are mainly characterized by the presence of *N*-donating 2.2'-bipyridine derivatives ligands and bridging oxygen atoms between two gold(III) centers. The peculiar characteristic is the presence of a "diamond core" Au_2O_2, which, along with the bypiridinic ligands, defines a square-planar geometry around the metal center (**Figure 11**).

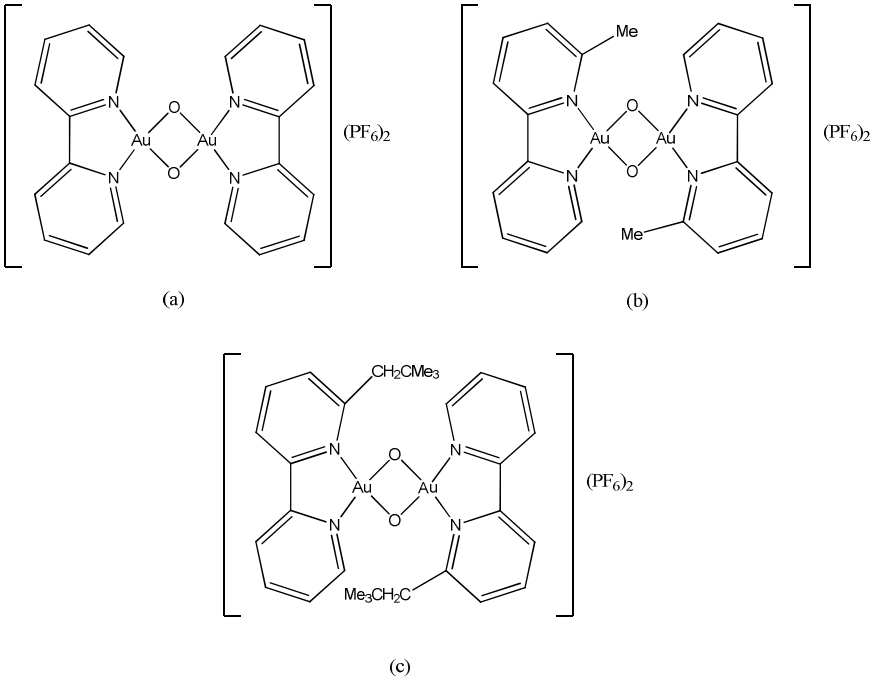

Figure 11: dinuclear complexes of gold(III): (a) $[\{Au(bipy)\}_2(\mu\text{-}O)_2](PF_6)_2$; (b) $[\{Au(6\text{-}Mebipy)\}_2(\mu\text{-}O)_2](PF_6)_2$; (c) $[\{Au(6\text{-}CH_2CMe_3bipy)\}_2(\mu\text{-}O)_2](PF_6)_2$.

The introduction of substituents on 6 and 6' positions influences weakly the overall structure of the complexes, determining indeed a strong variation of the metal center reactivity[80].

Gold(III)-based dithiocarbamato complexes: state of the art of our researches

Among the mononuclear complexes an important example of gold(III) complexes designed for anticancer therapy is represented by dithiocarbamato derivatives.

As previously mentioned, nephrotoxicity (*i.e.*, kidney toxicity) limits the use of cisplatin and related platinum-based therapeutics. This side-effect may be induced by platinum binding to thiol-containing renal enzymes, which leads to their consequent inactivation[81]. The high affinity of Pt(II) ion for sulfur-containing biomolecules, such as cysteine, methionine, glutathione, metallothionein and albumin, plays a central role in platinum toxicity as well as in its deactivation[82,83]. In this case, the adducts formed upon the irreversible binding to *S*-donor biomolecules are further metabolized and, successively, excreted through urine or bile (faeces).

Since sulfur is involved in the whole metabolic process of platinum drugs, a large number of sulfur-containing nucleophiles has been tested as chemoprotectants to modulate cisplatin nephrotoxicity[84].

The selective protection of non-tumor cells, together with reduced systemic toxicity, are two critical issues for the development of novel and efficient chemoprotectants. Many sulfur-based molecules have been designed and tested (**Figure 12**), some of them showing encouraging properties in the perspective of clinical use. However, the selective protection of normal tissues without inhibition of the anticancer activity still remains a challenging objective[85,86].

In this context, positive outcomes were achieved with sodium diethyldithiocarbamate (NaDEDT), that provides protection against renal, gastrointestinal and bone marrow toxicity induced by cisplatin without decreasing its antitumor activity[87].

The chemoprotective effect results from the capability to remove platinum from the thiol groups of proteins, without any reversal of platinum-DNA adducts responsible for its antitumor activity. Interestingly, platinum-DNA adducts (1,2-intrastrand cross-links) were shown to decrease by *ca.* 50% upon treatment with NaDEDT soon after cisplatin administration, causing a loss of therapeutic effect, whereas no change in anticancer activity was observed when NaDEDT was administered 3 h after the drug. This behavior can be ascribed to NaDEDT-cisplatin reaction, resulting in the inactivation of the drug, when diethyldithiocarbamate is administered soon after cisplatin. In particular, this reaction is 40,000-fold faster than hydrolysis, leading to the direct chloride substitution. Conversely, when NaDEDT is administered 3 h later, the drug has already started to react with DNA. In this case the dithiocarbamate is not able to cleave platinum-DNA adducts, wherein chlorides have been replaced by guanine residues, but it can remove platinum centers from a variety of other sulfur-containing molecules and, as a consequence, increase the amount of drug available to interact with DNA. Hence, the accurate use and dosing of NaDEDT as chemoprotectant reduces nephrotoxicity of cisplatin chemotherapy without decreasing the antitumor properties. Furthermore, few data showed DEDT ability to significantly reduce other non-renal toxicities, particularly the cumulative neuropathies, associated with cisplatin treatment. Nevertheless, the overall benefits of NaDEDT are somewhat limited by the acute inherent toxicity of dithiocarbamates themselves that excludes the possibility to treat patients with a dose-intensive program[86]. In fact, potential health hazards associated with free (*i.e.*, not coordinated) dithiocarbamates are still under investigation, including genotoxicity. However, clinical use of chemoprotectants has been forsaken and replaced by aggressive hydration, together with antiemetic prophylaxis during cisplatin treatment. In the meantime, a continuous effort is still being made by researchers in order to reduce cisplatin-induced toxicity.

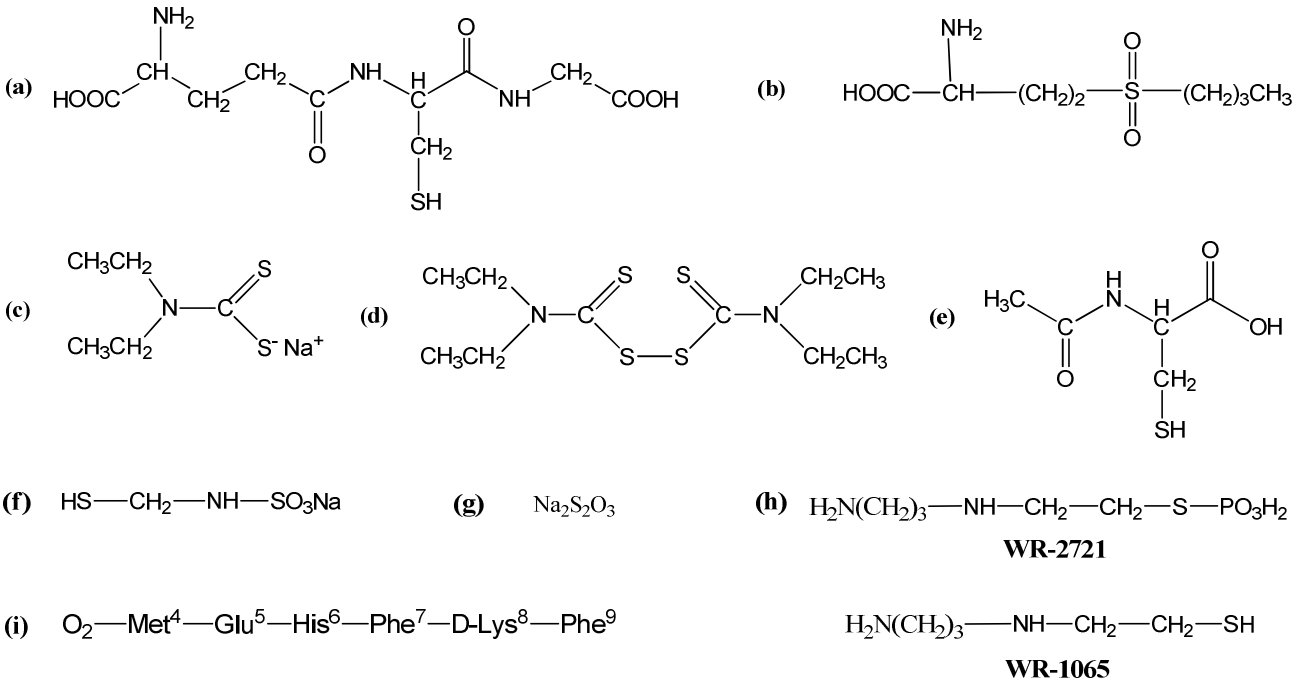

Figure 12: Cisplatin modulatory sulfydryls and peptide derivatives: glutathione (GSH, **a**), the GSH-depleting antimetabolite L-buthioninesulfoximine (L-BSO, **b**), the sulfydryl metabolite of disulfiramdiethyldithiocarbamate (DEDT, **c**), the parent disulfide disulfiram (antabuse, **d**), *N*-acetyl-L-cysteine (L-NAC, **e**), *S*-mercaptoethanesulfonatesodium salt (mesna, **f**), sodium thiosulfate (**g**), the phosphothiolamifostine (**WR-2721**) and its active metabolite actifostine (**WR-1065**) formed by alkaline phosphatase activity (**h**), and the melanocortin-derivedpeptide ORG-2766 (**i**).

On the basis of these considerations, our research group has been designing novel dithiocarbamato complexes potentially able to combine the cytotoxic activity of the related metal centers (*e.g.* Pt(II), Pd(II), Au(III), Ru(III), Ru(II), Zn(II), Cu(II)) with the lack of nephrotoxicity due to the inherent chemoprotective action of the ligand[88,89]. The rationale of our strategy is based on the chemical features possessed by the dithiocarbamato moiety (–$NCSS^-$). Dithiocarbamates are bidentate ligands that can form very stable complexes, due to the chelating effect; thus, the possible decomposition with subsequent loss of the dithiocarbamato ligand is unlikely to occur. Moreover, the solubility properties of the metal-dithiocarbamato derivatives may be, at least in principle, modulated by modifying the organic chain of the dithiocarbamato ligand.

Interestingly, the presence of a chelating dithiocarbamato ligand in a square-planar complexes should prevent from the coordination of additional *S*-donor ligands (*e.g.*, methionine and cysteine residues) in *trans* position with respect to the –$NCSS^-$ moiety, due to the strong *trans* effect of the dithiocarbamato sulfur atoms; this peculiarity potentially avoids any interaction of the metal center with thiol-containing renal enzymes and, consequently, reduces the risks of nephrotoxic side-effects.

To date, the toxicological profile and the anticancer activity of compounds points out the success of our design strategy, both in stabilizing the heavy metal center and in avoiding the non-specific reactivity of the compound, responsible of systemic toxicity. The most promising results were obtained with gold(III)-dithiocarbamato derivatives [$Au^{III}X_2$(dtc)] (X = Cl, Br; dtc = dithiocarbamato-derivatives ligands), whose design aimed to reproduce as much as possible the main features of cisplatin. All the compounds have been fully characterized by means of several techniques, confirming that coordination of the metal ion by the dithiocarbamato ligand takes place in a near square-planar geometry through the two sulfur-donating atoms in a bidentate symmetrical fashion. The two remaining coordination positions are occupied by two *cis*-halogen atoms which may undergo hydrolysis. When X-ray structures were not available, density functional calculations were performed, confirming the structural conclusions deduced by other characterization techniques[90].

In addition, the inherent electrochemical properties of our gold(III) compounds have been studied in a physiological-like solution by cyclic voltammetry, showing that both *N*,*N*-dimethyldithiocarbamate (DMDT) (AuL10 and AuL14) and sarcosine ethyl ester (ESDT) (AuL12 and AuL13) derivatives (**Figure 13**) undergo irreversible stepwise reduction processes, leading to the corresponding dinuclear gold(I) species [Au^{I}(DMDT)]$_2$ and [Au^{I}(ESDT)]$_2$, at *ca.* -300 mV and -180 mV (*vs.* saturated calomel electrode, SCE), respectively. Remarkably, these reductions occur at potentials considerably lower than the typical values for the Au(III)/Au(I) couple known for the corresponding K[AuX_4] (X = Cl, Br) precursors (*ca.* +1.29 V)[91]. Therefore, coordination by dithiocarbamates induces a large stabilization of the metal ion in the +3 oxidation state, owing to the electron-donating capability and the stabilizing chelate effect of the dithiocarbamato moiety.

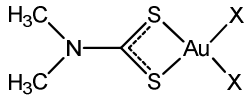

X =Cl, [$Au^{III}Cl_2$(DMDT)] (AUL10)
X =Br, [$Au^{III}Br_2$(DMDT)] (AUL14)

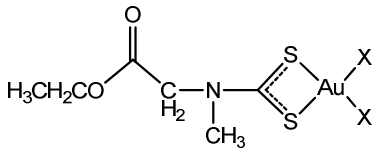

X =Cl, [$Au^{III}Cl_2$(ESDT)] (AUL13)
X =Br, [$Au^{III}Br_2$(ESDT)] (AUL12)

Figure 13: Selected Au(III)-dithiocarbamato derivatives.

Concerning their solution properties, these gold(III) complexes hydrolyze in a physiological-like environment, by delivering two moles of halide per mole of starting complex, leading to the corresponding Au(III)-diaquo counter-parts within 30-40 min. Intriguingly, the hydrolyzed

species were proved to be reasonably stable in physiological solution, reduction to gold(I) occurring after 12-24h.

From comparative *in vitro* cytotoxicity studies on our Pt(II)-, Pd(II)-, and Au(III)-MSDT derivatives on human squamous cervical adenocarcinoma (HeLa) cells and human leukemic promyelocytes (HL60), gold(III) complexes resulted to be significantly more active (GI_{50} *ca.* 1 μM) than cisplatin (GI_{50} *ca.* 2 μM) and with respect to Pt(II) and Pd(II)-dtc counter-parts (GI_{50} >15 and 5 μM, respectively) under the same experimental conditions, inducing apoptosis especially in HL60 cells[92]. $[Au^{III}X_2(MSDT)]$-type compounds were also tested on a panel of acute myelogenous leukemia cell lines, representing different French-American-British subtypes, and toward the Philadelphia-positive (K562) cells[93]. In this case, the gold complexes showed to inhibit cell growth in the tested myeloid cell lines with GI_{50} values *ca.* ten-fold lower than the reference drug[91].

Moreover, after short exposure (18 h), they induced strong and rapid apoptosis by down-regulating the antiapoptotic molecule Bcl-2 and up-regulating the proapoptotic molecule Bax, whereas cisplatin did not. Finally, after long exposure (72 h), they were proved to induce only modest cell cycle perturbations but high DNA fragmentation, whereas classical platinum(II) complexes are known to promote characteristic cell cycle alterations resulting in increased G_2M cell fraction. G_2M is an important DNA cell cycle check-point which prevents cells from initiating mitosis before they have a chance to repair damaged DNA after replication[26,94]. Therefore, $[Au^{III}X_2(MSDT)]$-type complexes are able to promote early apoptosis and membrane damage to a much greater extent than cisplatin, suggesting a different mechanism of action underlying its biological activity.

Within the family of $[Au^{III}(dtc)X_2]$ complexes, the derivatives AuL10, AuL14, AuL13 and AuL12, turned out to be much more cytotoxic *in vitro* than cisplatin, even toward human tumor cell lines intrinsically resistant to the Pt-based drug itself, such as Daudi, MeWo, LoVo and A549 cells, for which they have shown activity levels comparable to those recorded on the corresponding cisplatin-sensitive parent cell lines, ruling out the occurrence of cross-resistance phenomena (**Table 1**). As a whole, our complexes proved to be much more potent than cisplatin even at nanomolar concentrations, with GI_{50} values up to five orders of magnitude lower than the reference drug[95].

Table 1: *In vitro* cytotoxic activity of Au(III)-dithiocarbamato derivatives [$Au^{III}Cl_2$(DMDT)] (AUL10), [$Au^{III}Br_2$(DMDT)] (AUL14), [$Au^{III}Cl_2$(ESDT)] (AUL13) and [$Au^{III}Br_2$(ESDT)] (AUL12) compared to the reference metallodrug cisplatin toward different established human cancer cell lines: human squamous cervical adenocarcinoma (HeLa), human leukemic promyelocytes (HL60), human Burkitt's lymphoma (Daudi), human malignant melanoma (MeWo), human colon adenocarcinoma (LoVo), human non-small cell lung adenocarcinoma (A549), human ovarian carcinoma cisplatin-sensitive (2008) and cisplatin-resistant (C13*), human epidermoid carcinoma cisplatin-sensitive (A431) and cisplatin-resistant (A431-R), human osteosarcoma cisplatin-sensitive (U2OS) and cisplatin-resistant (U2OS-R) cells.

	GI_{50}±st.dev. (μM)				
Cell line	Compound				
	AUL10	AUL14	AUL13	AUL12	cisplatin
HeLa	2.10±0.01	3.5±0.01	8.2±0.2	7.6±0.2	15.6±0.4
HL60	$(0.80\pm0.01)\cdot10^{-2}$	$(0.70\pm0.01)\cdot10^{-2}$	0.43±0.09	0.14±0.02	25.6±0.3
Daudi	$(0.10\pm0.01)\cdot10^{-2}$	$(0.10\pm0.01)\cdot10^{-2}$	4.65±0.09	5.8±0.2	95±1
MeWo	2.0±0.3	$(0.10\pm0.01)\cdot10^{-2}$	12.4±0.9	10.0±0.9	48±2
LoVo	$(2.40\pm0.04)\cdot10^{-2}$	3.8±0.1	7.6±0.2	7.9±0.1	56±2
A549	$(0.35\pm0.01)\cdot10^{-2}$	0.41±0.03	4.73±0.04	9.6±0.2	35±1
2008	$(0.20\pm0.01)\cdot10^{-2}$	30.0±0.1	49.3±0.1	16.5±0.4	43.2±0.4
C13*	$(0.10\pm0.01)\cdot10^{-2}$	21.8±0.2	23.8±0.1	$(0.10\pm0.01)\cdot10^{-2}$	556±3
A431	$(1.20\pm0.01)\cdot10^{-2}$	1.8±0.1	0.29±0.01	$(1.50\pm0.01)\cdot10^{-2}$	77.4±0.4
A431-R	$(0.20\pm0.01)\cdot10^{-2}$	2.8±0.2	0.43±0.03	$(0.10\pm0.01)\cdot10^{-2}$	382±3
U2OS	4.8±0.3	18±1	5.8±0.4	0.49±0.09	35±2
U2OS-R	6.4±0.1	13±1	5.2±0.2	0.24±0.09	84±3

It is worth to highlight that usually *in vitro* anticancer activity of gold compounds is not confirmed by subsequent *in vivo* studies[96]. On the other hand, the *in vivo* antitumor activity of our gold(III)-dithiocarbamato derivatives, evaluated against human tumors implanted on immunodepressed nude mice (xenografts), was fully consistent with *in vitro* data. For example, treatment of MDA-MB-231 breast tumor-bearing nude mice with AuL14 resulted in significant inhibition of the tumor growth (*ca.* 50% inhibition after 29 days of daily treatment at 1 mg kg^{-1} body weight subcutaneous, s.c., compared to control). Interestingly, during the treatment, no toxicity was observed, and mice did not display signs of weight loss, decreased activity or anorexia[97]. Similarly, administration of 1 mg kg^{-1} s.c. every second day of AuL10 caused an overall 85% reduction of PC3 human prostate tumor implanted in nude mice after a 19-day treatment

(compared to control untreated mice). Again, chemotherapy was well tolerated by the treated animals which suffered from minimal systemic toxicity only, and histology showed no detectable damage to the main organs[93,94]. Among all, the Au(III)-dithiocarbamato derivative AuL12 has been selected for additional *in vivo* studies due to its overall favorable solubility, stability and antitumor properties. Thus, *in vivo* nephrotoxicity studies were also carried out with AuL12 by measuring some specific biomarkers in both urines (total urinary proteins (TUP), *N*-acetyl-β-D-glucosaminidase (NAG) and glutamine synthetase (GS)) and renal tissues (*p*-aminohippuric acid (PAH) and GS) of the treated rats[3]. In this investigation, cisplatin administration induced a significant increase of all the urinary biomarkers and a significant inhibition of GS activity in renal cortical slices, whereas the gold(III)-dithiocarbamato derivative caused negligible changes compared to untreated control rats (mainly observable at the higher dose, 20 mg kg^{-1} body weight), accounting for a substantial lack of nephrotoxic side-effects. The favorable toxicity profile was also confirmed by the LD_{50} value of 30 mg kg^{-1} recorded for AuL12 that is, as far as we know, among the higher ever reported for gold-based therapeutics (cisplatin LD_{50} = 11.4 mg kg^{-1}). Subsequent investigations showed that no significant histologically detectable toxicity involving treated animals' organs was observed. SEM (scanning electron microscopy) evaluation of the surface of all tissues examined was considered compatible with normal conditions, when compared to control animals. Surprisingly, no gold was detected in the investigated tissues, thus ruling out the accumulation of the metal in any of the organs taken into account (*i.e.*, heart, liver, spleen, kidneys, testicles, pancreas, lungs and brain). Accumulation around the injection site (*i.e.*, peritoneal area) was also excluded. These results together with excretion studies, suggest that gold is quickly cleared from the body (within 48 h), the large majority being excreted through the feces (>89%) and only about 10% *via* the urinary system[98]. This result is extremely positive when compared with the data reported in literature concerning the renal toxicity induced by gold derivatives. For instance, it is well known that the anti-arthritic drugs, auranofin and myochrysine, induce proteinuria and kidney dysfunctions and gold nanoparticles are able to penetrate renal cells causing nephrotoxicity[99].

Second Generation gold(III) dithiocarbamato complexes.

To improve the therapeutic effectiveness of the complexes and increase their cellular uptake, a "second generation" of gold(III)-dithiocarbamato complexes was designed[100,101]. Since cancer cells are known to overexpress specific biomarkers and receptors needed for carcinogenesis and tumor growth, targeted chemotherapies actually aim at blocking cancer cells proliferation exploiting such

specific upregulated biomolecules. This led to the development of efficient and innovative delivery systems in which conjugated drugs incorporating a tumor targeting group, can selectively reach the tissue of interest and deliver the cytotoxic agent directly into the tumor cells[102]. In particular specific peptide transporters (PEPTs), characterized by different tissue distributions (small intestine, kidney, lung, etc.), were selected as potential targets, because of their upregulation in various cancerous cells[103]. In particular, owing to their capability to promote cellular uptake of potentially all physiologically occurring di- and tripeptides, they represented an excellent target also for the delivery of some pharmacologically-active compounds (as β-lactam antibiotics and ACE inhibitors), and might have a central role also in the recognition and transport of our compounds.

According to the *in vitro* cytotoxicity studies, the complexes [$AuBr_2$(dtc-SarGlyO*t*Bu)] (AuD6) and [$AuBr_2$(dtc-SarAibO*t*Bu)] (AuD8) (**Figure 14**) resulted the most effective not only toward the evaluated human tumor cell lines (**Table 2**), but also in preliminary *in vivo* tests on xenografts, and were thus selected for further studies[104].

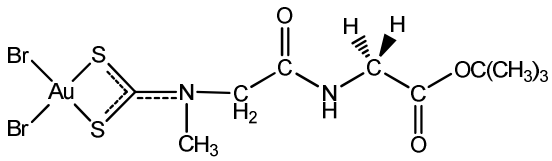

[$Au^{III}Br_2$(dtc-Sar-Gly-O*t*Bu)]

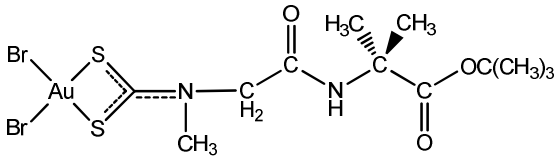

[$Au^{III}Br_2$(dtc-Sar-Aib-O*t*Bu)]

Figure 14: chemical structure of [$Au^{III}Br_2$(dtc-SarGlyO*t*Bu)] (AuD6) and [$Au^{III}Br_2$(dtc-SarAibO*t*Bu)](AuD8) compounds

AUD8, up to now the better characterized, showed no cross-resistance with cisplatin and was proved to inhibit tumor cell proliferation with different mechanism of action compared to clinically-established platinum drugs[100]. All the obtained results account for the interest in continuing the preclinical studies on AUD8 and other Au(III)-peptidodithiocarbamato derivatives, evaluating the possibility for these complexes to approach to phase I clinical trials.

Table 2: *in vitro* cytotoxic activity of AuD6 and AuD8 on established human cancer cell lines: human prostate cancer (PC3 and DU145), ovarian adenocarcinoma cisplatin-sensitive (2008) and cisplatin-resistant (C13*) and Hodgkin's lymphoma (L540) cells compared to the reference metallodrug, cisplatin.

Cell line	GI_{50} ± st.dev. (μM)		
	AuD6	AuD8	Cisplatin
PC3	1.3±0.1	0.8±0.1	3.3±0.3
DU145	4.5±0.9	1.4±0.1	4.5±0.1
2008	18±2	4.5±0.2	19±1
C13*	12±1	3.7±0.3	117±9
L540	2.1±0.2	1.5±0.2	2.5±0.1

General materials and methods

Instrumentation

Elemental analysis

Elemental analysis of carbon, nitrogen and hydrogen were obtained with a CARLO ERBA mod 1108 CHNS-O microanalyzer.

Termogravimetric analysis

Thermogravimeter analysis were carried out using a thermoanalyzer NETZSCH mod. STA42 in the range 25-1200°C in alumina crucibles, with an heating rate of 5°C/min under air, with a flow rate of 30 cm^3/min, using alumina as reference substance.

Thin layer chromatography

Silica gel 60 F254 (Merck) or Alugram® Sil G UV 254 (Macherey-Nagel) on aluminium foil was used to follow the reactions. Silica gel 60 F254 (Merck) on glass was used for TLC characterization. Retention factors (R_f) have been measured using three different solvent mixtures as eluents.

R_{f1}: $CHCl_3$/EtOH 9:1; **R_{f2}**: BuOH/AcOH/H_2O 3:1:1; **R_{f3}**: PhMe/EtOH 7:1.

Products were detected either by UV lamp irradiation, or with exposition to I_2 vapours or by warming with a heat gun and spraying firstly with a 1.5 % NaClO solution and then with a ninhydrin-TDM solution.

Flash chromatography

For flash chromathography (FC) purifications silica gel 60 Merck (40-63 μm diameter, mesh 230-400) was used. For the various purifications, the crude product was directly loaded on top of the column, after been dissolved in a small amount of the eluent used for the purification.

Polarimetric measurements

Optical rotations were measured on a Perkin-Elmer model 241 polarimeter with an Haake model D8 thermostat at the mercury line wavelength, using a cell with an optical pathlength of 10 cm. Concentrations are expressed in g/100 mL. [α] are calculated using the formula $[\alpha] = \alpha/(c \cdot l)$, where "c" is the concentration (in g/mL) and "l" is the optical path (in dm). Spectrophotometric grade MeOH was used as solvent.

IR Spectroscopy

FT-IR spectra were recorded in nujol on a Nicolet Nexus 870 spectrophotometer (1000 scans, resolution 2 cm^{-1}) for the range 50-600 cm^{-1}, and in solid KBr on either a Nicolet 55XC or a Perkin-Elmer 580B spectrophotometer (32 scans, resolution 2 cm^{-1}) for the range 400-4000 cm^{-1}. Data processing was carried out using OMNIC version 5.1 (Nicolet Instrument Corp.).

NMR Spectroscopy

All NMR spectra were acquired in the appropriate deuterated solvent at 298 K on a Bruker Avance DRX 300 spectrometer using a BBI [^{1}H,X] probe-head equipped with *z*-field gradients. Data processing was carried out using MestReNova version 6.2 (Mestrelab Research S.L.).

Typical acquisition parameters for 1D ^{1}H NMR spectra (1H: 300.13 MHz): 16 transients, spectral width 7.5 kHz, using 32k data points and a delay time of 5.0 s. Spectra were processed using exponential weighting with a resolution of 0.5 Hz and a line-broadening threshold of 0.1 Hz.

Typical acquisition parameters for 1D **^{13}C{^{1}H} NMR** spectra (^{13}C: 75.48 MHz): 8k transients, spectral width 18.8 kHz, using 32k data points and a delay time of 7.0 s. Sequences were optimized for $^{1}J(^{13}C,^{1}H)$ = 145 Hz, and ^{1}H decoupling was achieved by using WALTZ16 pulse sequence. Spectra were processed using exponential weighting with a resolution of 2.0 Hz and a line-broadening threshold of 2.8 Hz.

Typical acquisition parameters for 2D **[^{1}H,^{13}C] HMQC NMR** spectra (^{1}H: 300.13/^{13}C: 75.48 MHz): 512 transients of 32 scans/block, spectral width 7.5/18.8 kHz, 1k/1k data points and a delay time of 2.0 s. Sequences were optimized for $^{1}J(^{13}C,^{1}H)$ = 145 Hz, and ^{1}H decoupling was achieved by using GARP pulse sequence. Spectra were processed by using cosine-square weighting with a resolution of 1.0/3.0 Hz and a line-broadening threshold of 0.3/1.0 Hz.

Typical acquisition parameters for 2D **[^{1}H,^{13}C] HMBC NMR** spectra (^{1}H: 300.13/^{13}C: 75.48 MHz): 512 transients of 16 scans/block, spectral width 7.5/18.8 kHz, 1k/1k data points and a delay time of 2.0 s. Sequences were optimized for $^{1}J(^{13}C,^{1}H)$ = 145 Hz/$^{n}J(^{13}C,^{1}H)$ = 5 Hz with no ^{1}H decoupling. Spectra were processed by using sine-square weighting with a resolution of 0.3/1.0 Hz and a line-broadening threshold of 0.3/1.0 Hz.

Typical acquisition parameters for 2D **[^{1}H,^{15}N] HSQC NMR** spectra (^{1}H: 300.13/^{15}N: 30.41 MHz): 512 transients of 16 scans/block, spectral width 7.5/12.1 kHz, 1k/1k data points and a delay time of 2.0 s. Sequences were optimized for $^{1}J(^{15}N,^{1}H)$ = 70 Hz, and ^{1}H decoupling was achieved by using WALTZ16 pulse sequence. Spectra were processed by using cosine-square weighting with a resolution of 2.2/3.7 Hz and a line-broadening threshold of 0.7/1.0 Hz.

Typical acquisition parameters for 2D **[^{1}H,^{15}N] HMBC NMR** spectra (^{1}H: 300.13/^{15}N: 30.41 MHz): 512 transients of 16 scans/block, spectral width 7.5/12.1 kHz, 1k/1k data points and a delay time of 2.0 s. Sequences were optimized for $^{1}J(^{15}N,^{1}H)$ = 70 Hz/ $^{n}J(^{15}N,^{1}H)$ = 3 Hz with no ^{1}H decoupling. Spectra were processed by using sine-square weighting with a resolution of 2.2/3.7 Hz and a line-broadening threshold of 0.7/1.0 Hz.

^{1}H and ^{13}C chemical shifts were referenced to TMS at 0.00 ppm *via* internal referencing to the residual peak of the deuterated solvent employed, and ^{15}N to external $^{15}NH_4Cl$ (1.5 M in 1 M HCl in 90% H_2O/10% D_2O) at 0.00 ppm.

UV-Vis spectroscopy

Electronic spectra were recorded using a Cary 100 Spectrophotometer (*Agilent Technologies*) in the range 200–800 nm (230-800 for aqueous samples containing DMSO), at a scan rate of 300 nm min^{-1} and a resolution of 2 nm. Sample temperature was kept constant at 37°C through a Varian Dual Cell Peltier device. Data processing was performed with Cary WINUV version 4.2 (*Varian Inc.*).

Circular Dichroism

CD measurements were registered at 25°C with a Jasco J-715 spectropolarimeter (scan rate: 50 nm min^{-1}) using Hellman quartz cells of 0.01 and 0.1 cm path length, respectively in the range 193–260 and 240–350 nm. Spectra (each being the average of eight subsequent accumulations) were recorded at standard sensitivity (100 mdeg) with a data-pitch of 1 nm in the continuous mode and a resolution of 2 nm. Data processing was carried out using SPECTRA MANAGER version 1.52 (*Jasco Inc.*), and values expressed in terms of total molar ellipticity [θ] (deg·cm^{2}·dmol^{-1}).

Fluorescence Spectroscopy

Emission spectra were recorded at room temperature on a Perkin Elmer LS50B Luminescence Spectrometer in 1 cm quartz cuvettes. The emission of BSA was measured in the range Δ_{em}=300-400 nm with an excitation wavelength of 288 nm. The excitation and emission slits were fixed at 5 nm, scanning speed 40 nm/min (10 accumulations).

Chapter 1

Design, synthesis and characterization of gold(III) peptidomimetics

The enhancement of the therapeutical effectiveness of drugs can be achieved by increasing their bioavailabilty and cellular uptake, which is usually limited by their capacity to pass the plasma membrane. In order to overcome this issue, carrier-mediated strategies were adopted to suitably modify drugs in order to be recognizable by specific transporters, thus enhancing the amount of compound entering the cell without losing their pharmacological activity. Moreover, since cancer cells are known to overexpress specific biomarkers and receptors needed for carcinogenesis and tumor growth, targeted chemotherapies aim at blocking cancer cells proliferation by exploiting such specific upregulated biomolecules. This led to the development of efficient and innovative delivery systems in which conjugated drugs incorporating a tumor targeting group can selectively reach the tissue of interest and deliver the cytotoxic agent directly into the tumor cells.

Starting from promising *in vitro* and *in vivo* antiproliferative activities of some gold(III)-dithiocarbamato complexes designed in our reasearch group, we carried out further functionalization with specific oligopeptides to exploit their recognition and transport by specific peptide transporters.

In particular, transporters named PEPTs were selected as potential targets for our compounds. They are integral membrane proteins expressed in mammals in two different isoforms, PEPT1 and PEPT2, which are known to promote cellular uptake of all physiologically occurring L-enantiomers of di- and tripeptides, regardeless sequence, size, charge and hydrophobicity. They are present predominantly in epithelial cells of small intestine, bile duct, mammary glands, lung, choroid plexus and kidney, but are also localized in other tissues (e.g. pancreas, liver, gastrointestinal tract) and are interestingly upregulated in different cancer cells[105]. Owing to their specificity in recognition and transport, they represented an excellent target for the delivery of some pharmacologically-active peptidomimetics (*e.g.* β-lactam antibiotics and ACE inhibitors), and might have a central role also in the uptake of our gold(III) peptide derivatives.

Recently we reported about the synthesis, characterization and biological evaluation of new gold(III)-dithiocarbamato complexes functionalized with short oligopeptides, of the type [$Au^{III}X_2$(dct-Sar-AA)] (X = Br, Cl; Sar = sarcosine, N-methylglycine; AA=different aminoacids). These complexes were tested on a large panel of cancer cell lines representatives of different cancer types, recording GI_{50} in the lower micromolar range, with values up to 5-times lower than the reference drug cisplatin. Interestingly they showed no cross-resistance with cisplatin and were proved to inhibit tumor cell

proliferation with a different mechanism of action if compared to clinically-established platinum drugs[100,101,106].

Since PEPTs are known to transport selectively only L-occuring natural aminoacids, the possibiity to enhance the cellular uptake of the complexes by using different chiral aminoacids was also explored.

Experimental

Chemicals and solvents

Acetone-d_6, DMSO-d_6, dichloromethane-d_2, chloroform-d_1, methanol-d_4, 4-dimethylaminopyridine (DMAP), triethylene glycol monomethyl ether (TEG-OH) (*Sigma Aldrich*); 1-hydroxy-1H-benzotriazole (HOBt), phosphoric anhydride P_2O_5, H-D-AlaOH, H-D-ProOH (*Acros-Janssen*); potassium tetrabromoaurate(III) dihydrate (*Alfa Aesar*); potassium hydrogen carbonate $NaHCO_3$, potassium hydrogen sulfate $KHSO_4$, sodium carbonate dodecahydrate, sodium hydroxide, sodium hypochlorite, sodium sulphate anhydrous, triethylamine (TEA, *Carlo Erba*); isobutene (*Siad*); isobutylchloroformiate (*Lancaster*); *N*-methylmorpholine (NMM), palladium (10% on carbon), HSarOH (*Fluka*); 1-ethyl-3-(3-dimethylaminopropyl)-carbodiimide hydrochloride (EDCl), *N*-(benzyloxycarbonyloxy)succinimide (ZOSu, *Iris Biotech*); Z-Aib-OH, Z-L-Ala-OH, Z-L-Pro-OH, Z-Sar-OH (synthesized in Prof. Formaggio laboratory, University of Padua)

All other reagents and solvents were used as purchased without any further purification.

Synthesis. The purity of all the synthesized compounds was ≥95%, as determined by elemental and thermogravimetric analysis (*vide infra*).

General synthetic route for tert-Butyl- or TEG-esterified dipeptide hydrochlorides and related intermediates. ZSarOH, Z-L-ProOH, Z-L-AlaO*t*Bu, Z-L-AibO*t*Bu) were prepared according to literature methods[107,108]. For the synthesis of Z-L-AibOTEG, 1 eq. of ZAibOH (15 mmol) was dissolved in CH_2Cl_2 and cooled to 0°C with ice bath. To the solution were subsequently added: 1.2 eq. of HOBt; 0.3 eq. of DMAP; 1.2 equiv. di EDCl; 2 eq. of TEG-OH, and the mixture was stirred for 48h. The solvent was evaporated at reduced pressure; the product was extracted with ethylacetate and washed with $KHSO_4$ and $NaHCO_3$ aqueous solutions. After removing water traces by treating with Na_2SO_4, the organic portion was dried obtaining a yellow oil which was purified by flash chromatography (eluent: petroleum ether/ethyl acetate 3:2 and subsequently 4.5:0.5, on silica).

Yellow oil; yield: 92%; R_{f1}: 0.94; R_{f2}: 0.74; R_{f3}: 0.43.

^{1}H NMR (300.13 MHz, DMSO-d_6, 298 K, TMS): 1.55 (s, 6H, ß-CH_3 Aib); 3.68 (s, 3H, O-CH_3 TEG); 3.50-3.55, 3.60-3.68, 4.25-4.29 (m, 12H, -CH_2 TEG); 5.08 (s , 2H, -CH_2 Z); 5.44 (s, 1H, N-H Aib); 7.27-7.36 (m, 5H, CH Z).

FT-IR (KBr): $\bar{\nu}$=3341 (ν, N-H); 2984/2929/2877 (ν, C-H); 1739 (ν, C=O ester); 1721 (ν, amide I); 1523 (ν, amide II); 1157 (ν, (TEG)-O).

For the aminoacids coupling reaction, generally, a THF solution (15–20 mL) of Z-Sar-OH (or Z-L/D-ProOH) was treated with NMM (22 mmol), cooled to −15 °C and then treated with isobutyl chloroformiate (22 mmol) under continuous stirring[109]. After 10 min, a cold $CHCl_3$ (10–35 mL) suspension of H-L/D-Ala-O*t*Bu (or H-Aib-O*t*Bu), H-Aib-OTEG; 22 mmol[110] was added, adjusting the pH to ca. 8 by adding NMM.

After stirring overnight at room temperature, the reaction mixture was concentrated under reduced pressure and the residue was dissolved with AcOEt, washed subsequently with 10% $KHSO_4$, H_2O, 5% $NaHCO_3$, H_2O, and dried over Na_2SO_4. The organic layer was then concentrated to dryness and purified by flash chromatography using AcOEt/petroleum ether 1:1 as eluent, in order to obtain the corresponding Z-protected dipeptides esters (yield = 70–90%).

Each Z-AA_1-AA_2-OR (AA_1= Pro, Sar; AA_2= Aib, Ala; R= *t*Bu, TEG) intermediate was then Z-deprotected by catalytic hydrogenation over Pd/C (20% w/w) in MeOH. The H-AA_1-AA_2-OR compound was dissolved in dry diethylether and dropwise treated with 1 equivalent of a dilute ether solution of HCl (0.2 mM) under vigorous stirring, leading to the formation of a white precipitate corresponding to the hydrochloride form of the dipeptide, HCl·H-AA_1-AA_2-OR (AA_1= Pro, Sar; AA_2= Aib, Ala; R= *t*-Bu, TEG).

HCl·H-Sar-D-Ala-O*t*Bu (P1)

White powder; yield: 65%. R_{f1}: 0.13; R_{f2}: 0.23; R_{f3}: 0.04; m.p.: 148-150°C; $[\alpha]^{20}_D$= 38.67° (c=0.5, MeOH); ^{1}H NMR (300.13 MHz, DMSO-d_6, 298 K, TMS): δ=9.00 [br, s, 2H, NH_2^+ Sar]. 8.88 [d, 1H, N*H* Ala], 4.17 [m, 1H, α-C*H* Ala], 3.70 [s, 2H, N-CH_2 Sar], 2.53 [s, 3H, N-CH_3 Sar], 1.40 [s, 9H, CH_3 *t*-Bu], 1.28 ppm [d, 3H, β-CH_3 Ala]; ^{13}C{^{1}H} NMR (75.48 MHz, DMSO-d_6, 298 K, TMS): δ= 171.22 (***C***=O Ala), 164.87 (***C***=O Sar), 80.55 (-***C***$(CH_3)_3$ *t*-Bu), 48.52 (N-***C***H_2 Sar), 48.29 (α-***C*** Ala), 32.41 (N-***C***H_3 Sar), 27.28 (***C***H_3 *t*-Bu), 16.76 ppm (β-***C***H_3 Ala); FT-IR (KBr): $\bar{\nu}$=3332 (ν, N-H); 2978/2960/2936 (ν, C-H); 2763 (ν_a, NH_2^+);2701 (ν_s, NH_2^+), 1735 (ν, C=O ester); 1669 (ν, amide I); 1564 (ν, amide II); 1266 (ν, amide III); 1221 (ν, C-O(*t*-Bu)); 1165 cm^{-1} (ν, *t*-Bu-O).

HCl·H-Sar-L-Ala-*O*tBu (P2)

White powder; yield: 82%; R_{f1}: 0.13; R_{f2}: 0.23; R_{f3}: 0.04; m.p.: 147-150°C; $[\alpha]^{20}_D$ = -39.1° (c = 0.5, MeOH)

^{1}H NMR (300.13 MHz, DMSO-d_6, 298 K, TMS): δ = 9.12 [br, s, 2H, N***H*** Sar], 8.96 [d, 1H, N***H*** Ala], 4.16 [m, 1H, α-C***H*** Sar], 3.69 [s, 2H, N-C$\boldsymbol{H}_2$ Sar], 2.52 [s, 3H, N-C$\boldsymbol{H}_3$ Sar], 1.40 [s, 9H, C$\boldsymbol{H}_3$ *t*-Bu], 1.27 ppm [d, 3H, β-C$\boldsymbol{H}_3$ Ala]; ^{13}C{^{1}H} NMR (75.48 MHz, DMSO-d_6, 298 K, TMS): δ =171.27 (***C***=O Ala), 164.86 (***C***=O Sar), 80.58 (-***C***$(CH_3)_3$ *t*-Bu), 48.53 (N-***C***H_2 Sar), 48.29 (α-***C*** Ala), 32.40 (N-***C***H_3 Sar), 16.75 (β-***C***H_3 Ala); 27.36 ppm (***C***H_3 *t*-Bu); FT-IR (KBr): $\bar{\nu}$=3332 (ν, N-H); 2978/2963/2939 (ν, C-H); 2766 (ν_a, NH_2^+); 2699 (ν_s, NH_2^+); 1735 (ν, C=O ester); 1669 (ν, amide I); 1564 (ν, amide II); 1266 (ν, amide III); 1220 (ν, C-O(*t*-Bu)); 1166 cm^{-1} (ν, *t*-Bu-O).

HCl·H-D-Pro-Aib-OtBu (P3)

White powder; yield: 49%; R_{f1}: 0.15; R_{f2}: 0.30; R_{f3}: 0.06; m.p.: 104-108°C; $[\alpha]^{20}_D$ = -32.8° (c = 0.6, MeOH);

^{1}H NMR (300.13 MHz, DMSO-d_6, 298 K, TMS): δ=9.34 [s, br, 2H, N$\boldsymbol{H_2}^+$ Pro]; 8.94 [s, 1H, N***H*** Aib], 4.14 [m, 1H, C$\boldsymbol{H}_2$ Pro], 3.16 [m, 2H, C$\boldsymbol{H}_2^5$ Pro], 2.29 [m, 1H, C$\boldsymbol{H}_3$' Pro], 1.83 [m, 3H, C$\boldsymbol{H}_3$'' Pro e C$\boldsymbol{H}_2^4$ Pro], 1.36 [s, 9H, C$\boldsymbol{H}_3$ *t*-Bu], 1.33, 1.37 ppm [2 s, 6H, β-C$\boldsymbol{H}_3$ Aib]; ^{13}C{^{1}H} NMR (75.48 MHz, DMSO-d_6, 298 K, TMS): δ = 172.06 (***C***=O Aib), 167.15 (***C***=O Pro), 79.65 (-***C***$(CH_3)_3$ *t*-Bu), 58.07 (***C***H_2 Pro), 55.69 (C(***C***$H_3)_2$ Aib), 45.32 (***C***H_2^5 Pro), 29.59 (***C***H_2^3 Pro), 27.13 (***C***H_3 *t*-Bu), 24.00, 24.77 (***C***H_3 Aib), 23.28 ppm (***C***H_2^4 Pro); FT-IR (KBr): $\bar{\nu}$=3437 (ν, N-H); 2979/2935 (ν, C-H); 2743 ($\nu_{a,s}$, NH_2^+); 1733 (ν, C=O ester); 1678 (ν, amide I); 1551 (ν, amide II); 1256 (ν, amide III); 1219 (ν, C-O(*t*-Bu)); 1146 cm^{-1} (ν, *t*-Bu-O).

HCl·H-L-Pro-Aib-OtBu (P4)

White powder; yield: 49%; R_{f1}: 0.15; R_{f2}: 0.30; R_{f3}: 0.06; m.p.: 104-108°C. $[\alpha]^{20}_D$ = -31.2° (c = 0.7, MeOH)

^{1}H NMR (300.13 MHz, DMSO-d_6, 298 K, TMS): δ= 9.80 [s, br, 2H, N$\boldsymbol{H}_2^+$ Pro], 8.92 [s, 1H, N***H*** Aib], 4.11 [m, 1H, C$\boldsymbol{H}^2$ Pro], 3.15 [m, 2H, C$\boldsymbol{H}_2^5$ Pro], 2.27 [m, 1H, C$\boldsymbol{H}_3$' Pro], 1.83 [m, 3H, C$\boldsymbol{H}_3$" and C$\boldsymbol{H}_2^4$ Pro], 1.32, 1.36 ppm [2 s, 15H, β-C$\boldsymbol{H}_3$ Aib and C$\boldsymbol{H}_3$ *t*-Bu]; ^{13}C{^{1}H} NMR (75.48 MHz, DMSO-d_6, 298 K, TMS): δ = 172.15 (***C***=O Aib), 167.75 (***C***=O Pro), 79.71 (***C***$(CH_3)_3$ *t*-Bu), 58.26 (**C**H_2 Pro), 55.70 (**C**$(CH_3)_2$ Aib), 45.55 (***C***H_2^5 Pro), 29.67 (***C***H_2^3 Pro), 27.19 (***C***H_3 *t*-Bu), 24.08, 24.78 (***C***H_3 Aib), 23.56 ppm (***C***H_2^4 Pro); FT-IR (KBr): $\bar{\nu}$= 3430 (ν, N-H); 2980/2936 (ν, C-H); 2744 ($\nu_{a,s}$, NH_2^+); 1733 (ν, C=O ester); 1678 (ν, amide I); 1551 (ν, amide II); 1256 (ν, amide III); 1219 (ν, C-O(*t*-Bu)); 1146 cm^{-1} (ν, (*t*-Bu)-O).

HCl·H-Sar-Aib-OTEG (P5)

Pale-yellow oil; yield: 97%; R_{f1}: 0.92; R_{f2}: 0.69; R_{f3}: 0.33;

^{1}H NMR (300.13 MHz, DMSO-d_6, 298 K, TMS): δ = 9.04 [s, 3H, N***H*** Aib e N$\boldsymbol{H_2}^+$ Sar], 4.10-4.13 [m, 2H, C$\boldsymbol{H_2}^1$ TEG], 3.66 [s, 2H, N-C$\boldsymbol{H}_2$ Sar], 3.57-3.60 [m, 2H, C$\boldsymbol{H}_2{}^2$ TEG], 3.41-3.54 [m, 8H, C$\boldsymbol{H}_2{}^{3,4,5,6}$ TEG], 3.24 [s, 3H, O-C$\boldsymbol{H}_3$ TEG], 2.51 [s, 3H, N-C$\boldsymbol{H}_3$ Sar], 1.39 ppm [s, 6H, β-C$\boldsymbol{H}_3$ Aib]; ^{13}C{^{1}H} NMR (75.48 MHz, DMSO-d_6, 298 K, TMS): δ =172.52 (***C***=O Aib), 163.80 (***C***=O Sar), 68.8-70.7 (***C***$H_2{}^{3,4,5,6}$ TEG), 67.44 (***C***$H_2{}^2$ TEG), 63.19 (***C***$H_2{}^1$ TEG), 57.26 (O-***C***H_3 TEG), 54.77 (**C**$(CH_3)_2$ Aib), 47.94 (N-***C***H_2 Sar), 31.84 (N-***C***H_3 Sar), 23.39 (β-***C***H_3 Aib); FT-IR (KBr): $\bar{\nu}$=3193 (ν, N-H); 2985/2937/2872 (ν, C-H); 2762 (**(**$\nu_{a,s}$, NH_2^+); 1739 (ν, C=O ester); 1684 (ν, amide I); 1554 (ν, amide II); 1256 (ν, amide III); 1217 (ν, C-OTEG); 1159 (ν, (TEG)-O).

General route for the synthesis of the complexes. The compound HCl·H-AA_1-AA_2-OR (AA_1= Sar, L/D-Pro; AA_2= L/D-Ala, Aib; 0.7 mmol) was dissolved in water and the solution was kept at 0°C with a water/ice bath. Under continuous stirring, cold CS_2 (1.4 mmol) and sodium hydroxide (0.7 mmol) were added to the solution. The variation of pH from 9 to 6 confirms the reaction of the dipeptide with CS_2 and the consequent formation of the dithiocarbamato derivative. The ligand solution was then added, under vigorous stirring, to an ice-cold water solution of K[$Au^{III}Br_4$] (0.35 mmol), leading to the formation of a ocher-brown precipitate. The solid was separated from the mother liquor and washed several times with ice-cold water before drying under reduced pressure with P_2O_5.

[$Au^{III}Br_2$(SSC-Sar-L-Ala-O*t*Bu)] (ITØ1)

Ocher powder; yield: 86%; ^{1}H NMR (300.13 MHz, acetone-d_6, 298 K, TMS): δ=7.93 (d, 1H, N***H*** Ala), 4.69,4.72 (s, 2H, NC$\boldsymbol{H_2}$ Sar), 4.37 (m, 1H, C***H*** Ala), 3.52, 3.55 (s, 3H, NC$\boldsymbol{H_3}$ Sar), 1.45 (s, 9H, C$\boldsymbol{H_3}$ *t*Bu), 1.36 ppm (d, 3H, C$\boldsymbol{H_3}$ Ala); ^{1}H NMR (300.13 MHz, DMSO-d_6, 298 K, δ/ppm, TMS): 8.79 (m, 1H, N***H*** Ala), 4.53 (m, 2H, NC$\boldsymbol{H_2}$ Sar), 4.18 (m, 1H, C***H*** Ala), 3.36, 3.38 (s, 3H, NC**H**$_3$ Sar), 1.40 (s, 9H, C$\boldsymbol{H_3}$ *t*Bu), 1.23 ppm (d, 3H, C$\boldsymbol{H_3}$ Ala); ^{13}C{^{1}H} NMR (75.48 MHz, acetone-d_6, 298 K, TMS): δ =196.49, 200.40 (***C***SS), 172.54 (***C***=O Ala), 164.48, 164.72 (*C*=O Sar), 82.36 (***C***$(CH_3)3$ *t*Bu), 54.99, 55.97 (N***C***H_2 Sar), 50.35 (***C***H Ala), 40.08, 41.06 (N***C***H_3 Sar), 28.35 (***C***H_3 *t*Bu), 18.34 (***C***H_3 Ala); IR (KBr): $\bar{\nu}$=3317 (ν, N-H); 2979/2932 (ν, C-H); 1733 (ν, C=O ester); 1668 (ν, amide I); 1564 (n, N-CSS+amide II); 1219 (ν, C-O(*t*Bu)+amide III); 1149 (ν, (*t*Bu)-O); 1003 cm^{-1} (ν_a, S-C-S). FT-IR (nujol): $\bar{\nu}$=567 (ν_s, S–C–S); 419 (ν_a, S–Au–S); 380 (ν_s, S–Au–S); 251 (ν_a, Br–Au–Br); 229 cm^{-1} (ν_s, Br–Au–Br). Elemental analysis: calcd (%) for $C_{11}H_{19}AuBr_2N_2O_3S_2$ (648.19 g mol^{-1}): C, 20.38; H, 2.95; N, 4.32; S, 9.89%; found: C, 20.52; H, 2.93; N, 4.41; S, 9.90%.

[$Au^{III}Br_2$(SSC-Sar-D-Ala-O*t*Bu)] (ITØ2)

Ocher powder; yield: 86%; ^{1}H NMR (300.13 MHz, acetone-d_6, 298 K, TMS): δ=7.94 (d, 1H, N***H*** Ala), 4.68, 4.72 (s, 2H, NC***H***$_2$ Sar), 4.37 (m, 1H, C***H*** Ala), 3.52, 3.55 (s, 3H, NC***H***$_3$ Sar), 1.45 (s, 9H, C***H***$_3$ *t*Bu), 1.36 (d, 3H, C***H***$_3$ Ala); ^{1}H NMR (300.13 MHz, DMSO-d_6, 298 K, TMS): δ =8,79 (m, 1H, N***H*** Ala), 4.53 (m, 2H, NC***H***$_2$ Sar), 4.17 (m, 1H, C***H*** Ala), 3.36 (s, 3H, NCH_3 Sar), 1.41 (s, 9H, C***H***$_3$ *t*Bu), 1.28 (d, 3H, C***H***$_3$ Ala); $^{13}C\{^1H\}$ NMR (75.48 MHz, acetone-d_6, 298 K, TMS): δ=195.83, 199.74 (***C***SS), 171.88 (***C***=O Ala), 163.57, 163.81 (***C***=O Sar), 81.70 (***C***$(CH_3)_3$ *t*Bu), 54.33, 55.30 (N***C***H_2 Sar), 49.68 (***C***H Ala), 39.42, 40.40 (N***C***H_3 Sar), 27.69 (***C***H_3 *t*Bu), 17.67 (***C***H3 Ala); FT-IR (KBr): $\bar{\nu}$=3311 (ν, N-H); 2979/2933 (ν, C-H); 1732 (ν, C=O ester); 1668 (ν, amide I); 1563 (ν, N-CSS+amide II); 1218 (ν, C–O(*t*Bu)+amide III); 1149 (ν, (*t*Bu)-O); 1003 (ν_a, S-C-S). IR (nujol): $\bar{\nu}$ =566 (ν_s, S–C–S); 419 (ν_a, S–Au–S); 380 (ν_s, S–Au–S); 251 (ν_a, Br–Au–Br); 228 cm^{-1} (ν_s, Br–Au–Br). Elemental Analysis calcd (%) for $C_{11}H_{19}AuBr_2N_2O_3S_2$ (648.19 g mol^{-1}): C, 20.38; H, 2.95; N, 4.32; S, 9.89%; found: C, 19.96; H, 2.86; N, 4.55; S, 9.89%.

[$Au^{III}Br_2$(SSC-L-Pro-Aib-O*t*Bu)] (ITØ3)

After the synthetic procedure described above, the complex was further purified by re-precipitation in water from a concentrated acetone solution, obtaining the compound as a dark-orange powder. Yield: 76%.; ^{1}H NMR (300.13 MHz, acetone-d_6, 298 K, TMS): δ=8.01 (s, br, 1H, N***H*** Aib), 4.91-4.95 (m, 1H, C***H***^{2} Pro), 3.97-4.02 (m, 2H, C***H***$_2^5$ Pro), 2.57-2.64 (m, 1H, C***H***$_3$' Pro), 2.25-2.39 (m, 3H, C***H***$_2^4$ + C***H***$_3$ Pro), 1.44 (s, 9H, C***H***$_3$' *t*Bu), 1.43, 1.47 ppm (s, 6H, C***H***$_3$ Aib); ^{1}H NMR (300.13 MHz, DMSO-d_6, 298 K, TMS): δ=8.71-8.78 (m, 1H, N***H*** Aib), 4.75-4.78 (m, 1H, C***H***^{2} Pro), 3.85-3.89 (m, 2H, C***H***$_2^5$ Pro), 2.41 (m, 1H, C***H***$_3$' Pro), 2.08 (m, 3H, C***H***$_2^4$ + C***H***$_3$ Pro), 1.38 (s, 9H, C***H***$_3$' *t*-Bu), 1.31, 1.34 ppm (s, 6H, C***H***$_3$ Aib); $^{13}C\{^1H\}$ NMR (75.48 MHz, acetone-d_6, 298 K, TMS): δ=190.22 (-***C***SS), 172.84 (***C***=O Aib), 166.69 (***C***=O Pro), 80.98 (***C***$(CH_3)_3$ *t*Bu), 64.87 (***C***H_2 Pro), 57.28 (C(***C***$H_3)_2$ Aib), 52.10 (***C***H_2^5 Pro), 30.84 (***C***H_2^3 Pro), 28.00 (***C***H_3 *t*-Bu), 24.56, 25.51 (***C***H_3 Aib), 23.09 (***C***H_2^4 Pro); IR (KBr): $\bar{\nu}$=3341 (ν, N-H); 2979/2931 (ν, C-H); 1730 (ν, C=O ester); 1680 (ν, amide I); 1553 (ν, N-CSS amide II); 1247 (ν, C-O(*t*Bu)+amide III); 1147 (ν, (*t*Bu)-O); 1000 cm^{-1} (ν_a, S-C-S). FT-IR (nujol): $\bar{\nu}$=535 (ν_s, S–C–S); 410 (ν_a, S–Au–S); 376 ($_{vs}$, S–Au–S); 252 (ν_a, Br–Au–Br); 222 cm^{-1} (ν_s, Br–Au–Br). Elemental Analysis calcd (%) for $C_{14}H_{23}AuBr_2N_2O_3S_2$ (688.26 g mol^{-1}): C, 24.43; H, 3.37; N, 4.07; S, 9.32%; found: C, 24.59; H, 3.47; N, 4.14; S, 8.98%.

[$Au^{III}Br_2$(SSC-D-Pro-Aib-O*t*Bu)] (ITØ4)

Dark-orange powder; obtained as described for the synthesis of IT03. Yield: 25%; ^{1}H NMR (300.13 MHz, acetone-d_6, 298 K, TMS): δ=8.00 (s, br, 1H, N***H*** Aib), 4.91-4.94 (m, 1H, C***H***$_2$ Pro), 3.97-4.02

(m, 2H, C$\boldsymbol{H_2^5}$ Pro), 2.54-2.64 (m, 1H, C$\boldsymbol{H_3}$' Pro), 2.28-2.38 (m, 3H, C$\boldsymbol{H_2^4}$ + C$\boldsymbol{H_3}$'' Pro), 1.44 (s, 9H, C$\boldsymbol{H_3}$ *t*Bu), 1.43, 1.47 (s, 6H, C$\boldsymbol{H_3}$ Aib); ^{1}H NMR (300.13 MHz, DMSO-d_6, 298 K, TMS): δ=8.78 (s, br, 1H, N$\boldsymbol{H}$ Aib), 4.75-4.78 (m, 1H, C$\boldsymbol{H^2}$ Pro), 3.83-3.91 (m, 2H, C$\boldsymbol{H_2^5}$ Pro) 3.83-3.91 (m, 2H, C$\boldsymbol{H_2^5}$ Pro), 2.41 (m, 1H, C$\boldsymbol{H_3}$' Pro), 2.07-2.12 (m, 3H, C$\boldsymbol{H_2^4}$ + C$\boldsymbol{H_3}$'' Pro), 1.34 (s, 9H, C$\boldsymbol{H_3}$ *t*-Bu), 1.24, 1.31 (s, 6H, C$\boldsymbol{H_3}$ Aib). ^{13}C{^{1}H} NMR (75.48 MHz, acetone-d_6, 298 K, TMS): δ=190.21 (-$\boldsymbol{C}$SS), 23.16 ($\boldsymbol{C}$H$_2^4$ Pro); 172.96 ($\boldsymbol{C}$=O Aib), 166.94 ($\boldsymbol{C}$=O Pro), 81.10 ($\boldsymbol{C}$(CH$_3$)$_3$ *t*Bu), 64.92 ($\boldsymbol{C}$H$_2$ Pro), 57.44 (C($\boldsymbol{C}$H$_3$)$_2$ Aib), 52.08 ($\boldsymbol{C}$H$_2^5$ Pro), 30.80 ($\boldsymbol{C}$H$_2^3$ Pro), 27.97 ($\boldsymbol{C}$H$_3$ *t*Bu), 24.67, 25.21 ppm ($\boldsymbol{C}$H$_3$ Aib); IR (KBr): $\bar{\nu}$=3363 (ν, N-H); 2982/2927 (ν, C-H); 1732 (ν, C=O ester); 1680 (ν, amide I); 1549 (ν, N-CSS+amide II); 1241 (ν, C-O(*t*Bu)+amide III); 1147 (ν, (*t*Bu)-O); 991 cm^{-1} (ν_a, S-C-S). FT-IR (nujol): $\bar{\nu}$=533 (ν_s, S–C–S); 410 (ν_a, S–Au–S); 376 (ν_s, S–Au–S); 251 (ν_a, Br–Au–Br); 222 cm^{-1} (ν_s, Br–Au–Br). Elemental analysis calcd (%) for $C_{14}H_{23}AuBr_2N_2O_3S_2$ (688.26 g mol^{-1}): C, 24.43; H, 3.37; N, 4.07; S, 9.32%; found: C, 24.30; H, 3.64; N, 4.06; S, 9.02%.

[Au^{III}Br$_2$(SSC-Sar-Aib-OTEG)] (ITØ5)

After the general synthetic procedure previously described, the compound was further purified to eliminate the presence of hydrolyzed compound at the ester function, by dissolving the product in dichloromethane and washing it with a water solution of $KHCO_3$ 5%.

Dark-brown powder, Yield: 56%. ^{1}H NMR (300.13 MHz, acetone-d_6, 298 K, TMS): δ=8.05 (s, br, 1H, N$\boldsymbol{H}$ Aib), 4.62, 4.65 (s, 2H, NC$\boldsymbol{H}_2$ Sar), 4.19-4.22 (m, 2H, C$\boldsymbol{H}_2^1$ TEG), 3.65-3.68 (m, 2H, -C$\boldsymbol{H}_2^2$ TEG), 3.50,3.53 (s, 3H, NC$\boldsymbol{H}_3$ Sar), 3.47-3.62 (m, 8H, C$\boldsymbol{H}_2^{3,4,5,6}$ TEG), 3.29 (s, 3H, OC$\boldsymbol{H}_3$ TEG), 1.50 ppm (s, 6H, C$\boldsymbol{H}_3$ Aib);^{1}H NMR (300.13 MHz, DMSO-d_6, 298 K, TMS): δ=8.83 (s, br, 1H, N$\boldsymbol{H}$ Aib), 4.47 (s, 2H, NC$\boldsymbol{H}_2$ Sar), 4.10-4.11 (s, br, 2H, -C$\boldsymbol{H}_2^2$ TEG), 3.36-3.58 (m, 13H, C$\boldsymbol{H}_2^{1,3,4,5,6}$ TEG, NC$\boldsymbol{H}_3$ Sar), 3.24 (s, 3H, OC$\boldsymbol{H}_3$ TEG), 1.39 (s, 6H, C$\boldsymbol{H}_3$ Aib); ^{13}C{^{1}H} NMR (75.48 MHz, acetone-d_6, 298 K, TMS): δ=195.38, 199.21 ($\boldsymbol{C}$SS), 173.63 ($\boldsymbol{C}$=O Aib), 163.54 ($\boldsymbol{C}$=O Sar), 72.35 (C$\boldsymbol{H}_2$ TEG), 70.8-71.2 ($\boldsymbol{C}$H$_2^{3,4,5}$ TEG), 69.25 (C$\boldsymbol{H}_2^2$ TEG), 64.52 (C$\boldsymbol{H}_2^1$ TEG), 58.52 (O$\boldsymbol{C}$H$_3$ TEG), 57.00 (C($\boldsymbol{C}$H$_3$)$_2$ Aib), 54.34, 55.17 (N$\boldsymbol{C}$H$_2$ Sar), 39.36, 40.38 (N$\boldsymbol{C}$H$_3$ Sar), 24.86 ($\boldsymbol{C}$H$_3$ Aib); FT-IR (KBr): $\bar{\nu}$ =3290 (ν, N-H); 2909/2872 (ν, C-H); 1735 (ν, C=O ester); 1683 (ν, amide I); 1576 (ν, N-CSS); 1549 (ν, amide II); 1253 (ν, amide III); 1210 (ν, C–OTEG); 1159 cm^{-1} (ν, TEG-O). IR (nujol): $\bar{\nu}$=569 (ν_s, S-C-S); 412 (ν_a, S-Au-S); 390 (ν_s, S-Au-S); 250 (ν_a, Br-Au-Br); 226 cm^{-1} (ν_s, Br-Au-Br). Elemental analysis calcd (%) for $C_{15}H_{27}AuBr_2N_2O_6S_2$ (752.30 g mol^{-1}): C, 23.95; H, 3.62; N, 3.72; S, 8.52%; found: C, 24.40; H, 3.55; N, 3.70; S, 8.57%.

X-ray Crystallography

Single crystal data were collected with a *Bruker Smart Breeze* area detector diffractometer, Mo Kα: λ = 0.71073 Å. The unit cell parameters were obtained using 60 ω-frames of 0.5° width and scanned from three different zone of reciprocal lattice. The intensity data were integrated from several series of exposures frames (0.3° width) covering the sphere of reciprocal space[111]. An absorption correction was applied using the program SADABS[111] with min. and max. trasmission factors of: 0.676-1.000. The structures were solved by direct methods (SIR2004[111]) and refined on F^2 with full-matrix least squares (SHELXL-97[112]), using the WinGX software package[113].

For IT05, the crystals were of poor quality and of small size, and this affected the overall quality of the data. For this reason, only the atoms comprising the coordination sphere were refined anisotropically, whereas the remaining atoms were refined isotropically. The hydrogen atoms were placed at their calculated positions. In the lattice, solvent molecules of crystallization (pentane) were found but could not be properly modelled during the refinement, and they were treated with the SQUEEZE program[114]. According to the residual electron density, the crystal lattice contained approximately one molecule of pentane per complex molecule. Graphical material was prepared with the ORTEP3 for Windows[115] and Mercury CSD 3.1[116].

Chromatography

Separation of the two forms of complex AuL23 was accomplished by preparative layer chromatography on silica gel Merck Kieselgel $60F_{254}$ precoated glass plates (2 mm thick) in dichloromethane/ethanol 97:3. Retention factors (R_f) of 0.9 and 0.3 were measured for the major and the minor species, respectively. Once detached from the plate, each fraction was washed with fresh dichloromethane, filtered and evaporated to dryness under reduced pressure.

Results and discussion

The synthesis of the esterified dipeptides HCl·Sar-L/D-AlaO*t*Bu (respectively **P1**, **P2**), HCl·L/D-ProAibO*t*Bu (respectively **P3**, **P4**), HCl·SarAibOTEG (**P5**) was performed in solution starting from the single protected amino acids, by using proper coupling agents. The synthesis in solution was preferred over the solid phase route since the preparation of the oligopeptides require a reasonable number of synthetic steps, moreover allowing the obtainment of higher amounts of products. The general procedure followed is described in **Scheme 1.1**.

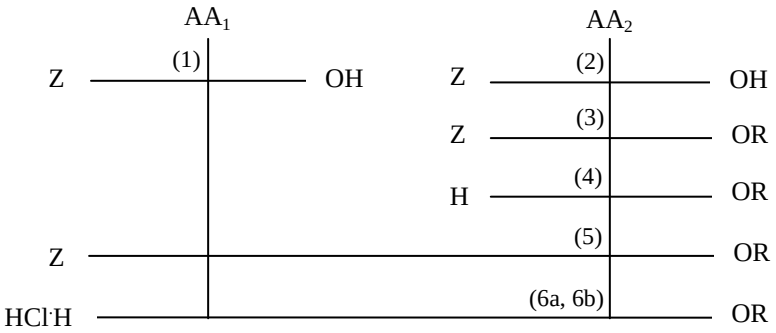

Scheme 1.1: schematic general synthetic route for the synthesis of hyrochloride dipeptides esters **P1-P5** (R= O*t*Bu, OTEG; AA_1= Sar, L/D-Pro; AA_2=L/D-Ala, Aib).

Briefly, the C-terminal aminoacid was first esterified to protect the carboxylate function. The *tert*-butyl function was introduced by reacting under pressure the Z-protected amino acid with isobutane for 1 week, while the TEG fraction was coupled to the Z-protected amino acid using as coupling agents EDCI/HOBt.

The esterified amino acid was then deprotected at the N-terminus through catalytic hydrogenation over Pd/C (10%) in organic solution, and then coupled to the Z-protected C-ter amino acid. Particular attention was paid in the choice of the coupling reagents in this step, since the use of isobutylchloroformiate usually causes racemization at the C-ter amino acid as a consequence of a mixed anhydride formation (**Figure 1.1**). This is not relevant when Sar is used as first amino acid in the oligopeptide sequence, but must be taken into account when chiral L/D-Pro are either used (*e.g.*, for the synthesis of **P2** and **P3)** as the optical purity of the amino acid must be conserved. For this reason, in such case a different method is adopted and EDCI/HOBt is rather used (**Figure 1.2**). In this way the racemization of the aminoacid is prevented due to the formation of an ester between L/D-Pro and HOBt, which results less reactive than the mixed anhydride and do not allow racemization.

After removing the *N*-ter Z-protecting group by hydrogenation all the dipeptides were transformed in their hydrochloride form by reacting the esterified dipeptide with HCl in ether solution.

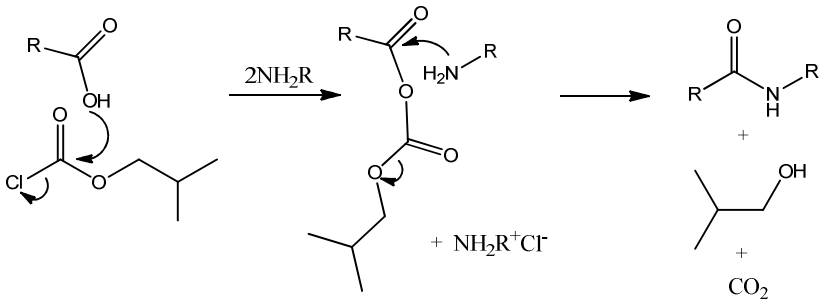

Figure 1.1: schematic representation of peptide bond formation using isobutylchloroformiate as coupling reagent.

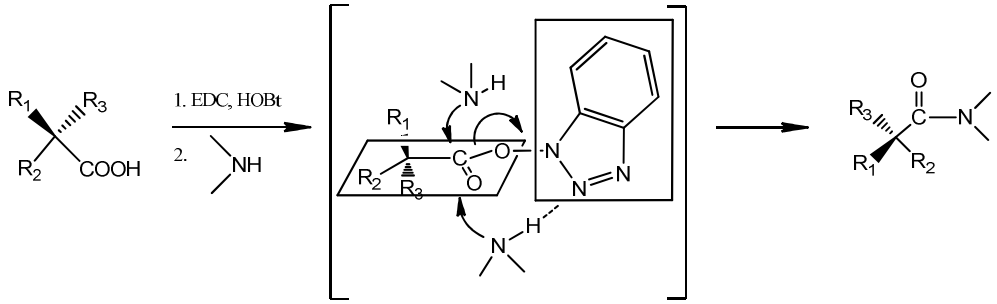

Figure 1.2: schematic representation of peptide bond formation using HOBt/EDC approach.

The *tert*-butyl ester was used as C-protecting group (*i.e.* COOR) since it has been previously shown that the COOH-containing derivatives are not active. Screening between -OMe, -OEt and -O*t*Bu esters as protecting groups, demonstrated that hydrophobic and sterically hindered ligand would be beneficial to the biological activity of the Au(III) complexes, and -O*t*Bu protected complexes are much better than the –OMe ester protected counterparts in terms of antitumor activity.

On the other hand, the more hydrophobic the complexes the less soluble in aqueous medium. This is an important issue to take into account when considering the biological application of the synthesized compounds. For this reason a complex with TEG-ester functionalization was prepared, enhancing water solubility through the presence of ethyloxy-groups, but keeping the hinderance to the C-terminus of the complex. The properties of the compound IT05 thus prepared was compared to the previously prepared -O*t*Bu esterified counterpart AuD8 [$Au^{III}Br_2$(dtc-Sar-Aib-O*t*Bu)][101].

The choice of Sar in **P1/P2** was suggested by the stability and the antiproliferative activity of previously synthesized compounds, as for example [$Au^{III}Br_2$(ESDT)] (AuL12) described in the *Introduction*. Conversely, in **P3** and **P4** sarcosine was substituted by Pro because it is a chiral *N,N*-substituted aminoacid and has also the advantage to be, almost in principle, more easily recognized by PEPT transporters, thus possibly enhancing the cellular uptake of the complexes.

The hydrochloride dipeptides were then used for the synthesis of the corresponding gold(III) dithiocarbamato complexes [$Au^{III}Br_2$(dtc-Sar-L/D-AlaO*t*Bu)] (**IT01** and **IT02,** respectively), [$Au^{III}Br_2$(dtc-L/D-Pro-AibO*t*Bu)] (**IT03** and **IT04,** respectively), [$Au^{III}Br_2$(dtc-SarAibOTEG)] (**IT05**) (**Scheme 1.2, Figure 1.3**). In particular, the dithiocarbamato functionalized oligopeptide was

prepared *in situ*, treating the water solution of the hydrocloride dipeptide with NaOH and CS_2. When the pH of the solution drops from 9 to 6, the reaction proceeds leading to the formation of the ligand, which is not sufficiently stable in this conditions and cannot be isolated. Therefore, it is added directly to a water solution containing 0.5 eq of $KAuBr_4$, leading to the precipitation of ocher-brown powdery solids. In some cases, further purification through flash chromatography was necessary to eliminate undesired side-products.

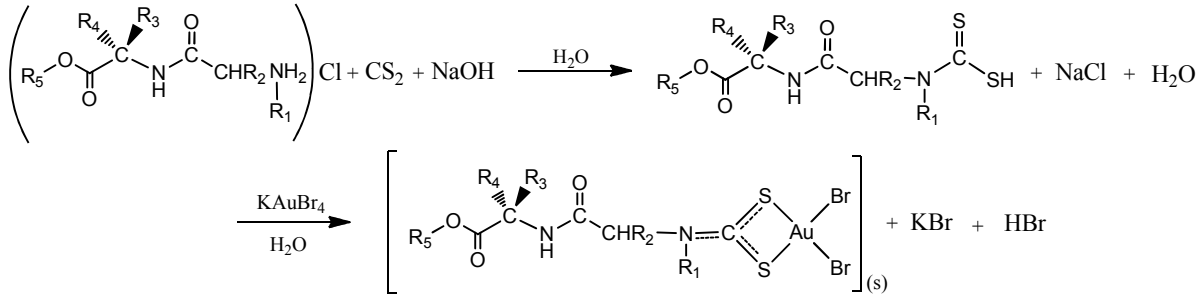

Scheme 1.2: schematic general synthetic route for the synthesis of gold(III) dithiocarbamato complexes (IT01/02 R_1= CH_3; R_2=H; R_3=CH_3; R_4=H; R_5= -*t*Bu. IT03/04 R_1+R_2= -(CH)$(CH_2)_3$-; R_3= R_4=CH_3; R_5= -*t*Bu. IT05: R_1= CH_3; R_2=H; R_3= R_4=CH_3; R_5= -TEG).

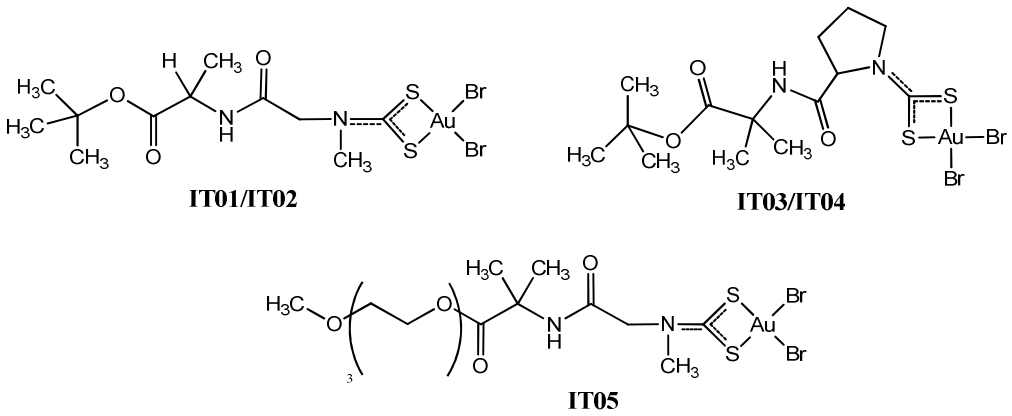

Figure 1.3: chemical structures of gold(III)-dithiocarbamato complexes IT01-05.

FT-IR analysis was proved useful to characterize the synthesized complexes (**Table 1.1**).

Concerning the vibration modes of the peptide chain, the main signals are generated by the ν(N-H) of the amide proton at 3550-3200 cm^{-1} (*Amide A band*), and by the three characteristic bands referred to as amide I, II and III, generated by combination of ν(C=O), δ(N-H) and ν(C-N) characteristic of the C(O)NH function.

In particular, amide I is the combination of the above mentioned modes in 80:10:10 ratios, respectively. It can be normally found between 1660-1620 cm^{-1} when C=O are involved in hydrogen bonds, and between 1710-1660 cm^{-1} when not. The amide II band is characterized by a contribution of δ(N-H) and ν(C-N) in a 60:40 ratio respectively, and can be either found at 1570-1540 cm^{-1} when

the N-H group is involved in the formation of H-bonds and at 1520-1500 cm^{-1} when the N-H group is "free" (the more the proton is involved in H-bonding, the more high the wavenumber of the vibration mode). The amide III is similarly constituted by a 40:30 contribution of δ(N-H) and ν(C-N), and is normally found in 1300-1240 cm^{-1} range, with a shift to higher wavenumber when the proton of the amide is involved in H-bonds.

The most diagnostic regions to verify the formation of the gold(III) dithiocarbamato complex are principally three:

- the 1580-1450 cm^{-1} region, primarily associated with the "thioureide" band of the ν(N-CSS) vibration;
- the 1060-940 cm^{-1} region, associated with ν(S-C-S) vibrations;
- the 420-350 cm^{-1} region, associated with ν(M-S) vibrations.

Upon complex formation, the deprotonation of the free dipeptide to form the corresponding dithiocarbamato moiety causes the disappearance of the signal at 2766-2743 cm^{-1} generated by the $\nu_{a/s}(NH_2^+)$ vibration mode, and the appearance of both the *ν*(N-CSS) band at 1580-1450 cm^{-1} (somewhat overlapped to amide II band) and the ν_a(S-C-S) band at 1060-940 cm^{-1}.

As described by Chatt et al.[117], the dithiocarbamato function is characterized by a strong delocalization of electrons in the dithiocarbamate moiety, and can be described by three main resonance structures (**Figure 1.4**). The position of the *ν*(N-CSS) band recorded for our compounds are consistent with the presence of a carbon-nitrogen bond which order lies between a single bond (ν=1350-1250 cm^{-1}) and a double bond (ν~=1690-1640 cm^{-1})[118]. This is consistent thus with a main contribution to the structure deriving from the resonance form III, consisting in a symmetric chelated coordination of the dithiocarbamato function to the gold(III) metal center[119].

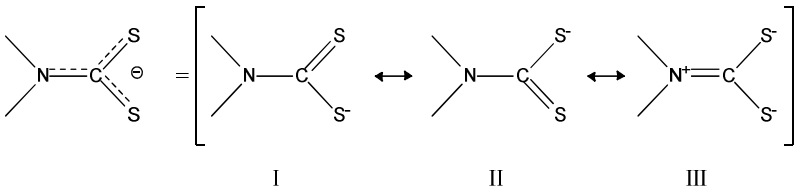

Figure 1.4: resonance forms of the dithiocarbamic –NCSS- moiety.

Moreover, following the Bonati-Ugo criterion[120], the presence of a single band for the ν_a(S-C-S) at 1022-991 and the ν_s(S-C-S) at 569-533 cm^{-1} further confirms the presence of a bidentate symmetric coordination (**Figure 1.5**).

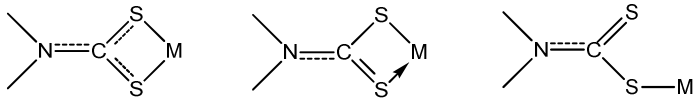

(a) (b) (c)

Figure 1.5: Different ways of metal-sulfur binding in dithiocarbamate complexes: symmetrical bidentate (**a**), asymmetrical bidentate (**b**) and monodentate (**c**).

The formation of a symmetrically chelated dithiocarbamato is demonstrated also by the metal-sulfur stretching vibrations signals $\nu_{a/s}$(S-Au-S) at 419-410/390-376 cm^{-1}, in accordance to previously reported data[119]. Moreover, the vibration of the *cis*-coordinated halides $\nu_{a/s}$(Br-Au-Br) can be rather found at 252-250/229-220 cm^{-1} [119,120,121].

Table 1.1: FT-IR frequencies of ligands **P1-P5** and corresponding complexes **IT01-IT05**

	Vibrational mode [cm^{-1}]									
Comp.	***ν* NH**	***ν*$_{a/s}$ NH_2^+**	***ν* C=O**	**amide I**	***ν N-CSS***	**Amide II**	**Amide III**	***ν*$_{a/s}$ SCS**	***ν*$_{a/s}$ SAuS**	***ν*$_{a/s}$ XAuX**
P1	3332	2736	1735	1669	-	1564	1266	-	-	-
IT01	3317	-	1733	1668	1564[a]		1219	1003/ 567	419/ 380	251/ 229
P2	3332	2766	1735	1669	-	1564	1266	-	-	-
IT02	3311	-	1732	1668	1563[a]		1218	1003/ 566	419/ 380	251/ 228
P3	3430	2744	1733	1678	-	1551	1265	-	-	-
IT03	3341	-	1730	1680	1553[a]		1247	1000/ 535	410/376	252/220
P4	3437	2743	1733	1678	-	1551	1256	-	-	-
IT04	3363		1732	1680	1549[a]		1241	991/ 533	410/ 376	251/ 222
P5	3193	2762	1739	1648	-	1554	1256	-	-	-
IT05	3290	-	1735	1683	1576	1549	1253	1022/ 569	412/ 390	250/ 226

[a] *ν N-CSS* and amide II are overlapped.

All the synthetized dipeptides, **P1-P5** and the corresponding gold(III) complexes **IT01-IT05** were analyzed by means of ^1H (**Table 1.2**) and ^{13}C (**Table 1.3**) NMR spectroscopy. In general, the proton signals of the dipeptide backbone undergo a downfield shift upon complex formation, less evident when the distance from the metal center increases as previously reported for similar compounds[119]. The protons located on -NCSS proximal groups undergo a chemical shift increase of about 1 ppm, while the amide signal follows an opposite trend, with chemical shift value lowered by 0.1-0.2 ppm

in the complex with respect to the free dipeptide. This trend is generally observed also for the ^{13}C signals (**Table 1.3**). The formation of the dithiocarbamato moiety is confirmed by the disappearance of the proton amine signal at 9.00-9.80 ppm of the free dipeptide, and by the appearance in the ^{13}C-NMR spectrum of the signal related to the dithiocarbamato carbon at 190.2-199.2 ppm (**Table 1.3**), in accordance with literature data for complexes with metals in high oxidation states, as gold(III)[122,123].

Table 1.2: ^{1}H NMR chemical shifts of ligands and complexes in DMSO-d_6.

		δ (^{1}H) [ppm]		
Compound	**RO**	**AA_1**	**AA_2**	**NH_3^+**
	R=O*t*Bu	AA_1=Sar	AA_2=L-Ala	
P1	1.40 ($(CH_3)_3C$)	2.53 (N-C***H***$_3$) 3.70 (N-C***H***$_2$)	1.28 (β-C***H***$_3$) 4.17 (α-C***H***) 8.88 (N***H***)	9.00
IT01	1.40 ($(CH_3)_3C$)	3.37 (N-C***H***$_3$) 4.53 (N-C***H***$_2$)	1.23 (β-C***H***$_3$) 4.18 (α-C***H***) 8.79 (N***H***)	
		AA_1=Sar	AA_2=D-Ala	
P2	1.40 ($(CH_3)_3C$)	2.52 (N-C***H***$_3$) 3.69 (N-C***H***$_2$)	1.27 (β-C***H***$_3$) 4.16 (α-C***H***) 8.96 (N***H***)	9.12
IT02	1.41 ($(CH_3)_3C$)	3.36 (N-C***H***$_3$) 4.53 (N-C***H***$_2$)	1.28 (β-C***H***$_3$) 4.17 (α-C***H***) 8.79 (N***H***)	
		AA_1=L-Pro	AA_2=Aib	
P3	1.32 ($(CH_3)_3C$)	1.83(C***H***3", C***H***$_2^4$) 2.27 (C***H***3') 3.15 (C***H***$_2^V$) 4.11 (C***H***$_2$)	1.36 (β-C***H***$_3$) 8.92 (N***H***)	9.80
IT03	1.38 ($(CH_3)_3C$)	2.08(C***H***$_3$, C***H***$_2^4$) 2.41 (C***H***$^{3'}$) 3.85-3.89 (C***H***$_2^5$) 4.75-4.78 (C***H***^{2})	1.31, 1.34 (β-C***H***$_3$) 8.75 (N***H***)	
		AA_1=D-Pro	AA_2=Aib	
P4	1.36 (($C\mathbf{H_3}$)$_3$C)	1.83(C***H***$_3$", C***H***$_2^4$) 2.29 (C***H***$_3$') 3.15 (C***H***$_2^5$) 4.14 (C***H***$_2$)	1.33, 1.37 (β-C***H***$_3$) 8.94 (N***H***)	9.34
IT04	1.38 ($(CH_3)_3C$)	2.07-2.12 (C***H***$^{3''}$, C***H***$_2^4$) 2.41 (C***H***$^{3'}$) 3.83-3.91 (C***H***$_2^5$) 4.75-4.78 (C***H***^{2})	1.31, 1.34 (β-C***H***$_3$) 8.78 (N***H***)	
		AA_1=Sar	AA_2=Aib	
P5	3.24 (O-C***H***$_3$) 3.41-3.54 (C***H***$_2^{3,4,5,6}$)	2.51 (N-C***H***$_3$) 3.66 (N-C***H***$_2$)	1.39 (β-C***H***3) 9.04 (N***H$_2$***)	9.04 (N***H***)

	3.57-3.60 (C***H***$_2^2$) 4.10-4.13 (C***H*^{1}**)**		
IT05	3.24 (O-C***H***$_3$) 3.36-3.58 (C***H***$_2^{1,3,4,5,6}$) 4.10-4.11 (C***H***$_2^2$) 4.10-4.13 (C***H*^{1}**)**	2.51 (N-C***H***$_3$) 4.47 (N-C***H***$_2$)	1.39 (β-C***H***3) 8.83 (N***H*$_2$**)

Table 1.3: ^{13}C NMR chemical shifts of ligands and complexes, in DMSO-d$_6$.

	δ (^{13}HC) [ppm]			
Compound	**RO**	**AA$_1$**	**AA$_2$**	***C*-SS**
	R=O*t*Bu	AA$_1$=Sar	AA$_2$=L-Ala	
P1	27.36 ((***C***H$_3$)$_3$C) 80.58 ((CH$_3$)$_3$***C***)	32.40 (N-***C***H$_3$) 48.53 (N-***C***H$_2$) 164.86 (***C***=O)	16.75 (β-***C***H$_3$) 48.29 (β-***C***H$_3$) 171.27 (β-***C***H$_3$)	
IT01	28.35 ((***C***H$_3$)$_3$C) 82.36 ((CH$_3$)$_3$***C***)	40.08, 41.06 (N-***C***H$_3$) 54.99, 55.97 (N-***C***H$_2$) 164.72 (***C***=O)	18.34 (β-***C***H$_3$) 50.35 (α-***C***H) 172.54 (***C***=O)	196.49, 200.4
	R=*t*Bu	AA$_1$=Sar	AA$_2$=D-Ala	
P2	27.28 ((***C***H$_3$)$_3$C) 80.55 ((CH$_3$)$_3$***C***)	32.41 (N-***C***H$_3$) 48.52 (N-***C***H$_2$) 164.87 (***C***=O)	16.76 (β-***C***H$_3$) 48.29 (α-***C***H) 171.22 (***C***=O)	
IT02*	27.69 ((***C***H$_3$)$_3$C) 81.70 ((CH$_3$)$_3$***C***)	39.42, 40.40 (N-***C***H$_3$) 54.33, 55.30 (N-***C***H$_2$) 163.81 (***C***=O)	17.67 (β-***C***H$_3$) 49.68 (α-***C***H) 171.88 (***C***=O)	195.83, 199.74
	R=*t*Bu	AA$_1$=L-Pro	AA$_2$=Aib	
P3	27.19 (-C(**C**H$_3$)$_3$) 79.71 (-**C**(CH$_3$)$_3$)	23.56 (**C**H$_2^4$) 29.67 (**C**H$_2^3$) 45.55 (**C**H$_2^5$) 58.26 (**C**H^2)	24.08, 24.78 (**C**H$_3$) 172.15 (**C**=O)	
IT03*	28.00 (-C(**C**H$_3$)$_3$) 80.98 (-**C**(CH$_3$)$_3$)	23.09 (**C**H$_2^4$) 30.84 (**C**H$_2^3$) 52.10 (**C**H$_2^5$) 64.87 (**C**H^2)	24.56, 25.51 (**C**H$_3$) 57.28 (**C**(CH$_3$)$_2$) 172.84 (**C**=O)	190.22
	R=*t*Bu	AA$_1$=D-Pro	AA$_2$=Aib	
P4	27.13 (-C(**C**H$_3$)$_3$) 79.65 (-**C**(CH$_3$)$_3$)	23.28 (**C**H$_2^4$) 29.59 (**C**H$_2^3$) 45.32 (**C**H$_2^5$) 58.07 (**C**H^2)	172.06 (**C**=O)	
IT04*	27.97 (**C**H$_3$ *t*-Bu) 81.10 (-**C**(CH$_3$)$_3$)	23.16 (**C**H$_2^4$) 30.80 (**C**H$_2^3$) 52.08 (**C**H$_2^5$) 64.92 (**C**H^2)	24.67, 25.21 (**C**H$_3$) 57.44 (**C**(CH$_3$)$_2$) 172.96 (**C**=O)	190.21
	R=TEG	AA$_1$=Sar	AA$_2$=Aib	

P5	57.26 (O-**C**H_3) 63.19 (**C**H_2^1) 67.44 (**C**H_2^2) 68.8-70.7 (**C**$H_2^{3,4,5,6}$)	31.84 (N-**C**H_3) 47.94 (N-**C**H_2)	23.39 (β-**C**H_3) 54.77 (**C**$(CH_3)_2$) 172.52 (**C**=O)	
IT05*	58.52 (O**C**H_3) 64.52 (**C**H_2^1) 69.25 (**C**H_2^2) 70.8-71.2 (**C**$H_2^{3,4,5}$)	39.36, 40.38 (N**C**H_3) 54.34, 55.17 (N**C**H_2)	24.86 (**C**H_3) 173.63 (**C**=O)	195.38, 199.21

***** acetone-d_6

In both the ^{1}H and the **[**^{1}H,^{13}C]-HMBC spectra of IT01 in acetone-d_6 and DMSO-d_6 (**Figures 1.6, 1.7** and **1.8** respectively), a set of signals (two singlets) is recorded for the protons of N-C*H*$_3$ and N-C*H*$_2$ groups of the sarcosine residue, and for the dithiocarbamic carbon *C*SS at nearly 192 ppm (**Figure 1.8**).

This can be explained by the presence in solution of two different isoforms of the compounds, whose relative abundance varies depending on the synthetic conditions[93]. Moreover, as we can see from **Figure 1.6** and **1.7**, the behavior of the compound is quite different in the two solvents, since in acetone-d_6 (**Figure 1.6**) the relative intensity of the two isomers changes with time, favouring the formation of the major species, while in DMSO-d_6 this interconversion does not occur and the relative abundance of the isomers does not change significantly even after 48 h (**Figure 1.7**).

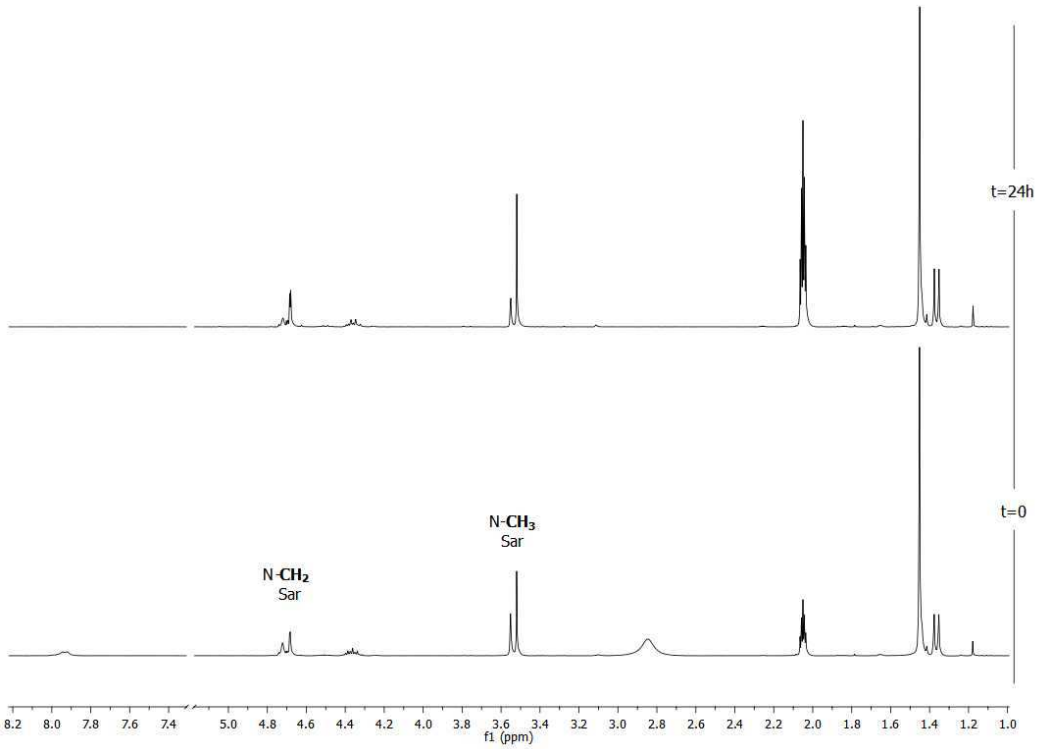

Figure 1.6: ^{1}H-NMR spectra of IT01 in acetone-d_6 over 24h.

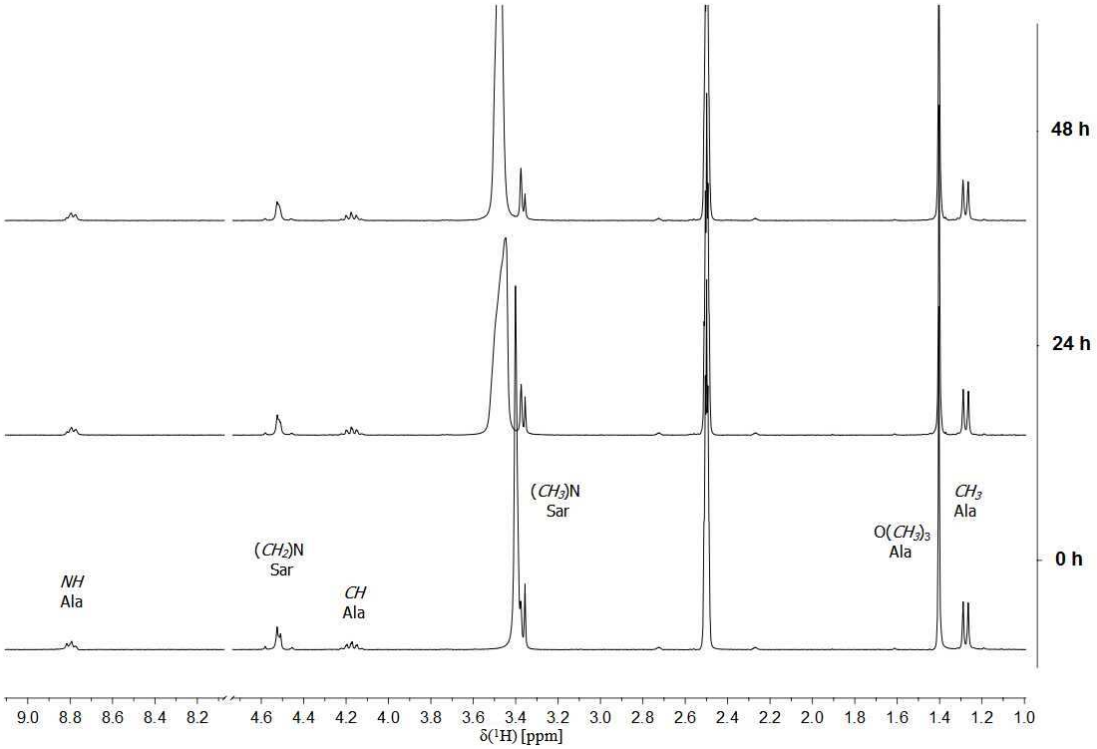

Figure 1.7: ^{1}H-NMR spectra of IT01 in DMSO-d_6.

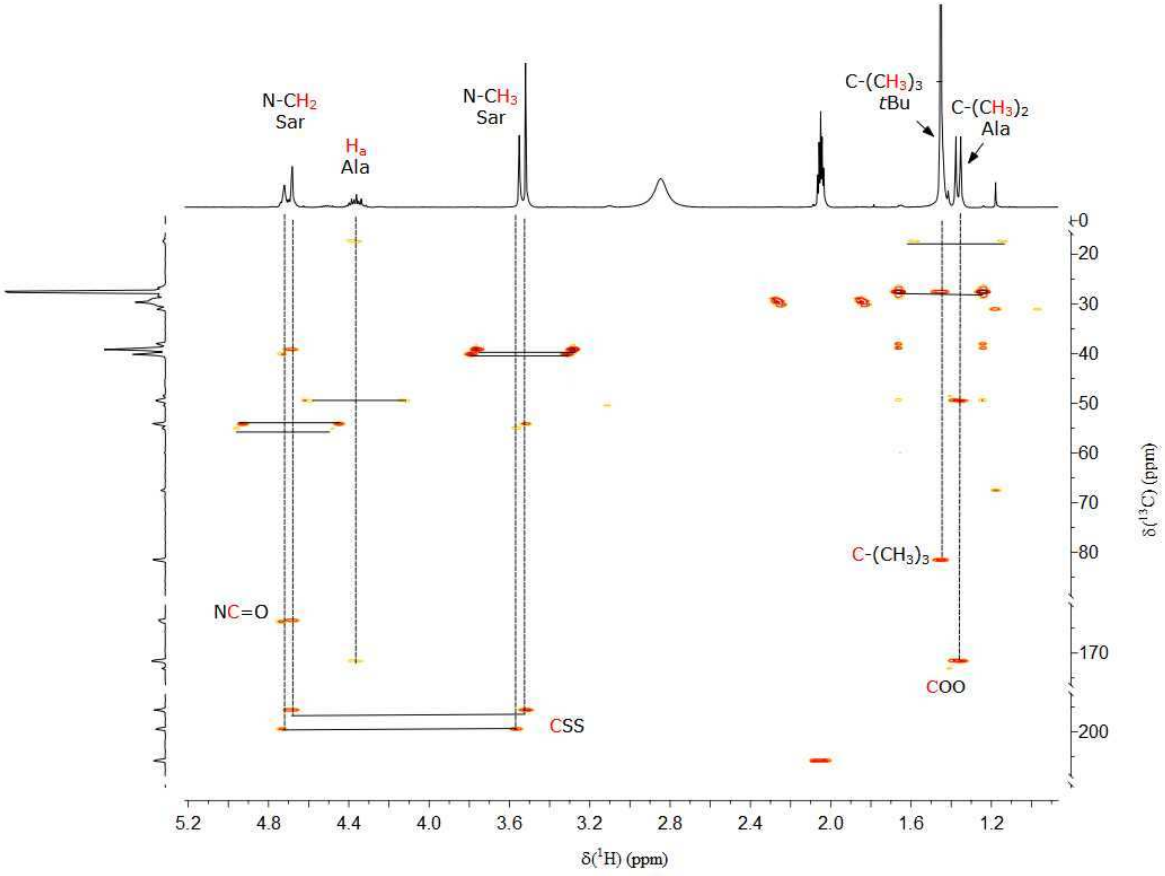

Figure 1.8: [^{1}H,^{13}C]-HMBC spectrum of IT01 in $(CD_3)_2CO$.

The two species were not resolved since recently, when we were able to separate the two forms of one of the most studied and characterized gold(III) dithiocarbamato complexes, AuL23 [$Au^{III}Br_2$(SSC-Sar-OMe)] (**Figure 1.9**), during the experiments aimed at obtaining high purity compounds for the *in vitro* and *in vivo* biological evaluations.

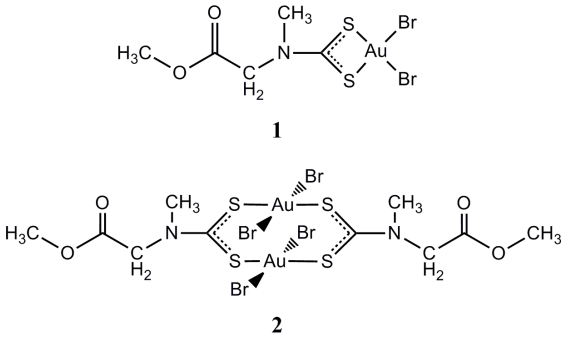

Figure 1.9: molecular structure of AuL23 forms, Au23-1 (above) and AuL23-2 (bottom).

In **Figure 1.10** the ^{1}H NMR spectra over time of crude AuL23 are shown. Similarly to what reported for IT01, two proton signals at 3.58/3.61 and 4.79/4.81 ppm were recorded in acetone-d_6 for the *N*-methyl and *N*-methylene groups, respectively. The NCH_3/NCH_2 couples at 3.58/4.79 and 3.61/4.81 ppm belong to two different species, as confirmed by the mutual long-range couplings observed in the [^{1}H,^{13}C] HMBC spectrum (**Figure 1.11**), thus accounting for the coexistence of two forms for complex AuL23. This is confirmed by the presence of two ^{13}C signals recorded for both the C=O and the NCSS carbons as well, each giving rise to long-range couplings with one set of NCH_3/NCH_2 signals. The analysis of the ^{1}H NMR spectra of the native complex AuL23 in acetone-d_6, confirmed the same behaviour recorded for IT01, with the minor species irreversibly interconverting into the major one over time, leading to its almost complete disappearance (**Figure 1.10A** and **1.10B**). The same behavior was observed also in $CDCl_3$ and CD_2Cl_2 (data not shown) whereas no interconversion occurred in either CD_3OD (data not shown) or DMSO-d_6 over 24 h (**Figure 1.10C** and **1.10D**), confirming the crucial role played by the solvent.

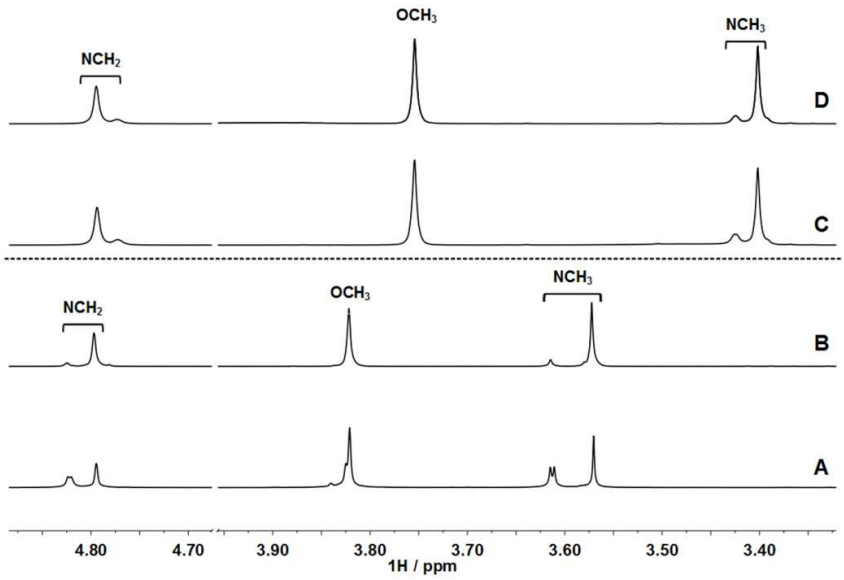

Figure 1.10: ^{1}H NMR spectrum of complex AuL23 over time in acetone-d_6 (A) soon after dissolution and (B) after 24 h, and in DMSO-d_6 (C) soon after dissolution and (D) after 24 h.

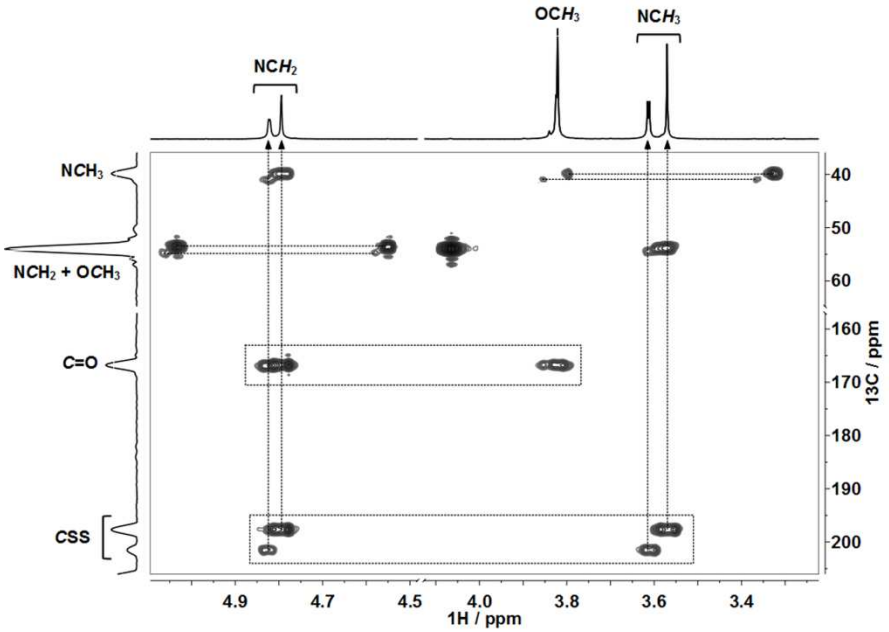

Figure 1.11: [^{1}H,^{13}C] HMBC spectrum of complex **1** in acetone-d_6 (dotted arrows indicate long-range ^{1}H-^{13}C couplings).

The two forms were isolated by preparative layer chromatography and characterized by FT-IR and ^{1}H-NMR spectroscopy (**Figure 1.12**). The major species was identified as the expected gold(III)-dithiocarbamato derivative AuL23-1 depicted in **Figure 1.9**, whose structure was confirmed by X-ray analysis (**Figure 1.13**). The minor species AuL23-2 is consistent with a gold(III) dimer in which two bridging dithiocarbamato ligands are bound to both gold(III) centers whose coordination sphere is completed by two *trans*-bromides, as suggested by the absence of both the symmetric S–Au–S and Br–Au–Br stretching vibrations in the far-IR spectrum (**Figure 1.12**).

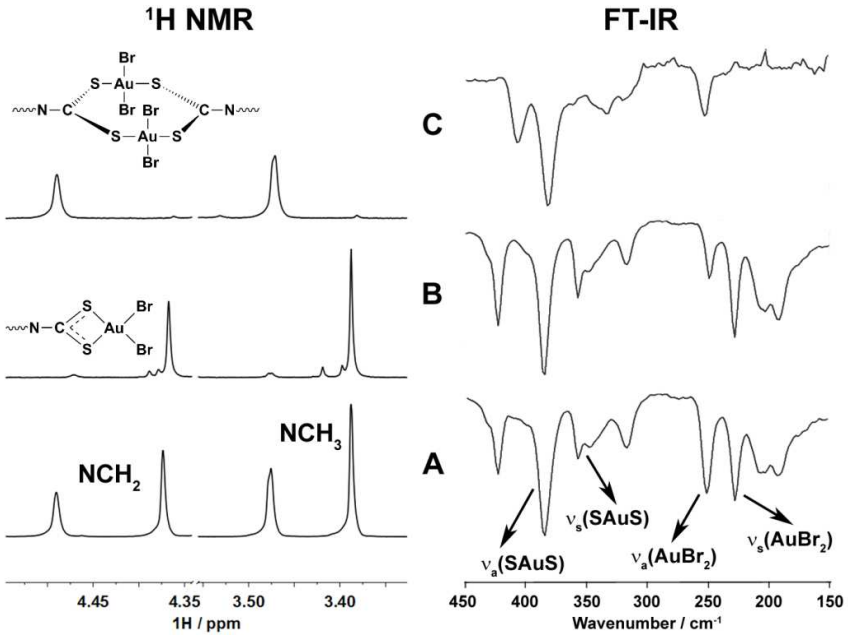

Figure 1.12: detail of the ^{1}H NMR (in CD_2Cl_2) and IR spectra of (A) native raw complex **1**, and (B) the major and (C) the minor forms as isolated by preparative layer chromatography.

Single crystals of compound Aul23-1 allowed the resolution of the 3D structure of the compound, reported in **Figure 1.13A** (for further details see *Appendix 1*).

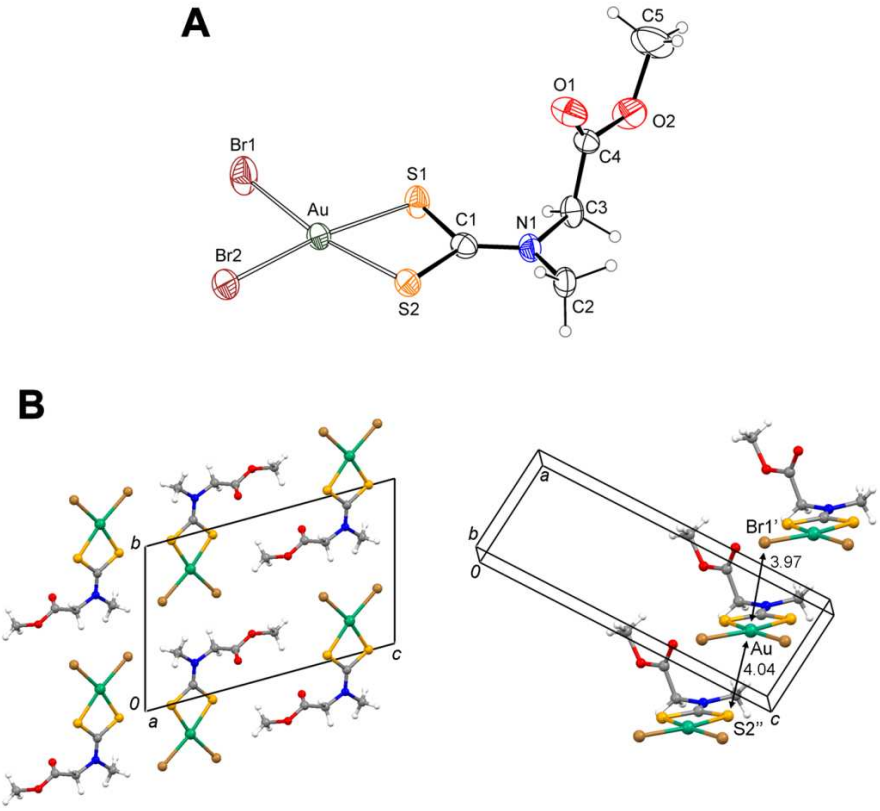

Figure 1.13: (A) X-ray crystal structure with atom numbering scheme for [$Au^{III}Br_2$(dtc-Sar-OCH_3)] (**1**), with thermal ellipsoids drawn at 30% probability. (B) Crystal packing of **1** with Au–S (2)" and Au–Br(1)' distances (Å) (symmetry codes: ' = 1+x; y; z, " = 1-x; y; z). The corresponding crystallographic data as well as a list of selected bond lengths and angles are reported in Table S1 and Table S2, respectively.

Going back to our gold(III)-peptidomimetic compounds IT01-IT05, the thermal behaviour of the synthesized complexes have been studied by thermogravimetric (TG) and differential scanning calorimetry (DSC) techniques in a dynamic atmosphere of air, in order to establish the different decomposition processes and to confirm the proposed stoichiometry. The experimental data agree to a good extent with the ones obtained by other spectroscopic techniques, and the results of such analysis summarized in **Table 1.4**, indicate a good correlation between calculated (to metallic gold) and found weight loss values for all the investigated compounds.

Table 1.4: Thermogravimetric (TG) and differential scanning calorimetric (DSC) data.

Compound	Weight loss (%)		DSC
	Found	Calculated	Peak temperature [°C] (process*)
IT01	67.95	69.61	158.0 (endo); 499.4 (exo)
IT02	67.90	69.61	151.0 (endo); 469.4 (exo)
IT03	72.00	71.38	113.7 (endo); 439.7 (exo)
IT04	71.89	71.38	178.0 (endo); 436.7 (exo)
IT05	73.82	72.61	122.6 (endo); 493.7 (exo); 542.1 (exo)

*endo/exo=endothermic/exothermic

The thermal degradation of all the complexes is likely to occur in two major steps, the first TG step corresponding to the pyrolysis, the decarboxylation and reduction elimination Au(III)→Au(I), thus leading to [Au(SCN)] as the residue, a commonly discovered intermediate in the thermal decomposition of metal dithiocarbamates[124]. The removal of the remaining ligand atoms at higher temperature is followed by complete degradation leading to metallic gold[125,126].

After the purification of the gold(III) dithiocarbamato complexes, the crystals of two complexes were grown, in particular for the racemate [$Au^{III}Br_2$(dtc-L/D-ProAibO*t*Bu)] (IT03/IT04) and [$Au^{III}Br_2$(dtc-SarAibOTEG)]·(IT05).

By exploiting the *Wallach rule*[127] ("racemates pack better"), a racemal mixture of [$Au^{III}Br_2$(dtc-L,D-Pro-Aib-O*t*Bu)] was prepared to grow single crystals and to solve the crystal structure (the D-enantiomer IT04 is shown in **Figure 1.14**).

As expected, Au adopts a planar square coordination. The Au-S and Au-Br bond values, as well as the bond angles, are comparable to those of the few available similar crystal structures[128,129]. The Pro *N* atom adopts a sp^2 hybridization. The values of the D-Pro and Aib ϕ, ψ torsion angles are 81°, –166° and 54°, 37°, respectively (*see Appendix 1*).

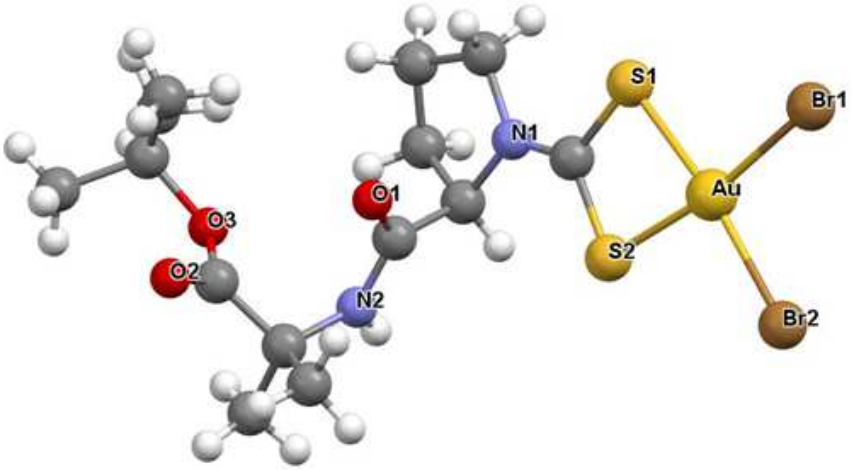

Figure 1.14: molecular structure of the racemate IT04 [$Au^{III}Br_2$(dtc-L,D-Pro-Aib-O*t*Bu)] (crystal obtained from a CH_2Cl_2/*n*-pentane mixture)

In summary, the solved molecular structure indicate that: (i) the planar geometry of the Au(III) complexes is not affected by a bulky ligand (a dipeptide); (ii) Pro and Aib are folded in their typical conformations (semi-extended and helical, respectively).

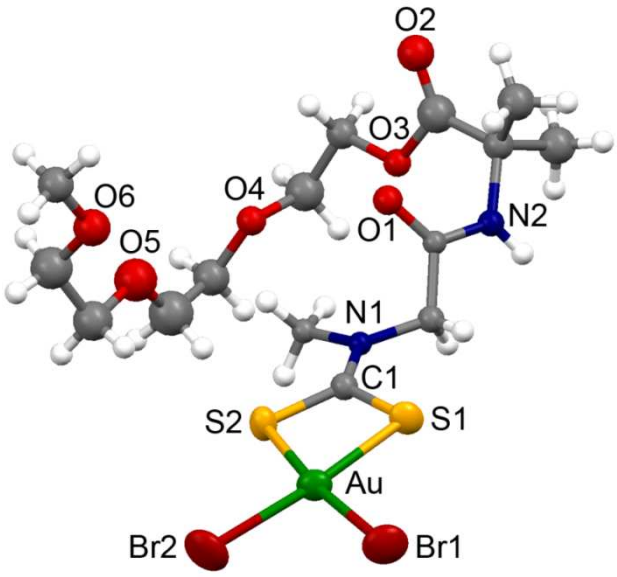

Figure 1.15. Molecular structure of [$Au^{III}Br_2$(dtc-Sar-Aib-OTEG)] (IT05). Thermal parameters are depicted at the 30% probability level.

The molecular structures of IT05 is reported in **Figure 1.15**. The metal exhibits a square planar geometry achieved by the *S*,*S* chelate dithiocarbamate ligand and by two bromine atoms. The coordination environment of the metal and the coordination distances (**Table A6**, *Appendix 1*) are in

agreement with previously reported data for gold complexes with a dithiocarbamate ligand and two bromide anions (*Appendix 1*)[129,130]. The peripheral methylated triethylene glycol is folded towards the dithiocarbamate moiety and the three ethereal oxygen atoms, O(4)-O(6), are capping the C(2) methyl group of the ditiocarbamate ligand. The crystal packing shows that the IT05 molecules are irregularly stacked along the *b* crystallographic axis (**Figure A3** in *Appendix 1*), and that the long arm of the ligand originating from the C(3) atom, is responsible of several C-H···O interactions (**Figure A4**, *Appendix 1*). In addition, there is a bifurcated hydrogen bond between the N(2)-H and the O(4)' and O(5)' atoms of a symmetry related triethylene glycol residue (symmetry code = 1/2-x; 1/2+y; z), d[N(2)··O(4)'] = 3.00(3) Å, and d[N(2)··O(5)'] = 3.18(4) Å, that is mainly responsible of the conformations adopted by the methylated triethylene glycol.

To sum up, in this Chapter is reported the synthesis and the characterization of newly synthetized gold(III)-peptidodithiocarbamato complexes, with possible application in targeted anticancer therapy. The oligopeptides were prepared using liquid phase synthesis approach, and further purified by flash chromatography. They were subsequently functionalized by reaction in aqueous condition with CS_2, to obtain the dithiocarbamato ligands, used *in situ* for the synthesis of the corresponding gold(III) derivative, which precipitate from solution. The synthetic procedure allowed the obtainement of the complexes with yields of 50-70%, depending on the substrate used. Nonetheless, the complexes were further purified, to separate the two isoforms obtained from the reaction crude (mononuclear and dinuclear gold(III) dithiocarbamato species) by exploiting the thin layer chromathography technique. Finally, the crystal structure of three compounds, IT03, IT04 and IT05 were obtained, confirming the geometry and stoichiometry proposed for the major species formed from the one-pot reaction.

Chapter 2

Synthesis of AuL12 and IT03 in MeOH in anhydrous conditions

So far, a general route has been followed for the synthesis of these complexes, which combined several steps (dithiocarbamic group formation, deprotonation and metal ion coordination) in a one-pot reaction. The main drawback of this procedure was identified in the conversion rate of starting material, which often do not exceed 50%.

Early studies focused on mechanistic details of this reaction, by using sarcosine ethyl ester (ES hereon) as substrate, has pointed out ester hydrolysis as the main cause of degradation of the substrate, together with the formation of a number of byproducts. The degradation process is favored by the presence of a base in aqueous solution, but these conditions also favored the establishment of an equilibrium between the neutral and the protonated substrate. This latter depletes the amount of substrate available to the dithiocarbamate conversion, by forming a cationic counterion (**Figure 2.1**).

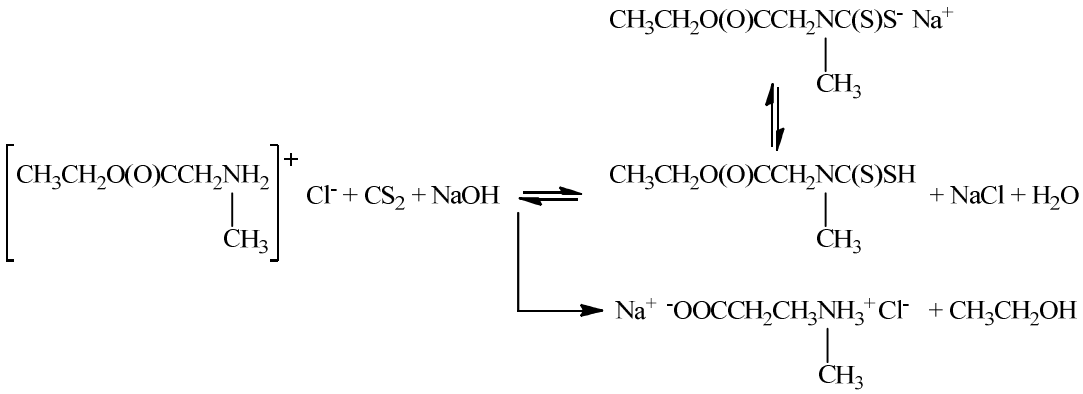

Figure .2.1: Reactions occurred during the template synthesis of ES dithiocarbamic acid.

In addition, the efficiency of this synthetic strategy is largely influenced by the nature of the substrate, leading in some cases to highly limited final yields or even to total starting material inertness, as in the case of primary amines (for which this procedure was proved to be not suitable), or more complex systems, such as long oligopeptides, for which unspecific metal binding on the side chain can occur. In order to overcome the limitations of the technique, the attention has been focused on the study of the mechanistic details of the synthetic pathway.

In this Chapter it has been reported a detailed study, mainly based on NMR spectroscopy, which has led to interesting results. In fact, by screening and modifying the reaction conditions, total conversion

of the starting material to dithiocarbamate derivative has been obtained for several substrates, leading to increase the final yields in Au(III) complexes in many cases.

The variety of the investigated substrates has led to the development of a methodology for the synthesis of dithiocarmabates that allows the total conversion of the starting material. In particular, the proposed methodology has been found successful also in case of more complex substrates.

Experimental section

All the synthetic operations were performed under inert atmosphere (N_2, Ar) by using Schlenk-line technique. A methanol solution of the hydrochloride substrate (HCl·ES, HCl·H-L-Pro-Aib-O*t*Bu; 2 mL, 1 eq) was cooled at 0°C. Cold carbon disulfide (CS_2, 2 eq) was added to the solution, followed by the dropwise addition of a methanol solution of NaOtBu (2 eq, 1 mL) under continuous stirring, in order to neutralize the starting material. The reaction has been kept under stirring for half an hour, after which cold $(K[AuBr_4])_{MeOH}$ solution (1 eq, 2 mL) has been added dropwise to the mixture, leading to direct precipitation of the complex. The solid was filtered-off, washed with cold water and finally dried in a dessicator with P_4O_{10}.

NMR spectra in CD_3OD (residual peak 3.31 ppm) have been recorded after half an hour from the addition of CS_2, to check the progress of the substrate conversion. For each experiment, an aliquot of reaction crude has been withdrawn, dried under nitrogen flux and newly dissolved in the proper deuterated solvent. NMR spectra of final complexes were registered, according to their solubility, in acetone-d_6 (residual peak 2.05 ppm) or DMSO-d_6 (residual peak 2.5 ppm).

Results and discussion

2.1 Synthesis of Aul12

Several substrates have been investigated with the aim to assess the applicability of the method. The ES has been used to obtain a promising Au(III)-based drug candidate synthesized in our lab, better known as AuL12. From a chemical point of view, the presence of sarcosine at the N-terminal, where the dithiocarbamato formation takes place, confers stability to the synthesized dithiocarbamate, as a hydrogen atom (N-H) is replaced by a methyl group (N-CH_3). Interestingly, for several gold(III)-dithiocarbamato complexes synthesized in our lab, promising biological activity have been exhibited when a Sar residue is placed at the N-terminal of the peptide moiety, pointing out an interesting structure/activity relationship[19,107].

As already mentioned above, early preliminary investigations on this substrate evidenced ester hydrolysis as the main issue correlated with the use of the traditional methodology. To overcome this inconvenience, presence of water has been minimized by using freshly distilled methanol and by performing all the operations in an inert atmosphere; in addition, stoichiometric amounts of base have been used. The substrate, available as chlorhydrate form, has been pre-treated with 1 equivalent of ^{t}BuONa, to make the amino group entirely available for the reaction with CS_2.

^{1}H-NMR spectrum in CD_3OD for ES chlorhydrate shows two singlets, attributable to N-CH_3 (δ 2.76 ppm) and to α-CH_2 (δ 3.96 ppm) hydrogen nuclei, both considered diagnostic of the reaction progress, as they result the most affected by dithiocarbamate formation. In addition, the spectrum shows a triplet (δ 1.32 ppm) and a quartet (δ 4.31 ppm) attributable to methyl and methylene groups of ethyl ester (**Figure 2.2**). Successively to the neutralization of the hydrochloride, the procedure developed with propyl-amine has been applied. After half an hour, the two singlets corresponding to N-CH_3 and α-CH_2 undergo considerable downfield chemical shift (δ 0.81 and 0.99 ppm, respectively) due to the formation of dithiocarbamato group (**Table 2.1**). The spectrum reveals the presence of only one species, confirming the total conversion of the substrate (**Figure 2.3**).

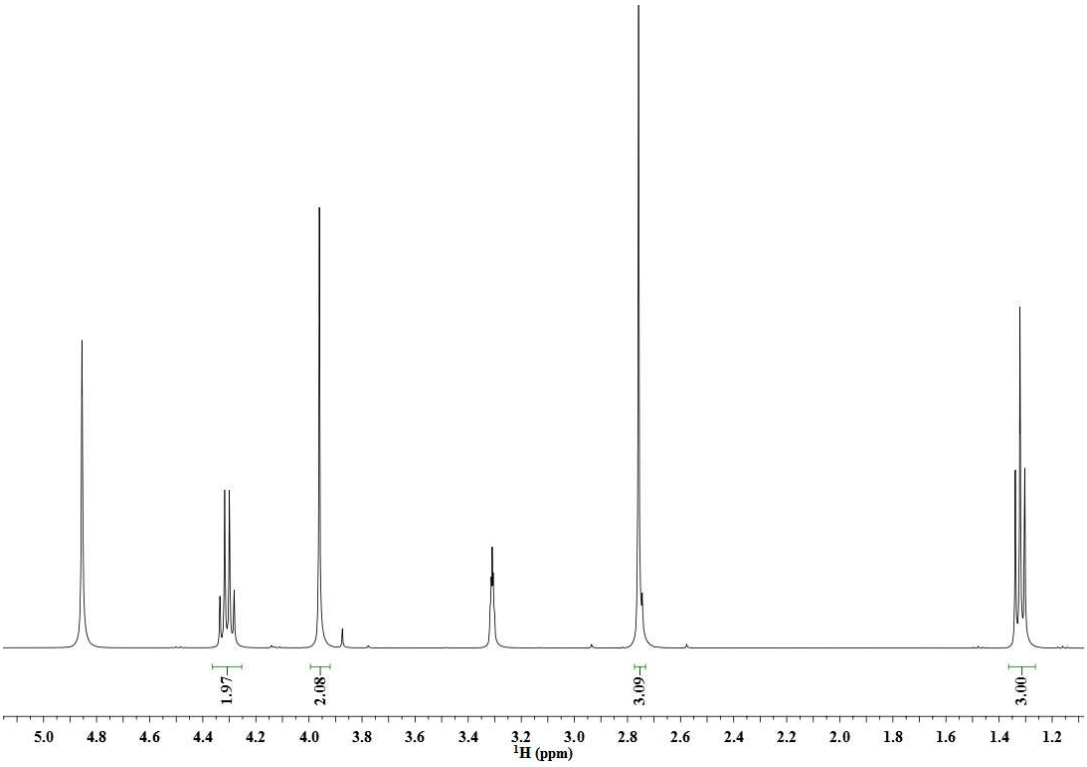

Figure 2.2: ^{1}H-NMR spectrum of the substrate ES (expanded view of the alkyl region). Solvent: methanol-d_4; 200MHz.

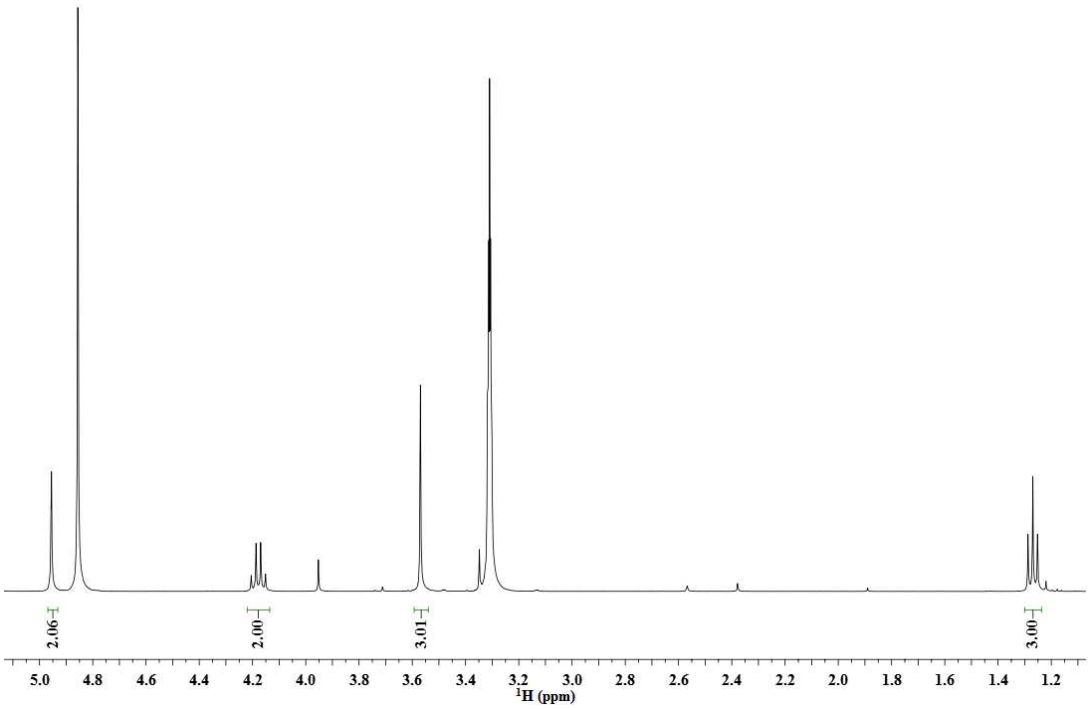

Figure 2.3: ^{1}H-NMR spectrum of the reaction between ES and CS_2 in presence of base after 1/2h (expanded view of the alkyl region). Solvent: methanol-d_4; 200MHz.

Table 2.1: ^{1}H-NMR spectral data for ES chlorhydrate and dithiocarbamic derivative (ESDT)

^{1}H-NMR	**ES-H^{+}**		**ESDT^{-}**	
	A*	**δ (ppm)**	**A**	**δ (ppm)**
O-C*H*$_2$	2	4.31 q	2	4.18
α-C*H*$_2$	2	3.96 s	2	4.96
N-C*H*$_3$	3	2.76 s	3	3.57
C*H*$_3$	3	1.32 t	3	1.27

**relative peak area integral*

In an attempt to assess the compatibility of the new reaction conditions with the formation of the final gold complex, a methanol solution containing one equivalent of K[Au(Br)$_4$] has been added dropwise to the dithiocarbamate solution. The addition has been performed inversely with respect to the procedure used in the template synthesis, to assess possible differences in the formed products. In this case, differently from the old strategy for which 0.5 equivalents of gold precursor were used for the complexation of 1 equivalent of ligand, a stoichiometric amount of metal precursor has been used. The formation of a brownish orange precipitate is soon observed and successively isolated from the orange mother liquor. The two fractions were investigated *via* ^{1}H-NMR spectroscopy (**Figure 2.4**).

The spectrum in acetone-d_6 for the isolated precipitate reveals the presence of two species with similar chemical shifts, similarly to what already described in **Chapter 1** for the analogous compound AuL23.

In fact, in the region of α-CH_2 two singlets are detected (δ 4.78 and δ 4.81 ppm, respectively), as well as for N-CH_3 region (δ 3.57 and δ 3.61 ppm, respectively), with a constant integral ratio of 1.5. On the other hand, the signals related to the ester group (δ 1.28 and δ 4.28 ppm for methyl and methylene, respectively) do not show duplicity and the ratio between integral values of these signals with respect to the integral sum of each couple of singlets found for α-CH_2 and N-CH_3 confirm that ester hydrolysis does not occur. In addition, the NMR spectrum registered in acetone-d_6 on the residual mother liquor shows the presence of both the species, but with a different integrals ratio (0.5), suggesting a higher solubility of the second species in MeOH with respect to AuL12 (**Figure 2.4**).

Similarly to what reported for AuL23 (**Chapter 1**), these findings suggest the presence of the same dithiocarbamato ligand coordinated to gold ion for both the species, either with a different geometry with respect to the coordination plane or with different ligands in *trans* to the two sulfur atoms that do not affect the ester moiety, where the signals corresponding to the major species can be attributed to the desired complex AuL12.

Moreover, NMR data collected on the reaction crude obtained by using the classical methodology report about the presence of the same number of additional peaks (falling at the same chemical shift) here described. These previous studies hypothesized the formation of a dinuclear gold species, having two bridging dithiocarbamato ligands and two bromide ions *trans*-coordinated for each gold center (**Figure 2.5**). The presence of the dinuclear species was supported by the occurrence of the conversion of the minor species into AuL12, observed in acetone after 24 hours: according to this finding the dinuclear species, upon breakage, could give rise to two AuL12 molecules.

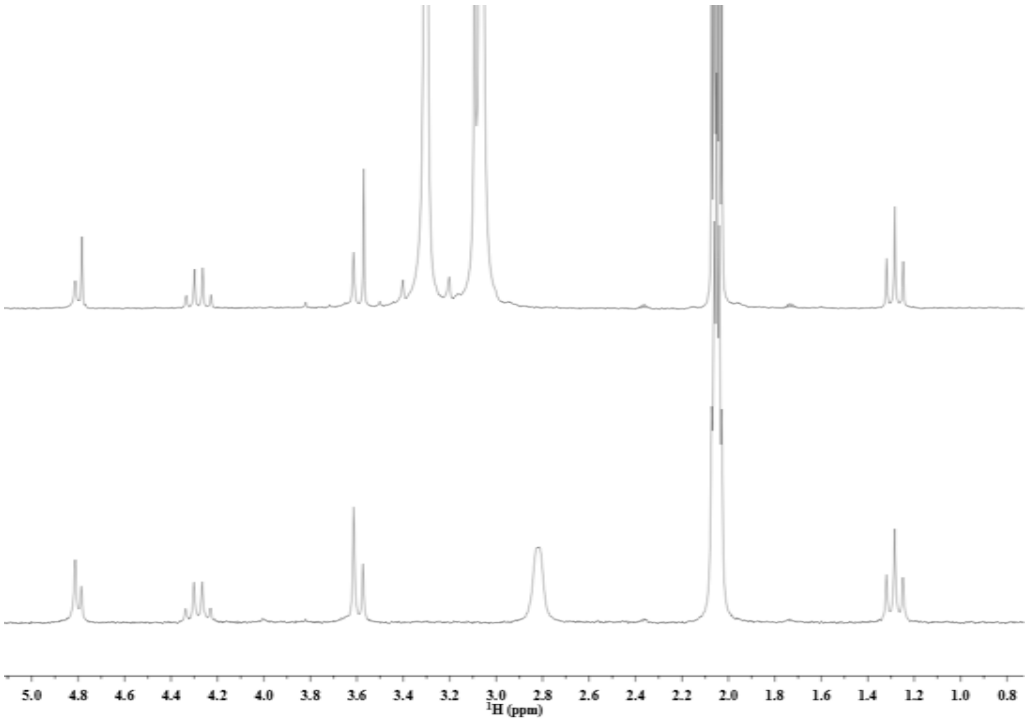

Figure 2.4: ^{1}H-NMR spectral comparison of the alkyl region for precipitate (top) and mother liquors (bottom) obtained by AuL12 new synthetic methodology. Solvent: acetone-d_6; 200 MHz.

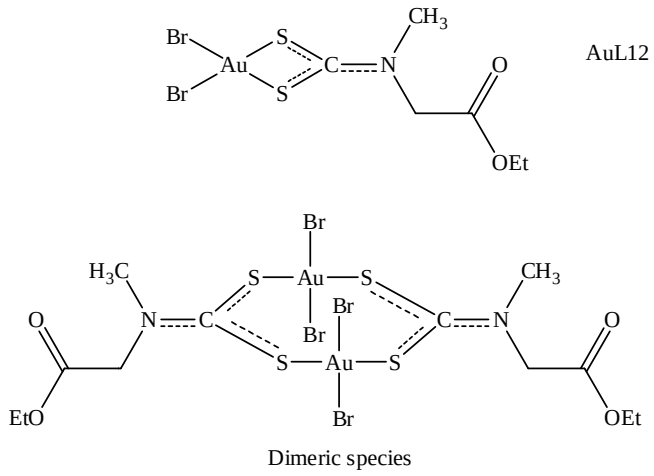

Figure 2.5: Molecular structure of AuL12 and hypothesized byproducts for the reported synthesis.

The similar behavior assumed by the mixture obtained with the new synthesis confirms the formation of the same minor species formed during the one-pot synthesis as a by product.

AuL12 has been successively purified from the minor species, by means of silica gel chromatography (eluent, DCM:MeOH, 97:3). The minor species mainly undergoes degradation upon interaction with silica. Interestingly, the final yield of AuL12 was 65% (calculated over ligand).

^{1}H-NMR spectrum registered in acetone-d_6 confirms the purity of the compound, with the presence of only one signal for each diagnostic region (4.78 and 3.57 ppm for α-CH_2 and N-CH_3, respectively) together with the signals related to the ethyl ester group (1.28 and 4.28 ppm) (**Figure 2.6**). The values of the chemical shifts are in accordance with those previously found in literature[100]. In addition, elemental analyses confirmed the structure proposed for AuL12 (**Table 2.2**).

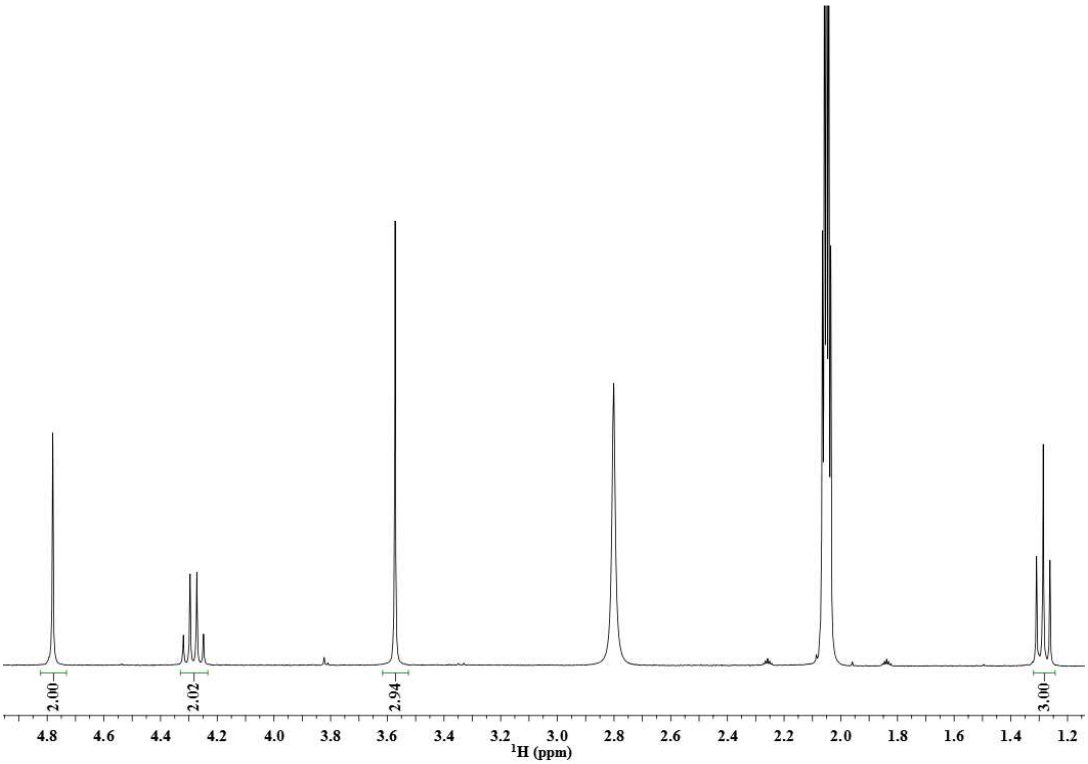

Figure 2.6: ^{1}H-NMR spectrum of purified AuL12 (expanded view of the alkyl region). Solvent: acetone-d_6; 200MHz.

Table 2.2: Elemental analysis data for AuL12.

AuL12	**C (%)**		**H (%)**		**N (%)**		**S (%)**	
	calcd	found	calcd	found	calcd	found	calcd	found
$C_6H_{10}AuBr_2NO_2S_2$	13.17	13.65	1.84	1.84	2.56	2.34	11.69	12.56

Far-IR spectrum (**Figure 2.7**) on AuL12 showed the typical bands for Au-S stretching (384-356 cm^{-1} for antisymmetrical and symmetrical, respectively) and for Au-Br stretching (249-228 cm^{-1} for antisymmetrical and symmetrical, respectively). Moreover, the band at 422 cm^{-1} is probably related to the out-of-plane bending of the 4-membered ring (C-S-Au-S) (**Table 2.3**).

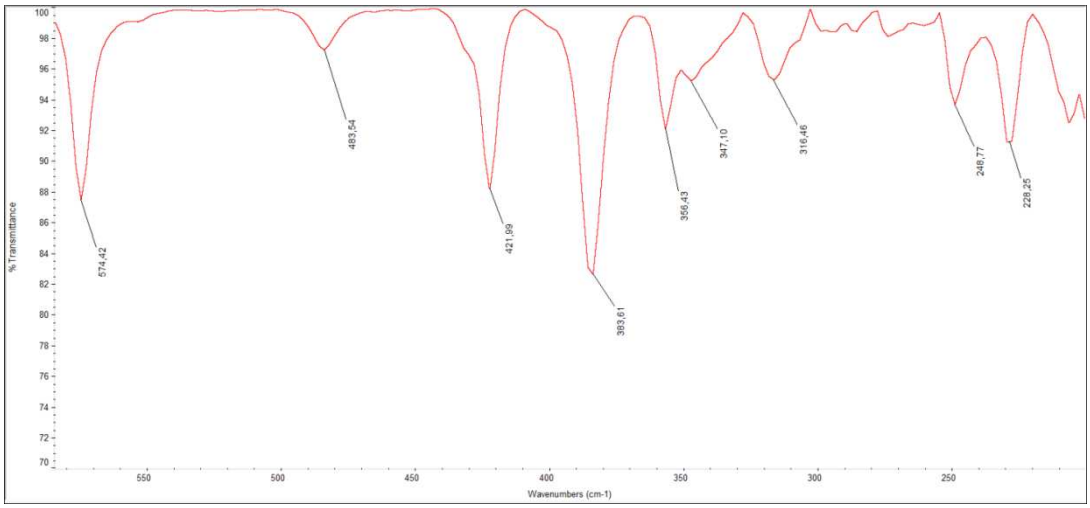

Figure 2.7:1 Far-IR spectrum of purified AuL12 (nujol suspension).

Table 2.3: Far-IR main values for AuL12 vibration modes.

	ν out-of-plane bending (cm^{-1})	**$\nu_{a/s}$ S-Au-S stretching (cm^{-1})**	**$\nu_{a/s}$ Br-Au-Br stretching (cm^{-1})**
AuL12	422	384/356	249/228

2.2 Synthesis of IT03

The dipeptide prolyl-α-amino isobutyric tertbutyl ester (HProAibO*t*Bu) has been then selected as substrate to test the methodology. The same experimental procedure was adopted also for the synthesis of the compound IT03 [$Au^{III}Br_2$(dtc-L-ProAibO*t*Bu)] (**Figure 2.8**), for which multistep purification procedures were usually adopted, and low yields were normally obtained.

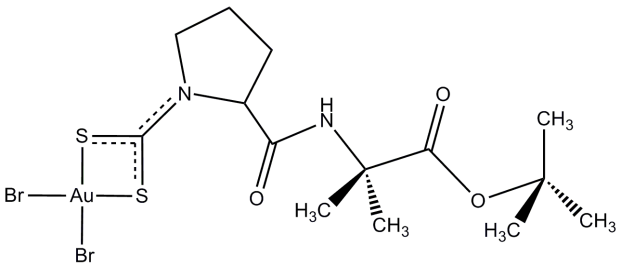

Figure 2.8: molecular structure of IT03.

Also in this case, total conversion of the substrate to the corresponding dithiocarbamato has been observed. The ^{1}H-NMR spectrum in CD_3OD (**Table 2.4**; **Figure 2.9**) of the substrate shows a multiplet corresponding to α-CH (Pro) (δ 3.74 ppm) and a doublet of multiplets for δ-CH_2 (Pro) (δ 3.04), which are the two most affected signals by the presence of CS_2. In addition, it is possible to recognize two groups of signals attributable to the two diasterotopic protons of β-CH_2 (Pro) (δ 2.18 and 1.85 ppm), superimposed to γ-CH_2 (Pro) (δ 1.80 ppm). The two β-CH_3 (Aib) groups, as well as the *tert*-butyl ester signals, are all overlapped at 1.41 ppm. The ^{1}H NMR spectrum of the reaction crude, half an hour after the addition of CS_2, shows a large downfield shift for α-CH (Pro) and δ-CH_2 (Pro) (about δ 1.5 and 1 ppm, respectively) (**Table 2.4**, **Figure 2.10**). The methyl groups are not affected by the reaction and remain unchanged (δ 1.43 ppm).

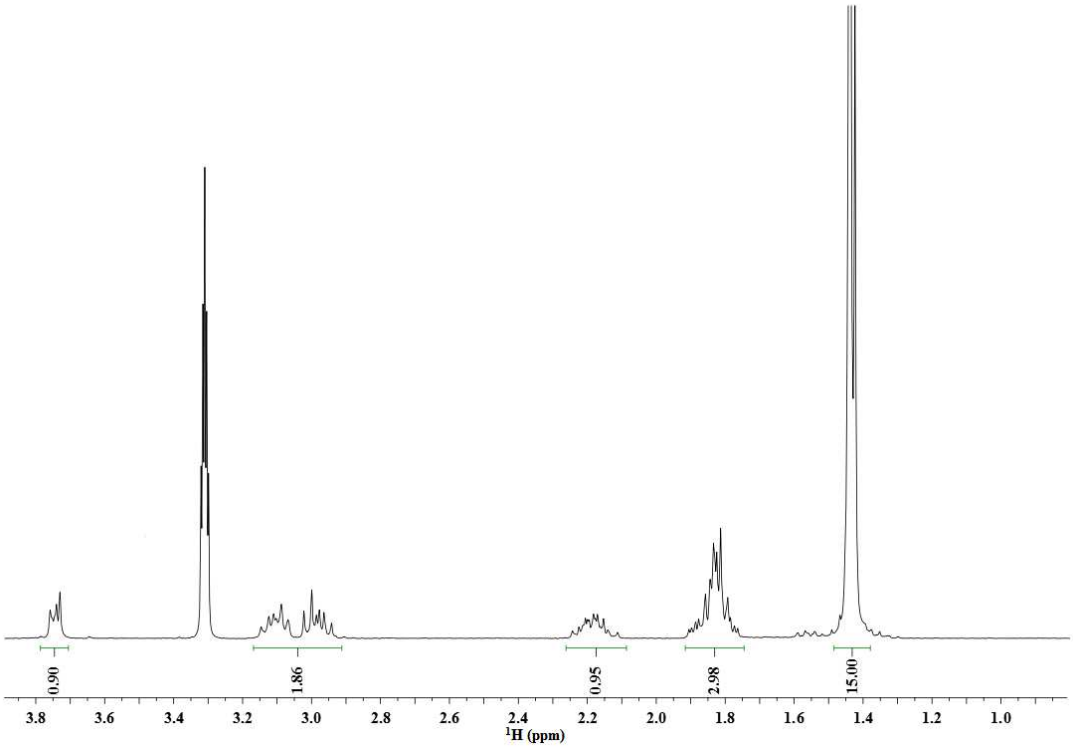

Figure 2.9: ^{1}H-NMR spectrum of the substrate HProAibO*t*Bu (expanded view of the alkyl region). Solvent: methanol-d_4; 300MHz.

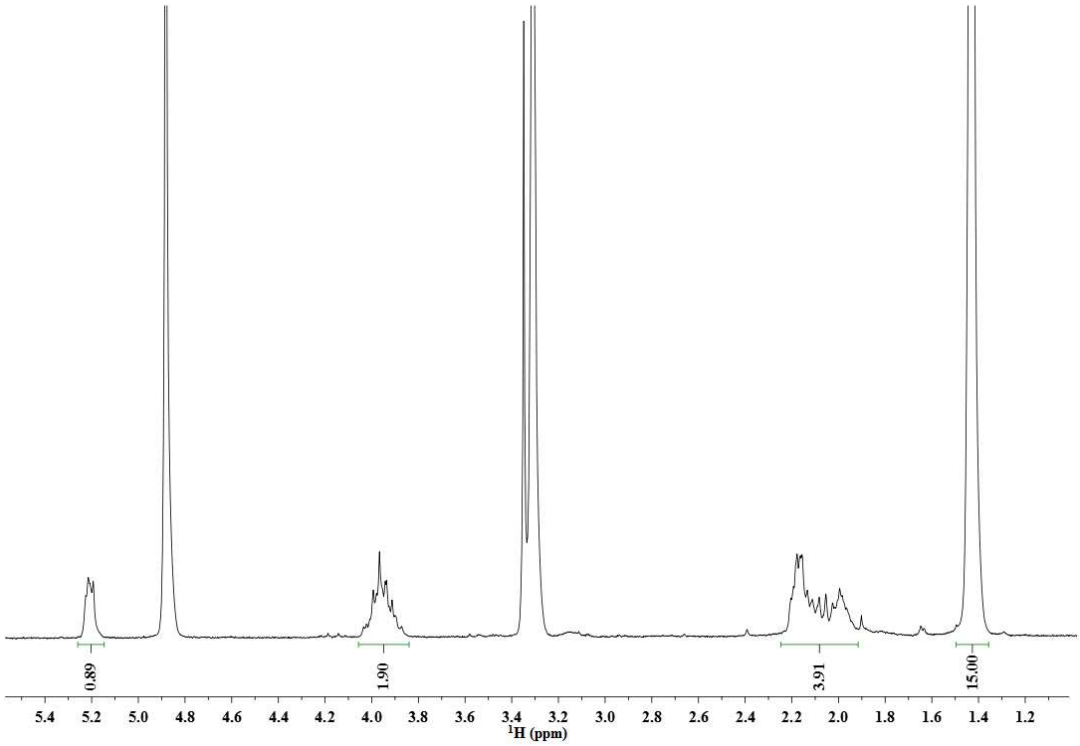

Figure 2.10: ^{1}H-NMR spectrum of the reaction between HProAibO*t*Bu and CS_2 in presence of base after 1/2h (expanded view of the alkyl region). Solvent: methanol-d_4; 300MHz.

Table 2.4: ^{1}H-NMR spectral data.

^{1}H-NMR		**HProAibOtBu**		**DTC^{-}-ProAibOtBu**	
		A	**δ (ppm)**	**A**	**δ (ppm)**
α-CH	Pro	1	3.70 m	1	5.21 m
β-CH_2 + γ-CH_2		2+2	2.18-1.80 m	2+2	2.25-1.85 m
δ-CH_2		2	3.05 m	2	3.97 m
α-$C(CH_3)_2$	Aib	6	1.41 s	6	1.43 s
O$C(CH_3)_3$		9	1.41 s	9	1.43 s

To obtain the IT03 complex, a methanol solution of one equivalent of K[Au(Br)$_4$] has been added dropwise to the obtained dithiocarbamate. The spectrum of the reaction crude, recorded in acetone-d_6, confirms the formation of the complex (**Figure 2.11**). A doublet is found for α-CH(Pro) (δ 5.04 ppm) together with a multiplet corresponding to δ-CH_2 (Pro) (δ 4.00 ppm). The two multiplets related to β-CH_2 (Pro) hydrogen nuclei are found at 2.60 and 2.35 ppm, respectively. Overlapped to this latter, the multiplet for γ-CH_2 (Pro) is found (δ2.30 ppm). Finally, the methyl groups are found at 1.43 ppm. After purification, an orange solid has been isolated and characterized by ^{1}H-NMR spectroscopy (**Figure 2.11**). Interestingly, upon the purification process (which is not carried out in inhert athmposphere) the spectrum of the purified compound seems to be more complicated. On the

basis of our previous studies, this is probably due the formation also in this case of a second minor species, already described for similar compound AuL23 in **Chapter 1**. The chemical shifts of this minor product suggest a similar structure for both the species as already reported.

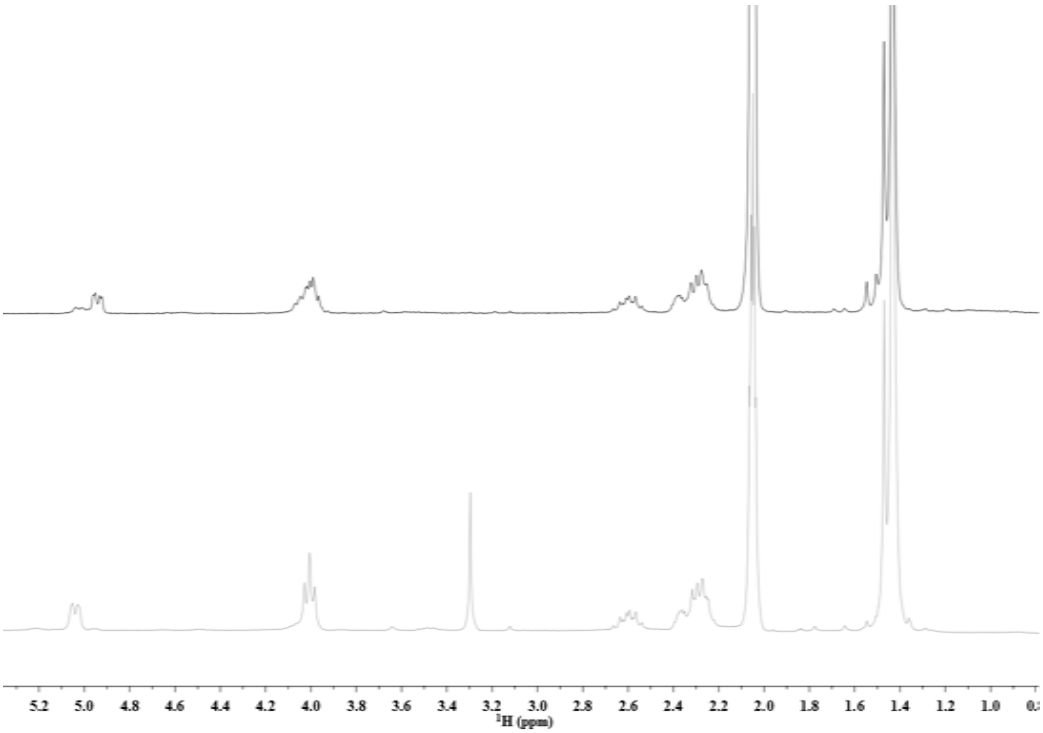

Figure 2.11: ^{1}H-NMR spectra comparison of the alkyl region for IT03 before (bottom) and after purification (top). Solvent: acetone-d_6; 300 MHz.

In fact, the similar chemical shift of the two sets of signals suggests the presence of a very similar coordination sphere for both the species. The differences between the two species affected also the α-CH_3 groups of Aib, which undergo a small downfield shift. ^{1}H-NMR investigations performed on the previous syntheses of IT03, obtained by means of the in water one pot methodology, revealed the same set of signals for the byproduct, which has been supposed to correspond to a dinuclear species of IT03.

The mixture has been purified by means of silica gel chromatography (DCM:EtOH 97:3) in order to isolate the desired complex. The final yield for IT03 is 61% (calculated on ligand).
Elemental analyses for this compound confirmed the purity of the isolated compound (**Table 2.5**).

Table 2.5: Elemental analysis data for mixed fraction.

IT03	**C (%)**		**H (%)**		**N (%)**		**S (%)**	
	calcd	found	calcd	found	calcd	found	calcd	found
$C_{14}H_{23}AuBr_2N_2O_3S_2$	24.43	24.41	3.37	3.30	4.07	4.03	9.32	9.1

In conclusion, a new methodology has been tested for the formation of dithiocarbamates aimed to the synthesis of Au(III) complexes suitable for antitumor therapy. Investigations on the secondary amine substrates employed were successful, exhibiting total conversion to dithiocarbamato derivative. In case of HCl·HProAibO*t*Bu, the synthesis of the related IT03 complex have been performed, obtaining higher yields as the whole substrate was available for the reaction. Interestingly, even though in the new methodology the metal precursor solution is added dropwise to the substrate (contrarily to the traditional method) the same gold-byproducts were produced after both the synthetic and purification pathways. Notwithstanding, using the reaction under anhydrous conditions allow an increase of final yield.

Chapter 3

Spectroscopic investigation of compounds' stability and reactivity in physiological-like conditions

To elucidate the pharmacological behavior of our compounds it is of crucial importance to better understand the possible modifications they can undergo in physiological conditions. Moreover, it could be of fundamental importance for the forthcoming pharmacokinetic studies, to predict if there can be an interaction or a stabilization in physiological medium by carrier proteins. Indeed, for the upcoming *in vivo* experiments, it could be significant to predict if the serum components can interfere with drugs activity and bioavailability, as a consequence of their well known binding properties which made them good transporters.

Among the gold(III) compounds under study, [$Au^{III}Br_2$(SSC-Sar-L-AlaO*t*Bu)] (IT01) was chosen as a model to investigate the behavior in different aqueous systems and in presence of putative protein carriers.

In particular, it is essential to analyze the interaction of serum albumins with our compounds, since they are the most abundant proteins in the circulatory system of a wide variety of organisms (30-50 $g{\cdot}L^{-1}$, in the human serum, 52-60% of plasma protein composition)[131].

The human serum albumin (HSA) is constituted by a single polypeptide chain having 585 amino acid residues, characterized by low tryptophan and high cystein content. Its secondary structure consists of 67% α-helix, 23% extended chains and 10% β-turns, having six turns and seventeen disulphide bridges. Under physiological conditions it assumes a heart-shaped three dimensional structure, with three homologous domains labeled as domains I-III. Each of these domains is further subdivided into two sub-domains (A and B), that consist of 4- and 6-helices, respectively. Conversely, more easily available bovine serum albumin (BSA) shares with HAS the 76% sequence homology, and is constituted by a single polypeptide chain of 583 amino acids residues, having molecular weight of 66 kDa. Like HAS, BSA also has seventeen disulphide bridges and one free -SH group (C34), which can be involved in the formation of a dimer. Both proteins show the presence of a Trp in the subdomain IIA (W214 for HSA and W212 for BSA). The fundamental difference between HSA and BSA consists mainly in an additional tryptophan residue (W135) located on the surface of the BSA protein[132].

Albumins play a fundamental role not only in the control of the osmotic blood pressure, but also in the transport of various endogenous compounds such as fatty acids, hormones, toxic metabolites (e.g.

bilirubin), bile acids, amino acids and metals. In recent years, human serum albumin (HSA) has been emerging as a reliable and versatile carrier for therapeutic and diagnostic agents, owing to its small size, flexibility and high abundance in the plasma[133].

Depending on their chemical properties, drugs can bound to HAS in the bloodstream, but in most cases only free drug molecules can interact with therapeutic targets to produce their therapeutic effect. Indeed, only the unbound molecules can passively diffuse through the barriers constituted by endothelial cells and tissue cells into organ tissue and undergo metabolism, biliary excretion or glomerular filtration in kidney, or be distributed intracellularly *via* specific transport systems (e.g. receptor-mediated endocytosis, protein-mediated transport)[134].

Any injected metal-based therapeutic is expected to have some kind of interaction with albumin. For many drugs and prodrugs it was demonstrated that the protein plays a crucial role in their stabilization and transport, modulating their bioavailability and toxicity[135]. Accordingly, without exception, also platinum-based drugs bind to HSA and such reactions may be related to the metabolism, effectiveness, and body distribution[136,137]. Indeed, the protein contains six methionine residues (i.e. Met-87, 123, 298, 329, 446, and 548) among which Met-298 is the most surface accessible and thus has been speculated to be the main cisplatin-binding site[138].

Considering the pharmacokinetic and pharmacological implications, the study of the interaction between the compounds and BSA become of great importance. This analysis was carried out combining different experimental techniques, as fluorescence and UV-Vis spectroscopy, together with CD analysis.

3.1 UV-Vis analysis of stability in physiological conditions

Since the compounds are not *per se* soluble in water, all the biological assays up to now were performed pre-dissolving the compounds in the minimum volume of DMSO before adding them to aqueous medium.

In this Chapter are in particular reported the results obtained for the compound IT01, that was chosen as a model for our gold(III)-peptidedithiocarbamato derivatives.

First of all, the stability of the compound in sole DMSO (used as stock solution) was evaluated. The compound was dissolved in the solvent at a final concentration of 50 μM, recording UV-Vis spectra at 25°C in the range 190-800 nm over 24h (**Figure 3.1**). In this solvent the complex shows three main absorption bands. The first two bands, hereafter called band I and band II, are assigned from the literature to intraligand $\pi^* \leftarrow \pi$ transitions (at nearly 260 and 310 nm) mainly located on the -NCS and -CSS moieties, respectively[93]. An intraligand $\pi^* \leftarrow n$ transition (where *n* is the in-plane non-bonding

sulfur orbital) is expected around 340 nm, but is not discernible because overlapped to higher intensity bands at very close wavelength. The third detectable band of weak intensity is rather found at higher wavelengths (around 370 nm), and is assigned to an electron transfer of the type $u \leftarrow g$, from a *4p* orbital (σ symmetry) of the bromide ligands to the lowest unfilled *5d* metal orbital (band III, **Table 3.1**).

No significant modification of neither the position of the bands and their intensity was detected over 24 h, confirming that the compound remains stable in this solvent. The only very slight variations registered are connected to the presence of water in the solvent, which increases over time. Indeed, upon water absorption by the system, partial hydrolysis of the complex takes place. The bromide ligands are thus substituted by one/two water molecules to form the corresponding aquo complex, which is still quite water soluble. This effect is also suggested by the slight shift in wavelength of the main two absorption bands, which move towards the band positions recorded for the complex in water (DMSO<5%).

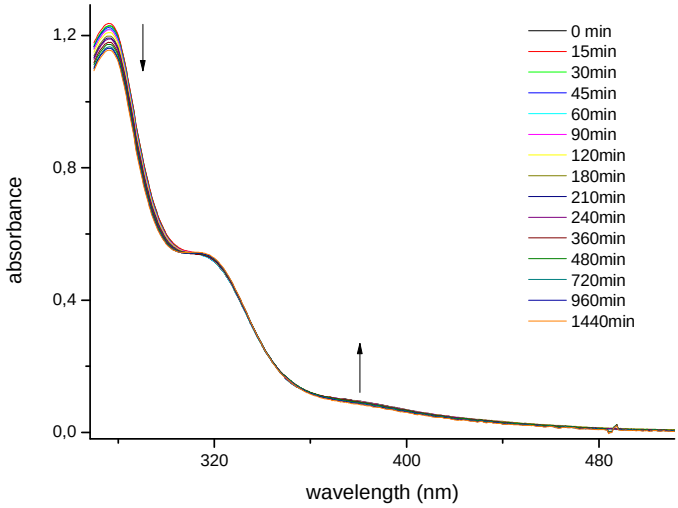

Figure 3.1: electronic spectra of IT01 (50 μM) in DMSO at 25°C for 24 h.

Moving to aqueous systems, the behavior in pure deionized water was first evaluated, confirming the tendency of the complex to undergo partial hydrolysis, with slow modifications over the first 24 h (**Figure 3.2**). The main absorption bands present opposite trends, with band I and band II undergoing a hypochromic and hyperchromic modifications with time, respectively. Simultaneously, a band at nearly 380 nm increases in intensity with time. All these variations have probably to be connected to the formation of the aquo-complex in solution. Anyway, after nearly 10 h, an hypochromic effect of all the absorption bands is detected, which can be correlated to the partial precipitation of the dihydroxo-complex (already described for other gold(III)-dithiocarbamato derivatives) which results

less water soluble than the corresponding aquo complex. The compound, which precipitates as a yellow powdery solid, was isolated and characterized by means of elemental analysis and FT-IR spectroscopy, allowing the identification of the hydroxo-derivative.

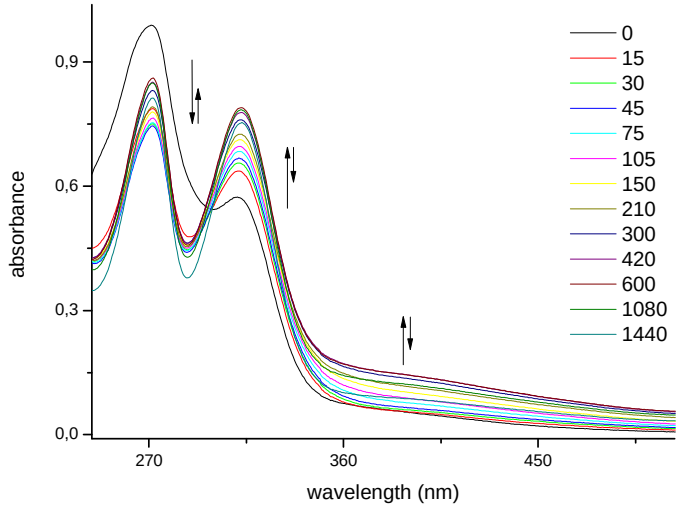

Figure 3.2: electronic spectra of IT01 (50 μM) in deionized water at 25°C for 24h.

The behavior of the complex IT01 in saline solution (0.9% NaCl), is slightly different with respect to what recorded in pure water (**Figure 3.3**). In this case an hyperchromic effect is registered for both band I and band II, along with the formation of a band at nearly 380 nm due to the coordination of aquo groups to the gold(III) metal center.

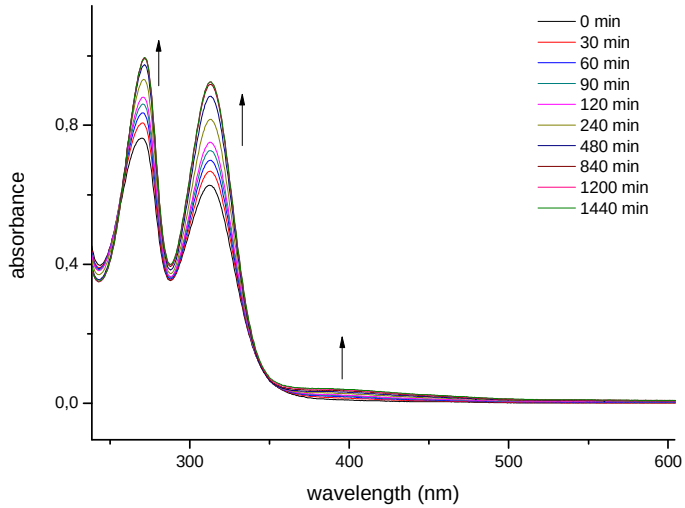

Figure 3.3: electronic spectra of IT01 (50 μM) in saline solution (NaCl 0.9%) at 25°C for 24h.

The hyperchromic effect recorded for both bands can be explained with the substitution of the bromine ligands with chlorines, as a consequence of the higher concentration of Cl^- ions in solution. Subsequently, the substitution of one/two chloride ligands with water molecules can lead to the formation of the aquo-derivative, as suggested by the appearance of an absorption band at 380 nm (metal-to-ligand charge transfer). In this case, however, no precipitates were detected in solution over 24h, suggesting that the hydroxo complex does not form until this time.

Otherwise, the behavior of IT01 in PBS (phosphate buffered solution) seems to be completely different (**Figure 3.4**). After only 4 h from dissolution, the complex undergoes fast hydrolysis, leading to the formation of the dihydroxo complex which precipitates as a yellow powdery solid. The process is accelereted with respect to the trend registered in pure deionized water. The more basic pH of the solution (buffered at 7.4) can favor the formation of the dihydroxo derivative, along with the presence of the phosphato ions, which can directly interact with the metal by coordination causing the precipitation of the corresponding phosphato-derivative.

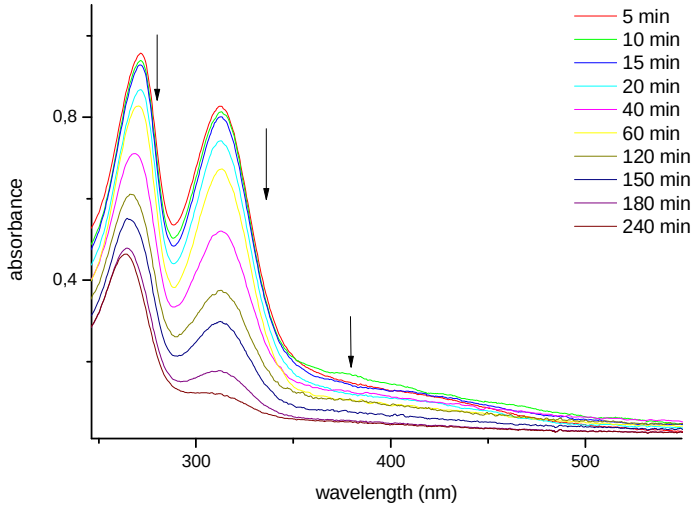

Figure 3.4: electronic spectra of IT01 (50 μM) in PBS buffer pH=7.4 at 25°C over 4 h.

Moving to more complex environments, the stability of the gold(III) complex in complete cell culture medium was analyzed. The electronic spectra, registered in presence of 20% complete medium (RPMI-1640 medium supplemented with 10% fetal calf serum) in PBS show two main absorption bands at 273 and 307 nm, both assignable to the IT01 complex (**Figure 3.5**). The main absorption band of the medium itself is otherwise present at 276 nm. The behavior of the complex in this environment is similar to that registered in PBS, even if the formation of a precipitate is not detectable in this case, probably as a consequence of the interaction with proteins or other medium components which lowers the rate of the hydroxo-derivative precipitation. Similarly to the previous

spectra, an intensity reduction of the bands related to the $\pi^* \leftarrow \pi$ transitions, is accompanied by an hyperchromic effect of the band at 362 nm, correlated to the formation of a gold-oxygen bond (as already described above).

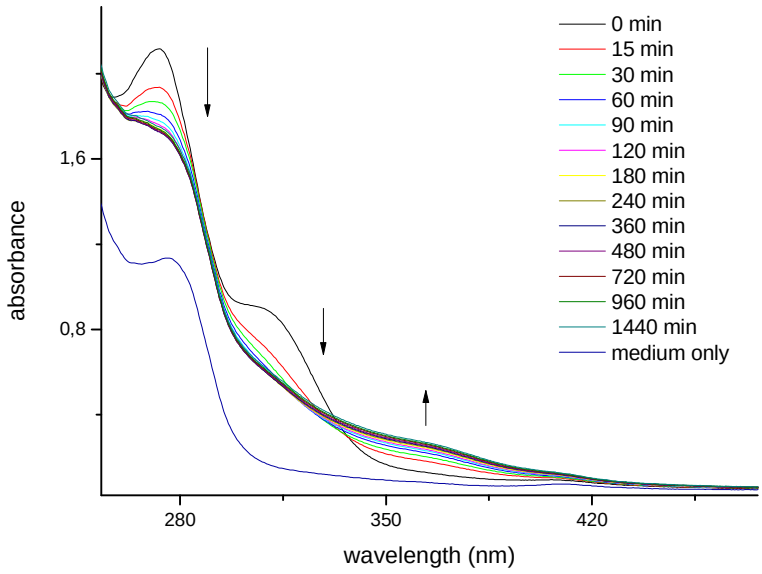

Figure 3.5: electronic spectra of IT01 (30 μM) in RPMI-1640 mod and FCS (10%) at 25°C for 24.

Table 3.1: main absorption bands wavelength (nm) in different solvents.

	λ_{max}/nm		
	Band I	Band II	Band III
DMSO	276	316	378
Bidistilled water	272	310	370
Saline solution 0.9% NaCl	261	312	--
PBS	262	313	375
Cell culture media + 10% bovine fetal serum	273	307	362

*λ_{max} determined soon after dissolution

3.2 Interaction with BSA

To analyze the possible interaction of the compound IT01 with BSA, different spectroscopic techniques were employed.

Firstly, the compound was incubated at equimolar ratio with BSA (30 μM), and electronic spectra were recorded over time. The UV-Vis spectrum of BSA is characterized by two main absorption bands at 198 and 280 nm, which correspond to $\pi^* \leftarrow \pi$ transition located on the peptide group and the aromatic ring aminoacids (Trp and Tyr), respectively.

In the UV-Vis spectra recorded soon after incubation, the main absorption bands previously described for IT01 are detected, with band I almost overlapping the BSA absorption band at 280 nm (**Figure 3.6**).

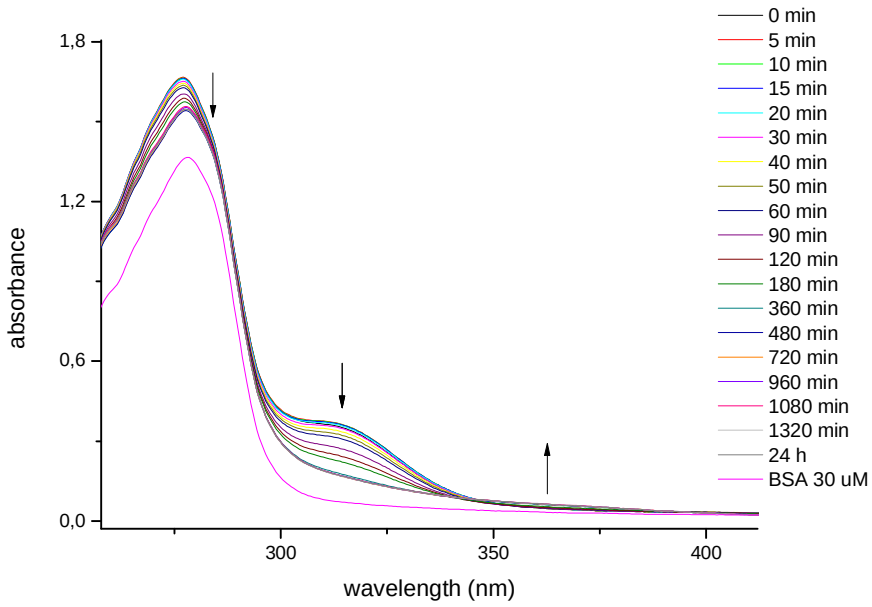

Figure 3.6: electronic spectrum of BSA and IT01 (equimolar, 30 μM) in PBS at 25°C over 24h.

Upon incubation with BSA, no stabilizing effect in reducing complex hydrolysis rate seems to take place, as an hypochromic effect of both band I and band II is recorded. This is accompanied by the the slight increase in the intensity of a band at 360 nm, probably due to the complex-protein interaction (through metal coordination) which can stabilize the hydrolized compound in solution preventing its precipitation.

The possible interaction with BSA was analyzed also by CD spectroscopy, to evaluate possible modification in protein secondary structure upon incubation with the complex. The interaction of equimolar quantities of each component (15 μM) in PBS solution (after dissolution of IT01 in DMSO; final DMSO concentration < 1.5%) was monitored over time showing only slight and not coherent variation in protein α-helix content (data not shown). Contrarily, the CD spectra recorded soon after incubation of IT01 with BSA (15 μM) at different molar ratios (**Figure 3.7**) showed variations in the protein secondary structure which were significant only at IT01:BSA molar ratio of 1 or higher. These modifications can be correlated with more extended conformation, or to an increase in β-sheet or random contributions to the structure. Anyway, this behavior is detectable only at high complex concentrations (with respect to BSA) that are far from the physiological-like conditions.

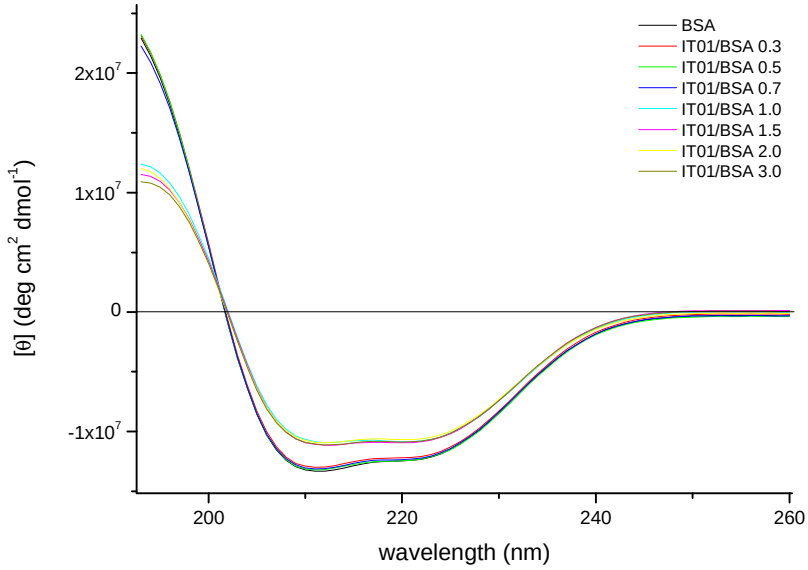

Figure 3.7: CD spectra of IT01 incubated with IT01 at different molar ratios (from 0 to 3) in PBS at 25°C.

Further studies, aimed at elucidating the result obtained with the CD experiments, were performed recording fluorescence spectra at constant temperature (25°C) in the same time ranges and concentrations used in the CD experiments above reported.

It is known that the intrinsic fluorescence of BSA derives from two tryptophan (Trp) residues per chain which are known to be excellent fluorogenic structural probes. They are characterized by strong emission signals at room temperature, and are very sensitive to the local microenvironment. The first residue is buried inside the protein where it is sheltered from energy loss or fluorescence quenching, thus resulting in increased fluorescence quantum yield. The second one is located on protein surface. The change in either fluorescence intensity or emission band position can be correlated to a modification of the two Trp environmental polarity or rigidity and consequently to the protein modifications.

This intrinsic fluorescence can be quenched by a variety of molecules and the mechanism may be either through static or dynamic quenching[139]. Static quenching refers to quenching through fluorophore-quencher complex formation, and dynamic quenching refers to a process where the fluorophore and the quencher come into contact during the transient existence of the excited state.

In the first experiment the molar ratio between protein and IT01 was kept constant (1:1; 15 μM), and the fluorescence spectra were recorded at different times, starting from incubation, over 24 h.

As we can see from **Figure 3.8-3.9**, there is a progressive quenching of BSA fluorescence intensity with time. The quenching phenomena may account for a direct interaction of the metal compound with the protein fluorophores or for an increasing amount of endogenous quenchers such as water

molecules or oxygen approaching the site of fluorescence. In the recorded spectra, only slight modifications in the fluorescence intensity of the emission bands are recorded, but the position of the emission bands are not affected, thus suggesting that no changes in the polarity of the Trp sites take place.

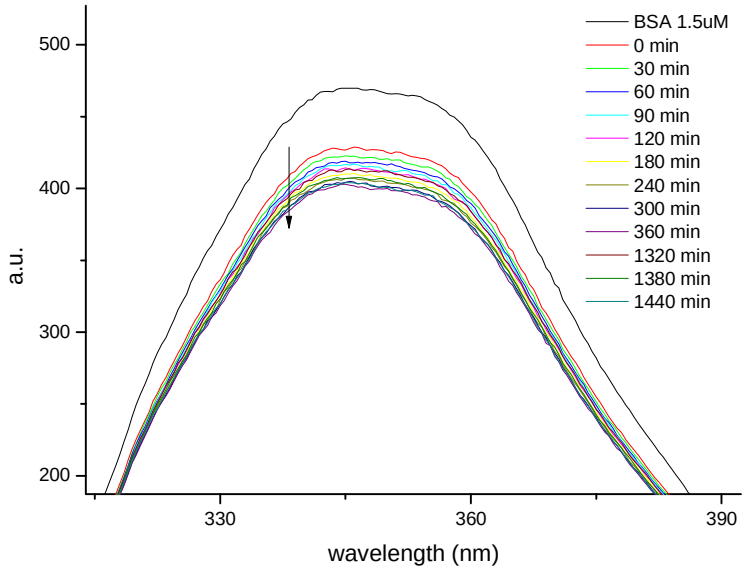

Figure 3.8: fluorescence spectra of BSA (1.5 μM) in presence of IT01 (1.5 μM) in PBS at 25°C over 24h.

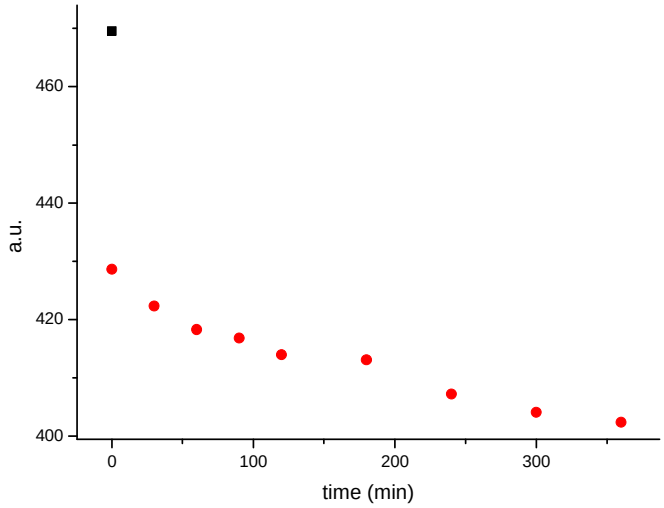

Figure 3.9: intensity fluorescence at the λ_{em} maximum (349 nm) of BSA (alone, ■) incubated with IT01 as a function of time (●, 0-6h)

The same exeriment was repeated changing the molar ratio of BSA and IT01, and recording the fluorescence spectra soon after incubation at the constant temperature of 25°C (**Figure 3.10**). In this

case it was detected a decrease in the fluorescence intensity that was proportional to the increase of IT01/BSA molar ratio (the DMSO content was kept constant for each sample).

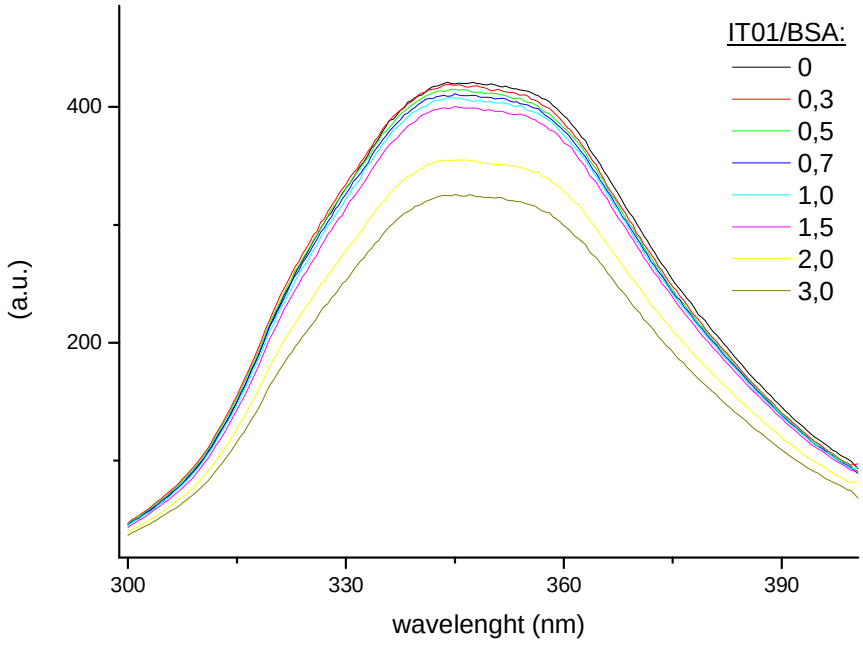

Figure 3.10: fluorescence spectra of BSA (1.5 μM) in presence of IT01 at different molar ratios (from 0 to 3) soon after mixing, in PBS at 25°C.

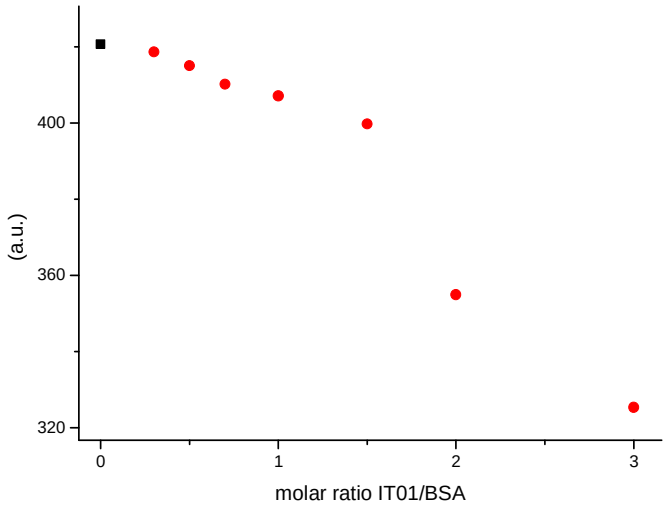

Figure 3.11: intensity fluorescence at the λ_{em} maximum (349 nm) of BSA (alone, ■) and incubated with IT01 at different IT01/BSA molar ratios (From 0.3 to 3; ●)

The decrease in fluorescence intensity may be correlated either to the direct interaction of Trp134/213 with the metal based compound, or to interactions with other sites of the protein which can modify the overall BSA structure. In fact, as before stated, each fluorophore may undergo a small structural change upon interaction of the complex with different sites of the protein, resulting in a different local environment at molecular level and thereby justifying the decrease of the quantum yield.

From the analysis of the spectra reported in **Figure 3.10**, it is evident that only slight modifications are recorded for IT01:BSA molar ratios equal or lower than 1, suggesting that only weak interaction take place between the gold(III) complex and the protein.

To sum up, the stability of the model compound IT01 was firstly evaluated under physiological-like conditions, to analyze their reactivity for the subsequent biological tests. It was shown that the compound (previously solubilized in DMSO) behaves differently depending on the conditions used. Indeed, it was shown that the compound undergoes hydrolysis both in pure water and in saline solution, by exchanging the bromido ligands with water molecules.

Conversely, upon dissolution in PBS, rapid formation of the hydroxo-derivative (not water-soluble) was detected. The precipitation of a yellow powdery compound was connected to the precipitation of the dihydroxo derivative or either to the formation of the corresponding gold(III)-phosphato compound, formed by the coordination of the phosphato anion to the metal center.

Anyway, when considering the cell culture medium, the precipitation of the hydroxo-derivative is likely reduced, probably thanks to the interaction of the compound with biomolecules and proteins present in the medium.

This behaviour reflected the results recorded for the interaction of the gold(III) compound with BSA in PBS. Considering the informations collected from the CD and fluorescence analysis, it can be concluded that IT01 does not significantly modify the secondary structure of the protein when incubated at low molar ratio (representative of the physiological-like condition). The slight modifications in the overall secondary structure might be due to weak secondary interaction with the complex, which can account for slight stabilizing effect that make BSA, almost in principle, a possible carrier for our compounds *in vivo*.

Chapter 4.

Evaluation of the *in vitro* and *in vivo* antiproliferative activity, and *ex vivo* toxicological effects

As reported in the Introduction, "first generation" complexes were already tested for their anticancer activity both *in vitro* and *in vivo*, showing outstanding antiproliferative properties.

In this work we carried out the screening for the newly synthesized compounds IT01-IT05 (belonging to the "second generation" of gold(III)-peptidedithiocarbamato derivatives). Firstly, they were tested *in vitro* for their cytotoxic activity toward different human cancer cell lines. Subsequently, the compounds were tested on MDA-MB-231 human breast cancer xenografts, to check their capability to induce tumor growth inhibition in mice.

The toxicity of selected compounds representatives of the "first" and "second generation" complexes was also assayed, comparing the obtained results to the reference drug cisplatin. Finally, the complexes were tested *ex vivo* on rat tissues of different organs (liver, colon and kidney) excised from healthy animals, in order to preliminary determine their toxicological profile without using living animals during the compounds' administration. These experiments were performed at the Groningen Research Institute of Pharmacy of the University of Groningen (Groningen, The Netherlands) under the supervision of Prof. A. Casini.

Experimental

Cell lines and culture conditions

Human non-small cell lung carcicoma A549 cells, human embryonic kidney HEK cells and human breast adenocarcinoma MCF-7 cells (*ATCC*) were cultured in DMEM (Dulbecco's Modified Eagle Medium, *Life Technologies*), while human ovarian cancer A2780 cells, A2780cisR (A2780 cells made resistant to cisplatin), human large cell lung cancer H460 cells and non-small cell lung cancer H1975 cells (*ATCC*) were grown in RPMI-1640 (Roswell Park Memorial Institute, *Sigma Aldrich*). Human breast cancer

MDA-MB-231 cells (*ATCC*) were instead grown in DMEM/F12 1:1 medium enriched with 1 mM sodium pyruvate and 10 mM HEPES. Each media was further supplemented with 10% Fetal Calf Serum (FCS) and 1% penicillin and streptomycin (*Invitrogen*). Cells were incubated at 37°C in the presence of 5% CO_2 and moisture-enriched atmosphere.

***In vitro* cytotoxicity**

Cells were seeded at a concentration between 3.0-5.0 x 10^4 cell mL^{-1} (depending on cell line) in either 96-well flat-bottomed microplates or 24-well culture plates, and incubated in standard conditions for 24h to allow cells adhesion. Afterwards, the medium was discarded and replaced with fresh new medium containing the test compounds at different concentrations. Gold(III) derivatives were previously dissolved in DMSO and added to each well at a maximum final DMSO concentration of 1%. Otherwise, cisplatin (*Sigma-Aldrich*), micellar and vesicular formulations of the gold(III) complexes were dissolved in saline solution (0.9% NaCl). Cells were incubated with the compounds for either 24 or 72 h (depending on the experiment) and the induced cell growth inhibition was assayed by MTT or by Trypan Blue Exclusion assay. The final GI_{50} (μM) (*i.e.* concentration of the test compound that induce a reduction of cells viability equal to 50%) were calculated from data collected from almost three independent experiments.

Human breast xenograft tumor experiments

Seven-week-old Female athymic nude mice were purchased from Harlan Laboratories (Horst, The Netherlands) and housed in accordance with protocols approved by the ethical committee of University of Groningen. Human breast cancer MDA-MB-231 cells suspended in 0.1 mL of serum-free DMEM/F12 cell growth medium were inoculated subcutaneously (*s.c.*) into the right flank of each mouse. When tumors reached sizes of around 115 mm^3, the mice were randomly allocated in three groups of seven mice per group, and treated by daily *s.c.* injection of either vehicle [1:1:1 v/v PBS, DMSO, Cremophore/ethanol (1:4)] or medium containing 1.0 mg/kg of IT03. Tumor length (L) and width (W) were measured every other day using a caliper, and tumor volumes were evaluated according to the standard formula $(\pi \cdot L \cdot W^2)/6$. Mouse weights were monitored twice a week. Mice were sacrificed after 27 days of treatment when control tumors reached ~ 1,800 mm^3. The tumors were collected and weighed.

Toxicity studies on animals

Male Wistar (HsdCpb:WU) rats were purchased from Harlan (Horst, The Netherlands). Rats were housed in a temperature- and humidity-controlled room on 12h light/dark cycle with food (Harlan Chow no. 2018 or standard RMH Chow, *Hope Farms, Woerden, The Netherlands*) and tap water *ad libitum.* All the experiments were conducted with the approval of the Ethical Committee of the University of Groningen (NL).

Preparation of precision-cut colon, liver and kidney rat slices

Krebs-Henseleit buffer (KHB), 3% agarose solution and University of Winsconsin organ preservation solution (UW) were prepared as described elsewhere[140].

After influxing the rats with isofurane/N_2/O_2 anesthesia, the liver and colon of the animal were excised and conserved in oxygenated ice-cold UW solution. Liver and kidney cores of 8 mm diameter were obtained using a mechanical drill (*Metabo*), while colon was excised in ca. 2 cm long pieces, washed with UW solution and filled with agarose. The cores obtained from each organ were than fitted in supports and sliced with a Krumdieck tissue slicer (*ARD*), obtaining slices of ca. 300 µm and 10-15 mg for liver and kidney, and 300 µm and 2 mg for colon.

Liver and kidney slices were preincubated for 1h in 12-well plates containing 1 mL/well of WME (*Williams Medium E, Invitrogen*) enriched with D-glucose (2.75 $mg \cdot mL^{-1}$) and gentamicine (50 $mg\ ml^{-1}$). The slices were then transferred to 12-well plate containing the compounds at different concentration dissolved in complete medium, and incubated for 24 h. Control slices were collected soon after slicing, after 1 h preincubation and after 24 h incubation in complete medium only.

Colon slices were directly incubated after slicing for 5 h in medium containing the test compounds at different concentrations. In addition to D-glucose and gentamicine, as previously reported, also amphotericine B (250 $\mu g\ ml^{-1}$) was added to WME. Control samples for colon were collected both after slicing and after 5 h incubation in sole complete medium.

Each sample was quickly frozen in 1 mL Sonop solution[140], and stored at -80°C.

ATP determination assay

ATP content of the samples was determined using the *ATP Bioluminescence Assay Kit CLS II* (*Roche*), following producer instructions. The slices stored in 1 mL Sonop solution were homogenized with a Minibeadbeater (*BioSpect Products*) for 45 seconds after

addition of glass beads, and the homogenates were centrifuged for 2 min at 4°C and 13000 rpm. All the samples were stored in melting ice during all the procedure. For each sample 5 µL of supernatant solution were diluted in a 96-well black plate with 45 µL of 100 mM Tris-HCl buffer containing EDTA (2 mM). Different dilutions of an ATP standard solution in Tris/EDTA buffer were prepared for calibration, and ATP content was determined reading the luminescence of each sample after addition of 50 µL/well of Luciferase reagent (*Roche*). Each sample of the assay was prepared in duplicate, and final ATP content expressed in ($nmol \cdot ml^{-1}$).

Protein determination assay

The protein content of each sample was determined using the *BIO-rad DC Protein Assay* based on Lowry method (*BIO-rad*), following the manufacturer's protocol. The homogenized samples prepared for the ATP determination were dried overnight and incubated with 200 µL of 5N NaOH at 37°C in shaking water bath. After dilution with 800 µL milliQ water, the samples where homogenized again with a Minibeadbeater (*BioSpect Products*) for 40 s. Calibration curve was prepared using different dilution of a BSA standard solution, at final concentrations between 0 and 1,2 $mg \cdot mL^{-1}$. The samples or either the standards were then added to a 96-well clear plate, together with 25 µL of reagent A and 200µL of reagent B *(BIO-rad DC Protein assay)*. The plate was gently shaken for 1 min and, after 15 min of incubation in the dark at r.t., the absorbance at 650 nm was read with a ThermoMax Microplate Reader (*Molecular Devices*). The protein content of each sample was calculated on the bases of the calibration curve made with BSA, and expressed as concentration of $mg \cdot mL^{-1}$.

Results and discussion

4.1 *In vitro* cytotoxic activity on human cancer cells

The compounds were tested on a broad panel of cancer cells to assess their cytotoxic activity on different tumor types. The GI_{50} values were calculated for each compound after 72h incubation, and the number of viable cells was evaluated by MTT test (or Trypan Blue Exclusion assay, were indicated). The results are summarized in **Table 4.1**.

All gold(III) complexes belonging to the "second generation" of compounds show quite a similar activity on the same cell lines, with the exception of IT05 on MCF-7 and H1975,

which seems to be less effective than the other compounds of the series. These results can be probably connected to their different solubility and steric hindrance properties (due to the presence of either -TEG or -O*t*Bu functions).

Among the tested complexes, IT03 and IT04 resulted the most active with GI_{50} values comparable to the antiprolferative data recorded for cisplatin on the same cell line.

In particular, the tested compounds present higher cytotoxic activity towards A2780 cell line, with GI_{50} values lower than 0.50 µM, 10 times more effective than cisplatin.

Good results were obtained also on H1975 cells, with GI_{50} in the submicromolar range. The cytotoxicity of the compounds on breast adenocarcinoma MCF-7 cells seems to be promising as well, with GI_{50} values 5-fold higher than that obtained after cisplatin treatment.

Generally, even if comparable, their antiproliferative activity resulted slightly lower to the "first generation" compound AuL12 on all the cell lines tested.

Table 4.1: GI_{50} ± st.dev. (µM) on A549 (human non-small cell lung carcinoma), HEK (human embryonic kidney) and MCF-7 (human breast cancer), A2780 (human ovarian carcinoma cells) H1975 (human non-small cell lung cancer) and H460 (human large cell lung carcinoma), A431 (human epidermoid carcinoma) cells calculated after incubation for 72 h for the compounds IT01, IT02, IT03, IT04, IT05, AUL12 or cisplatin. Viable cells were determined via MTT test or via Trypan Blue dye exclusion method.

	GI_{50}±st.dev. (µM)						
	IT01	**IT02**	**IT03**	**IT04**	**IT05**	**AUL12**	***Cisplatin***
A549	20.04±2.80	26.62±3.20	10.28±3.31	9.06±2.14	13.5±1.56	12.27±1.62	8.00±0.50
HEK	5.88±1.44	4.17±1.25	7.07±2.58	4.52±1.03	5.20±0.69	2.85±0.95	11.00±2.90
MCF-7	3.44±0.93	4.30±0.80	4.00±0.70	3.2±1.6	8.50±0.85	6.40±0.70	20.00±3.00
A2780	0.59±0.16	0.32±0.17	0.44±0.11	0.21±0.12	0.46±010	0.40±0.08	5.20±1.90
H1975 [a]	0.56±0.13	0.57±0.19	0.71±0.10	0.66±0.06	5.78±1.30	0.158±0.008	0.99±0.09
H460 [a]	3.83±2.13	3.38±0.40	3.63±0.51	2.99±0.64	4.25±0.22	2.15±0.260	0.76±0.11
A431 [a]	16,10±3,90	14,01±2,52	8,37±2,57	10,07±1,91	13,51±2,62	9,59 ± 2,53	3,22± 0,50

[a]values calculated with Trypan Blue dye exclusion method.

Moreover, the cytotoxic activity of the compounds IT03 and IT04 was determined after 24 h incubation on large cell lung cancer H460 cells, to analyze the GI_{50} time-dependence. Interestingly, the obtained values (**Table 4.2**) highlight how the complexes are able to exert a cytotoxic effect already after shorter incubation times. Cisplatin, on the contrary, normally induces good inhibitory effects on cells proliferation only for incubation times of 72 h (data not shown).

Table 4.2: comparison between cytotoxicity values calculated on H460 cells after 24 h and 72 h incubation with IT03 and IT04.

	IC_{50} ± st.dev. (μM) on H460 cells	
	24 h	72 h
IT03	10,45 ± 3,97	3,63 ± 0,51
IT04	10,01±3,08	2,99±0,64

Generally, the compounds differing only for the stereochemical configuration (D, L entantiomers) of the second aminoacid of the dipeptide ligand, show similar cytotoxic activity. This highlights that probably there is no correlation between the stereochemical features of the compounds and their cytotoxic activity and/or transporter recognition. In particular this is evident on A549 cells, known to overexpress PEPT2 transporter. Both IT01 and IT02 (similarly to IT03 and IT04) exert the same cytotoxic activity on this cell line, even if, almost in principle, the transporters would be more selective in the L-isomer recognition.

Nevertheless, the selectivity for L-configuration derivatives is recognized for naturally occuring aminoacids or oligopoetides, but since PEPTs are responsible also for the transport of peptido-mimetics which resemble the main features of their physiological substrates, it is possible that similar recognition occurs for both the gold(III) isomers, despite their chirality.

Anyway, deeper studies about the overexpression of PEPTs by selected cell lines will be performed to analyze if differences in the internalization rates the two gold(III) configurational isomers can be detected.

4.2 Preliminary *in vivo* studies

Preliminary studies on human xenografts were performed to determine the capability of a selected compound IT03 to induce tumor growth inhibition in *in vivo* conditions. The compound was in particular tested towards a breast cancer cell line MDA-MB-231, which is known to be highly metastatic and invasive.

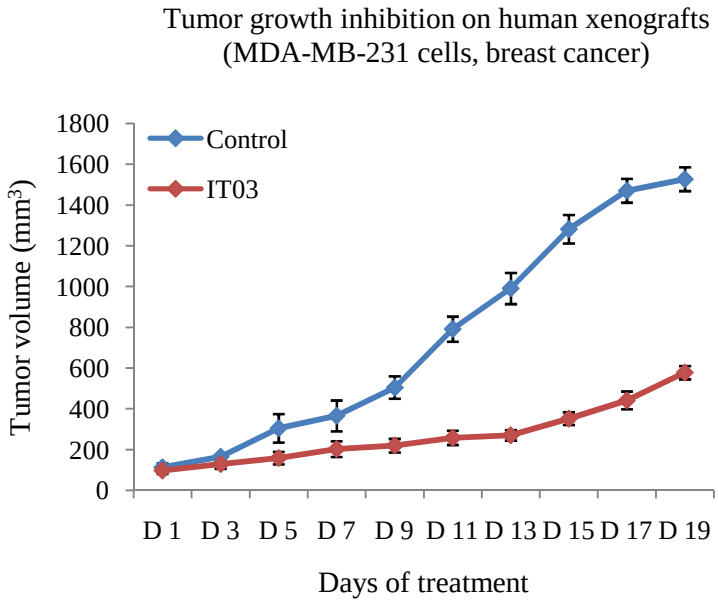

Figure 4.2: tumor growth inhibition on human xenografts treated with IT03 with respect to the controls treated only with vehicle.

In vitro tests on the MDA-MB-231 cells were preliminarily done to determine the cytotoxicity of the compound on this tumor cell type. After 24h incubation of cells with different concentrations of IT03, MTT test was performed to calculate cell viability, obtaining a GI_{50} value of 10.3±0.7 μM.

The *in vivo* experiment was performed on athymic nude mice inoculated subcutaneously with human breast cancer cells MDA-MB-231, and then treated with 1 $mg \cdot kg^{-1}$ of IT03 every day.

The tumor volume was measured every other day both in control animals and in treated animals. As we can see from **Figure 4.2**, the tumor growth in the mice administered with IT03 is inhibited by almost 60% after 19 days of treatment, without any evident sign of suffering or weight loss in the animals administered with the gold compound.

4.3 *Ex vivo* studies

Figura 4.1: *upper part***:** procedure adopted to obtain liver cores (a-b) and liver slices (c-f), that are subsequently incubated with different test compounds for toxicological studies (a-g); *lower part*: preparation of colon cores (a-j) and obtainment of colon cores (h-j) suitable for slicing (k-l).

The toxicity of selected complexes was tested on different organ tissues exploiting *ex vivo* experiments that consist in the incubation of drugs or other compounds with small slices of tissue derived from organs excised from healthy rat. This method allows the study of drug metabolism and toxicity in intact tissues, with great advantages with respect to both *in vitro* cell culture and *in vivo* animal testing. The use of slices permit to reduce the number of animals used for the experiments, since a large number of slices can be obtained from the same organ (about 80–100 slices 8 mm thick or 200–250 slices 5 mm thick can be obtained from 10 g of rat liver), allowing the testing of more than one compound at different concentrations in parallel. Moreover, although being an *in vitro* experiment, it has the advantage of using intact tissues where enzyme systems, cofactors and transporters are present in their physiological levels, resulting in a reliable model for the *in vivo* conditions[141]. The slices used in the experiments are easy to prepare and to process and can be obtained (with slight modifications of the method) from a large variety of different organs as liver, intestine, kidney and lungs.

From the *in vitro* tests carried out on different cancer cell lines, it emerged that the compound IT03 was one of the most promising for its antiproliferative activity on all the tested cell lines, and was thus selected for the *ex vivo* toxicity experiments.

The toxicity of IT03 on healthy tissues was preliminarily determined on rat liver and colon slices, since these two organs are generally mainly involved in drug metabolism. Afterwards, toxicity of the compounds on kidneys was also tested, since they are usually

strongly affected by cisplatin treatment. The slices, characterized by both similar size and weight, were freshly prepared on the day of the experiment from excised organs[140].

Cylindrical liver and kidney cores were cut from each organ with the use of a mechanic drill (for liver) or manual cutter (for kidney), while intestine was first washed and flushed with UW solution and then filled with 3% solution of agarose, in order to obtain cylindrical sections with dimensions comparable to those obtained for the liver (**Figure 4.1**). Both cores were subsequently sliced with a Krumdieck tissue slicer (*ARD*), adjusting knife speed and position to obtain slices with the final desired characteristics.

Previous studies were aimed at establishing the viability of incubated slices as a function of time, so to assess the best incubation times for each experiment type. Since the slices are obtained from normal tissues with no further modification, their viability with time decreases fast, with rates depending on tissue type.

It was found that soon after slicing the ATP content is low, with values depending on the time they are preserved cold, and it rises again to higher viability values after 1 to 3 h incubation in medium at 37°C. For liver and kidney slices it was noticed that ATP level remains in the range between 10-12 $nmol \cdot mg^{-1}$ for almost 72 h. Thus, after slicing, 1h preincubation in WME is necessary to allow viability recover and to eliminate debris and other residues from the tissue before the experiment.

The viability of colon slices decreased faster with respect to liver and kidney (with ATP values that go from 3-4 $nmol \cdot mg^{-1}$ to about 1 $nmol \cdot mg^{-1}$ after only 24 h), so the experiments should be carried out during the first 8 hours following the slicing. Unlikely from liver and kidney, colon slices should be stored in ice cold KHB instead of UW solution which allow a better preservation, and no preincubation is needed before starting the experiment.

The viability after incubation with the test compounds was thus evaluated after 24 h for liver and kidney slices, and after 5 h for colon slices. These times were chosen as the best compromise for the determination of possible toxic effects of the compounds on tissues while maintaining constant the viability of non treated slices.

The viability was expressed as a function of their ATP levels, with values normalized by their total protein content to eliminate the differences deriving from slices of different weight and dimensions.

The compounds to test were previously dissolved in DMSO, and then diluted in complete medium to the desired final concentrations ranging from 1 to 100 µM (final DMSO content. < 1%).

In each experiment, control samples were also incubated with medium containing the maximum concentration of DMSO, so to determine any intrinsic toxic effect of the solvent on the slices. On none of the organ tissues the concentration of DMSO added to the samples resulted toxic, with values of tissue viability comparable to the control samples incubated with sole medium.

Each experiment was performed almost in triplicate and the viability of each slice was expressed in terms of moles of ATP per grams of protein, while the toxicity was expressed in terms of TC_{50} values (toxic concentration, defined as the concentration of compound that decreases viability of the slices by 50%).

Table 4.3: TC_{50} and st.dev. for IT03, AUL12 and cisplatin on liver, colon and kidney slices.

Organ	$TC_{50\pm}$st.dev. (µM)		
	IT03	**AuL12**	**Cisplatin**
Liver	36.6±7.1	43.5±6.4	16.92±8.7
Colon	38.3±8.7	51.1±10.2	>100
Kidney	42.6±9.2	52.6±8.8	39.1±3.7

As we can see from the values calculated in **Table 4.3**, the toxicity of compound IT03 on liver, colon and kidney is quite similar, with 36.6, 38.3 and 42.6 µM respectively. The standard deviations for the mean values of toxicity are sometimes quite high, but we have to take in account the great different responses that may arise from the individuality of the treated animals with the same compound.

The toxicity values determined for AuL12 on the same tissues are quite similar, but they result in both cases less toxic than the reference drug cisplatin. Only exception is colon, where cisplatin seems to be much less toxic than the gold(III) dithiocarbamato complexes screened.

The toxicity values measured on colon slices resulted comparable to those detected in the other organs, even if shorter incubation times were adopted in these sets of experiments.

The values of TC_{50} obtained for the gold(III) compounds on the other organs were anyway improved, even if slightly, when compared to cisplatin. This is more evident in

particular on liver, where IT03 displays a toxicity that is 50% lesser with respect to cisplatin treatment.

From the results reported in this Chapter we can conclude that the newly synthesized compounds show outstanding antiproliferative activity on all the tested human cancer cell lines, proving to be particularly promising towards the ovarian cancer cell line A270 and breast cancer cell line MCF-7. Their antiproliferative activity was confirmed *in vivo,* by the preliminary experiment on the breast cancer cell line MDA-MB-231 inoculated into immunodepressed mice. After only 19 days of treatment the reduction of the tumor mass was about 60%, with no evident signs of suffering detected in the animals.

Subsequently IT03, choosen as a model for the "second generation" compounds, was tested *ex vivo* on precision-cut slices of different organs to determine its toxicity, in comparison with AuL12 and the reference drug cisplatin.

The results highlighted how the two gold(III) compounds have similar toxicity on the tissues tested (liver, kidney and colon), resulting less toxic than cisplatin in particular on liver.

Chapter 5

Targeting and delivering of gold(III) complexes through the encapsulation into vesicular and micellar systems

As previously assessed, our gold(III) dithiocarbamato complexes were proved to be very promising for their biological activity as antiproliferative agents, but are characterized by very low water solubility. Indeed, they dissolve in isotonic saline solution to a lesser extent than cisplatin, which is clinically *i.v.* administered in the presence of sugars, such as mannitol and dextrose[142], to improve its solubility.

Efficient carriers can be thus used to enhnce the properties of drugs which exhibit poor solubility, undesired pharmakokinetics and low stability in physiological environment, furthermore increasing their circulation times[143].

For the delivery of our gold(III) dithiocarbamato complexes we explored different approaches, based on the encapsulation in supramolecular aggregates. This allowed to avoid the use of organic solvents, normally exploited to solubilize the compounds for the biological tests, excluding additive toxic effects.

In particular, the internalization of our gold(III) complexes was carried out in either micellar or vesicular systems to improve both their solubility and their bioavailability in physiological conditions. Moreover, micellar functionalization with a targeting moiety, as the cholecystokinin octapeptide CCK8, was performed to obtain tumor-selective delivery, thus further improving the chemotherapeutic index of our compounds (which is defined as the ratio between the lethal dose (LD_{50}) and the effective dose (ED_{50}) of a drug).

An important feature to consider when selecting nanocarriers for drug delivery are the dimensions of the aggregates, since variations in the nanoscale range strongly affect blood circulation times and the bioavailability of the particles within the body[144].

In particular, it was proved that the encapsulation of drugs in micelles can diminish their extravasation into normal tissues and provide for a passive drug targeting to tumors *via* the enhanced permeability and retention (EPR) effect[145]. Indeed, being unable to penetrate through tight endothelial junctions of normal blood vessels, the concentration of the drug-loaded systems can build up in the plasma increasing their half-lifes. More importantly, they can selectively extravasate in tumor tissues due to their abnormal vascular nature and escape renal clearance. Overtime the tumor concentration of drug will

increase reaching values several-folds higher than those found in the plasma, due to lack of efficient lymphatic drainage in solid tumor, thus becoming an ideal application for EPR-based selective anticancer nanotherapy[146].

For pharmaceutical applications, the preferred size range goes from 10 to 100 nm. Particles ranging from 10 to 70 nm in particular, are known to offer effective distribution in certain tissues and are preferred to obtain faster drainage from the site of injection[147,148]. Particles smaller than 100 nm can also be accommodated in endocytotic vesicles, allowing the entrance into target cells *via* endocytosis[149]. Particles going from 70 to 200 nm demonstrate the most prolonged circulation times[150]. However, the use of particles with higher diameters, likely more than 200 nm, are not recommended since they are frequently sequestered by the spleen as a result of mechanical filtration[151], followed by eventual removal by the phagocyte system of the cells. On the other hand, small particles with diameters less than 5-10 nm are rapidly removed through extravasation and renal clearance[144].

The polymer-based nanotechnology is becoming one of the most attractive and fast growing area of the pharmaceutical research. The main nanoscale sized materials which are used as delivery agents for not water soluble compounds are polymeric micelles, polymer-DNA complexes ("polyplexes"), nanogels and liposomes, and are commonly referred to as nanomedicines[145]. These polymeric molecules can be thus specifically arranged to efficiently and safely deliver drugs, genes, antigenes and imaging molecules[143].

For the delivery of our gold(III)-dithiocarbamato complexes two different types of dispersing systems were employed; the first is based on the self-assembly of DPPC (dipalmitoylphosphatidylcholine) molecules to form vesicular structures, the second exploits the formation of micellar structures based on the aggregation of the Pluronic F127 amphiphilic polymer.

DPPC vesicles

The first dispersant system was chosen among the class of lipid nanosystems which, because of their high degree of biocompatibility, have been used to improve the pharmacological profiles of various anticancer drugs, otherwise discarded because of their low water solubility, poor bioavailability or either rapid biotransformation.

Liposomes are synthetic phospholipid vesicles with sizes ranging from approximately 50 to 1,000 nm that can be loaded with a variety of drugs[152]. As for micelles, liposomes used for delivery purposes have several advantageous properties such as biocompatibility, biodegradability, low toxicity and capacity to modify the pharmacokinetic profile of the loaded drug, which can help in the preferential delivery of a drug to a desired target tissue. Although liposomes have attracted extensive attention during the past 30 years as pharmaceutical carriers, the currently available marketed liposomal formulations are not capable of selectively target cancer cells at a molecular level[153]. The introduction of PEG functionalizations was widely used to increase liposomes longevity in the circulatory system, since the presence of the polymer sterically hinders the interaction of blood components with the liposome surface, reducing the binding to plasma proteins[154,155] and their interaction with opsonins (molecules that act as a binding enhancers for the process of phagocytosis) subsequent to capture by the RES (reticuloendothelial system)[156].

Thus so far, four formulations based on liposomes have been just clinically approved: Doxil® (Caelyx® in Europe), Myocet®, DaunoXome® and DepoCyt®[157]. The first two formulations include respectively PEGylated and non-PEGylated liposomes encapsulating doxorubicin which, at therapeutic concentrations, has severe cardiotoxic effects which limits its dosage when administered in a standard formulation. DaunoXome® is a non-PEGylated liposomal formulation of daunorubicin[1580,159], while DepoCyt® is the commercial name of a non-PEGylated liposomal cytarabine[160], a hydrophilic chemotherapeutic drug.

In addition to the previous formulations on the market, a huge variety of antineoplastic liposomes are still under clinical evaluation.

Most recently, the concept of “stimuli-sensitive” nanocarriers has been developed within the field of drug delivery. Such nanocarriers bear site-specific targeting ligands which are expected to be released in targeted tissues or cell compartments when exposed to certain internal or external stimuli, such as low pH[161], elevated temperature[162,163], magnetic field[164,165] or altered redox potentials[166], thus greatly increasing the drug’s efficacy.

The choice of lipid composition is also crucial for maintaining the stability of liposomes in the circulatory system. The correct choice of lipids can indeed reduce the binding of serum proteins[167] or stabilize the drug formulation, diminishing the rate of drug leakage. In fact, liposomes characterized by particular compositions have shown more rapid RES uptake increasing their size[168].

The effect of surface charge on liposome clearance was demonstrated using eggPC/cholesterol (PC=phosphatidylcholine) liposomes with anionic lipids added in a 1:10:5 ratio (anionic lipid/eggPC/cholesterol)[169]. It was found that liposomes containing phosphatidylglycerol (PG), phosphatidic acid (PA), and phosphatidylserine (PS; PS>PA>PG) were cleared more rapidly than neutral liposomes. Addition of ganglioside GM1 or phosphatidylinositol (PI) resulted in longer circulation times.

Pluronic micelles

The second dispersant system was chosen among the Pluronic amphiphilic molecules, a class of tri-block copolymers characterized by an A-B-A architecture of polyoxyethylene-polyoxypropylene-polyoxyethylene (PEO_x-PPO_y-PEO_x) units. Pluronics are a class of surfactants available in a wide range of molecular weights and PEO/PPO ratios. They are usually identified with an alphanumeric code, the first letter indicating the physical form at room temperature (with "L" stating for liquid, "P" for paste and "F" for flakes). The next two (or three) numbers give information about the composition and molecular weight of the compound, since the first number (or two numbers, in case of three number codes) multiplied by 300 gives the approximately molecular weight of PPO, while the last one, by a factor 10, gives the weight percentage of PEO in the structure.

For the encapsulation of our gold(III) dithiocarbamato complexes, the Pluronic F127 was chosen. It is characterized by a PEO_{98}-PPO_{57}-PEO_{98} (**Figure 4.1**) structure with an average molecular weight of 12600 g mol^{-1}. Above the critical micelle concentration ($2.8 \cdot 10^{-6}$ M at 37 °C, pH 7.4)[170] it self-assembles in solution, giving rise to spherical micelles (**Figure 5.2**).

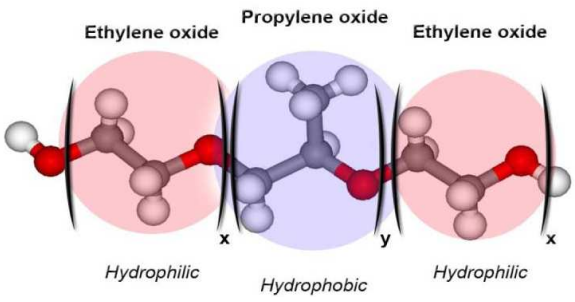

Figure 5.1: structure of Pluronic F127 triblock copolymer.

These types of structures are characterized by two well-defined regions: a central core which has hydrophobic properties and can incorporate lipophilic substances and an

external hydrophilic layer which can establish hydrophilic interaction with polar solvents like water (**Figure 5.2**).

The hydrophobic core of Pluronic® F127 system is one of the most used nanocarriers studied for biomedical applications and demonstrated a good solubilization capability for our compounds. Regarding the biocompatibility, it is worth emphasizing that this class of organic carriers remains metabolically intact until renal clearance and has proved to be little or not toxic[171].

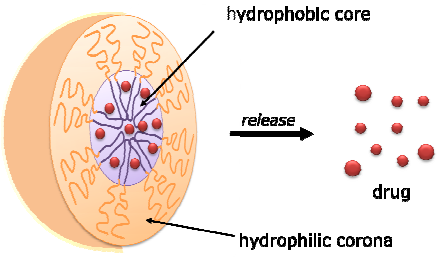

Figure 5.2: schematic representation of Pluronic® F-127 used as carrier system for hydrophobic molecules.

The use of Pluronic F127 for different clinical applications is already reported in literature, since it was firstly used in clinical trials for the delivery of doxorubicin (Dox, an anticancer compound) in a mixed formulation named SP1049C, which contains two different types of Pluronic, F127 and L61[172]. Analysis of the pharmacokinetics and biodistribution of Dox encapsulated in micelles demonstrated that, with respect to the administration of the free drug, there was a more efficient accumulation of Dox into the tumor site, with delayed peak levels and prolonged residence time of the drug[173]. Not only Dox, but also other anticancer drugs as Paclitaxel and Carboplatin were encapsulated in this type of nanocarriers and tested *in vivo*, showing in all cases an enhanced drug activity, being furthermore capable to overcome multidrug resistance (MDR) in cancer cells[145]. Even if the polymers used for drug delivery were usually considered as biologically inert components, that have only the role to protect drugs from degradation, prolong the exposure of tissues to drugs and enhance the transport into cells, it was demonstrated that in some selected cases they can also drastically alter specific cellular responses[143].

Experimental

Materials

Protected N^{α}-Fmoc-amino acid derivatives, coupling reagents and Rink amide *p*-methylbenzhydrylamine (MBHA) resin were purchased from Calbiochem-Novabiochem (Lafelfingen, Switzerland). The Fmoc-21-amino-4,7,10,13,16,19-hexaoxaheneicosanoic acid (Fmoc-Ahoh-OH) was purchased from Neosystem (Strasbourg, France). The *N,N*-dioctadecylsuccinamic acid was synthesized according to published methods[174]. A tri-block copolymer, containing ethylene oxide (EO) and propylene oxide (PO) groups, with the trade name Pluronic® F127 (PF127) and an approximate formula of $PEO_{98}PPO_{57}PEO_{98}$ (average molecular weight of 12600 g mol^{-1}) was obtained from BASF Svenska AB (Helsingborg, Sweden). All other chemicals were commercially available by Sigma-Aldrich (Bucks, Switzerland) or LabScan (Stillorgan, Dublin, Ireland) and were used as received unless otherwise stated. Snake skin dialysis tubing 3.5 K MWCO was purchased by Pierce Protein (USA). All solutions were prepared by weight with bidistilled water. Solid phase peptide synthesis was performed on a 433A Applied Biosystems automatic synthesizer (Carlsbad, California). Analytical LC-MS analyses were performed by using Finnigan Surveyor MSQ single quadrupole electrospray ionization (Finnigan/Thermo Electron Corporation San Jose, CA) column: C4-Phenomenex eluted with H_2O/0.1% TFA (A) and CH_3CN/0.1% TFA (B) from 20–80% over 20 min at a flow rate of 0.8 mL/min. The crude peptide was purified by RP-HPLC on a LC8 Shimadzu HPLC system (Shimadzu Corporation, Kyoto, Japan) equipped with a UV lambda-Max Model 481 detector using a Phenomenex (Torrance, CA) C4 (300 Å, 250 x 21.20 mm, 5 μ) column eluted with H_2O/0.1% TFA (A) and CH_3CN/0.1% TFA (B) from 20–80% over 20 min at a flow rate of 20 $mLmin^{-1}$. UV-Vis measurements were performed on a UV-Vis Jasco V-5505 spectrophotometer (Easton, MD) equipped with a Jasco ETC-505T Peltier temperature controller with a 1-cm quartz cuvette (Hellma).

Peptide Synthesis

$(C18)_2$-PEG1000-G-CCK8 amphiphilic peptide was synthesized by using standard solid-phase 9-fluorenylmethoxycarbonyl (Fmoc) procedures. The Rink amide MBHA resin (substitution 0.65 mmol g^{-1}) was used as the solid-phase support, and the synthesis was performed on a scale of 0.1 mmol. The peptide Gly-CCK8 was prepared by sequential condensation of Fmoc-AA-OH using PyBOP/HOBt/DIPEA (1/1/2) as coupling reagents

in DMF in pre-activation mode. All the reactions were performed twice for 1 hour, by using an excess of 4 equivalents for the single amino acid. Fmoc deprotection was carried out by 30% solution of piperidine in DMF after the coupling of each amino acidic residue. When completed the Gly-CCK8 synthesis, the Fmoc *N*-terminal protecting group was removed and three residues of Fmoc-Ahoh-OH hexaoxoethylene linker and the *N*,*N*-dioctadecylsuccinamic acid were sequentially condensed as previously reported[174,175]. Then, the amphiphic peptide was fully deprotected and cleaved from the resin with TFA and 2.5% (v/v) water and 2.5% (v/v) TIS as scavengers, at room temperature, and then precipitated with ice-cold water, filtered, dissolved in H_2O/CH_3CN mixture, and lyophilized. The crude peptide derivative was purified by RP-HPLC. Purity and identity were assessed by analytical LC-MS analysis.

$(C18)_2$-PEG1000-G-CCK8. Rt=17.26 min; MS (ESI): m/z: 2724 calcd. for $C_{136}H_{226}N_{15}O_{37}S_2$; $[M+2H]^{2+}$= 1363.0

Synthesis of AuL12

$[Au^{III}Br_2$(SSC-Sar-OEt)] (Sar=*N*-methylglycine, Et=ethyl; AuL12) was synthesized and fully characterized according to our procedure, reported elsewhere[93].

Stability studies by UV-Vis spectrophotometry

Stability of the compound AuL12 or IT01 alone (pre-dissolved in DMSO) in saline solution at a final concentration of 100 μM was studied recording several electronic spectra over 24 h at 25 °C between 240 and 450 nm. The stability of AuL12 loaded in either targeted or non-targeted PF127-based micelles, and of IT01 in non-targeted ones, was evaluated by UV-Vis spectrophotometry over 72 h acquiring spectra in the wavelength range 210÷500 nm. Other experimental settings were: scan speed (300 nm/min), spectral bandwidth (2.0 nm), average time (0.100 s) and data pitch (0.5 nm).

Determination of log*P*

The determination of the partition coefficient (*P*) was performed dissolving the gold(III) compounds at a concentration of 5 mM in 50 mL *n*-octanol. The solution was mixed with 50 mL bidistilled water in a separating flask, and equilibrated for 2h. After the equilibrium was reached, the two non miscible solutions were separated, and the

concentration of compound in *n*-octanol was determined before and after equilibration *via* UV-VIs spectroscopy, obtaining indirectly the concentration of complex in water.

Micelles formulation

Pure micelles of PF127 were prepared by dissolving copolymer at 2% w/w in aqueous solution at the physiological conditions. Mixed PF127/$(C18)_2$-PEG1000-G-CCK8 micelles were prepared by adding 4% w/w of the CCK8 amphiphilic peptide with respect to PF127. Briefly, the two amphiphile compounds were dissolved in a small amount of MeOH/$CHCl_3$ (50:50); subsequently a thin film was obtained by evaporating the solvent by slowly rotating the tube containing the solution under nitrogen flux. Lipid film was hydrated in physiological solution (1 mL) for 5 min by vortex, sonicated for 10 min and used without further treatment. Concentrations of CCK8-containing solutions were determined by absorbance on a UV-Vis Jasco (Easton, MD) Model 440 spectrophotometer with a path length of 1 cm using a molar absorptivity (ε_{280}) of 6845 M^{-1} cm^{-1} for CCK8. This value was calculated according to the Edelhoch method[175], taking into account contributions from tyrosine and tryptophan present in the primary structure, which amount to 1215 and 5630 M^{-1} cm^{-1}, respectively[176].

AuL12 and IT01 micelles loading

Loading of either AuL12 or IT01 compounds in PF127 pure micelles and of AuL12 in PF127/$(C18)_2$-PEG1000-G-CCK8 mixed micelles was performed *via* film method[177]. Briefly, after lipid film preparation previously described, AuL12 or IT01 (0.35 mg or 0.36, respectively, in 20 mg of PF127) were dissolved in chloroform/methanol (50/50) mixture. Organic solvent was then evaporated under nitrogen flux and saline solution added as previously described. Subsequently, unloaded AuL12/IT01 was removed using a Sephadex G50 column pre-equilibrated with a NaCl 0.9% w/w aqueous solution.

The AuL12 concentration (0.5 mM) and drug loading content (DLC), defined as the weight percentage of Au complex encapsulated in the micelles, was quantified by using ICP-AES analysis (Inductively Coupled Plasma Atomic Emission Spectroscopy) after subtraction of the amount of AuL12/IT01 removed from the column from the total amount of AuL12/IT01 loaded.

AuL12 release from PF127 micelles

Non-targeted AuL12-containing aggregates (lyophilized) were dissolved in 1 mL of water. The solution was then transferred into a dialysis bag (MW cutoff = 3500 Da) which was placed into 15 mL (hereinafter, $\mathbf{V_0}$) of saline solution and incubated under stirring for 72 h at 37°C. At different time points, 2 mL ($\mathbf{V_D}$) of the dialyzed solution were withdrawn to evaluate the released drug amount over time; such volume was immediately replenished with fresh saline solution. It was assumed that the crossing of gold species through the dialysis membrane occurred quickly, and that the overall release of AuL12 from micelle vehicle to the dialysis bag medium was the rate determining step process.

The extent of gold complex released was evaluated by ICP-AES analysis (Au^I λ_{em}= 242.795 nm) as ratio of the concentration of released metal ($\mathbf{C_J}$) to the total metal previously loaded into the micelles. In particular, $\mathbf{C_J}$ is the released concentration immediately after drawing of each sample (labelled as *J*) and refilling of the removed volume $\mathbf{V_D}$. In **Equation 1** defines $\mathbf{C_J}$ (wherein the subscript *a* stands for "analyzed") and the first term takes into account the effects of both drawing (system resulting in a volume of 13 mL=$\mathbf{V_R}$) and dilution (system volume =$\mathbf{V_0}$) whereas the second term considers all the 2 mL aliquotes related to the J^{th} drawing and the i^{th} previous aliquotes, α and β being V_R/V_D and V_D/V_0, respectively. The second term could be neglected only if $V_D<<V_0$ which is not our case.

$$C_J = C_{J,a} \cdot \alpha + \sum_{i=1}^{J} C_{i,a} \cdot \beta = C_{J,a} \cdot \frac{V_R}{V_0} + \sum_{i=1}^{J} C_{i,a} \cdot \frac{V_D}{V_0} \qquad (1)$$

Then, we analyzed the overall release kinetics from the micelles *via* experimental data fitting, assuming a first-order dissociation process[178]. **Equation 2** describes that AuL12 is released from the supramolecular aggregates owing to two parallel dissociation events (not identified yet). The parameters a_1 and a_2 are the maximum amount of gold compound released by means of the first or the second event, respectively. The parameters *k* (s^{-1}) are the overall experimental rate constants which correspond to the combination of single microscopic rate constants associated with the unloading processes from the micelle hydrophobic core of the different AuL12 isoforms (present in the sample).

By fitting the $\mathbf{C_J}$ vs. *t* profile with **Eq. 2**, the following parameters were obtained: a_1= 3470 ± 26 ppb; a_2 = 1730 ± 57; k_1 = (6.7 ±0.3) · $10^{-4}s^{-1}$; k_2 = (8.7 ±0.8) · $10^{-6}s^{-1}$.

$$y = a_1(1 - e^{-k_1 x}) + a_2(1 - e^{-k_2 x}) \qquad (2)$$

Vesicles formulation and AuL12 and IT01 loading

Vesicles based on dipalmitoylphosphatidylcholine (DPPC, *Sigma Aldrich;* CMC=0.46nM) containing either IT01 or AuL12 were prepared dissolving phospholipids (3.8 mg) and test compound (0.35 or 0.38 mg respectively) in chloroform/ethanol. The solvent was slowly evaporated under a gentle $N_{2(g)}$ flux in a flask, obtaining an homogeneous DPPC/AuL12 or DPPC/IT01 thin film, that was dried overnight at reduced pressure to eliminate any trace of solvent. The thin layer was then rehydrated above the critical temperature of the phospholipids T_c (about 50°C) with 1 mL of saline solution (NaCl 0.9% aqueous solution). The suspension was stirred for 30 min and then submitted to 5 cycles of quick freezing/defreezing in liquid nitrogen and 37°C water bath to obtain large unilamellar vesicles (LUV) with heterogeneous dimensions. The solution was then extruded through a porous membrane of polycarbonate with mean pores diameter of 100 nm, to obtain small unilamellar vesicles (SUV). The solutions before and after extrusion were analyzed by means of DLS analysis to assess the dimensional properties of the vesicles. The extruded vesicles were then dialyzed for 2 h against saline solution to eliminate gold(III) complex and phospholipids not entrapped in the vesicles system.

DLS (Dynamic Light Scattering) Analysis

Mean diameter was measured using a ZetasizerNano-S (*Malvern Instruments*, Westborough, MA) at 25 °C using disposable sizing cuvettes. DLS samples were prepared at $2.0 \cdot 10^{-4}$ M in saline solution NaCl 0.9% and centrifuged at room temperature at 13,000 rpm for 5 min. For each batch, hydrodynamic radius and size distribution were the mean of three measurements and final values were calculated as the mean of three different batches.

ICP-AES analysis

ICP-AES measurements were carried out by ICP-AES spectrometer (ICP SPECTRO Arcos with EndOnPlasma torch; Spectro Analytical, Kleve, Germany) equipped with

capillary cross-flow nebulizer. Analytical determinations were carried out with a plasma power of 1.4 kW, a radiofrequency generator of 27.12 MHz and an argon gas flow with nebulizer, auxiliary, and coolant set at 0.8, 0.8 and 13 $L \cdot min^{-1}$, respectively.

Samples were diluted with 5% *aqua regia* (HCl/HNO_3 3:1 v/v) in bidistilled water. The extent of gold complex release was evaluated by ICP-AES analysis [$\lambda_{em}(Au^I)$= 242.795 nm] through external calibration method.

Cell Lines and cultures

A431 cells (human epidermoid carcinoma) and H460 (human large cell lung cancer) were obtained from *American Type Culture Collection* (ATCC). Cells were grown in a humidified atmosphere containing 5% CO_2 at 37°C in either Dulbecco Modified Eagle medium (DMEM, *Sigma Aldrich*) supplemented with D-glucose (final concentration 4.5 g/L, *Sigma*; A431) or RPMI-1640 (Roswell Park Memorial Institute, *Sigma Aldrich*; H460), both supplemented with 10% heat-inactivated fetal bovine serum (*Invitrogen*), 100 $U \cdot mL^{-1}$ penicillin (*Sigma*), 100 $\mu g \cdot mL^{-1}$ streptomycin (*Sigma*) and 0.25 $\mu g \cdot mL^{-1}$ amphotericin B (*Sigma*). The human epidermoid carcinoma cell line A431 overexpressing the CCK2-R by stable transfection, kindly provided by Dr. L. Aloj (Istituto Nazionale Tumori, Fondazione G. Pascale, Napoli, Italy), was cultured as exponential growing subconfluent monolayer on 100-mm plates in DMEM supplemented with 10% FCS (*Fetal Calf Serum*), 2 mM L-glutamine, and 250 g/mL neomycin analog G418 (*Gibco BRL*) in a humidified atmosphere containing 5% CO_2 at 37°C.

In Vitro cytotoxicity assays

A431, A431-transfected and H460 cells ($3 \cdot 10^4$ cells mL^{-1}) were seeded into each well of 24-well cell culture plates. After 24 h incubation, the medium was discarded from the plates and replaced with an equal volume of fresh medium containing the test complexes at different concentrations. Then, cells were incubated for 72 h. A DMSO solution of either AuL12 or IT01 was added for the tests in amounts of organic solvent not exceeding the 0.4% v/v per well. Cisplatin (*Sigma*) was stocked in saline solution (0.9% w/w NaCl in water) at a concentration up to 4 mM. The formulations of micelles or vesicles loading either AuL12 or IT01 were likely hydrated in saline solution, at a final stock solution concentration of $5.0 \cdot 10^{-4}$ M. The Trypan Blue dye exclusion assay was performed to determine cell viability. Cytotoxicity data were expressed as GI_{50} values (μM), *i.e.* the

concentration of test compound inducing 50% reduction in cell number compared to control cultures. Control samples of F127 and DPPC vesicles were furthermore tested to confirm the absence of intrinsic toxicity due to the carriers.

Results and discussion

5.1 Determination of the partition coefficient P

Before loading the gold(III)-dithiocarbamato compounds into micelles or vesicles, the lipophilic properties of the analyzed complexes were defined through the determination of their partition coefficient (*P*) between water and *n*-octanol, usually expressed in the logarithmic form, log*P* (**Equation 3**). The value of *P* is defined as the ratio between the concentrations of a compound in a mixture of two immiscible solvents at equilibrium.

$$\log P = \log \frac{[complex]_{octanol}}{[complex]_{water}} \qquad (3)$$

In particular, the partition of the complexes was evaluated between a hydrophobic solvent such *n*-octanol, and a hydrophilic one, like water, which are immiscible. In medical use, this parameter is evaluated to achieve information about the network of inter- and intramolecular forces affecting drug transport through lipid structures as well as drug's interactions with target proteins. Indeed, at the organism level, lipophilicity and hydrophilicity are important factors defining the pharmacokinetics and pharmacodynamics of a drug substance[179].

In this case, since the scarce solubility of our compounds in water, the evaluation of the partition coefficient was carried out determining the concentration of the complexes in a *n*-octanol solution before and after the mixing with a well-defined volume of water (**Table 5.1**).

Tabella 5.1: log*P* values measured for the three complexes AuL12, IT01 and IT03.

	log P
AuL12	0.13
IT01	0.51
IT03	0.87

Positive values for the logarithm of *P* have to be correlated to a more lipophilic character of the compounds. The determination was performed both for the "first generation" reference compound AuL12 and for the "second generation" dipeptide derivatives, IT01 and IT03. The determination on the correspondent IT02 and IT04 isomers was not carried out, since they differ from the above mentioned compounds only for the configuration of the chiral aminoacid, property which does not affect the chemico-physical behaviour of the compounds, neither their solubility.

In all cases, the compounds showed higher affinity for hydrophobic environments, with values of log*P* increasing from the more hydrophylic AuL12 to the more hydrophobic IT03.

For the further solubilization studies, which include two different types of dispersant nanosystems, IT01 was chosen as a model upon the peptido-functionalized gold(III)-dithicarbamato complexes while AuL12 was taken as a reference compound.

In the first case we exploited the encapsulation of the gold(III) compound in the hydrophobic core of Pluronic F127 non-targeted and targeted micelles. In the second case, the complexes were loaded in hydrophobic corona of DPPC-based vesicles (**Figure 5.3**).

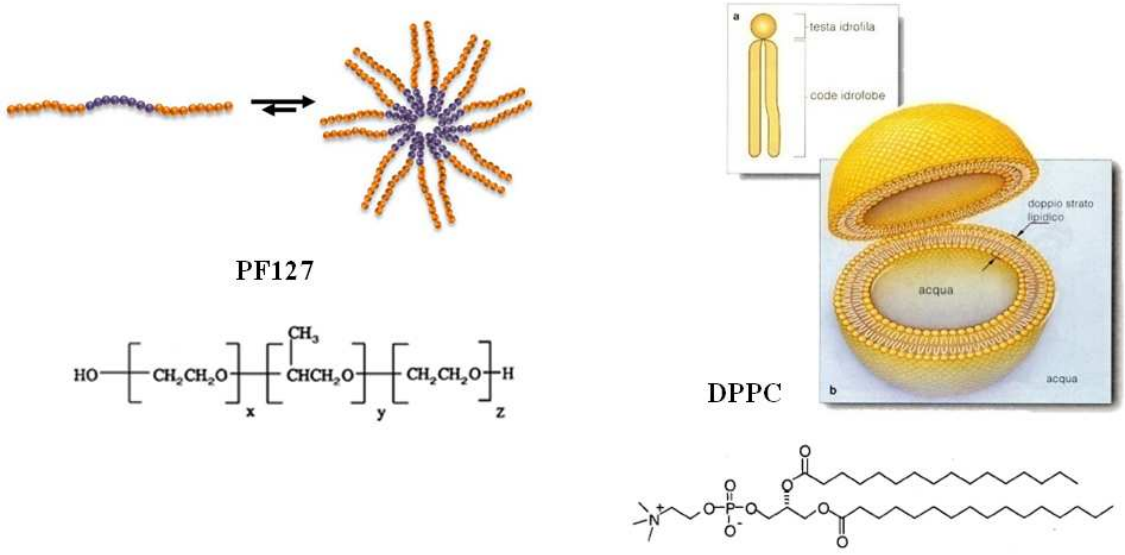

Figure 5.3: schematic representation of Pluronic F127 monomer (x=z=98, y=57) and the corresponding micelle architecture (**left**) and of phospholipid DPPC and the corresponding vesicular system upon surfactant organization in solution (**right**).

5.2 *Targeting and delivery of AuL12 with Pluronic-based micelles*

The gold(III)-dithiocarbamato complex AuL12 (**Figure 5.4A**, compound **2**) was selected among the "first generation" compounds due to its good antiproliferative rates recorded both *in vitro* and *in vivo*[2,180]. Such gold(III) derivative was loaded in two types of self-assembling supramolecular aggregates, namely consisting of Pluronic® F127 (PF127, **Figure 5.4B**) or its combination with the amphiphilic peptide $(C18)_2$-PEG1000-G-CCK8 (**Figure 5.4C**), thus yielding the formation of either non-targeted and targeted micelles, respectively.

In fact, upon self-assembling, the second type of drug carrier is characterized by the presence of the octapeptide CCK8 bound to the external hydrophilic corona of the resulting micelles (**Figure 5.4D**).

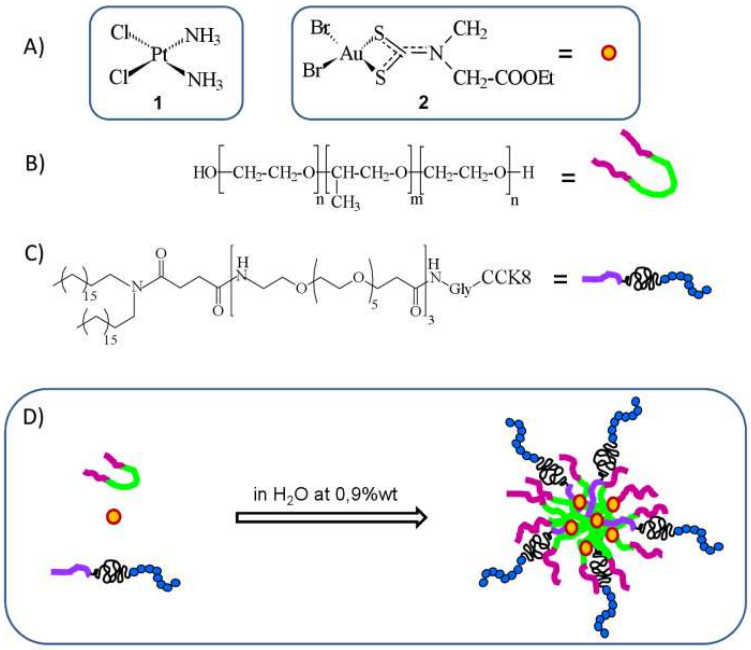

Figure 5.4: Chemical drawing of *cis*-diaminodichloroplatinum(II) (cisplatin) **(A-1)**, dibromo[ethyl *N*-(dithiocarboxy-k*S*,k*S'*)-*N*-methylglycinato]gold(III) (AuL12) **(A-2)**, non-ionic surfactant Pluronic® F127 with n=98 and m=57 **(B)**, $(C18)_2$-PEG1000-G-CCK8 **(C)** and schematic representation of AuL12 loaded in PF127/$(C18)_2$-PEG1000-G-CCK8 targeted micelles **(D)**.

The targeting peptide CCK8 belongs to the family of cholecystokinin (CCK) peptides whose receptors[181,182] are normally present on the cell surface and are known to be up-regulated after malignant transformation. Two different receptor types, called CCK1-R and CCK2-R, recognize CCK and mediate its action[183]. Both are located predominantly in the gastrointestinal tract and in the central nervous system[184]. The CCK1-R was found

overexpressed in a number of pancreatic adenocarcinomas and in gastro-entero-pancreatic neuroendocrine tumors (38%), in meningiomas (30%) and in some neuroblastomas (19%), while the CCK2-R in stromal ovarian cancers (100%) and it was shown to be up-regulated in a high percentage of medullary thyroid cancers (92%), in astrocytomas (62%) and in small-cell lung cancers (57%)[182-185]. Also the octapeptide amide-CCK8 (amino acid sequence: Asp^{26}-Tyr^{27}-Met^{28}-Gly^{29}-Trp^{30}-Met^{31}-Asp^{32}-Phe^{33}-amide) binds with nanomolar affinity both receptor subtypes, also when modified on its *N*-terminus with chelating agents or alkyle chains[186]. In fact, it has been successfully used to deliver, in a selective way, contrast agents for nuclear medicine applications[187] or supramolecular aggregates carrying gadolinium complexes and/or anticancer drugs.

In this work the amphiphilic CCK8-functionalized surfactant $(C18)_2$-PEG1000-G-CCK8 (**Figure 5.4C**) was synthesized by solid-phase methods on a Rink-amide resin. After CCK8 assembling, a Gly residue, three units of Fmoc-Ahoh-OH and *N*,*N*-dioctadecylsuccinamic acid were subsequently condensed step by step. After cleavage and purification, the amphiphilic peptide derivative was obtained in high yield and purity.

The preparation of both AuL12-loaded PF127 non-targeted micelles and PF127/CCK8 targeted micelles was carried out exploiting the thin film hydration method[188]. Briefly, a homogeneous lipid layer has been obtained by dissolution of the amphiphilic monomers [0.020 g of PF127 alone or along with 0.0008 g of $(C18)_2$-PEG1000-G-CCK8] and AuL12 (0.00035 g) in a small volume of chloroform/methanol (50/50) mixture, followed by evaporation of the solvent under a mild nitrogen flow. Afterwards, the layer was hydrated by addition of aqueous solution (10 mM HEPES at pH 7.4, 10 mM PBS at pH 7.4 or saline solution at 0.9% w/w NaCl pH=5.0), resulting in a suspension containing 2% of PF127 with respect to water weight, which was then vortexed until obtaining a clear solution.

Dynamic Light Scattering (DLS) measurements were performed to assess the dimensions of the two, empty or filled, self-assembled systems. As previously reported, the mean hydrodynamic diameter of PF127 micelles at 2% w/w and 25 °C is 25 nm, accordingly to literature data[189],[190], and no significant variation occurs after loading of AuL12 at 0.035 % w/w (diameter=26 nm). A slight increase in size was observed for mixed, empty or filled, targeted micelles (mean diameter values calculated from DLS were 34 and 32 nm, respectively, **Table 5.2**).

Table 5.2: Structural parameters (mean hydrodynamic diameters, polydispersity indexes and diffusion coefficients) determined from dynamic light scattering measurements for the studied systems.

Systems	Micelle diameter± SD (nm)	P.I.± SD	diffusion coefficient $[m^2s^{-1}]x10^{-12}$
PF127	25±14	0.23±0.01	20±11
AuL12-PF127	26±13	0.23±0.01	19± 10
PF127/CCK8	34±11	0.43±0.02	15± 5
AuL12-PF127/CCK8	32±12	0.48±0.01	15± 6

Electronic spectra of free AuL12 in saline solution (**Figure 5.5**) and AuL12-loaded micelles in different solution systems (**Figure 5.6**) were recorded to assess the stability of the metal complex over time (until either 24 or 72 h). The wavelength range 210-500 nm, wherein only the gold(III) complex shows significant absorption bands, was explored. In saline solution, the electronic spectrum of AuL12 alone (previously dissolved in DMSO at 0.5% v/v) displays two strong absorption bands at around 270 (band I) and 312 (band II) nm, ascribed to the transition already described for IT01 complex (see **Chapter 3**).

As can be observed in **Figure 5.5**, the compound undergoes partial hydrolysis, as shown by the appearance of a band at 380 nm assignable to the coordination of water molecules to the metal center.

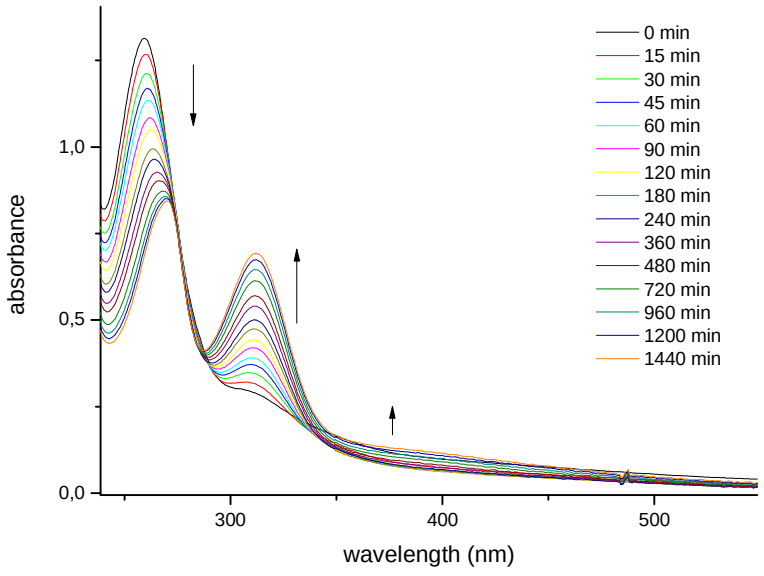

Figure 5.5: UV-Vis spectra of AuL12 dissolved in DMSO collected over time in saline solution (NaCl 0.9%) at 25°C.

However, the spectral features varitions reported for AuL12 differ from those of IT01 recorded in the same experimental conditions (**Chapter 3**). This different behaviour can

be explained with different solubility properties and hydrolysis rates for the two complexes. Nevertheless, deeper and more accurate evaluations will be performed to elucidate this subject.

Considering the AuL12-encapsulating micelles, the UV-Vis spectrum recorded soon after their re-suspension in PBS shows a slight change in the values of λ_{max} for band I and band II (258 and 312 nm; **Figure 5.6A**) with respect to those recorded for the complex alone in saline solution. However, a strong hypochromic effect accompanied by a bathochromic shift is detected over time for both bands, together with the appearance of a new band at 380 nm (band III), thus highlighting the reactivity of the compound in this medium, in agreement with literature data[106].

On the contrary, no notable changes in terms of spectral features (*e.g.*, intensity, λ_{max}), have been observed in the kinetic trend recorded for the AuL12-loaded micelles prepared in saline solution (**Figure 5.6B**), pointing out a higher stability of the compound in such an aqueous medium. On the whole, the position of the bands (270 and 313 nm) is basically unchanged with time, indicating that the gold center remains in the +3 oxidation state due to the stabilization effects played by the chelating dithiocarbamato ligand[106,191].

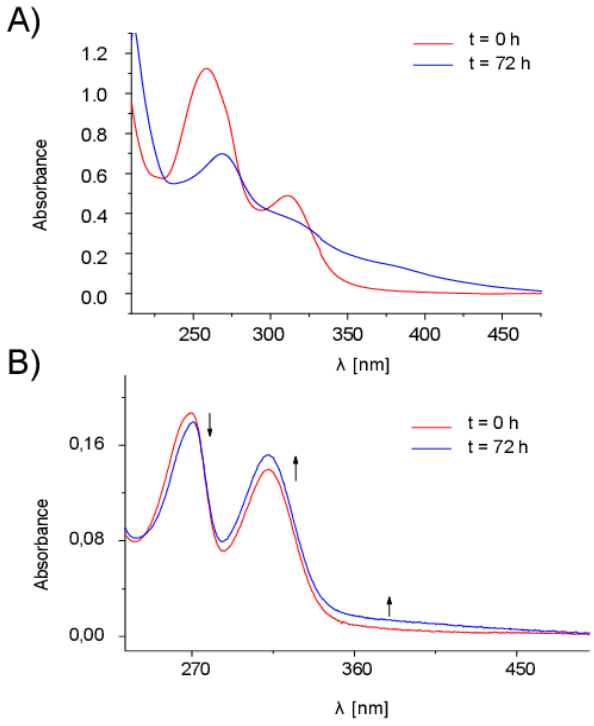

Figure 5.6: UV-Vis spectra of AuL12/PF127 micelles collected over time in: (**A**) 10 mM phosphate buffered saline and (**B**) saline solution.

The slight changes in spectral intensity (hypochromic and hyperchromic effect for band I and II, respectively) have been ascribed to the progressive hydrolysis of gold(III)-bound

bromide ions, leading to the formation of an aquo complex (as already described for IT01 in saline solution, **Chapter 3**). The changes in spectral intensity (hypochromic and hyperchromic effects for band I and II, respectively) have been attributed to the progressive hydrolysis of gold(III)-bound bromide ions, resulting in the formation of the corresponding water-soluble aquo-complex[81,82] (as already described for IT01 in saline solution, **Chapter 3**).

Furthermore, the band III (*M→L* charge transfer involving the M *nd* orbitals and the dithiocarbamato π^* system)[192,193] intensity increase at about 385 nm may be explained considering the effects of the Br/OH substitution on the transition dipole moment and, hence, on the transition probability.

Based on the higher stability of the formulation in saline solution compared to PBS, all subsequent studies were carried out in the first medium.

The drug release from the micelle carriers was evaluated using a dialysis membrane (MW_{cutoff} = 3500). **Figure 5.7** shows the release profile obtained at 37 °C over 72 h. The amount of released complex was evaluated by ICP-AES analysis (Inductively Coupled Plasma Atomic Emission Spectroscopy) as percentage of released gold(III) complex on the total compound previously encapsulated in the aggregates. It is worth noting that most of the drug (around 73%) is released after 72 h and that the process takes place quite quickly as after 30 min the 35% of the compound is out of the micelles, with 56% release reached after 12 h.

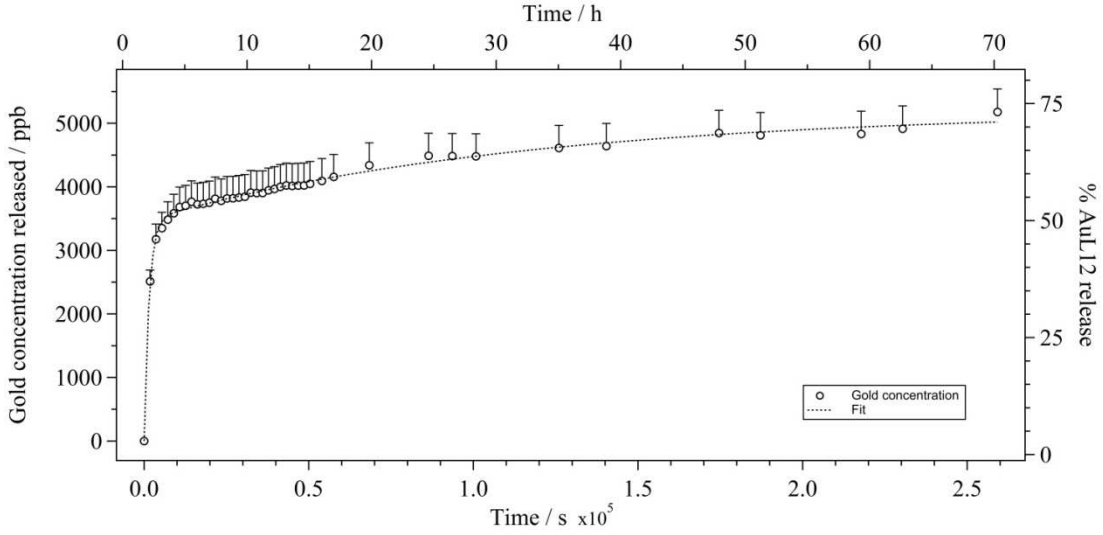

Figura 5.7: Gold concentration (C_J, according to equation 1) evaluated over 72 h in saline solution at 37 °C, namely AuL12 release from non-targeted micelles (%, with respect to total compound previously encapsulated in the aggregates). Error bars were determined by means of the error propagation equation.

The antiproliferative activity (**Table 5.3, Figure 5.8**) was evaluated on two tumor cell lines, namely A431 (epidermoid carcinoma) and A431 overexpressing the CCK2 receptor (CCK2-R) by stable transfection (kindly provided by Dr. L. Aloj, Istituto Nazionale Tumori, Naples, Italy). AuL12 dissolved in DMSO (AuL12-DMSO) and AuL12-encaspulating non-targeted micelles (AuL12-PF127) display similar GI_{50} values on both tumor cell lines.

Table 5.3: *In vitro* antiproliferative activity of AuL12 dissolved in DMSO (AuL12), encapsulated in non-targeted micelles (AuL12/PF127) and in CCK8-receptor targeting micelles (AUL12/Pf127-CCK8). GI_{50} data are calculated as average value of at least three experiments ± S.D.

Samples	GI_{50} (μM)	
	A431	**CCK2-R transfected A431**
AuL12*	9.50± 2.00	9.50± 2.40
AuL12/PF127	9,01 ± 0.70	6.80 ± 1.90
AuL12/PF127-CCK8	7.50 ± 2.10	0.75±0.08
Cisplatin	4.00± 1.80	6.00± 2.10

*dissolved in DMSO

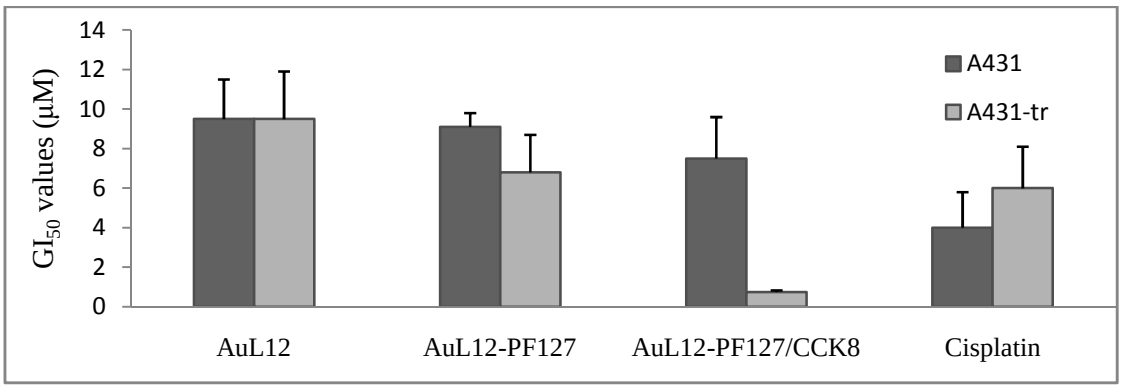

Figure 5.8: Barchart related to **Table 5.3** cytotoxicity values of the tested formulation with respect to Ciplatin, on A431 and CCK2R transfected A431 cells (A431-tr).

Anyway, cisplatin remains the most potent compound against A431 cells, showing a cytotoxic effect about 2-fold higher than the two AuL12 micellar formulations, and only a slightly higher effect on A431 CCK2-R-transfected cells. However, when AuL12 is loaded in the peptide-conjugated micelles (AuL12-PF127/CCK8), the GI_{50} value determined on A431 CCK2-R-transfected cells decreases of one order of magnitude with respect to those of cisplatin, AuL12-DMSO and AuL12-PF127. Thus, in agreement with the release data, it is possible to suppose that the endocytic process occurs faster (in the

order of minutes) with respect to the rate of AuL12 released from the micelles, thus allowing tumor cell targeting and cell internalization before the loss of active gold(III) complex from the supramolecular aggregates.

To sum up, one of our poorly water-soluble gold(III)-based complexes (AuL12) has been loaded in the lipophilic core of PF127-based micelles. Overall, here we have demonstrated that:

- AuL12 encapsulated in micelles proved to be stable in saline solution up to 72 h.
- the studied supramolecular aggregates have proved to be good carriers, thus enhancing the water solubility together with keeping or increasing the antiproliferative activity of the model compound (compared to the DMSO vehicle).
- the release from the micelle systems into the aqueous medium was shown to occur very fast, reaching 50% after 2 h.
- if a targeting moiety is present on the hydrophilic shell of micelles, the designed supramolecular scaffold, besides being a vehicle, it also acts as a targeted bullet. In fact, on passing from A431 cells to CCK2-R-transfected counterparts, the cytotoxicity of the loaded AuL12 compound is 10-fold increased.

In conclusion, loading of metal-based antiproliferative compounds in labeled micelles of Pluronic® seems to be a winning approach both to increase water solubility and to favor tumor selectivity in a single strategy. Based on these preliminary promising results, we evaluate the loading of some gold(III)-peptidomimetics into Pluronic® aggregates to enhance their bioavailability in the prospect to enter phase I clinical trials[101].

5.3 Delivey of IT01with Pluronic micelles and DPPC vesicles

IT01-loaded micelles and vesicles were prepared by using the thin film hydration method[194]**,** as above reported. After resuspension of the lipidic film in saline solution NaCl 0.9%, a heterogeneous mixture of large unilamellar vesicles (LUV) was obtained. To control liposomes dimensions, the samples were thus extruded through a polycarbonate membrane of 100 nm porosity (as described in the Experimental Section of this Chapter). By mechanically forcing the LUVs to pass through the pores of the membrane, vesicles reorganize in smaller homogeneous systems (SUV, small unilamellar vesicles) of mean diameter comparable to the membrane pore dimension employed.

Dynamic Light Scattering (DLS) measurements were performed to assess the dimensions of the loaded or unloaded systems (**Table 5.4**). The mean hydrodynamic diameter of PF127 at 2% w/w and 25 °C is 25 nm, accordingly to literature data[189,190], and no significant variation occurs after loading of AuL12 at 0.035 % w/w (diameter=26 nm). Hydrodynamic diameters of nearly 80 nm were obtained for vesicles, slightly smaller than expected since a membrane porosity of 100 nm diameter was used for the extrusion. It is worth noting that even in this case, no significant structural changes were detected passing from the loaded to the unloaded systems.

Table 5.4: Structural parameters (mean hydrodynamic diameters, polydispersity indexes and diffusion coefficients) determined from dynamic light scattering measurements for the studied systems.

	Hydrodynamic diameter ± st.dev (nm)	**P.I.± SD**	**diffusion coefficient $[m^2s^{-1}]x10^{-12}$**	**Au content ($x10^{-4}M$)**
F127/IT01	22 ± 4,7	0.45±0.12	18±3	5.00±0.06
F127/AuL12	26±13	0.23±0.01	19± 10	5.00±0.10
F127 control	25±14	0.23±0.01	20±11	--
DPPC/IT01	81 ± 16	0.60±0.22	5.3±0.3	4.37±0.30
DPPC/AuL12	100 ± 40	0.34±0.23	4.4±0.1	4.30±0.20
DPPC control	83±20	0.64± 0.18	5.6±0.4	--

Each sample was then analyzed *via* ICP-AES analysis to determine the content of gold(III) complex encapsulated in the two different systems. As reported in **Table 5.4**, the amount of gold internalized in the liposomes is slightly lower than the amount found in the Pluronic micelles. This can be probably due to the multistep procedure used to obtain the complex-loaded liposomes, if considering in particular that the process of extrusion through the polycarbonate membrane can determine a loss of compound, as a consequence of the possible adsorption of the complex on the membrane itself.

The stability of the IT01/DPPC and IT01/F127 systems was evaluated through UV-Vis analysis of the sample in saline solution NaCl 0.9% (final IT01 concentration 50.0 μM) at 37°C for 24 h. From the analysis of the electronic spectra recorded for the IT01-loaded pluronic system (**Figure 5.9**), it can be noticed that the main absorption bands of IT01 undergo a hyperchromic effect with time, accompained by a slight shift in λ_{max} for the $\pi^* \leftarrow \pi$ transition (from 264 to 271 nm). Contrarily, the position of the $\pi^* \leftarrow n$ transition does not change with time, while an absorption band of low intensity appears at nearly 360 nm.

This situation is coherent with the release of the compound from the micelles, since hydrolysis of the complex could take place upon release from the hydrophobic core to the aqueous saline solution. Indeed, the position of the bands after 24 h is similar to those recorded in saline solution for the compound alone (added form a DMSO solution, **Chapter 3**).

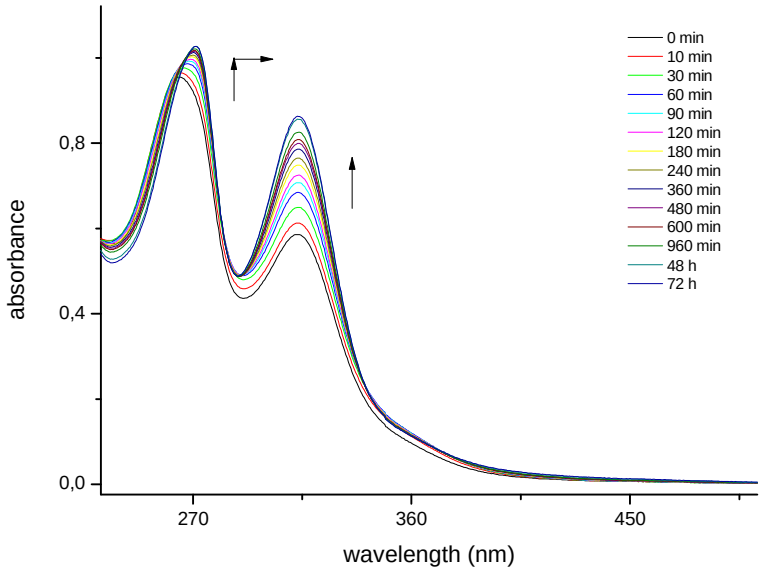

Figure 5.9: UV-Vis spectrum of IT01-loaded (50 μM) Pluronic F127 micelles recorded at 25°C over 72h.

Differently, for IT01-loaded DPPC vesicles in saline solution NaCl 0.9%, a hyperchromic effect on all the absorption bands is recorded without significant shift of their λ_{max} (**Figure 5.10**). This behaviour can be explained as the effect of an increase in scattered light due to the formation of larger aggregates in solution. This was furthermore confirmed by DLS analysis of the sample after 72h, which shows that the vesicles dimensions (in terms of hydrodynamic diameter) after 72h incubation at 37°C varies from 82±16 to 1868±520 nm, assessing the tendency of the vesicles to aggregate in solution.

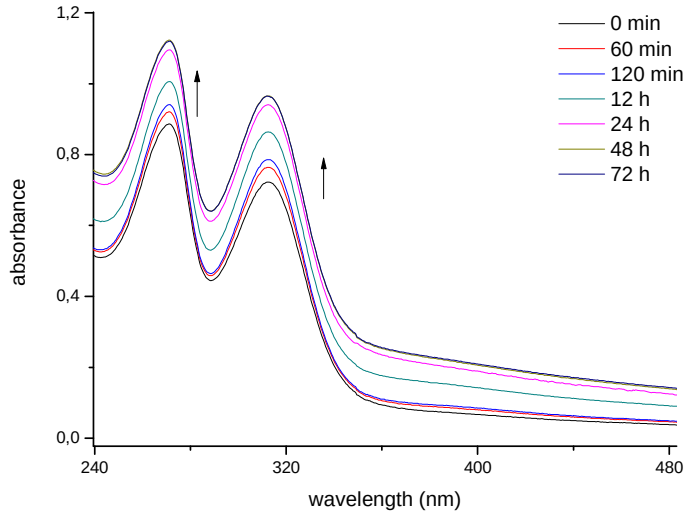

Figure 5.10: UV-Vis spectrum of IT01-loaded (50 μM) DPPC vesicles recorded at 25°C over 72h.

The DPPC and Pluronic F127 systems loading either the compound IT01 or AuL12, were subsequently tested on H460 human cancer cells, to check whether their cytotoxicity is maintained after the encapsulation in the two different dispersant systems. As we can see from **Table 5.5**, the activity of both the IT01- and AuL12-loaded vesicles and micelles is comparable to the cytotoxic activity of the compounds alone (administered to cells from a DMSO solution).

Table 5.5: *in vitro* cytotoxic activity of IT01- and Aul12-loaded in Pluronic F127 micelles and DPPC vesicles on H460 cells after 72h.

	GI_{50} ± dev.st.(μM)
DPPC/IT01	3.20 ± 1.93
F127/IT01	2.89 ± 1.62
IT01	3.83 ± 2.13
DPPC/AuL12	3.51 ± 0.48
F127/AuL12	2.13 ± 0.13
AUL12	2.15 ± 0.26

The toxicity of pure DPPC and Pluronic F127 on H460 cells was also checked, to assure the absence of any contribution to the decreased cell viability deriving from the intrinsic effect of the carrier. DPPC did not exhibit any cytotoxic effect on H460 cells even at concentration 2-fold higher then the highest concentration employed for the cytotoxicity studies with AuL12- or IT01-loaded liposomes ($[DPPC]_{max}=2.47\cdot10^{-4}M$). Otherwise, Pluronic F127 showed a slight decrease in cell viability while increasing its administered

concentration. At the maximum concentration used for cytotoxicity test of the gold(III) derivatives ($[F127]_{max}=2.89\cdot10^{-5}M$) it was shown that it determined a cell viability decrease of 17% with respect to the reference control (83% cell viability), which approached the 30% with Pluronic concentration of $4.00\cdot10^{-5}M$.

Concluding, in this section we evaluated the possibile encapsulation of the new gold(III) complexes in biocompatible carrier systems, in order to enhance their stability in physiological conditions and thus increase their bioavailability for the forthcoming *in vivo* studies. The results obtained for both the Pluronic F127-based micelles and for the DPPC-based liposomes were promising. In both cases the stability of the gold(III) complexes was enhanced, and the cytotoxic activity was maintained in comparison with that of the compound previously dissolved in DMSO.

With respect to DPPC liposomes, the Pluronic F127 formulations should be preferred if considering the simpler and faster procedure adopted for their preparation. Anyway, the intrinsic toxicity (even if low) of Pluronic F127 and the lower stabilization of the complexes, with respect to the liposomal systems, must be taken into account when considering their application to forthcoming *in vivo* experiments.

Chapter 6

Insights into the mechanism of action of gold(III)-dithiocarbamato derivatives

Considering the good cytotoxic properties of our compounds on human cancerous cells *in vitro* and the promising antiproliferative activity verified *in vivo*, it resulted of peculiar importance to obtain more details about the mechanism of action of our compounds.

In this context, the interaction with biomolecules already identified as putative targets for other anticancer metallodrugs have been explored.

In particular, we focused on the evaluation of selected gold(III) compounds interaction with different macromolecules, as DNA, proteasome, thioredoxin reductase and PARP enzymes.

As already mentioned, the most known metallodrug used in cancer chemotherapy is cisplatin. Even if its antiproliferative activity was discovered in 1969 and more than 30 years passed since its approval by FDA (Food and Drug Administration), its effective mechanism of action is still not fully understood yet. It is generally accepted that DNA is its principal target. As already described in the *Introduction*, cisplatin is activated intracellularly by the substitution of one or two chlorido ligands with water molecules, and it is known to subsequently covalently bind to DNA, forming DNA adducts. This activates various signal-transduction pathways, for example those involved in DNA-damage recognition and repair, cell-cycle arrest and programmed cell death/apoptosis[195].

It is also well known that only 5% of the internalized drug reaches the nucleus, and there are extensive evidences that it can interact with other molecules in the cells. Indeed at the basis of resistance occurrence to cisplatin therapy, there are increased levels of cytoplasmic thiol-containing species, such as tripeptide glutathione and metallothioneins, which are rich in sulphur-containing amino acids cystein and methionine, and cause detoxification due to the high affinity of platinum for sulfur atoms.

The evaluation of the action mechanism of gold(III)-dithiocarbamato compounds started from the assessment of their stability and reactivity under physiological conditions.

Since the physiological environment is generally reducing, the potential reduction of gold(III) compounds to the less active gold(I) counterparts could result a major drawback for the pharmacological development of gold(III)-based anticancer agents.

The high stabilization of the +3 oxidation state due to the presence of the dithiocarbamato chelating moiety was demonstrated by the lower redox potentials registered for $[Au^{III}Br_2(ESDT)_2]$ (AuL12) in physiological-like solution by cyclic voltammetry. It was shown that AuL12 undergoes irreversible stepwise reduction to gold(I) dinuclear species, $[Au^{I}(ESDT)_2]$, at *ca.* -180 mV (*vs.* saturated calomel electrode, SCE), which resulted significantly lower than the typical reduction potential for Au(III)/Au(I) of the corresponding $KAuX_4$ (X=Cl, Br) precursor (+1.29 V). Concerning their solution properties, the gold(III) complexes hydrolyze in physiological-like environment delivering two moles of halide per mole of starting complex, leading to the corresponding Au(III)-diaquo counterparts within 30-40 min. The hydrolyzed species were proved to be reasonably stable in physiological-like solution, and reduce to gold(I) species only after 12-24 h.

With reference to the interaction with DNA, experimental results highlighted that there is a dramatic inhibition of both DNA and RNA synthesis in a non-dose-dependent way, whereas cisplatin promoted a strong inhibition of DNA without significantly affecting RNA synthesis, as expected. In addition, gold (III) dithiocarbamato complexes showed extremely fast rates of DNA binding (100% to calf thymus DNA after 3h), with respect to cisplatin (51% after 24h) under the same experimental conditions. They were also proved to form intrastrand cross-links with a faster kinetics than cisplatin, but they were unable to induce DNA-protein cross-links[196].

This ability of Au(III)-dithiocarbamato derivatives to bind DNA to a greater extent than cisplatin, seems to be a consequence of their higher reactivity toward isolated biological-relevant macromolecules, rather than undoubtedly assign DNA as their ultimate target[195]. As the mechanism of action of our gold(III)-compounds differs from that of the classical platinum(II)-based anticancer drugs and DNA seems not to be the only and/or the major target, interaction with other biomolecules were explored.

Thioredoxine reductase

The thioredoxine system, along with the glutathione one, is one of the main machineries involved in the cellular control of the thiol redox state.

In particular, the enzyme thioredoxine reductase (TrxR) has been recently described as potential target for some gold anticancer compounds[197].

Trx is a small ubiquitary protein (12 kDa) expressed in cells in two isoforms, the cytosolic Trx1 and the mithocondrial Trx2. Both human isoforms keep the active site, characterized by the sequence {Cys-Gly-Pro-Cys} unmodified, and it is highly conserved in other species as {Cys-X-X-Cys}. It plays different roles in cells, comprehending reduction of ribonucleotide reductase enzyme during DNA synthesis, and activation of ROS (reactive oxygen species) scavengers through reduction of peroxiredoxine enzyme (Prx). Moreover it was demonstrated that it can activate, by reduction, different transcription factors involved in the regulation of different aspects of cellular proliferation and differentiation (AP-1, SP-1), cellular migration (NF-κB) and apoptosis (p53)[77].

The cytosolic form is overexpressed in many human carcinomas, and its cellular levels are linked to the tumor aggressiveness and inhibition grade of the apoptotic processes. It was so often identified as possible target for the pharmacological development of new anticancer drugs.

TrxR was found to be a potential target for gold(III) complexes, as well. It is a homodimeric selenoenzyme which controls the redox state of thioredoxine. In mammals, its catalytic site {Cys-Val-Asn-Val-Gly-Cys} is highly conserved, and the presence of a selenocystein in the C-ter is fundamental for the redox catalytic process.

Since gold compounds are known to have high affinity for selenium residues, TrxR results a good target candidate for these compounds, also considering that the redox center of the enzyme is located on a flexible chain exposed to the solvent and reactive to electrophilic agents[197].

TrxR was proved to be inhibited by a number of gold derivatives, thus triggering alterations of the mitochondrial functions and inducing severe oxidative stress, eventually leading to cell apoptosis. Our gold(III)-dithiocarbamato complexes were proved to induce cancer cell death through both apoptotic and non-apoptotic mechanisms, and to inhibit TrxR activity[129].

For some first generation gold(III)-dithiocarbamato complexes, it was hypothesized that a potential mechanism of action involves the deregulation of the Trx/TrxR system through the inhibition of both the cytosolic and mithocondrial forms of TrxR, allowing uncontrolled ROS production and modification of some mitochondrial functions (for example: alteration of membrane potential, induction of mitochondrial swelling without modifying the respiratory chain), ultimately causing cell death.

Gold(III) complexes presumably inhibit TrxR by covalently irreversible binding to its active site, avoiding the possibility for the enzyme to act as a mediator in the active

transport of electrons from nicotinamideadenindinucleotide phosphate (NADPH) to Prx, thus determining the increase of ROS concentration levels in cells. Deregulation of Trx/TrxR system activates other pathways in cells, as the one connected to the dissociation of the Trx-ASK-1 (Trx-apoptosis signal-regulating kinase 1) complex, with consequent activation of MAPK (mitogen-activated protein kinase) system. High levels of ROS, along with activation of MAPK system, induce a persistent presence of phosphorylated ERK-1 and ERK-2 (Extracellular signal-Regulated Kinases-1(/2)), which induces cell death. (**Figure 6.1**).

Nonetheless, phosphorylation of ERK-1 and consequent cell death, can be prevented through the action of an antioxidant agent as L-NAC (N-acetyl-L-cysteine) which, by keeping Trx in the reduced form, can prevent the dissociation of the Trx-ASK-1 complex. On the contrary, the antioxidant Trolox (6-hydroxy-2,5,7,8-tetramethylchroman-2-carboxylic acid) is not able to prevent cell death, since does not interact with thiols but only with free radicals, like peroxo species[129].

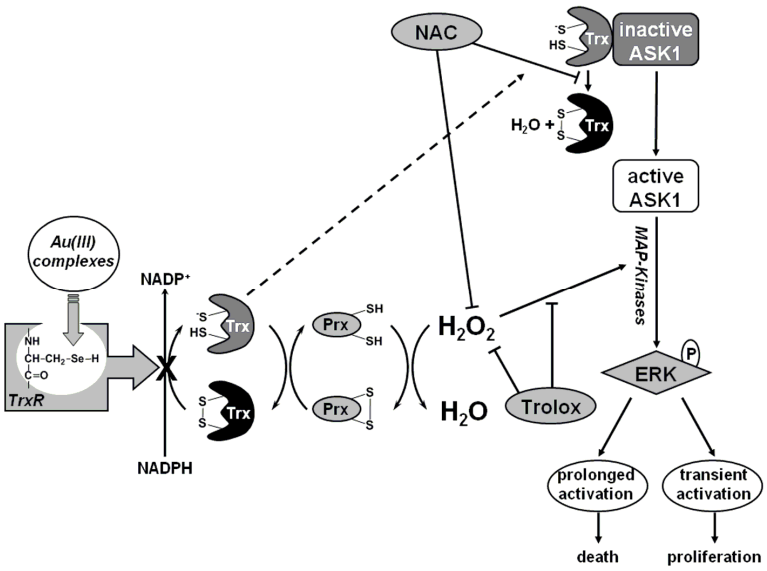

Figura 6.1: molecular mechanism of apoptotic death induction through Trx/TrxR system inhibition by gold(III)-dithiocarbamato complexes (adapted from[129]).

Thus, it was hypothesized that the persistent activation of ERK-1/2 by ROS, followed by the deregulation of ASK-1, can be responsible for cell death through both apoptotic and non-apoptotic processes (as demonstrated by the % of PARP (poly-(ADPribose)-polymerase) cleavage, known to be an apoptotic marker[129].

High levels of Trx and TrxR (with respect to those observed in healthy cells) were detected in many cancer types[198,199], including prostate cancer[200], and were proved to be connected to the insurance of platinum[201] and docetaxel resistance[202] in this cancer type.
For this reason, gold(III) complexes were tested *in vitro* on two human cancer cell lines androgen-resistant (namely PC3 and DU145)[2]. In particular, $[Au^{III}Br_2(ESDT)]$ (AuL12) showed lower GI_{50} values on PC3 and DU145 cell lines than cisplatin. Moreover, the results were comparable to those registered on the PC3 cisplatin-resistant counterpart, PC3-R. In that case, it was demonstrated that the compound inhibits the activity of TrxR in PC3 cells, inducing ROS formation and depolarization of the mitochondrial membrane, activating preferentially the intrinsic mitochondrial apoptotic pathway[2].

Proteasome

Also proteasome was recently identified as possible target for our gold(III) complexes. The proteasome 26S is a large protease complex (>2400KDa) constituted by different subunits (19S and 20S), present both in the cellular nucleus and cytosol. It is a fundamental part of the ubiquitin-proteasome system (**Figure 6.2**), which plays an important role in the proteolytic degradation processes in eukaryotic cells and is essential in controlling the concentration of many intracellular proteins, preserving the normal cell functions. Its role consists principally in the degradation of proteins implicated in processes concerning the proliferation, apoptosis, and progression of cell cycle, along with the degradation of abnormal proteins generated from oxidative stress or mutations.
The degradation process is possible only after the targeting of the substrates by covalent binding to ubiquitin molecules. Ubiquitin (Ub) is a small protein made of 76 amino acidic residues which binds to substrate-proteins through the subsequent action of three distinct enzymes, which favor the activation (E1), conjugation (E2) and binding (E3) to the molecule to be degraded.
The protein is marked by one or more ubiquitin molecules (ubiquitinated) and delivered to proteasome 26S, characterized by the 20S catalytic core and the two 19S regulatory units. These last two units are localized at the two opposite ends of the catalytic *core*, and recognize the ubiquitinated proteins regulating their entrance to 20S subunit, characterized by a "barrel"-like structure made of 28 subunits (14 of type α and 14 of type β) organized in four eptameric rings (7α-7β-7α) piled to form a cylindrical structure with the catalytic site in the middle.

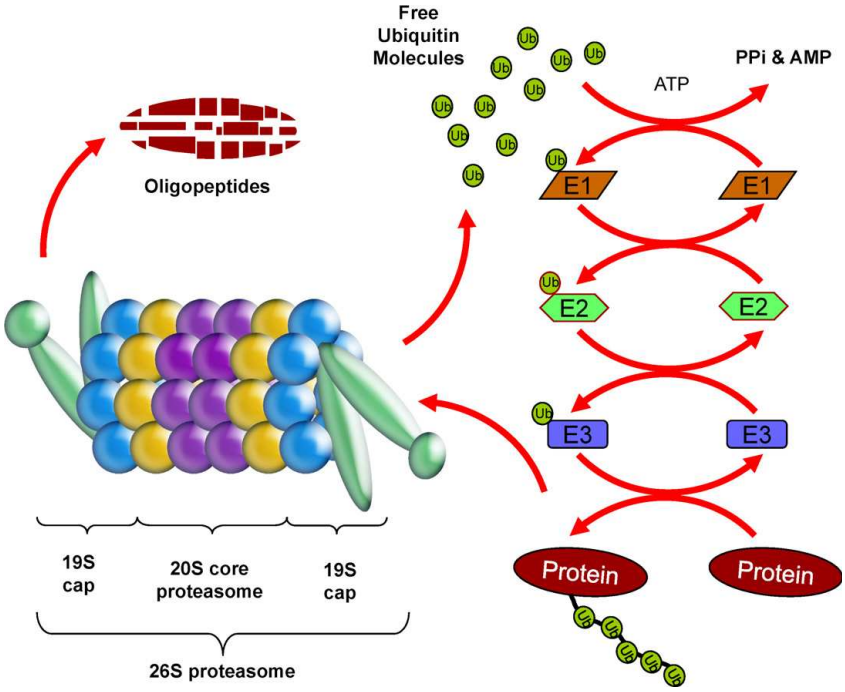

Figura 6.2: The ubiquitin-proteasome pathway. A target protein degraded by the ubiquitin-proteasome pathway is first covalently modified by multiple ubiquitin (Ub) molecules in a three-stepped, highly regulated enzymatic process involving an Ub-activating (E1), Ub-conjugating (E2), and the Ub-ligating (E3) enzymes. The ubiquitinated protein is then escorted to the 26S proteasome, recognized by the 19S cap, de-ubiquitinated and then degraded by the catalytic 20S core into oligopeptides. The ubiquitin molecules are released and recycled[201].

The proteolytic activity is executed in the β-subunits and comprehends chimotripsyn-like (cut after hydrophobic residues), caspase-like or PGPH-like (Peptidylglutamyl Peptide Hydrolizing-like, cut after acidic residues) and tripsyn-like (cut after basic residues) activity, while the two α-subunits regulate the access to the catalytic *core*, allowing the passage of only non-folded and extended substrates[203].

In some pathologies, like cancer, it has been observed an anomalous proteasome activity, which leads to the overexpression of some antiapoptotic proteins and the degradation of other pro-apoptotic ones, thus determining an uncontrolled proliferation of unhealthy cells and the progression of the disease.

In the case of colorectal carcinoma, leukemia and prostate cancer, the level of proteasome alteration was demonstrated to be strictly connected to the grade of malignity and to tumor aggressiveness[204,205].

Cell cycle arrest and apoptotic death of tumor cells are thus activated in cancerous cells upon inhibition of the ubiquitin-proteasome system, as consequence of the accumulation of tumor suppressor factors and pro-apoptotic proteins[206].

The inhibition of this system can be achieved preventing the binding of ubiquitinated substrates to the enzyme catalytic core, made by Thr1, Glu17 and Lys33 residues[207], where the N-ter amino acid threonine is directly responsible for the substrate degradation. Around the active site of the enzyme are located binding pockets, which allow the recognition of the amino acids side chains which undergo to the proteolitic cleavage. The identification of this specific binding sites allowed the design of suitable compounds capable of selectively and irreversibly binding them, acting as inhibitors of the proteasome activity[203]. Nonetheless, the inactivation of the enzyme could take place also indirectly, for example by oxidative modification and inactivation upon exposure to free radical-generating systems.

In this context, a "first generation" complex was tested as possible proteasome inhibitor, since it was known to exhibit high cytotoxic activity on different breast cancer cell lines. In particular, the compound was tested *in vitro* on the human breast cancer cell line MDA-MB-231, an highly metastatic and invasive cancer type, registering a cellular growth inhibition of nearly 85% (at a concentration of 5 μM), with respect to the 20% inhibition caused by cisplatin treatment.

The same gold(III) compound was proved to strongly inhibit the chymotrypsin-like proteasomal activity on MDA-MB-231 whole cell extract, in a dose-dependent way. This result is particularly important since this effect is associated to the induction of cell growth inhibition in cancer cells, and activation of apoptotic processes[208].

Proteasome inhibition was also detected after treatment of intact MDA-MB-231 cells with the same compound, leading to the increase of the ubiquitinated proteins and of proteasome target protein, p27.

Moreover, *in vivo* tests on immunodepressed mice inoculated with the same breast tumor type, demonstrated how the treatment with the gold compound caused a significant reduction of tumor mass, by 49% with respect to non-treated mice, accompanied by proteasome activity inhibition.

It is important to underline that after 29 days of treatment with daily 1 or 2 $mg \cdot kg^{-1}$of gold(III) compound, the mice have not shown signs of prostration, anorexia of weight loss[209].

All these results identify the proteasome as primary target for our gold(III) complexes, without anyway excluding the possible affection of the Trx/TrxR system.

Indeed, our gold(III)-dithiocarbamato complexes are known to cause a consistent production of ROS in cells. This can hence favor the production of high levels of

persistent phosphorylated ERK-1/2, which can affect the TrxR/Trx system. But, at the same time, the increase in ROS concentration levels can oxidize and thus inactivate the proteasomal activities.

This process was indeed recently reported also for Bortezomib, the first and only proteasome inhibitor recently approved by FDA for the treatment of multiple myeloma, which can induce apoptotic death in treated cells through either direct or indirect inactivation of the enzyme functions.

PARP-1

Exploring the possible targets responsible for the cytotoxicity of our class of compounds on cells, also the DNA damage repair route was taken into account.

As above reported, the results of direct interaction of our gold(III) compounds with DNA show that, even if the compounds have a great affinity for DNA purified molecule, it does not seem to be *in vivo* a major target. Nonetheless, enzymes involved in the repair and regulation mechanisms of DNA can be affected by the action of the gold(III) dithiocarbamato complexes.

In particular, our investigation focused on the interaction of the compounds with PARP-1 (poly-adenosine diphosphate (ADP)-polymerases-1), a zinc-finger protein essential for DNA repair and also relevant in activation of resistance mechanisms to cisplatin in cancer cells[210].

Among the PARP family, PARP-1 enzyme is one of the most studied and well-characterized[211], playing a central role in the repair of subtle DNA damages caused for example by alkylation, oxidative stress or single-strand breaks principally *via* the base excision repair pathway[212].

The human homologue of PARP-1 (hPARP-1) is a highly conserved nuclear enzyme of 113kDa, characterized by the presence of three major domains[213]:

- the amino-terminal DNA binding domain (DBD), which contains two zinc-finger motifs (ZnF1 and ZnF2) that are sensitive for DNA-damage and bind to it specifically;
- the auto-modification domain, which binds to poly-ADP-ribose (PAR)[214];
- the C-terminal catalytic domain, containing the third zinc finger motif (ZnF3).

Among the three zinc finger domains, ZnF2 has the strongest affinity for DNA breaks, while ZnF1, with the cooperation of ZnF3, is responsible for PARP-1 activation[215,216].

Any damage in the DNA structure activates PARP-1, which breaks nicotinamide-adenine-dinucleotide (NAD^+) in ADP-ribose and nicotinamide. Subsequently, ADP-ribose unites are linked together to form long chains of poly-ADP-ribose (PAR) which covalently attaches to acceptor proteins as PARP-1, histones, and other DNA-repair proteins. This long negatively charged polymer located closely to the damaged DNA site acts like a scaffold, recruiting other proteins that are involved in the BER/SSB (Base Excision Repair/Single Strand Break) mechanism and resulting in the repair of the damaged DNA. On the other end, the over-activation of PARP-1 may cause a depletion of NAD^+ pools, which conversely activates the necrosis response of the cell. Upon PARP-1 inactivation, a cascade of signals that promote apoptosis is started, preventing both the repair of DNA damages and the activation of necrosis caused by huge consumption of NAD^+. The overexpression of this enzyme, both at mRNA and protein expression levels, was detected in a variety of cancer types. In particular, nuclear levels of PARP-1 in breast cancer (especially in triple-negative tumors) have been directly correlated to the level of progression of the malignant transformation, representing a parameter to predict poor prognosis in operable invasive breast cancer[217]. The connection between PARP-1 overexpression and cancer progression has not been fully elucidated yet. Nonetheless, it is known its contribution to the regulation of important transcription factors as NF*k*B[218,219], which overexpression is connected to the tumor progression and malignancy[220,221], being also directly involved in the angiogenenic process, important for cancer development[222].

In the past, cellular dysfunctions in the DNA repair were exploited to cause irreversible DNA modification that couldn't be recognized by DNA repair enzymes, and ultimately led to cell death. Today an alternative approach has been evaluated, and compounds were designed to specifically target components involved in the DNA damage repair process, as topoisomerase or PARP enzymes[222].

The importance of targeting PARP enzymes arises mostly from their ability to act as initiators of a signal cascade that lead to cell death through an apoptotic mechanism.

In the last decades compounds capable to inhibit PARP-1 emerged as potential anticancer drugs, either to be used alone or in combination with other well-established drugs which cause DNA damage, thus amplifying their cytotoxic effect[223].

PARP enzymes, in particular, are playing a dual role in the DNA damage response, acting not only as DNA damage sensors but also as signal transducers to down-stream effectors.

Many compounds have been developed in the last years to specifically target PARP-1 or PARP-2, and are now in the early stages of clinical trials[224]. One of them, Olaparib

(*AstraZeneca*), showed an IC_{50} value of 0,005 µM for the inhibition of PARP-1 enzyme in the *in vitro* screenings, and is now in clinical phase studies for the treatment of ovarian, breast and colon rectal cancer[225].

Experimental section

Analysis of the proteasomal activity on purified 20S proteasome

The purified human 20S proteasome (0.5 nM) was incubated in triplicate with three different proteasomal fluorogenic substrates (20 µM) and the compound (IT03) (previously dissolved in DMSO) at various concentrations ranging from 0.1 to 10 µM, or an equivalent volume of solvent DMSO as control in 100 µL assay buffer [20 mM Tris-HCl (pH 7.5)]. After 1 hour incubation at 37°C, inhibition of each proteasomal activity was measured recording the fluorescence of the hydrolyzed AMC groups by means of a Wallac Victor^3 1420 multilabel counter (Perkin Elmer, excitation wavelength = 355 nm, emission wavelength = 460 nm, measurement time 0.1 s).

PARP-1 inhibition assay on purified protein

The ability of the test compounds to inhibit PARP-1 enzyme was evaluated on the pure protein using the *HT Universal Colorimetric PARP Assay Kit* (*Trevigen*). The assay is based on the detection and quantification of biotinylated-poly(ADP-ribose) linked onto histone proteins in a 96-well strip plate. PARP-1was purified after expression from *E.Coli* containing recombinant plasmid harboring the human PARP gene. The protein is generally quantified in Units, defined as the amount of enzyme incorporating 10 fmol of NAD^+ onto 5 µg of immobilized histones in 30 minutes at room temperature.

The compounds dissolved in DMSO (with exception of cisplatin, dissolved in saline solution containing 0.9% NaCl) were diluted in water and incubated with 0.5 U of recombinant human PARP-1 in PARP Buffer (*Trevigen*) to different final concentrations and then incubated with 0.5 U for 1h at room temperature (final DMSO content per sample < 0,1%). Samples not containing PARP-1 were used as negative controls for reading the background absorbance, while positive controls containing only PARP-1 solution were used as reference for determine the 100% of enzyme activity.

After the incubation with the compounds, the amount of active PARP-1 was evaluated by adding Streptavidine-HRP to the samples in presence of a mixture of NAD^+, biotinylated-

NAD^+ and activated DNA. The Streptavidine-HRP-biotine conjugates so formed were subsequently quantified incubating the samples with TACS-Sapphire for 30 min in the dark[226]. The absorance for each well was then recorded at 630 nm using a ThermoMaxMicroplate Reader (*Molecular Devices*).

Results and discussion

6.1 *In vitro* inhibition of proteasome 20S

The second generation compound IT03, one of the most active gold(III)-peptidedithiocarbamato complexes screened, was tested for the inhibition of all the three principal proteolitical activities present in the proteasome core 20S (**Table 6.1**), and the results were compared to those recorded for the first generation compound, AuL12.

In particular, IT03 inhibitory activity resulted significative especially for the chimotripsine-like function, which is known to be strongly connected with the activation of apoptotic response. Its inhibitory potency seems to be slightly improved if compared with the test compound AuL12. The IC_{50} values are anyways still higher than the values obtained for the reference proteasome inhibitor Velcade® (Bortezomib, *N*-acyl-dipeptidyl boronic acid; *Millennium Pharmaceuticals*, **Figure 6.4**).

Table 6.1: IC_{50} values for inhibition of proteasome activities by selected gold(III) dithiocarbamato compounds, with respect to the activity of the reference proteasome inhibitor *Velcade.*

	IC_{50} (μM)		
	IT03	**AuL12**	***Velcade***
Chimotrypsyne-like (CL)	0,68	1,13	*0,002*
Trypsine-like (TL)	1,7	-	
Peptidyl-glutamyl-peptide-hydrolysis-like (PGPHL)	0,77	-	

Up to now Velcade® is the only proteasome inhibitor approved by the *Food and Drug Administration* (FDA) and is currently used for the treatment of relapsed multiple myeloma and mantle cell lymphoma[18].

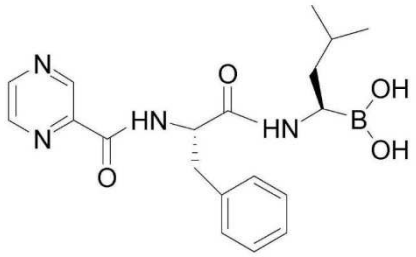

Figure 6.4: molecular structure of Velcade® (Bortezomib).

It consists in a small boronic acid dipeptide molecule that binds reversibly to the subunit of the 20S catalytic cavity, responsible for the chimotrypsine-like activity of the enzyme. In particular, the compound binds through the boron atom (that shows Lewis acidity properties) to the oxygen of an *N*-terminus threonine sited in the catalytic pocket of the enzyme[18].

The mechanism of action of our gold(III) dithiocarbamato complexes towards proteasome is not fully understood yet, and different pathways can be correlated to the final inhibitory outcome. At least two (or three) mechanisms could be responsible for the inactivation of proteasome by our compounds *in vivo*. These include direct binding to the active site, redox processes involving Au(III) and sulfur containing biomolecules, as for example glutathion (GSH), and ROS production. So, apart from the direct inactivation or oxidation, also secondary redox effects can take place, emphasizing the enzyme inhibition effect.

Therefore, the mechanism of proteasome inhibition of gold(III) dithiocarbamato complexes seems to be different from the one hypothesized for bortezomib, and the evaluation of IT03 inactivation *in vitro* describes only partially the situation that could occur *in vivo*, where secondary effects could participate to the effective inactivation of the enzyme. In fact, contrary to bortezomib, IT03 affects all the three principal proteasome activities presented by the 20S core, as shown in **Table 6.1**.

6.2 *In vitro* inhibition of PARP-1 enzyme

PARP enzymes are essential proteins involved in cancer resistance to chemotherapies. They play a key role in DNA repair by detecting DNA strand breaks and catalyzing poly(ADP-ribosylation), and consequently PARPs have been referred to as “the guardian angels” of DNA. PARP-1, in particular, is activated by mild to moderate genotoxic

stimuli, which facilitates DNA repair by signaling cell cycle arrest and by interacting with DNA repair enzymes. Severe DNA damage may even induce hyperactivation of PARP, which ultimately leads to apoptosis[210]. The initiation of the apoptotic process is characterized by the activation of caspases (cysteinyl aspartate specific protease), causing the cleavage of multiple targets in cells. PARP, being a specific substrate for caspases 3 and 7, is recognized as a marker for apoptosis. Studies regarding "first generation" compounds have shown how, upon treatment of cells with gold(III) compounds, the levels of cleaved PARP were not dose-dependent, thus highlighting that also other cell death mechanisms can be involved (*i.e.* necrosis).

Since it is known that PARP-1 can be a pharmacological target for some anticancer compounds[213], the direct inhibition of the enzyme by our gold(III) complexes was investigated. For other gold(III) compounds it was indeed demonstrated that the metal can inhibit the enzyme by directly binding to the zing-finger domain, thus competing with Zn(II) for the binding site[210].

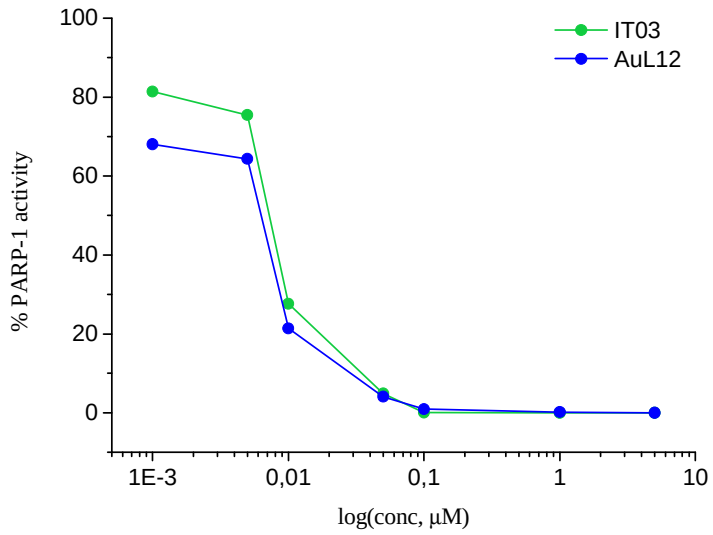

Figure 6.5: inhibition of PARP-1 activity by test compounds at different concentrations (from 10 to 0.01 µM). For the assay each compound was incubated for 1 h with 0.5 U of purified protein.

Our gold compounds were tested as inhibitors of PARP-1 purified protein, using a universal colorimeter PARP assay (*Trevigen*), and the values were compared to the those obtained for other gold(III) compounds[210] and for drugs now in clinical trials as specific PARP-1 inhibitors.

The inhibitory activity of the model compound IT03 and the first generation compound AuL12, obtained after 1 h incubation with the purified enzyme, are shown in **Figure 6.5.** The corresponding IC_{50} values were correlated to those obtained for cisplatin, the PARP-inhibitor Oliparib and the gold(I) antiartritic drug auranofin (calculated after 24h incubation), and are reported in **Table 6.2** only for comparative purposes.

Table 6.2: inhibitory activity of selected compounds on purified PARP-1. IC_{50} values and st.dev. (μM) are the result of data collected in three independent experiments.

	IC_{50} ±st.dev (μM)
IT03	0,017±0,006
AuL12	0,019±0,004
cisplatin	*12,3±2,0*[¥]
auronofin	*0,079±0,009*[¥]
oliparib®	*0.00500±0,00001*[¥]

[¥] evaluated after 24h incubation

As we can see from the data shown above, our gold(III)-dithiocarbamato compounds result as good inhibitors of the purified PARP-1, with IC_{50} value in the nanomolar range. The inactivation of PARP-1 by AuL12 was evaluated not only on the purified protein, but also on the total cell extracts.

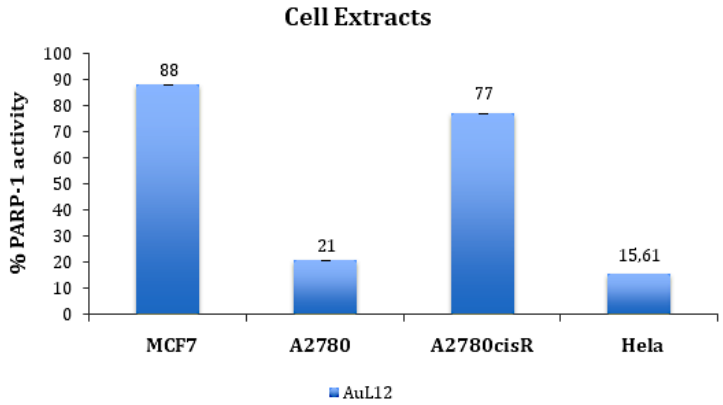

Figure 6.6: inhibition of PARP-1 from cell extracts.

The cultured cells were detached, centrifuged at 10,000 g/min at 4°C for 10 min and then resuspended in lyses buffer (*Trevigen*). After 15 min on ice, lysates were centrifuged obtaining a pellet of cellular debris, while the supernatant was removed.

The total protein content in each sample was determined by using the DC Protein Assay Kit (*BIO-Rad*). For each sample, 50 µg of cell extracts was then incubated with the gold compounds at fixed concentration. Non treated samples were also collected as controls.

Preliminary experiments with AuL12 were performed on MCF-7, A2780, A2780cisR and HeLa cells (**Figure 6.6**).

Also the results obtained for the cell extracts show an inactivation of PARP-1 by our compound, with higher values in particular on A2780 and HeLa cells. It is interesting to notice how the inactivation of PARP-1 from A2780cisR cell extracts with respect to normal A2780 is relevantly different (**Figure 6.6**).

Moreover, comparing the PARP-1 inactivation with compounds' cytotoxicity on cell lines, we can notice that apparently there is no direct correlation between cytotoxic activity and PARP-1 inactivation. Indeed, MCF-7 and HeLa cells, which are similarly sensitive to the tested compounds, show very different values of PARP-1 inactivation from the cell extracts.

The reported results are representative only of a preliminary study that we are currently performing on the gold(III)-oligopeptide dithiocarbamato derivatives as well. Further investigation should be done on cell extract deriving from cultured cells incubated with the compound for 24 h.

To sum up, the model compound IT03 was chosen among the newly synthetized compounds, to achieve more insights into their mechanism of action.

Two enzymes involved in two different pathways of apoptotic activation, known as targets for other anticancer drugs, were selected for leading the preliminary assays *in vitro*. The results demonstrated that the "second generation" compound is able to inhibit all the three proteolytic functions of 20S proteasome and affects PARP-1 activity with IC_{50} values in the nanomolar range. Nevertheless, further experiments on intact cells should be carried out to achieve more information about the effective targets *in vivo*.

Chapter 7

Real-time cell growth inhibition profile analysis and Au uptake kinetic studies

From the results presented in the previous Chapter, we continued the investigation of the mechanism of action of our gold(III)-peptidedithiocarbamato complexes through the evatution of the kinetic cellular response upon their administration to cancer cells.

In particular, the inhibitory effect of our compounds on cell proliferation was monitored real-time through an electronic device which provides also informations about morphological changes and cell adhesion variations.

Interestingly, it was demonstrated that the analysis of the cellular growth inhibition profiles with time results diagnostic for the discrimination of different mechanism of action exerted by drugs on cells.

As shown in **Figure 7.1**, cells exposed to selected compounds were dynamically monitored over 70 h, using real-time electrical impedance as a measure of viable cell number. Using this methodology, five well-characterized cytotoxic compounds were found to have different kinetics responses. Digitonin (**Figure 7.1A**), a mild detergent, and tamoxifen (**Figure 7.1E**), a Ca^{2+} influx stimulator, were fully cytotoxic to HepG2 cells after only 10 min of exposure. Potassium dichromate (**Figure 7.1B**) and doxorubicin (**Figure 7.1D**), both DNA-damaging agents, demonstrated a slower onset of activity and induced complete cytotoxicity only after 35 h of exposure. Finally, cycloheximide (**Figure 7.1C**), a protein synthesis blocker, inhibited cell proliferation but did not decreased cell number below the amount present at the time of addition[227].

All these results highlight how, almost in principle, it is possible to discriminate between drugs having different mechanisms of action, by comparing their time-dependent cell growth inhibition profiles. Similarly, for new drugs it can be possible to achieve more insights into their mechanism of action by correlating the experimental data to the profiles recorded for well characterized drugs.

Lastly, the data obtained from the analysis of the cellular growth and adhesion profiles over time, were subsequently correlated to the results obtained for kinetics experiments which evaluate the kinetics of gold uptake by cells after treatment with the complexes (determined *via* ICP-AES analysis).

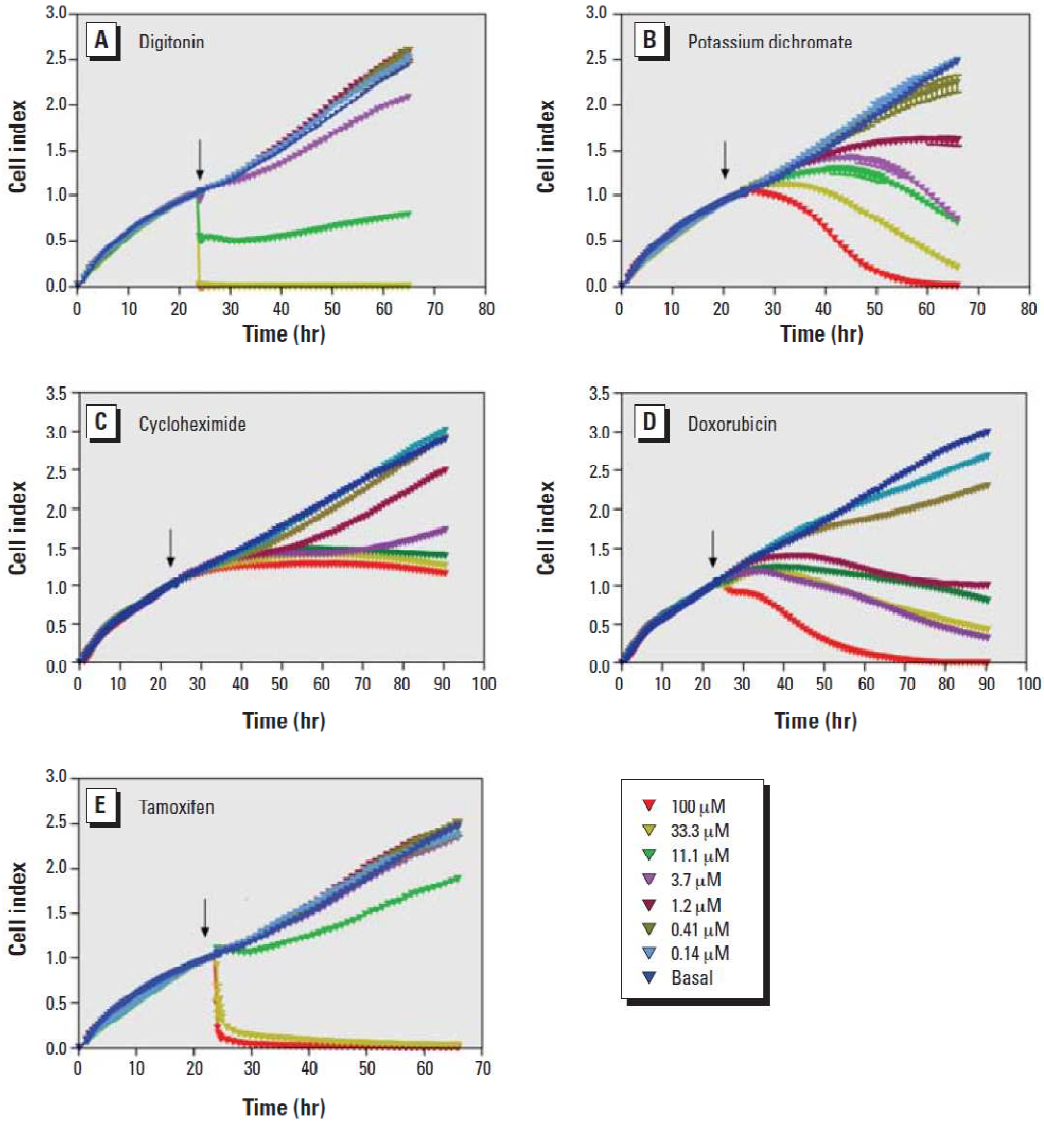

Figure 7.1: Kinetics of cytotoxicity responses for digitonin (A), potassium dichromate (B), cycloheximide (C), doxorubicin (D), and tamoxifen (E) in HepG2 cells monitored by the RT-CES system. 10,000 cells/well were plated in 16-well strips for the RT-CES cytotoxicity assay. ↓, time of compound addition. Different compound concentrations are indicated by different colors. Data are normalized to the time of compound additionat 22–24 h of cell culture[227].

Experimental section

Cell inhibition growth profile with time

Human non-small-cell lung carcinoma A549 cells (*ATCC*) were cultured using the same conditions described in **Chapter 4**. Cell attachment and proliferation was continuously monitored for 96 h in 16-microtiter plates (E Plate 16, *Roche*), characterized by well bottoms covered with gold microelectrodes. The cell-sensor impedance measured at each

well was expressed in arbitrary units called Cell Index, defined as (Rn-Rb)/15 where Rn is the cell-electrode impedance of the well when it contains cells and Rb is the background impedance of the well with the media alone. The Cell Index can be than normalized setting the Cell Index value at treatment to 1. Before the cytotoxicity experiments, the cell proliferation pattern was followed for 24 h in order to determine the optimum number of cells to seed. Cells were seeded at a concentration of 5000 cell·mL^{-1} in 100 µL of media and Cell Index values were collected every 15 minutes. After 24h from seeding, each well was supplemented with the compounds dissolved in 100 µL of medium, to obtain the final desired concentrations. Gold(III) complexes were dissolved in DMSO prior addition to the medium, while cisplatin was dissolved in 0.9% NaCl water solution. Cells were also treated with only vehicle, corresponding to 1% DMSO in medium, as control.

Kinetic experiments of gold dithiocarbamato complex uptake

Materials

Nitric acid 70% v/v and hydrochloric acid 37% for ultratrace analysis were purchased from *Sigma Aldrich*, and the standard Au solution (concentration of 1000 µg mL^{-1}) from *Inorganic Ventures*. ICP measurements were carried out using ICP SPECTRO Arcos with the same equipment and experimental condition described in **Chapter 5**. All solutions were prepared with final *aqua regia* content of 3% v/v.

Method

Human large cell lung cancer H460 cells (*ATCC*) were grown in RPMI-1640 (Roswell Park Memorial Institute, *Sigma Aldrich*) further supplemented with 10% Fetal Calf Serum (FCS), 1% penicillin and streptomycin (*Invitrogen*). Cells were incubated at 37°C in presence of 5% CO_2 and moisture-enriched atmosphere. For the experiment, cells were seeded in 4 mL Petri dishes ($1{,}25 \cdot 10^5$ cell·mL^{-1}) and incubated for 48 h to allow cells to attach and grow.

After 48 h from seeding, the medium was removed and replaced with fresh new one. In the first experiment the uptake kinetics was followed in time, and all the samples were incubated with the compound IT01 at the concentration of 20 µM, with exception of control samples. For the experiment of uptake kinetics at different concentration of compound, each Petri dish was incubated with gold(III) compound at different

concentrations (ranging from 10 to 100 μM) for two hours. In both experiments, each sample was collected following the same procedure: the medium was removed and collected in a Falcon tube, while attached cells were washed with 2 mL saline solution (0.9% NaCl) and incubated with 2 mL trypsin to allow cell detachment. Cells in trypsin solution were put in a Falcon tube and collected with 2 mL saline solution used to wash the Petri dish. 100 μL of solution were withdrawn from each sample to determine the cell number. Cell suspensions were then centrifuged for 5 min at 5000 rpm, the solution discarded and cells washed again with 2 mL saline solution. Death or detached cells were also collected from the medium and gathered to the ones detached from the dishes, after careful washing/centrifuging with saline solution to eliminate possible contaminants coming from the medium. Samples were stored at -20°C. Before ICP-AES analysis, cell pellets were transferred in Pyrex vials and mineralized with *aqua regia*, to obtain samples at final acidic concentration of 3% v/v.

Results and discussion

7.1 Real-time cell proliferation profile after treatment

To achieve more insights into the mechanism of action of our gold(III) compounds, the cellular growth inhibition induced by the treatment with our compounds was followed real-time.

The most common methods used for establish the cytotoxicity of compounds on cells are based on assays which use optical detection methods, that usually involve multi-step protocols. These protocols normally comprehend significant manipulation of the samples in order to obtain detectable species that are related to the percentage of viable cells. Moreover, these methods allow only the determination of the cell viability at a precise time for each experiment, with no information about the development of the system up to that time.

To monitor the real-time proliferation and viability of adherent cells, we exploited the xCELLigence system (*ACEA Biosciences and Roche*). This apparatus allows the determination of viable cells *in situ* through an electronic device that is based on the use of 200 μL/well microplates with bottoms covered with gold electrodes, which allow the measurement of the impedance at the base of each well (**Figure 7.2**).

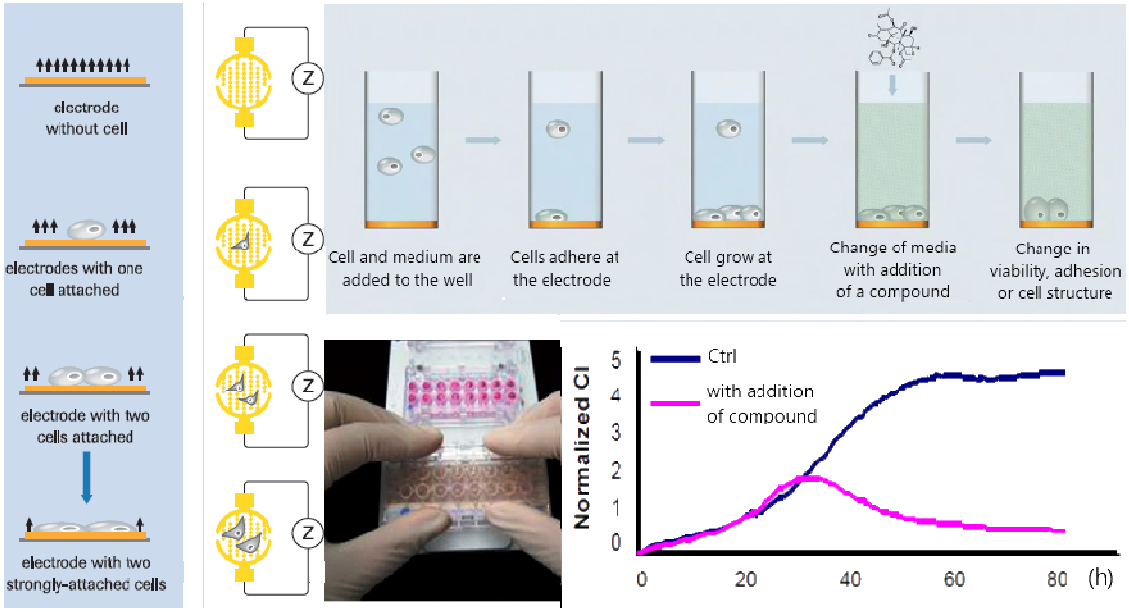

Figure 7.2: detection of cell growth/adhesion modification on gold-coated plates for A549 cells treated with reference compound. Impedance is measured as a function of time in every well, giving a curve with a trend that for cisplatin, could resemble the one reported in this picture.

When only medium is in contact with the electrode a stated value of impedance is measured, that is usually taken as the zero-value. But when cells start to adhere to the well bottom, the measured impedance changes by a value that is proportional to the area of the electrode that is modified. The impedance difference from the zero-value is measured with time and could arise from a change in cell number, efficiency of adhesion, changes of size or morphology. This method allows the real growth or morphology change after the addition of a cytotoxic compound to the cells.

As we can see from **Figure 7.3**, a different adhesion/growth profile can be detected for the treatment of A549 cells with different concentrations of either AuL12 or cisplatin. In the case of cisplatin the cytotoxic effect is evident only after 24 h after the treatment, with a progressive decrease of cell adhesion correspondent to cell death and detachment.

For the compound AuL12, instead, the recorded cellular growth profile is completely different with respect to cisplatin, showing a dramatic lowering of Cell-Index during the first 3 hours after the addition of the compound. This fast modification likely corresponds to a change in the morphology of the cells, which acquire a more rounded shape, as shown in **Figure 7.4**.

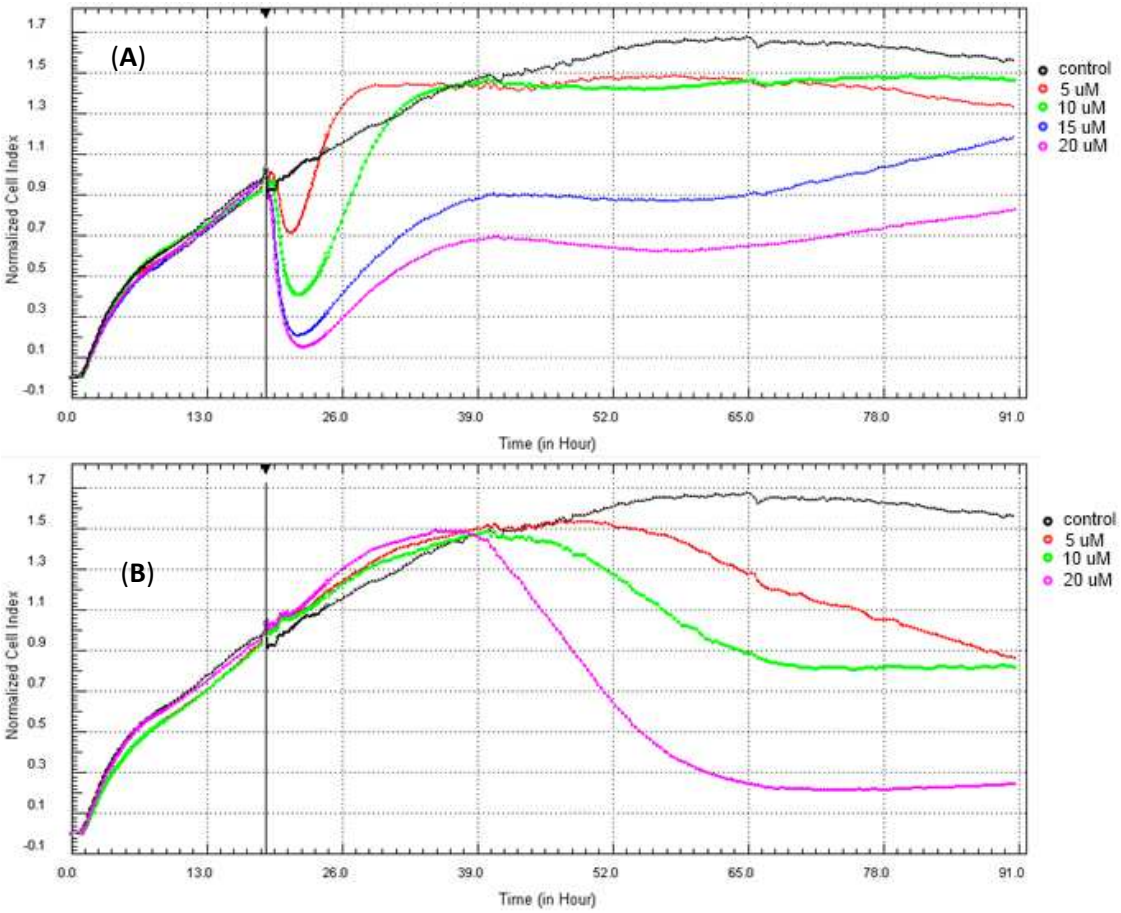

Figure 7.3: profile of cell adhesion/growth after treatment of A549 cells with AuL12 (**A**) or cisplatin (**B**) at different concentrations compared to non-treated cells.

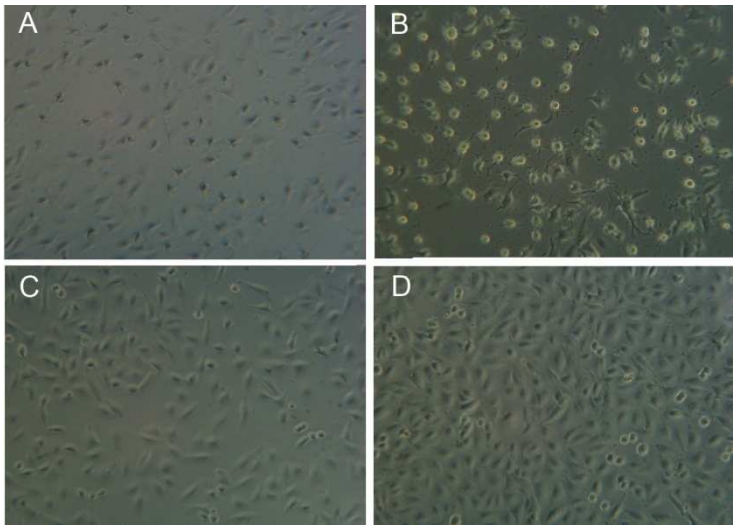

Figure 7.4: photos of A549 cells after 3h from the treatment with AuL12 (A) with respect to the control cells at the same time (C); A549 cells after 24h after treatment with AuL12 (B) with respect to the control cells (D).

The different cellular growth inhibition profile recorded for the two compounds can be presumably correlated to a different mechanism of action of the two compounds in

inducing cell death and allows, almost in principle, to differentiate between compounds acting on different cellular targets and pathways.

As reported in **Figure 7.5**, compounds as Etoposide and Methotrexate, which are both known to be involved in mechanisms of DNA damage, show similar effect on cells proliferation to the one recorded for cisplatin (**Figure 7.3B**), which is known to have DNA as an ultimate target.

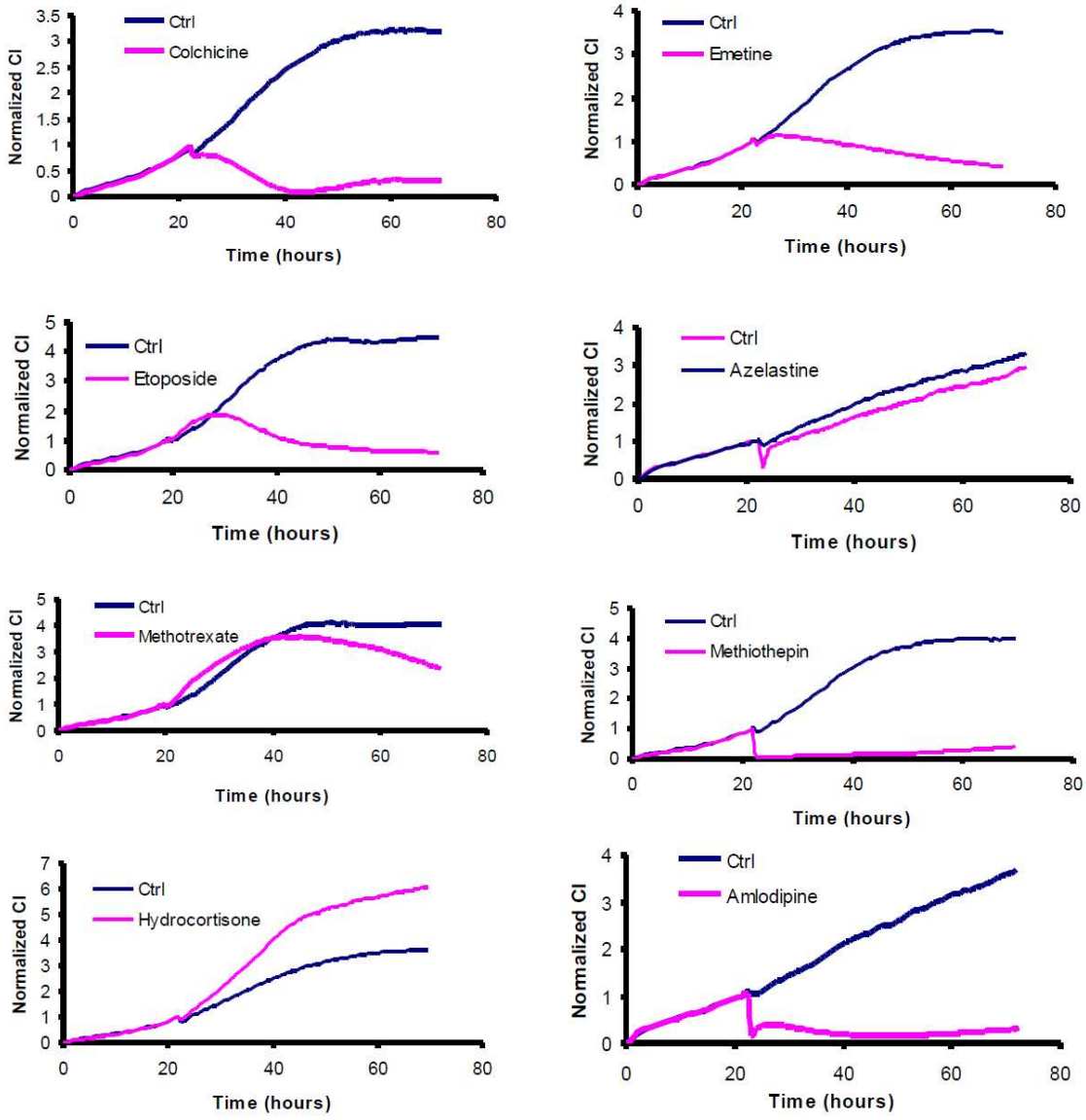

Figure 7.5: Real-time monitoring of apoptosis using the xCELLigence System. HeLa cells were treated with different drugs for which are recognized different mechanisms of action. Cell Index values were monitored continuously for 72 hours.

Otherwise, compounds as Azelastine, Methiothepin and Amlodipine present very fast effects in cellular growth/adhesion profiles since they exert their cytotoxic effect at a membrane level, acting or different receptors. Indeed, Azelastine is a well known

histamine antagonist, Methiothepin acts as a dopamine and seratonine antagonist, while Amlodipine interferes with Ca^{2+} transporters.

The curve shape recorded for AuL12 highlights how the mechanism of action for our gold(III) compounds is completely different from the one recorded for cisplatin and resembles the curve shapes characteristic for the above reported drugs Azelastine, Methiothepin and Amlodipine.

From these data it can be deduced that our compounds interfere (upon direct binding or indirect perturbation) with proteins and receptors present on the cell membrane double layer. This is suggested by the very fast response detected in the variation of Cell Index (CI) which can be correlated to a rapid shape modification (cell rounding within the first 3h) upon the incubation of cells with the compounds, thus resulting in a lowered cellular adhesion to the culture plate bottom. These alterations can be actually due to membrane interactions, which activate cell death processes after few hours from compound administration.

For the second generation compound IT01 similar trends with respect to AuL12 were predictably recorded (**Figure 7.6**), even if at the same concentration the effect on cell growth inhibition was lower. This is consistent with the higher value of GI_{50} calculated for IT01 on A549 cells with respect to AuL12 (20.0 μM and 12.3 μM) respectively (See **Chapter 4**).

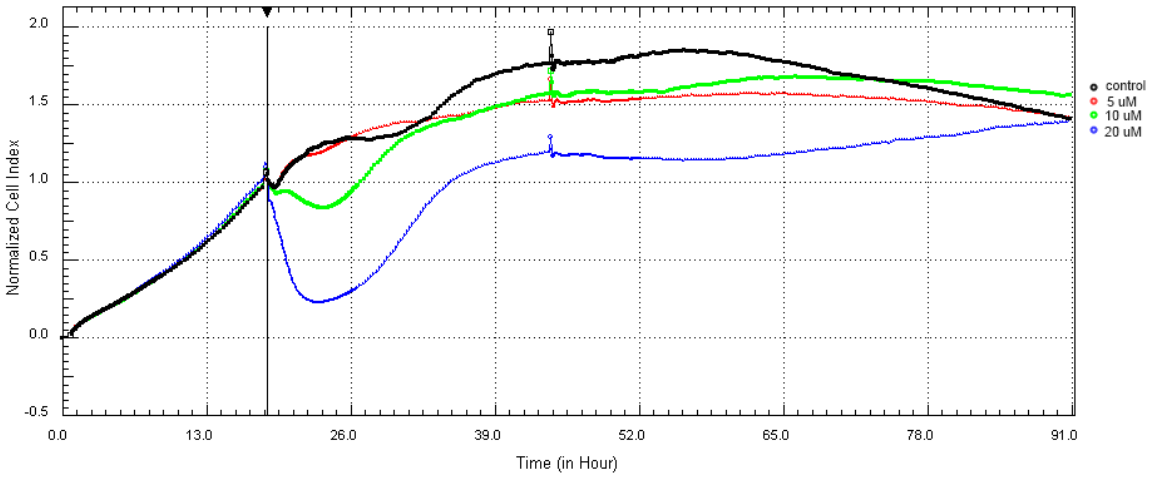

Figure 7.6: profile of cell adhesion/growth after treatment of A549 cells with IT01 at different concentrations (from 1 to 20 μM) compared to non-treated cells.

As we can appreciate from the curves recorded after both AuL12 and IT01 treatment, the cells present their maximum cytotoxic effect after nearly 24 h from compound administration and following tend to recuperate their viability. To assure that the recovery

in Cell Index was not due to secondary effects derived from the precipitation of gold(I) or gold(0) species on the culture plates bottoms, the effect of the sole compounds in complete cell culture medium was tested. The compound was dissolved in culture medium solution and added to the wells, in absence of cells, monitoring the Cell Index over time to detect possible variations in the registered inductance. As reported in **Figure 7.7B**, it can be seen that no contributions to the Cell Index derive from the effect of possible degradation products deriving from modifications of the compounds in medium.
Moving beyond, to prevent the effect of regained viability after 24-48 h from compound administration, cells were treated with AuL12 again after 24 h from the first addition. As we can see from **Figure 7.7A**, the cellular proliferation after the second treatment is completely inhibited and complete cell death is reached after 72h even for the lower concentration of compound used. This result is encouraging if taking into account that in the *in vivo* experiments the compound is administered every day or on alternate days, so complete tumor growth inhibition can predictably be achieved by administration of consequent even not lethal doses of the gold(III) cytotoxic compounds.

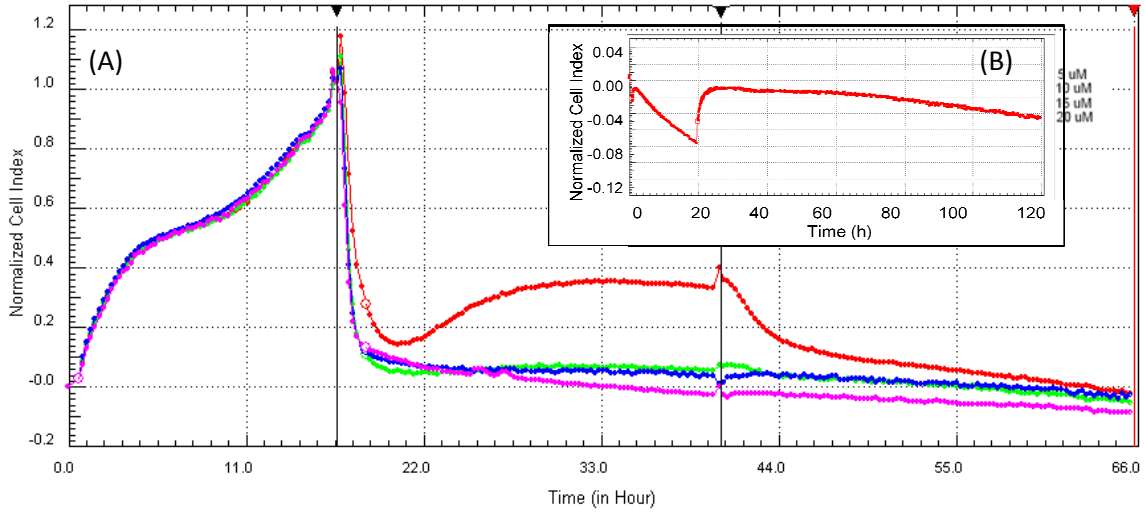

Figure 7.7: (A) profile of cell adhesion/growth after treatment of A549 cells with AuL12 at different concentrations (from 1 to 20 μM) at time t_1=0 and t_2=24h; **(B)** effect on Cell Index of compound dissolved in complete cell culture medium in absence of cells.

For comparison purposes, we have decided to perform some real-time *in vitro* experiments with a ruthenium(III)-dithiocarbamato complex, α-$[Ru^{III}_2(pdt)_5]Cl$, that was tested in the same experimental conditions (**Figure 7.8**).

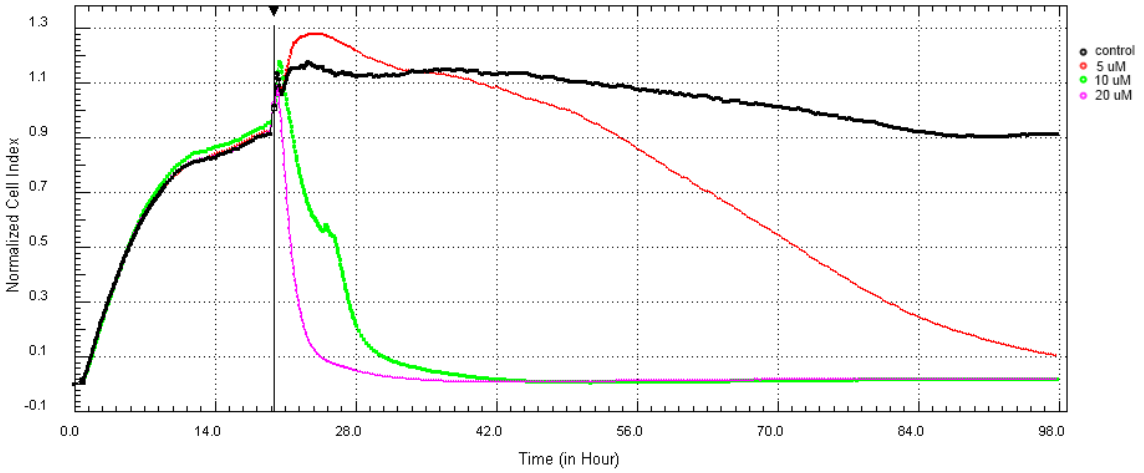

Figure 7.8: profile of cell adhesion/growth after treatment of A549 cells with α-$[Ru^{III}_2(pdt)_5]Cl$ at different concentrations compared to non-treated cells (from 1 to 20 μM).

The selected Ru(III) compound was chosen among the series synthesized in our laboratory for its encouraging antiproliferative properties, since it was found to be active on human non-small cell lung cancer cells H1975 with GI_{50} values of 0.059 μM[19]. In this case, the shape of the recorded curves is completely different from the characteristic curves obtained for our gold(III) complexes. Since the compounds share the same type of ligands attached to the metal center, the different mechanism of action can thus be related to the different properties of the metal itself, or to its different geometrical and coordinative properties.

7.2 Kinetic studies of cellular gold uptake

To gain more information about the rapid morphological changes recorded on cells after treatment with the gold(III) complexes, as reported in previous section, kinetic experiments of cellular uptake upon their administration to cancer cells was evaluated, setting up two different types of experiments. In the first one, the uptake of the gold(III) compound IT01 (chosen as reference) was evaluated over time. Cells were incubated with a fixed amount of IT01 complex (20 μM). At certain time point after compound administration (from 5 minutes to 8 h), the cellular pellets were collected, following the procedure described in the Experimental Section of this Chapter.

The gold content in each sample was thus determined by means of ICP-AES (Inductively Coupled Plasma-Atomic Emission Spectroscopy) analysis, after their mineralization with *aqua regia* (nitric acid hydrochloride; final acid concentration of 3% v/v).

Figure 7.9 shows the amount of gold detected in the collected cell samples as a function of the incubation time with the gold(III) compound IT01. The gold content is expressed as the nanograms of gold detected in one million of cells. The choice to normalize the gold content with the number of cells per sample was suggested by the variability on cell number between the different culture plates employed for the experiment, which depend not only on varition deriving from the seeding procedure itself, but also on the intrinsic variation in cell number due to the different cell proliferation with time in the different samples. Surprisingly, the highest amount of gold internalized by cells have been found right after administration to the cell cultures (5 min), while the gold concentration per cells decreases over time, reaching a plateau after nearly 4 h (**Table 7.1**).

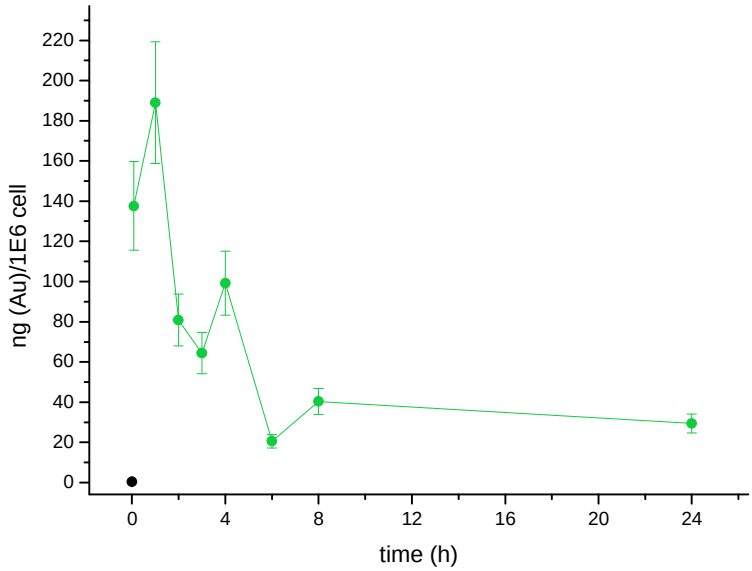

Figure 7.9: amount of Au in cells treated with IT01 (dissolved in DMSO), expressed as nanograms of Au *per* million of cells (nmol/10^6 cells), at different time points after compound administration to cell culture.

These results are consistent with the data obtained from the xCELLigence experiments, since the maximum modification in cell adhesion/viability detected through the xCELLigence curves (**Figure 7.6**) coincides with the time interval in which the maximum amount of gold is internalized by the system (**Figure 7.9**). After few hours, when the gold measured inside the cells reaches its minimum, no further increase in cell proliferation is detected, highlighting that the antitumor effect is activated by the compounds in the very first hours after internalization.

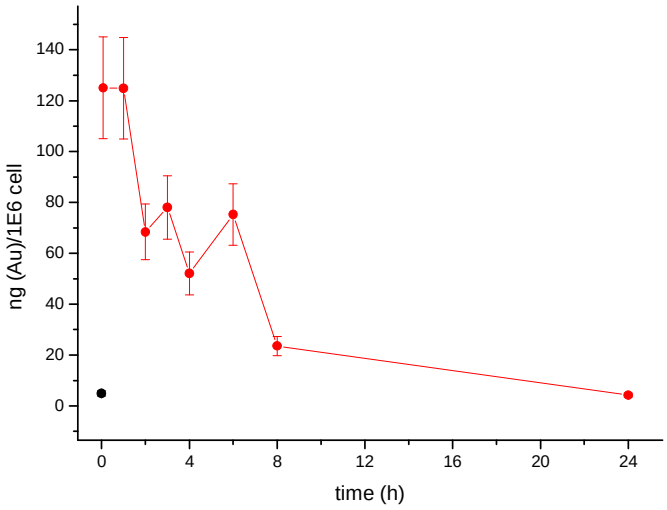

Figure 7.10: amount of Au in cells treated with IT01-loaded F127 micelles, expressed as nanograms of Au *per* million of cells (nmol/10^6), at different time points after compound administration to cells.

The results achieved after administration of cells with IT01-loaded Pluronic F127 micelles (**Figure 7.10**) were very similar to those obtained after treatment of cells with IT01 dissolved in DMSO. This suggests that the release from the micelles is very quick (as already reported for AuL12/F127 systems, **Chapter 5**) also for the IT01-loaded micelles, and that the uptake mechanism is the same for both the systems.

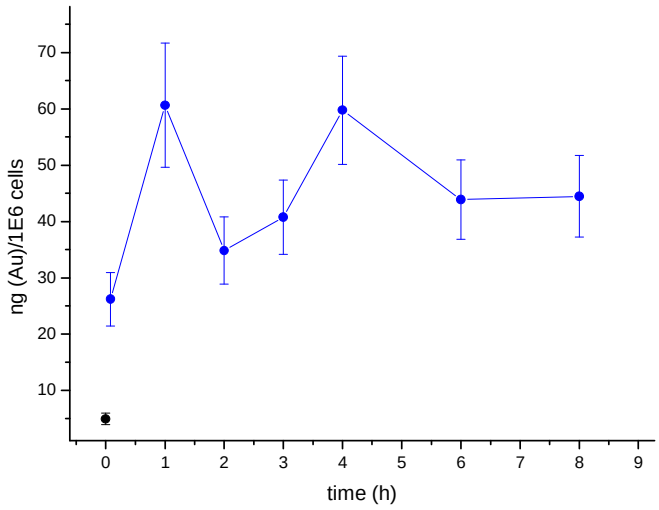

Figure 6.11: amount of Au in cells treated with IT01-loaded DPPC vesicles, expressed as nanograms of Au *per* million of cells (nmol/10^6), at different time points after compound administration to cells.

A different behavior was instead recorded when IT01-loaded DPPC vesicles were used (**Figure 7.11**). Even if in this case the data reported are only preliminary, the concentration of gold determined in the cell pellets increases during the first hour, but then remains almost constant over the following time. This probably suggests a different release rate of the compound from the liposomal system (in particular with respect to the micelles) or a different mechanism of cellular uptake of the compound when it is encapsulated in the vesicles, possibly mediated by the vesicular system itself.

Table 6.1: quantity of Au present in cellular pellets after incubation of cell with IT01 μM for different times, expressed as nanograms of gold per 1 million cells.

	mean ±error (ng of Au/10^6 cells)		
Time (min)	IT01/DMSO	IT01/F127	IT01/DPPC*
0	0,301±0,05	0,023±0,004	4,93±1,03
5	137,60±22,03	125,08±20,02	26,20±4,72
60	189,02±30,26	124,89±20,00	60,64±11,02
120	80,80±12,93	68,41±10,98	34,82±5,97
180	64,43±10,31	78,06±12,49	40,77±6,58
240	99,19±15,89	52,08±8,42	59,76±9,57
360	20,56±3,29	75,24±12,09	43,88±7,07
480	40,33±6,45	23,56±3,77	44,46±7,26
1440	29,40±4,71	4,24±0,72	-

* *preliminary data*

In a second set of experiments, the effect of different concentration of the test compound IT01 was evaluated after incubation with cells for a fixed time. The cellular uptake of gold by cells was determined after 2 h from the administration of the compound either dissolved in DMSO or loaded in F127 micelles or DPPC vesicles. After the selected incubation time, cell pellets were collected following the same procedure above described, and the samples were prepared for gold content determination *via* ICP-AES analysis.

The choice of the incubation time was in particular suggested by the analysis of the cell growth inhibition curves previously determined by xCELLigence analysis, which highlighted that a significant effect in cell growth inhibition/adhesion is detectable just after 4 h from the compound administration. It can be noticed that the higher the amount of compound administered to cells, the higher the gold content measured in the cells

pellets, thus the maximum uptake of gold is in this range of concentrations is only dependent on the amount of administered gold(III) complex to cells, and this behaviour can be found for every of formulation tested. As an example, the amount of gold detected after 2 h incubation of cells H460 with IT01 loaded in Pluronic micelles at different concentrations is reported in **Figure 7.12.**

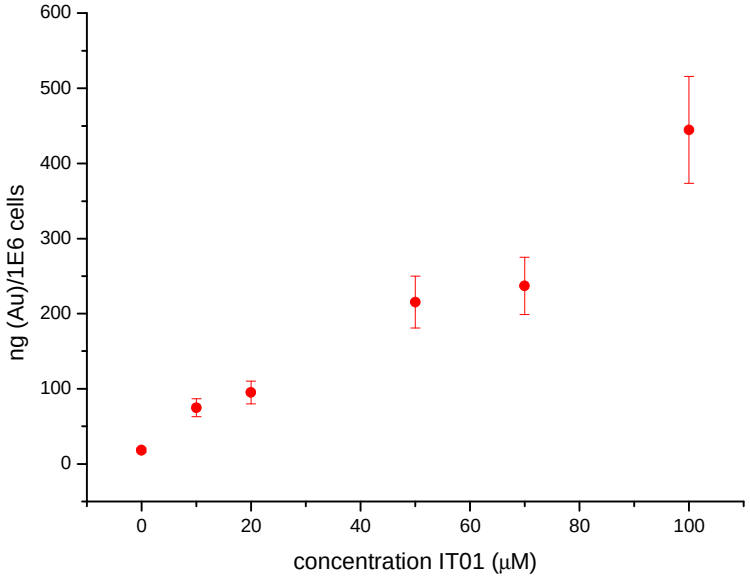

Figure 7.12: amount of Au in cells treated with IT01-loaded F127 micelles, expressed as nanomoles of Au *per* million of cells (nmol/10^6), after 2h incubation of different amounts of compound with cells.

In conclusion, the real-time proliferation curves recorded for the A549 cells after treatment with the selected compound in different formulations, remark the completely different mechanism of action exerted by our gold(III) complexes, with respect to cisplatin. In particular, the gold(III) dithiocarbamato complexes were demonstrated to strongly affect cell adhesion and cell viability during the first 4-5 h form the treatment, with curve shapes very similar to those obtained for drugs acting as modulators of calcium transporters. Combining these results to those obtained from the kinetic studies of compound internalization, a mechanism of action involving the inhibition of membrane receptors or other biomolecules at a membrane level was hypotesized.

The gold uptake kinetic experiments carried out by ICP-AES measurements confirmed that the interaction of the compounds with cells is very fast and occurs in the first hours after treatment.

Appendix 1

Crystallographic data for crystals of AuL23

The gold(III) complex adopts a distorted square-planar geometry achieved through the bidentate dithiocarbamato ligand and the two *cis*-bromides. The four donor atoms and the metal center lie on a plane and the distortion from the ideal geometry is a consequence of the small bite angle of the dithiocarbamato moiety (*ca.* 75°). The Au−S distances (2.294(4) and 2.310(4) Å) are approximately 0.1 Å shorter than those of Au−Br (2.428(2) and 2.421(2) Å). The dithiocarbamato nitrogen atom is functionalized with an *N*-methyl group (C(2)) and a methyl ester residue, the latter lying in a plane which is approximately perpendicular to the coordination plane (*ca.* 88°).

The crystal packing is composed of layers in which the molecules are arranged in an alternate way. Each molecule on one side approaches a symmetry-related one with a methyl group, a sulfur and a bromine atoms whereas, on the other side, couples of molecules approach each other with the methyl ester moieties. By inspecting the packing along the *a* crystallographic axis, the metal ion is interposed at a non-interacting distance between a sulfur and a bromine atoms of two symmetry-related molecules.

Table A1. Crystallographic data and refinement details for [$Au^{III}Br_2$(dtc-Sar-OCH_3)].

	[$Au^{III}Br_2$(dtc-Sar-OCH_3)]
Empirical formula	$C_5H_8AuBr_2NO_2S_2$
Molecular weight	535.03
Color, habit	Orange, block
Temperature [K]	293(2)
λ [Å]	0.71073
Crystal system	Triclinic
Space group	*P*-1
a [Å]	4.846(3)
b [Å]	9.200(5)
c [Å]	14.521(8)
α [deg]	74.464(7)
β [deg]	84.119(7)
γ [deg]	85.989(7)
V [$Å^3$]	619.5(6)

Z	2
ρ (calc) [mg m^{-3}]	2.868
μ [mm^{-1}]	18.633
θ range [deg]	1.46 to 27.45
No. of rflcn/unique	6605/2788
GoF	1.009
$R1$	0.0551
$wR2$	0.1096

$R1 = \Sigma||Fo|-|Fc||/\Sigma|Fo|$.
$wR2 = [\Sigma[w(Fo^2-Fc^2)^2]/\Sigma[w(Fo^2)^2]]^{½}$, $w = 1/[\sigma^2(Fo^2) + (aP)^2 + bP]$, where $P = [\max(Fo^2,0) + 2Fc^2]/3$.

Table A2. Selected bond lengths (Å) and angles (°) for [$Au^{III}Br_2$(dtc-Sar-OCH_3)].

Au–S(1)	2.294(4)
Au–S(2)	2.310(4)
Au–Br(1)	2.421(2)
Au–Br(2)	2.428(2)
C(1)–S(1)	1.72(2)
C(1)–S(2)	1.74(1)
C(1)–N(1)	1.28(2)
S(1)–Au–S(2)	75.1(1)
S(1)–Au–Br(1)	93.7(1)
S(2)–Au–Br(2)	96.8(1)
Br(1)–Au–Br(2)	94.43(8)
C(1)–S1–Au	88.6(5)
C(1)–S2–Au	87.8(6)
S(1)–C1–S(2)	108.5(9)

Crystallographic data for crystals of IT03 and IT04 racemate

Refinement data for IT03 and IT04 racemate crystals whose structure was reported (for IT04) in **Chapter 1** was not sufficiently resolved, even if connectivity assignment was undoubt.

Crystallographic data for crystals of Z-L-ProAibO*t*Bu

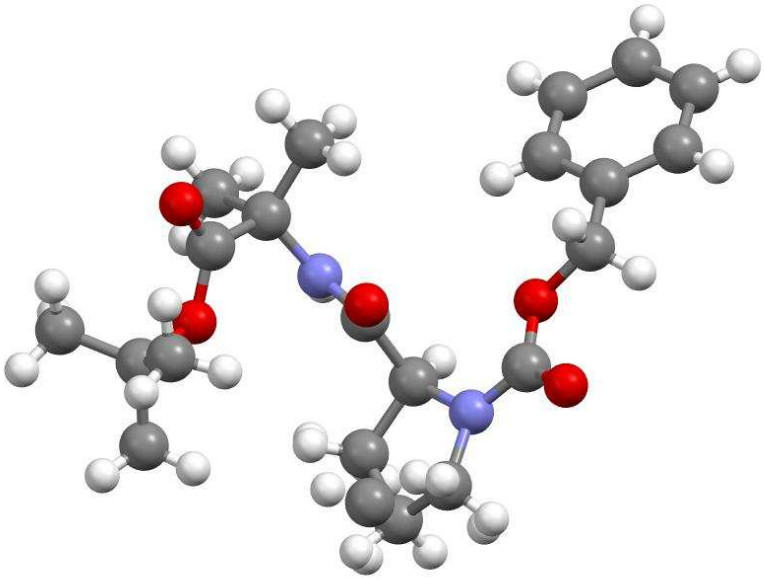

Figure A1: molecular structure of Z-L-Pro-Aib-O*t*Bu

Table A3. Crystal data and structure refinement for Z-L-Pro-Aib-O*t*Bu.

Identification code	**Z-L-Pro-Aib-O*t*Bu**	
Empirical formula	C21 H30 N2 O5	
Formula weight	390.47	
Temperature	293(2) K	
Wavelength	1.54178 Å	
Crystal system	Orthorhombic	
Space group	P 21 21 21	
Unit cell dimensions	a = 10.050(2) Å	α= 90°.
	b = 10.460(2) Å	β= 90°.
	c = 21.305(3) Å	γ = 90°.
Volume	2239.6(7) $Å^3$	
Z	4	

Density (calculated)	1.158 Mg/m^3
Absorption coefficient	0.674 mm^{-1}
F(000)	840
Crystal size	0.50 x 0.35 x 0.20 mm^3
Theta range for data collection	4.15 to 59.97°.
Index ranges	-1<=h<=11, 0<=k<=11, 0<=l<=23
Reflections collected	2158
Independent reflections	2121 [R(int) = 0.1078]
Completeness to theta = 59.97°	99.9 %
Max. and min. transmission	0.8770 and 0.7293
Refinement method	Full-matrix-block least-squares on F^2
Data / restraints / parameters	2121 / 4 / 250
Goodness-of-fit on F^2	0.992
Final R indices [I>2sigma(I)]	R1 = 0.0611, wR2 = 0.1612
R indices (all data)	R1 = 0.0774, wR2 = 0.1735
Absolute structure parameter	-0.1(5)
Largest diff. peak and hole	0.258 and -0.174 e.$Å^{-3}$

Table A4. Bond lengths [Å] and angles [°] for Z-L-Pro-Aib-O*t*Bu.

C01-C02	1.39
C01-C06	1.39
C01-C07	1.491(5)
C02-C03	1.39
C03-C04	1.39
C04-C05	1.39
C05-C06	1.39
C07-OU	1.421(5)
OU-C0	1.335(5)
C0-O0	1.231(5)
C0-N1	1.325(5)
N1-C1D	1.456(6)
N1-C1A	1.464(5)

C1A-C1	1.523(6)
C1A-C1B	1.528(6)
C1B-C1G	1.480(8)
C1B-C1G'	1.487(8)
C1G-C1D	1.499(8)
C1G'-C1D	1.497(8)
C1-O1	1.230(5)
C1-N2	1.345(5)
N2-C2A	1.444(6)
C2A-C2B2	1.519(6)
C2A-C2B1	1.536(6)
C2A-C2	1.536(6)
C2-O2	1.204(5)
C2-OT	1.335(5)
OT-CT1	1.481(5)
CT1-CT2	1.501(8)
CT1-CT4	1.501(8)
CT1-CT3	1.507(8)
C02-C01-C06	120
C02-C01-C07	122.4(3)
C06-C01-C07	117.6(3)
C01-C02-C03	120
C02-C03-C04	120
C05-C04-C03	120
C04-C05-C06	120
C05-C06-C01	120
OU-C07-C01	109.0(3)
C0-OU-C07	116.0(3)
O0-C0-N1	124.8(4)
O0-C0-OU	123.3(4)
N1-C0-OU	111.8(3)
C0-N1-C1D	122.1(4)
C0-N1-C1A	122.6(4)
C1D-N1-C1A	112.3(3)
N1-C1A-C1	110.3(3)
N1-C1A-C1B	102.9(3)
C1-C1A-C1B	112.2(4)
C1G-C1B-C1A	106.7(5)
C1G-C1B-C1G'	28.6(7)
C1A-C1B-C1G'	103.9(5)
C1B-C1G-C1D	107.9(6)
C1D-C1G'-C1B	107.6(6)
N1-C1D-C1G'	103.9(5)
N1-C1D-C1G	100.9(5)
O1-C1-N2	122.6(4)
O1-C1-C1A	122.6(4)
N2-C1-C1A	114.9(3)

C1-N2-C2A	123.3(3)
N2-C2A-C2B2	111.3(4)
N2-C2A-C2B1	108.1(4)
C2B2-C2A-C2B1	109.4(4)
N2-C2A-C2	112.0(3)
C2B2-C2A-C2	109.9(4)
C2B1-C2A-C2	106.0(3)
O2-C2-OT	124.9(4)
O2-C2-C2A	123.1(4)
OT-C2-C2A	111.8(3)
C2-OT-CT1	120.8(3)
OT-CT1-CT2	109.8(4)
OT-CT1-CT4	108.3(5)
CT2-CT1-CT4	115.2(6)
OT-CT1-CT3	102.1(4)
CT2-CT1-CT3	110.7(6)
CT4-CT1-CT3	109.9(5)

Crystallographic data for crystals of IT05

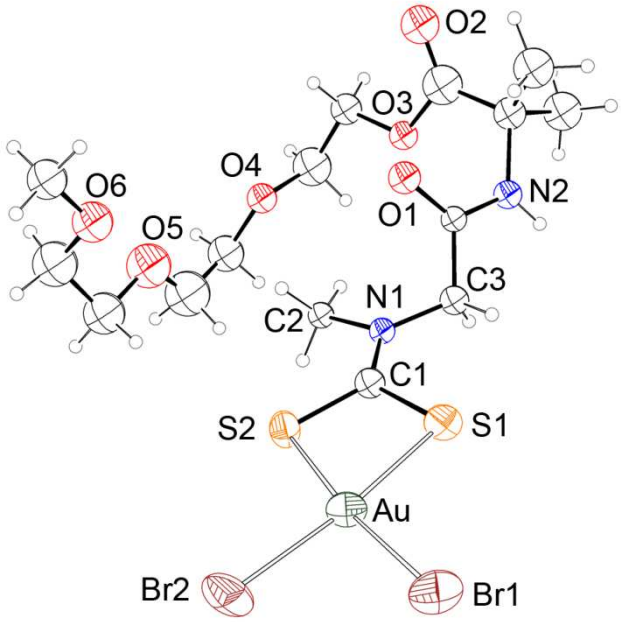

Figure A2. Ortep drawing of IT05·pentane. Thermal parameters are depicted at the 30% probability level.

Table A5. Summary of X-ray crystallographic data for IT05·pentane.

Empirical formula	$C_{20}H_{39}AuBr_2N_2O_6S_2$
Formula weight	824.44
Colour, habit	Yellow, block
Crystal size, mm	0.07x0.04x0.04
Crystal system	Orthorhombic
Space group	*P*bcn
a, Å	22.15(2)
b, Å	9.599(9)
c, Å	25.88(2)
α, deg.	90
β, deg.	90
γ, deg.	90
V, Å^3	5503(8)
Z	8
T, K	293(2)
ρ (calc), Mg/m^3	1.990
μ, mm^{-1}	8.440
ϑ range, deg.	1.82 to 20.75
No.ofrflcn/unique	9221 / 2636
GooF	1.028

*R*1	0.0877
*wR*2	0.1774

$R1 = \Sigma||F_o|-|F_c||/\Sigma|F_o|$, $wR2 = [\Sigma[w(F_o^2-F_c^2)^2]/\Sigma[w(F_o^2)^2]]^{½}$, $w = 1/[\sigma^2(F_o^2) + (aP)^2 + bP]$, where $P = [\max(F_o^2,0) + 2F_c^2]/3$

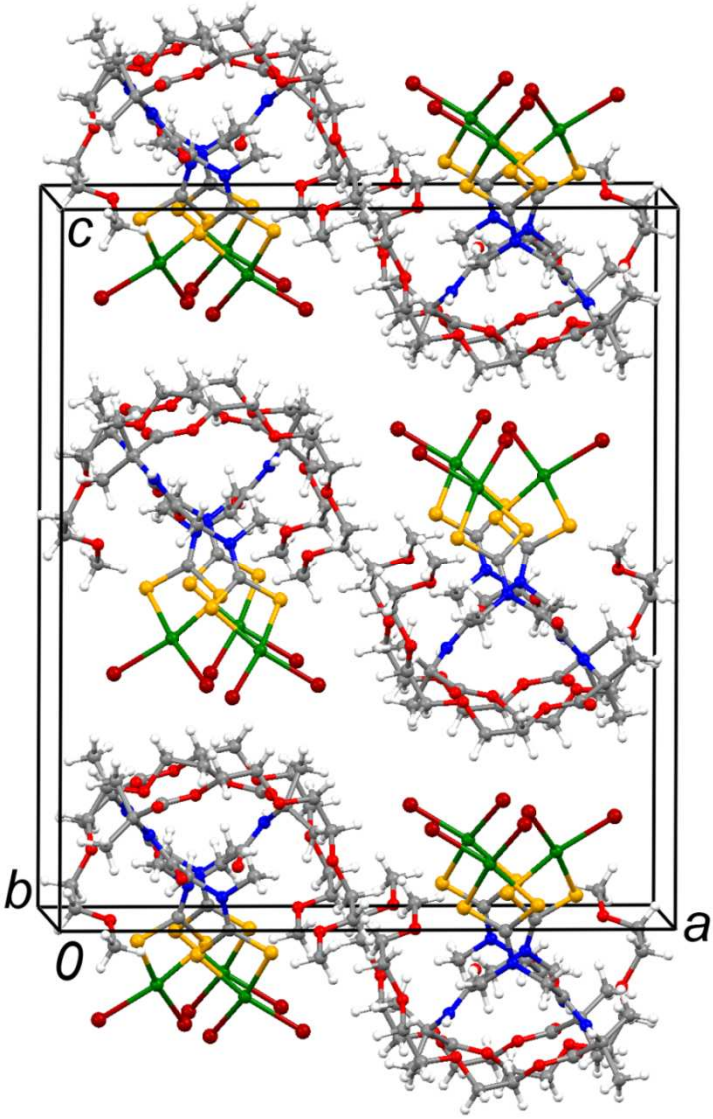

Figure A3: Crystal packing of IT05·pentane viewed along the b crystallographic axis.

Table A6. Selected bond lengths (Å) and angles (°) for IT05·pentane.

Au-Br(1)	2.429(4)	C(1)-N(1)	1.32(3)
Au-Br(2)	2.431(5)	C(4)-O(1)	1.27(3)
Au-S(1)	2.310(9)	C(4)-N(2)	1.33(3)
Au-S(2)	2.306(9)	C(8)-O(2)	1.21(4)

C(1)-S(1)	1.78(3)	C(8)-O(3)	1.36(4)
C(1)-S(2)	1.71(3)		
Br(1)-Au-Br(2)	94.0(2)	S(1)-C(1)-S(2)	108(2)
S(1)-Au-S(2)	75.7(3)	C(1)-S(1)-Au	87(1)
Br(1)-Au-S(1)	96.1(2)	C(1)-S(2)-Au	89(1)
Br(2)-Au-S(2)	94.1(2)		

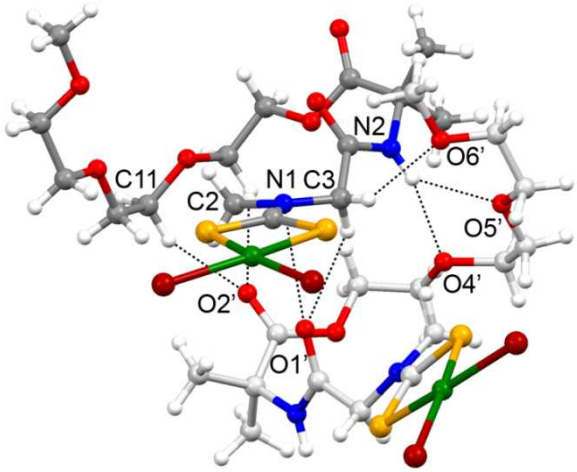

Figure A4: Depiction of intermolecular contacts between two symmetry related molecules of IT05·pentane. Symmetry code ’ = 1/2-x; 1/2+y; z.

Final remarks

The development of new anticancer therapies is nowadays focusing on compounds designed to show both strong antiproliferative effects on cancerous cells and low or even absent toxicity on healthy tissues. In other words, to selectively target tumor cells without affecting healthy tissues is a goal of paramount importance. In this context, the complexity of neoplastic physiology and the peculiarities of different cancer types and subtypes make this aim not so trivial to achieve. From the molecular point of view, targeted therapies have been exploiting biomarkers, transporters and receptors, normally present on the cell membrane, which become up-regulated upon malignant transformation. These overexpressed membrane biomolecules promote carcinogenesis and tumor growth. Remarkably, their inhibition or channel/pocket stoppage may result in a slowdown in cancer proliferation by interfering with intracellular downstream pathways.

In this work, we selected specific peptide transporters named PEPTs, known to be overexpressed in several neoplasias, and exploited them as targets for the site-specific delivery of an antitumor "cargo" (*viz*, a properly stabilized transition metal center as gold(III)). Five new gold(III)−dithiocarbamato peptidomimetics of the type [$Au^{III}Br_2$(dtc-AA_1-AA_2-OR] (AA_1= Sar, L/D-Pro; AA_2 =L/D-Ala, Aib; R = O*t*Bu, TEG) have been synthesized, characterized and studied from the biological point of view, with the final aim of obtaining complexes with enhanced bioavailability and tumor selectivity with respect to the our previously studied gold(III)-dithicarbamato derivatives of aminoacids. In particular, the dithiocarbamato moiety was functionalized with selected esterified dipeptides, differing for either the aminoacidic sequence or the configuration of the chiral aminoacid.

Taking into account their application as anticancer compounds, their stability was first analyzed under physiological-like conditions by means of UV-Vis spectrophotometry. In these studies, our poor water-soluble compounds were previously solubilized in DMSO (organic solvent normally used as a vehicle for biological *in vitro* tests) prior to addition to different investigated aqueous media (pure water, saline solution 0.9% w/w, PBS). It was shown that the model compound undergoes hydrolysis both in pure water and in saline solution, by exchanging the bromido ligands with water molecules. Conversely, upon dissolution in in PBS, a rapid formation of the hydroxo-derivative (not water-soluble) was detected. The presence of the phosphate anion in solution may further interfere with the stability of the complex since, following coordination to the metal center, can lead to the precipitation of the corresponding gold(III)-phosphato derivative. When considering more complicated environments, such as the cell culture medium, the formation of the hydroxo-derivative may take place, but its precipitation is likely prevented by the interaction of the compound with the biomolecules, including proteins, present in the examined aqueous medium. Indeed, when we

investigated the interaction of the model gold(III) compound with BSA in PBS, secondary stabilizing weak interactions were hypothesized to establish, thus suggesting a role of BSA as a carrier under physiological conditions.

The antiproliferative activity of all complexes was tested *in vitro* on different human cancer cell lines, showing encouraging results, in particular on A2780 and MCF7 cell lines, with GI_{50} values up to 10-fold lower than the reference metallodrug cisplatin. Since IT03 was proved the most cytotoxic compound against all the studied cell lines, it was selected for preliminary *in vivo* studies on human breast MDA-MB-231, highly aggressive and metastatic tumor, subcutaneously inoculated into nude mice. After 19 days of treatment, a tumor xenograft growth inhibition of 60% was recorded, with no sign of suffering or weight loss in the treated animals.

Preliminary toxicity studies were performed *ex vivo* on healthy rat tissues of liver, colon and kidney. The toxicity profiles recorded for the two tested gold(III) compounds were very similar and toxic concentration evaluated on each organ was slightly improved if compared to cisplatin. This result was more evident on liver, wherein IT03 was 50% less toxic than cisplatin. In this context, it should be highlighted that previous toxicological experiments performed *in vivo* with the gold complex AuL12 ("first generation") assessed that neither accumulation of the metal nor tissue damage were detected in the examined organs.

To overcome the poor water-solubility of our compounds, micellar and vesicular systems encapsulating the gold(III) complexes IT01 and AuL12 were prepared, characterized and tested on cancer cells *in vitro*, in order to both avoid the use of organic solvents as a vehicle for biological testing and improve their therapeutic index under physiological conditions. After determination of the log*P* values for the gold(III) compounds, Pluronic F127 micelles and DPPC vesicles were loaded with the gold(III)-peptidodithiocarbamato compounds, pointing out that the cytotoxic activities are maintained also upon encapsulation in the two supramolecular aggregates. Moreover, the loading of the "first generation" compound AuL12 into micellar systems based on Pluronic F127 functionalized with the cholecystokinin octapeptide CCK8, has been carried out to obtain tumor-selective delivery, thus further improving the chemotherapeutic index of our compounds. The treatment of the CCK2-R-overexpressing cells with CCK8-functionalized micelles showed a 10-fold increase of the AuL12 antiproliferative activity with respect to the AuL12-loaded non-functionalized supramolecular counterpart against the same tumor cell line. These results are very encouraging and led us to plan new *in vivo* experiments with our gold(III) compounds encapsulated in functionalized nanosystems.

To gain further insights into the mechanism of action of the investigated compounds, some inhibition assays were performed *in vitro* on purified selected enzymes. It was demonstrated that the compound IT03 is able to inhibit all the three proteolytic functions of 20S proteasome and affects PARP-1

activity, which is involved in mechanisms of DNA repair and activation of apoptosis, with IC_{50} values in the nanomolar range.

The real-time proliferation of tumor cells by an innovative technique was then analyzed, showing our compounds to be able to affect cell adhesion in the first 4-5 h treatment. In addition, in agreement with literature data, the shape of the recorded curves were directly correlated to well-known mechanisms of action of some clinically used anticancer drugs. The curves observed for our compounds were very similar to those obtained for drugs acting, for example, as modulators of calcium transporters.

The very fast response detected in cell adhesion variations and cytotoxic effect was furthermore confirmed by gold uptake kinetic experiments carried out by ICP-AES measurements.

Considering all the obtained results, it can be concluded that treatment with our compounds leads to cell death by a mechanism of action which is completely different from the one exerted by the reference drug cisplatin, for which DNA is the major known target. Indeed, our gold(III) complexes could more likely cause an effect at the cell membrane level, for instance either by bonding to the cell surface or by internalization after a few minutes from the incubation.

The encouraging antiproliferative results collected so far (mainly regarding the *in vitro* and *in vivo* antiproliferative tests and the preliminary *ex vivo* toxicological studies) make our compounds good candidates for the conclusion of the preclinical phase studies. Moreover, micellar and vesicular formulations will be employed in *in vivo* experiments aimed at assessing the drug pharmacokinetics, thus paving the way to the possibility to study the antiblastic activity of our complexes upon intravenous administration.

Acknowledgments

I firstly want to aknowledge my supervisor Prof. Dolores Fregona and all her Research Group, in particular the Post Docs Eszter Nagy, Simone Scintilla and Chiara Nardon, and all the Master and PhD Students with whom I shared everyday lab's life: Andrea, Elia, Valeria, Arianna, Cinzia, Claudia, Leonardo and Nicolò.

A particular thanks goes to Prof. Dalla Via, for giving me the possibility to approach to cell culture labs techniques, Prof. Formaggio for introducing me to peptide synthesis and Prof. Di Noto for the help with ICP-AES and FAR-IR experiments.

I want also to acknowledge Prof. Angela Casini for the ospitality in her Research Group at the Research Institute of Pharmacy of the University of Groningen (The Netherlands), where I spent 6 months carring out part of the Research presented in this work.

A special thank goes to Fondazione CARIPARO (Cassa di Risparmio di Padova e Rovigo), for funding this PhD project.

Finally, I want to thank the Doctoral School of Molecular Sciences, its Coordinator Prof. Antonino Polimeno and the members of my three-year committee: Prof. Formaggio, Prof. Badocco and Prof. Zagotto.

Bibliography

1. Milacic, V.; Dou, Q. P. The tumor proteasome as a novel target for gold(III) complexes: Implications for breast cancer therapy. *Coord. Chem. Rev.* **2009**, *253*, 1649-1660.

2. Cattaruzza, L.; Fregona, D.; Mongiat, M.; Ronconi, L.; Fassina, A.; Colombatti, A.; Aldinucci, D. Antitumor activity of gold(III)-dithiocarbamato derivatives on prostate cancer cells and xenografts. *Int. J. of Cancer* **2011**, *128*, 206-215.

3. Marzano, C.; Ronconi, L.; Chiara, F.; Giron, M. C.; Faustinelli, I.; Cristofori, P.; Trevisan, A.; Fregona, D. Gold(III)-dithiocarbamato anticancer agents: activity, toxicology and histopathological studies in rodents. *Int. J. Cancer* **2011**, *129*, 487-496.

4. Kramer, W. Transporters, Trojan horses and therapeutics: suitability of bile acid and peptide transporters for drug delivery. *Biol. Chem.* **2011**, *392*, 77-94.

5. Brandsch, M. Transport of drugs by proton-coupled peptide transporters: Pearls and pitfalls. *Expert Opin. Drug Metab. Toxicol.* **2009**, *5*, 887-905.

6. Boyle, P.; Levin, B. International Agency for Research on Cancer (IARC) and World Health Organization (WHO), *Word Cancer Report 2008*.

7. Mathers, C. D.; Loncar, D. Projections of global mortality and burden of disease from 2002 to 2030. *PLoS Med.* **2006**, *3*, 442.

8. Bhowmick, N. A.; Neilson, E. G.; Moses, H. L. Stromal fibroblasts in cancer initiation and progression. *Nature* **2004**, *432*, 332-337.

9. Cheng, N.; Chytil, A.; Shyr, Y.; Joly, A.; Moses, H. L. Transforming growth factor-ß signaling-deficient fibroblasts enhance hepatocyte growth factor signaling in mammary carcinoma cells to promote scattering and invasion. *Mol. Cancer Res.* **2008**, *6*, 1521-1533.

10. Hanahan, D.; Weinberg, R. Hallmarks of Cancer: The Next Generation. *Cell* **2011**, *144*, 646-674.

11. Junttila, M. R.; Evan, G. I. P53 a Jack of all trades but master of none. *Nature Reviews Cancer* **2009**, *9*, 821-829.

12. Shay, J. W.; Wright, W. E. Hayflick, his limit, and cellular ageing. *Nature Reviews Molecular Cell Biology* **2000**, *1*, 72-76.

13. Blasco, M. A. Telomeres and human disease: Ageing, cancer and beyond. *Nature Reviews Genetics* **2005**, *6*, 611-622.

14. Hanahan, D.; Folkman, J. Patterns and emerging mechanisms of the angiogenic switch during tumorigenesis. *Cell* **1996**, *86*, 353-364.

15. Emsley, J. *Nature's Building Blocks: An A-Z Guide to the Elements;* 2001.

16. Miessler, G. L.; Tarr, D. A. *Inorg Chem;* 2011.

17. Anonymous *American Pharmaceutical Association, The National Formulary of Unofficial Preparations;* ed.American Pharmaceutical Association: Baltimore, 1906.

18. Dalla Via, L.; Nardon, C.; Fregona, D. Targeting the ubiquitin-proteasome pathway with inorganic compounds to fight cancer: a challenge for the future. *Future Med. Chem.* **2012**, *4*, 525-543.

19. Nagy, E. M.; Pettenuzzo, A.; Boscutti, G.; Marchiò Luciano; Dalla Via Lisa; Fregona, D. Ruthenium(II/III)-based compounds with encouraging antiproliferative activity against non-small-cell lung cancer. *Chemistry* **2012**, *18*, 14464-14472.

20. Nagy, E. M.; Nardon, C.; Giovagnini, L.; Marchiò, L.; Trevisan, A.; Fregona, D. Promising anticancer mono- and dinuclear ruthenium(iii) dithiocarbamato complexes: Systematic solution studies. *Dalton Transactions* **2011**, *40*, 11885-11895.

21. Rosenberg, B.; VanCamp, L.; Trosko, J. E.; Mansour, V. H. Platinum compounds: A new class of potent antitumour agents [24]. *Nature* **1969**, *222*, 385-386.

22. Peyrone, M. *Ann. ,* **1845**, *51*, 15.

23. Mellor, D. P. . *Chem. Rev.* **1943**, *33*, 137-183.

24. Kauffman, G. B. *Plat. Met. Rev.* **1997**, *41*, 34-40.

25. Werner, A. Z. . *Anorg. Chem.* **1893**, *3*, 267.

26. Kelland, L. The resurgence of platinum-based cancer chemotherapy. *Nature Reviews Cancer* **2007**, *7*, 573-584.

27. Eastman, A. In: *Cisplatin: Chemistry and Biochemistry of a Leading Anticancer Drug*; Lippert, B.: Germany, 1999; pp 111-134.

28. Gately, D. P.; Howell, S. B. Cellular accumulation of the anticancer agent cisplatin: a review. *Br. J. Cancer* **1993**, *67*, 1171-1176.

29. Ishida, S.; Lee, J.; Thiele, D. J.; Herskowitz, I. Uptake of the anticancer drug cisplatin mediated by the copper transporter Ctr1 in yeast and mammals. *Proc. Natl. Acad. Sci. U. S. A.* **2002**, *99*, 14298-14302.

30. Davies, M. S.; Berners-Price, S. J.; Hambley, T. W. Slowing of cisplatin aquation in the presence of DNA but not in the presence of phosphate: improved understanding of sequence selectivity and the roles of monoaquated and diaquated species in the binding of cisplatin to DNA. *Inorg. Chem.* **2000**, *39*, 5603-5613.

31. Cohen, G. L.; Ledner, J. A.; Bauer, W. R.; Ushay, H. M.; Caravana, C.; Lippard, S. J. Sequence dependent binding of cis-dichlorodiammineplatinum(II) to DNA *J. Am. Chem. Soc.* **1980**, *102*, 2487-2488.

32. Hambley, T. W. *Dalton Trans.* **2001**, 2711-2718.

33. Guo, Z.; Sadler, P. J. J. *Adv. Inorg. Chem.* **2000**, *49*, 183-306.

34. Fuertes, M. A.; Castilla, J.; Alonso, C.; Perez, J. M. Novel concepts in the development of platinum antitumor drugs. *Curr. Med. Chem. Anticancer Agents* **2002**, *2*, 539-551.

35. Kartalou, M.; Essigmann, J. M. Recognition of cisplatin adducts by cellular proteins. *Mutation Research - Fundamental and Molecular Mechanisms of Mutagenesis* **2001**, *478*, 1-21.

36. Wong, E.; Giandomenico, C. M. Current Status of Platinum-Based Antitumor Drugs. *Chem. Rev. (Washington, D. C.)* **1999**, *99*, 2451-2466.

37. Weiss, R. B.; Christian, M. C. New cisplatin analogues in development. A review. *Drugs* **1993**, *46*, 360-377.

38. Lebwohl, D.; Canetta, R. Clinical development of platinum complexes in cancer therapy: an historical perspective and an update. *Eur. J. Cancer* **1998**, *34*, 1522-1534.

39. Raymond, E.; Faivre, S.; Woynarowski, J. M.; Chaney, S. G. Oxaliplatin: mechanism of action and antineoplastic activity. *Semin. Oncol.* **1998**, *25*, 4-12.

40. Zhao, H.; Ning, Y. *Gold Bull.* **2001**, *33*, 24.

41. Reedijk, J. New clues for platinum antitumor chemistry: kinetically controlled metal binding to DNA. *Proc. Natl. Acad. Sci. U. S. A.* **2003**, *100*, 3611-3616.

42. Arnesano, F.; Natile, G. Mechanistic insight into the cellular uptake and processing of cisplatin 30 years after its approval by FDA. *Coord. Chem. Rev.* **2009**, *253*, 2070-2081.

43. Graham, J.; Muhsin, M.; Kirkpatrick, P. *Nature Reviews Drug Discovery* **2004**.

44. Thompson, K. H.; Orvig, C. Boon and bane of metal ions in medicine. *Science* **2003**, *300*, 936-939.

45. Block, W. D.; Van Goor, K. *Metabolism, Pharmacology and Therapeutic Uses of Gold Compounds;* Springfield, IL, **1956**.

46. Sutton, B. M. In: Sutton, B. M., Franz, R. G. e., Eds.; *Bioinorganic Chemistry of Gold Coordination Compounds*; Philadelphia, PA, **1983**; pp 6.

47. Grahmann, A.; Schmidbaur, H. In: Abel, E. W., Stone, F. G. A. and Wilkinson, G., Eds.; *Comprehensive Organometallic Chemistry 2. A Review of the Literature 1982-1994*; **1995**.

48. Rapson, W. S. The science and technology of gold. A twenty-year perspective. *Gold Bull.* **1988**, *21*, 10-16.

49. Jacobson, D. M.; Humpston, G. *Interdisc. Sci. Rev.* **1992**, *17*, 244.

50. Mehringer, G.; Simon, J. The hydrometallurgical recycling of gold by biological degradable thiourea instead of cyanide leaching. *Metall (Berlin)* **1989**, *43*, 624-627.

51. Watkins II, J. W.; Elder, R. C.; Greene, B.; Darnall, D. W. Determination of gold binding in an algal biomass using EXAFS and XANES spectroscopies. *Inorg. Chem.* **1987**, *26*, 1147-1151.

52. Jones, P. G. X-ray structural investigations of gold compounds. *Gold bulletin* **1983**, *16*, 114-124.

53. Jiang, Y.; Alvarez, S.; Hoffmann, R. Binuclear and polymeric gold(I) complexes. *Inorg. Chem.* **1985**, *24*, 749-757.

54. Antonova, L. V.; Busygina, T. E.; Polovnyak, V. K.; Usachev, A. E. Stability of Gold(II) Complexes. *Russian Journal of General Chemistry* **1997**, *67*, 491-494.

55. Tiekink, E. R. T. Gold derivatives for the treatment of cancer. *Crit. Rev. Oncol.* **2002**, *42*, 225-248.

56. Li, D.; Che, C.; Kwong, H.; Yam, V. W. Photoinduced C-C bond formation from alkyl halides catalysed by luminescent dinuclear gold(I) and copper(I) complexes. *Journal of the Chemical Society, Dalton Transactions* **1992**, 3325-3329.

57. King, C.; Khan, M. N. I.; Staples, R. J.; Fackler Jr., J. P. Luminescent mononuclear gold(I) phosphines. *Inorg. Chem.* **1992**, *31*, 3236-3238.

58. Zeller, E.; Beruda, H.; Kolb, A.; Bissinger, P.; Riede, J.; Schmidbaur, H. Change of coordination from tetrahedral gold-ammonium to square-pyramidal gold-arsonium cations. *Nature* **1991**, *352*, 141-143.

59. Roulet, R.; Zolkin, A.; Faltens, M. O.; Templeton, D. H. *Inorg. Chem.* **1974**, *13*, 1836.

60. Hydes, P. C.; Middleton, H. *Gold Bull.* **1979**, *12*, 90.

61. Melpolder, J. B.; Burmeister, J. L. Antisymbiosis and the trans-influence in gold(I) thiocyanate complexes. *Inorg. Chim. Acta* **1981**, *49*, 115-120.

62. Muir, J. A.; Muir, M. M.; Arias, S. *Acta Crystallogr., Sect. B,* **1982**, *38*, 1318.

63. Skibsted, L. H.; Bjerrum, J. Acta Chem. Scand., Ser. A, **1977**, *31*, 155.

64. Puddephat, R. J. *The Chemistry of Gold;* Elsevier: Amsterdam, 1978.

65. Greenwood, N. N.; Earnshaw, A. N. *The Chemistry of the Elements;* Oxford, 1986.

66. Landé, K. *Münch. Med. Wachenschr*. **1927**, *74*, 1132.

67. Forestier, N. *J. Lab. Clin. Med.,* **1935**, *20*, 827.

68. Empire Rheumatism Council. *Ann. Rheum. Dis.* **1960**, *19*, 95.

69. Lipsky, P. In: Utsinger, P. D., Zvaifler, N. J. and Ehrlich, G. E., Eds.; *Arthritis: Etiology, Diagnosis and Management*; Lippincott: Philadelphia, PA, **1989**; pp 601.

70. Gordon, D. A. In: Kelly, W.W.; Harris, E.D.; Ruddy, D.;Sledge, C.B.; Saunders, W.B.: **1989**; pp 804.

71. Shaw III, C. F. Gold-based therapeutic agents. *Chem. Rev.* **1999**, *99*, 2589-2600.

72. Shaw, C. F. In: Fricker, S. P., Ed.; *Metal Compounds in Cancer Therapy*; Chapman & Hall: **1994**; pp 46.

73. Ward, J. R. Role of disease-modifying antirheumatic drugs versus cytotoxic agents in the therapy of rheumatoid arthritis. *Am. J. Med.* **1988**, *85*, 39-44.

74. Berners-Price, S. J.; Jarrett, P. S.; Sadler, P. J. *Inorg.Chem.* **1987**, *26*, 3074.

75. Che, C.; Sun, R. W.; Yu, W.; Ko, C.; Zhu, N.; Sun, H. Gold(III) porphyrins as a new class of anticancer drugs: Cytotoxicity, DNA binding and induction of apoptosis in human cervix epitheloid cancer cells. *Chemical Communications* **2003**, *9*, 1718-1719.

76. Messori, L.; Marcon, G.; Cinellu, M. A.; Coronnello, M.; Mini, E.; Gabbiani, C.; Orioli, P. Solution chemistry and cytotoxic properties of novel organogold(III) compounds. *Bioorganic and Medicinal Chemistry* **2004**, *12*, 6039-6043.

77. Nobili, S.; Mini, E.; Landini, I.; Gabbiani, C.; Casini, A.; Messori, L. Gold compounds as anticancer agents: Chemistry, cellular pharmacology, and preclinical studies. *Med. Res. Rev.* **2010**, *30*, 550-580.

78. Wang, Y.; He, Q. Y.; Sun, R. W.; Che, C. M.; Chiu, J. F. Gold(III) porphyrin 1a induced apoptosis by mitochondrial death pathways related to reactive oxygen species. *Cancer Res.* **2005**, *65*, 11553-11564.

79. Coronnello, M.; Mini, E.; Caciagli, B.; Cinellu, M. A.; Bindoli, A.; Gabbiani, C.; Messori, L. Mechanisms of cytotoxicity of selected organogold(III) compounds. *J. Med. Chem.* **2005**, *48*, 6761-6765.

80. Gabbiani, C.; Casini, A.; Messori, L.; Guerri, A.; Cinellu, M. A.; Minghetti, G.; Corsini, M.; Rosani, C.; Zanello, P.; Arca, M. Structural characterization, solution studies, and DFT calculations on a series of binuclear gold(III) oxo complexes: Relationships to biological properties. *Inorg. Chem.* **2008**, *47*, 2368-2379.

81. Messori, L.; Abbate, F.; Marcon, G.; Orioli, P.; Fontani, M.; Mini, E.; Mazzei, T.; Carotti, S.; O'Connell, T.; Zanello, P. Gold(III) complexes as potential antitumor agents: Solution chemistry and cytotoxic properties of some selected gold(III) compounds. *J. Med. Chem.* **2000**, *43*, 3541-3548.

82. Marcon, G.; Carotti, S.; Coronnello, M.; Messori, L.; Mini, E.; Orioli, P.; Mazzei, T.; Cinellu, M. A.; Minghetti, G. Gold(III) complexes with bipyridyl ligands: solution chemistry, cytotoxicity, and DNA binding properties. *J. Med. Chem.* **2002**, *45*, 1672-1677.

83. Casini, A.; Kelter, G.; Gabbiani, C.; Cinellu, M. A.; Minghetti, G.; Fregona, D.; Fiebig, H. H.; Messori, L. Chemistry, antiproliferative properties, tumor selectivity, and molecular mechanisms of novel gold(III) compounds for cancer treatment: a systematic study. *J. Biol. Inorg. Chem.* **2009**, *14*, 1139-1149.

84. Pabla, N.; Dong, Z. Cisplatin nephrotoxicity: Mechanisms and renoprotective strategies. *Kidney Int.* **2008**, *73*, 994-1007.

85. Appleton, T. G.; Connor, J. W.; Hall, J. R.; Prenzler, P. D. NMR study of the reactions of the cis-diamminediaquaplatinum(II) cation with glutathione and amino acids containing a thiol group. *Inorg. Chem.* **1989**, *28*, 2030-2037.

86. Andrews, P. A.; Howell, S. B. Cellular pharmacology of cisplatin: Perspectives on mechanisms of acquired resistance. *Cancer Cells* **1990**, *2*, 35-43.

87. Dorr, R. T.; Lagel, K. Interaction between cisplatin and mesna in mice. *J. Cancer Res. Clin. Oncol.* **1989**, *115*, 604-605.

88. Borch, R. F.; Dedon, P. C.; Gringeri, A.; Montine, T. J. In: Nicolini, M.; *Platinum and Other Metal Coordination Compounds in Cancer Chemotherapy*; Boston, 1988; pp 216-281.

89. Huang, H.; Zhu, L.; Reid, B. R.; Drobny, G. P.; Hopkins, P. B. Solution structure of a cisplatin-induced DNA interstrand cross-link. *Science* **1995**, *270*, 1842-1845.

90. Segovia, N.; Crovetto, G.; Lardelli, P.; Espigares, M. In vitro toxicity of several dithiocarbamates and structure - Activity relationships. *Journal of Applied Toxicology* **2002**, *22*, 353-357.

91. Koelle, U.; Laguna, A. Electrochemistry of Au-complexes. *Inorg. Chim. Acta* **1999**, *290*, 44-50.

92. Giovagnini, L.; Ronconi, L.; Aldinucci, D.; Lorenzon, D.; Sitran, S.; Fregona, D. Synthesis, characterization, and comparative in vitro cytotoxicity studies of platinum(II), palladium(II), and gold(III) methylsarcosinedithiocarbamate complexes. *J. Med. Chem.* **2005**, *48*, 1588-1595.

93. Ronconi, L.; Giovagnini, L.; Marzano, C.; Bettio, F.; Graziani, R.; Pilloni, G.; Fregona, D. Gold dithiocarbamate derivatives as potential antineoplastic agents: Design, spectroscopic properties, and in vitro antitumor activity. *Inorg. Chem.* **2005**, *44*, 1867-1881.

94. Giovagnini, L.; Ronconi, L.; Aldinucci, D.; Lorenzon, D.; Sitran, S.; Fregona, D. Synthesis, characterization, and comparative in vitro cytotoxicity studies of platinum(II), palladium(II), and gold(III) methylsarcosinedithiocarbamate complexes. *J. Med. Chem.* **2005**, *48*, 1588-1595.

95. Aldinucci, D.; Lorenzon, D.; Stefani, L.; Giovagnini, L.; Colombatti, A.; Fregona, D. Antiproliferative and apoptotic effects of two new gold(III) methylsarcosinedithiocarbamate derivatives on human acute myeloid leukemia cells in vitro. *Anticancer Drugs* **2007**, *18*, 323-332.

96. Aldinucci, D.; Cattaruzza, L.; Lorenzon, D.; Giovagnini, L.; Fregona, D.; Colombatti, A. Antiproliferative and apoptotic effects of two new Pd(II) methylsarcosinedithiocarbamate derivatives on human acute myeloid leukemia cells in vitro. *Oncol. Res.* **2008**, *17*, 103-113.

97. Cuddihy, A. R.; O'Connell, M. J. Cell-cycle responses to DNA damage in G2. *Int. Rev. Cytol.* **2003**, *222*, 99-140.

98. Kostova, I. Gold coordination complexes as anticancer agents. *Anti-Cancer Agents in Medicinal Chemistry* **2006**, *6*, 19-32.

99. Milacic, V.; Chen, D.; Ronconi, L.; Landis-Piwowar, K. R.; Fregona, D.; Dou, Q. P. A novel anticancer gold(III) dithiocarbamate compound inhibits the activity of a purified 20S proteasome and 26S proteasome in human breast cancer cell cultures and xenografts. *Cancer Res.* **2006**, *66*, 10478-10486.

100. Kouodom, M. N.; Boscutti, G.; Celegato, M.; Crisma, M.; Sitran, S.; Aldinucci, D.; Formaggio, F.; Ronconi, L.; Fregona, D. Rational design of gold(III)-dithiocarbamato peptidomimetics for the targeted anticancer chemotherapy. *J. Inorg. Biochem.* **2012**, *117*, 248-260.

101. Kouodom, M. N.; Ronconi, L.; Celegato, M.; Nardon, C.; Marchio, L.; Dou, Q. P.; Aldinucci, D.; Formaggio, F.; Fregona, D. Toward the selective delivery of chemotherapeutics into tumor cells by targeting peptide transporters: tailored gold-based anticancer peptidomimetics. *J. Med. Chem.* **2012**, *55*, 2212-2226.

102. Han, H. K.; Amidon, G. L. Targeted prodrug design to optimize drug delivery. *AAPS PharmSci* **2000**, *2*, E6.

103. Rubio-Aliaga, I.; Daniel, H. Peptide transporters and their roles in physiological processes and drug disposition. *Xenobiotica* **2008**, *38*, 1022-1042.

104. Fregona, D.; Ronconi, L.; Formaggio, F.; Dou, Q. P.; Aldinucci, D. , 2010.

105. Brandsch, M.; Knutter, I.; Bosse-Doenecke, E. Pharmaceutical and pharmacological importance of peptide transporters. *J. Pharm. Pharmacol.* **2008**, *60*, 543-585.

106. Ronconi, L.; Fregona, D. The Midas touch in cancer chemotherapy: From platinum- to gold-dithiocarbamato complexes. *Dalton Transactions* **2009**, 10670-10680.

107. Valle, G. Linear oligopeptides. Chemical and crystallographic study of the reaction between benzyloxycarbonyl chloride and a-aminoisobutyric acid. *J.Chem.Soc., Perkin Trans.* **1986**, *2*, 1371-1376.

108. McGahren, W. J.; Goodman, M. Synthesis of peptide oxazolones and related compounds. *Tetrahedron* **1967**, *23*, 2017-2030.

109. Vaughan, J. R.; Osato, R. L. Preparation of Peptides Using Mixed Carboxylic Acid Anhydrides. *J. Am. Chem. Soc.* **1951**, *73*, 5553-5555.

110. Green, T. W.; Wuts, P. G. M. *Protective Groups in Organic Synthesis;* Wiley-Interscience: New York, 1999; .

111. Burla, M. C.; Caliandro, R.; Camalli, M.; Carrozzini, B.; Cascarano, G. L.; De Caro, L.; Giacovazzo, C.; Polidori, G.; Spagna, R. SIR2004: an improved tool for crystal structure determination and refinement. *Journal of AppliedCrystallography* **2005**, *38*, 381-388.

112. Sheldrick, G. M. *SHELX97. Programs for Crystal Structure Analysis* **1997** (Release 97-2), University of Göttingen, Germany. .

113. Farrugia, L. J. WinGX suite for small-molecule single-crystal crystallography. *Journal of Applied Crystallography* **1999**, *32*, 817-838.

114. Sluis, P.; Spek, A. L. Bypass - An Effective Method for the Refinement of Crystal-Structures Containing Disordered Solvent Regions. *ActaCrystallographica Section* **1990**, *46*, 194-201.

115. Farrugia, L. J. WinGX and ORTEP for Windows: an update. *Journal of Applied Crystallography* **2012**, *45*, 849-854.

116. Macrae, C. F.; Bruno, I. J.; Chisholm, J. A.; Edgington, P. R.; McCabe, P.; Pidcock, E.; Rodriguez-Monge, L.; Taylor, R.; van de Streek, J.; Wood, P. A. Mercury CSD 2.0 - new features for the visualization and investigation of crystal structures. *Journal of Applied Crystallography* **2008**, *41*, 466-470.

117. Chatt, J.; Duncanson, L. A.; Venanzi, L. M. Dithiocarbamates, infrared spectra and structure. *Suom. Kemistil. B* **1956**, *29B*, 75-84.

118. Herlinger, A. W.; Wenhold, S. L.; Long II, T. V. Infrared spectra of amino acids and their metal complexes. II. Geometrical isomerism in bis(amino acidato) copper (II) complexes. *J. Am. Chem. Soc.* **1970**, *92*, 6474-6481.

119. Ronconi, L.; Giovagnini, L.; Marzano, C.; Bettio, F.; Graziani, R.; Pilloni, G.; Fregona, D. Gold dithiocarbamate derivatives as potential antineoplastic agents: design, spectroscopic properties, and in vitro antitumor activity. *Inorg. Chem.* **2005**, *44*, 1867-1881.

120. Bonati, F.; Ugo, R. Organotin(IV) N,N-disubstituted dithiocarbamates. *Journal of Organometallic Chemistry* **1967**, *10*, 257-268.

121. Forghieri, F.; Preti, C.; Tassi, L.; Tosi, G. Preparation, properties and reactivity of gold complexes with some heterocyclic dithiocarbamates as ligands. *Polyhedron* **1988**, *7*, 1231-1237.

122. Ronconi, L.; Maccato, C.; Barreca, D.; Saini, R.; Zancato, M.; Fregona, D. Gold(III) dithiocarbamate derivatives of N-methylglycine: An experimental and theoretical investigation. *Polyhedron* **2005**, *24*, 521-531.

123. Van Gaal, H. L. M.; Diesveld, J. W.; Pijpers, F. W.; Van Der Linden, J. G. M. 13C NMR spectra of dithiocarbamates. Chemical shifts, carbon-nitrogen stretching vibration frequencies, and p bonding in the NCS2 fragment. *Inorg. Chem.* **1979**, *18*, 3251-3260.

124. Macias, B.; Criado, J. J.; Vaquero, M. V.; Villa M.V. *Thermochim. Acta* **1993**, *223*, 213.

125. Criado, J. J.; Lopez-Arias, J. A.; Macias, B.; Fernandez-Lago, L. R.; Salas, J. M. Au(III) complexes of tris-dithiocarbamate derivatives of α-amino acids: spectroscopic studies, thermal behaviour and antibacterial activity. *Inorg. Chim. Acta* **1992**, *193*, 229-235.

126. Criado, J. J.; Fernandez, I.; Macias, B.; Salas, J. M.; Medarde, M. Novel chelates of Pd(II) dithiocarbamates. Spectroscopic studies and thermal behaviour. *Inorg. Chim. Acta* **1990**, *174*, 67-75.

127. Wallach, O. *LiebigsAnn. Chem.* **1895**, *90*, 286.

128. Beurskens, P. T.; Blaauw, H. J. A.; Cras, J. A.; Steggerda, J. J. Preparation, structure, and properties of bis(N,N-di-n-butyldithiocarbamato)gold(III) dihaloaurate(I). *Inorg. Chem.* **1968**, *7*, 805-810.

129. Saggioro, D.; Rigobello, M. P.; Paloschi, L.; Folda, A.; Moggach, S. A.; Parsons, S.; Ronconi, L.; Fregona, D.; Bindoli, A. Gold(III) - Dithiocarbamato complexes induce cancer cell death triggered by thioredoxin redox system inhibition and activation of ERK pathway. *Chem. Biol.* **2007**, *14*, 1128-1139.

130. Wijnhoven, F. T. H. M.; Bosman, W. P.; Willemse, J.; Cras, J. A. *ecl. J. R. Neth. Chem. Soc. R*, **1979**, *98*, 492-495.

131. Anand, U.; Mukherjee, S. Binding, unfolding and refolding dynamics of serum albumins. *Biochim. Biophys. Acta* **2013**, *1830*, 5394-5404.

132. Anguizola, J.; Matsuda, R.; Barnaby, O. S.; Hoy, K. S.; Wa, C.; Debolt, E.; Koke, M.; Hage, D. S. Review: Glycation of human serum albumin. *Clin. Chim. Acta* **2013**, *425*, 64-76.

133. Elsadek, B.; Kratz, F. Impact of albumin on drug delivery--new applications on the horizon. *J. Control. Release* **2012**, *157*, 4-28.

134. Yamasaki, K.; Chuang, V. T.; Maruyama, T.; Otagiri, M. Albumin-drug interaction and its clinical implication. *Biochim. Biophys. Acta* **2013**, *1830*, 5435-5443.

135. Timerbaev, A. R.; Hartinger, C. G.; Aleksenko, S. S.; Keppler, B. K. Interactions of antitumor metallodrugs with serum proteins: Advances in characterization using modern analytical methodology. *Chem. Rev.* **2006**, *106*, 2224-2248.

136. Nagai, N.; Okuda, R.; Kinoshita, M.; Ogata, H. Decomposition Kinetics of Cisplatin in Human Biological Fluids. *J. Pharm. Pharmacol.* **1996**, *48*, 918-924.

137. Timerbaev, A. R.; Hartinger, C. G.; Aleksenko, S. S.; Keppler, B. K. Interactions of antitumor metallodrugs with serum proteins: advances in characterization using modern analytical methodology. *Chem. Rev.* **2006**, *106*, 2224-2248.

138. Ivanov, A. I.; Christodoulou, J.; Parkinson, J. A.; Barnham, K. J.; Tucker, A.; Woodrow, J.; Sadler, P. J. Cisplatin binding sites on human albumin. *J. Biol. Chem.* **1998**, *273*, 14721-14730.

139. Vignesh, G.; Nehru, S.; Manojkumar, Y.; Arunachalam, S. Spectroscopic investigation on the interaction of some surfactant-cobalt(III) complexes with serum albumins. *J Lumin* **2014**, *145*, 269-277.

140. de Graaf, I. A.; Olinga, P.; de Jager, M. H.; Merema, M. T.; de Kanter, R.; van de Kerkhof, E. G.; Groothuis, G. M. Preparation and incubation of precision-cut liver and intestinal slices for application in drug metabolism and toxicity studies. *Nat. Protoc.* **2010**, *5*, 1540-1551.

141. van de Kerkhof, E. G.; de Graaf, I. A.; de Jager, M. H.; Meijer, D. K.; Groothuis, G. M. Characterization of rat small intestinal and colon precision-cut slices as an in vitro system for drug metabolism and induction studies. *Drug Metab. Dispos.* **2005**, *33*, 1613-1620.

142. Hincal, A. A.; Long, D. F.; Repta, A. J. Cis-platin stability in aqueous parenteral vehicles. *J. Parenter. Drug Assoc.* **1979**, *33*, 107-116.

143. Kabanov, A. V. Polymer genomics: an insight into pharmacology and toxicology of nanomedicines. *Adv. Drug Deliv. Rev.* **2006**, *58*, 1597-1621.

144. Torchilin, V. P. In: *In vitro and in vivo availability of liposomes* Kabanov, A. V., Felgner, P. L. and Seymour, L. W., Eds.; Self-assembling Complexes for Gene Delivery: From Laboratory to Clinical Trial; Wiley: Chichester, UK, **1998**; pp 277-293.

145. Batrakova, E. V.; Kabanov, A. V. Pluronic block copolymers: evolution of drug delivery concept from inert nanocarriers to biological response modifiers. *J. Control. Release* **2008**, *130*, 98-106.

146. Greish, K. In *Enhanced Permeability and Retention (EPR) Effect for Anticancer Nanomedicine Drug Targeting;* Grobmyer, S. R., Moudgil, B. M., Eds.; Humana Press: **2010**; Vol. 624, pp 25-37.

147. Stolnik, S.; Illum, L.; Davis, S. S. Long circulating microparticulate drug carriers. *Adv. Drug Deliv. Rev.* **1995**, *16*, 195-214.

148. Hawley, A. E.; Davis, S. S.; Illum, L. Targeting of colloids to lymph nodes: influence of lymphatic physiology and colloidal characteristics. *Adv. Drug Deliv. Rev.* **1995**, *17*, 129-148.

149. Ogawara, K. -.; Yoshida, M.; Furumoto, K.; Takakura, Y.; Hashida, M.; Higaki, K.; Kimura, T. Uptake by hepatocytes and biliary excretion of intravenously administered polystyrene microspheres in rats. *J. Drug Target.* **1999**, *7*, 213-221.

150. Ishida, O.; Maruyama, K.; Sasaki, K.; Iwatsuru, M. Size-dependent extravasation and interstitial localization of polyethyleneglycol liposomes in solid tumor-bearing mice. *Int. J. Pharm.* **1999**, *190*, 49-56.

151. Schiffelers, R. M.; Bakker-Woudenberg, I. A. J. M.; Snijders, S. V.; Storm, G. Localization of sterically stabilized liposomes in Klebsiella pneumoniae-infected rat lung tissue: influence of liposome characteristics. *Biochimica et Biophysica Acta (BBA) - Biomembranes* **1999**, *1421*, 329-339.

152. Lasic, D. D. *Liposomes: from physics to applications.* Amsterdam, **1993**.

153. Klibanov, A. L.; Maruyama, K.; Torchilin, V. P.; Huang, L. Amphipathic polyethyleneglycols effectively prolong the circulation time of liposomes. *FEBS Lett.* **1990**, *268*, 235-237.

154. Lasic, D. D.; Martin, F. J.; Gabizon, A.; Huang, S. K.; Papahadjopoulos, D. Sterically stabilized liposomes: a hypothesis on the molecular origin of the extended circulation times. *Biochimica et Biophysica Acta (BBA) - Biomembranes* **1991**, *1070*, 187-192.

155. Woodle, M. C.; Lasic, D. D. Sterically stabilized liposomes. *Biochim. Biophys. Acta* **1992**, *1113*, 171-199.

156. Senior, J. H. Fate and behavior of liposomes in vivo: a review of controlling factors. *Crit. Rev. Ther. Drug Carrier Syst.* **1987**, *3*, 123-193.

157. Hofheinz, R.; Gnad-Vogt, S.; Beyer, U.; Hochhaus, A. Liposomal encapsulated anti-cancer drugs. *Anticancer Drugs* **2005**, *16*.

158. Gaitanis, A.; Staal, S. In *Liposomal Doxorubicin and nab-Paclitaxel: Nanoparticle Cancer Chemotherapy in Current Clinical Use;* Grobmyer, S. R., Moudgil, B. M., Eds.; Humana Press: 2010; Vol. 624, pp 385-392.

159. Harris, L.; Batist, G.; Belt, R.; Rovira, D.; Navari, R.; Azarnia, N.; Welles, L.; Winer, E.; TLC D-99 Study Group Liposome-encapsulated doxorubicin compared with conventional doxorubicin in a randomized multicenter trial as first-line therapy of metastatic breast carcinoma. *Cancer* **2002**, *94*, 25-36.

160. Gill, P. S.; Wernz, J.; Scadden, D. T.; Cohen, P.; Mukwaya, G. M.; von Roenn, J. H.; Jacobs, M.; Kempin, S.; Silverberg, I.; Gonzales, G.; Rarick, M. U.; Myers, A. M.; Shepherd, F.; Sawka, C.; Pike, M. C.; Ross, M. E. Randomized phase III trial of liposomal daunorubicin versus doxorubicin, bleomycin, and vincristine in AIDS-related Kaposi's sarcoma. *Journal of Clinical Oncology* **1996**, *14*, 2353-2364.

161. Drummond, D. C.; Zignani, M.; Leroux, J. Current status of pH-sensitive liposomes in drug delivery. *Prog. Lipid Res.* **2000**, *39*, 409-460.

162. Yatvin, M.; Weinstein, J.; Dennis, W.; Blumenthal, R. Design of liposomes for enhanced local release of drugs by hyperthermia. *Science* **1978**, *202*, 1290-1293.

163. Ponce, A. M.; Vujaskovic, Z.; Yuan, F.; Needham, D.; Dewhirst, M. W. Hyperthermia mediated liposomal drug delivery. *Int. J. Hyperthermia* **2006**, *22*, 205-213.

164. Sabaté, R.; Barnadas-Rodríguez, R.; Callejas-Fernández, J.; Hidalgo-Álvarez, R.; Estelrich, J. Preparation and characterization of extruded magnetoliposomes. *Int. J. Pharm.* **2008**, *347*, 156-162.

165. Fortin-Ripoche, J.; Martina, M. S.; Gazeau, F.; Menager, C.; Wilhelm, C.; Bacri, J.; Lesieur, S.; Clement, O. Magnetic Targeting of Magnetoliposomes to Solid Tumors with MR Imaging Monitoring in Mice: Feasibility. *Radiology* **2006**, *239*, 415-424.

166. West, K. R.; Otto, S. Reversible covalent chemistry in drug delivery. *Curr. Drug Discov. Technol.* **2005**, *2*, 123-160.

167. Papahadjopoulos, D.; Jacobson, K.; Nir, S.; Isac, I. Phase transitions in phospholipid vesicles Fluorescence polarization and permeability measurements concerning the effect of temperature and cholesterol. *Biochimica et Biophysica Acta (BBA) - Biomembranes* **1973**, *311*, 330-348.

168. Abra, R. M.; Hunt, C. A. Liposome disposition in vivo. III. Dose and vesicle-size effects. *Biochim. Biophys. Acta* **1981**, *666*, 493-503.

169. Gabizon, A.; Papahadjopoulos, D. The role of surface charge and hydrophilic groups on liposome clearance in vivo. *Biochimica et Biophysica Acta (BBA) - Biomembranes* **1992**, *1103*, 94-100.

170. Batrakova, E.; Lee, S.; Li, S.; Venne, A.; Alakhov, V.; Kabanov, A. Fundamental relationships between the composition of pluronic block copolymers and their hypersensitization effect in MDR cancer cells. *Pharm. Res.* **1999**, *16*, 1373-1379.

171. Chiappetta, D. A.; Sosnik, A. Poly(ethylene oxide)-poly(propylene oxide) block copolymer micelles as drug delivery agents: improved hydrosolubility, stability and bioavailability of drugs. *Eur. J. Pharm. Biopharm.* **2007**, *66*, 303-317.

172. Valle, J. W.; Lawrance, J.; Brewer, J.; Clayton, A.; Corrie, P.; Alakhov, V.; Ranson, M. A phase II, window study of SP1049C as first-line therapy in inoperable metastatic adenocarcinoma of the oesophagus. *ASCO Meeting Abstracts* **2004**, *22*, 4195.

173. Alakhov, V.; Klinski, E.; Li, S.; Pietrzynski, G.; Venne, A.; Batrakova, E.; Bronitch, T.; Kabanov, A. Block copolymer-based formulation of doxorubicin. From cell screen to clinical trials. *Colloids and Surfaces B: Biointerfaces* **1999**, *16*, 113-134.

174. Roettger, B. F.; Rentsch, R. U.; Pinon, D.; Holicky, E.; Hadac, E.; Larkin, J. M.; Miller, L. J. Dual pathways of internalization of the cholecystokinin receptor. *J. Cell Biol.* **1995**, *128*, 1029-1041.

175. Edelhoch, H. Spectroscopic determination of tryptophan and tyrosine in proteins. *Biochemistry* **1967**, *6*, 1948-1954.

176. Pace, C. N.; Vajdos, F.; Fee, L.; Grimsley, G.; Gray, T. How to measure and predict the molar absorption coefficient of a protein. *Protein Sci.* **1995**, *4*, 2411-2423.

177. Chen, L.; Sha, X.; Jiang, X.; Chen, Y.; Ren, Q.; Fang, X. Pluronic P105/F127 mixed micelles for the delivery of docetaxel against Taxol-resistant non-small cell lung cancer: optimization and in vitro, in vivo evaluation. *Int. J. Nanomedicine* **2013**, *8*, 73-84.

178. Dalla Via, L.; Di Noto, V.; Gia, O.; Marciani Magno, S. Photoaddition of thienocoumarin derivatives to DNA: stoichiometry and kinetics of binding. *J. Photochem. Photobiol. B.* **2005**, *79*, 59-65.

179. Rutkowska, E.; PajIk, K.; Jozwiak, K. Lipophilicity--methods of determination and its role in medicinal chemistry. *Acta Pol. Pharm.* **2013**, *70*, 3-18.

180. Zhang, J.; Jin, W.; Wang, X.; Wang, J.; Zhang, X.; Zhang, Q. articles A Novel Octreotide Modified Lipid Vesicle Improved the Anticancer Efficacy of Doxorubicin in Somatostatin Receptor 2 Positive Tumor Models. **2010**, *7*, 1159-1168.

181. Reubi, J. C. Peptide receptors as molecular targets for cancer diagnosis and therapy. *Endocr. Rev.* **2003**, *24*, 389-427.

182. Reubi, J. C.; Schaer, J. C.; Waser, B. Cholecystokinin(CCK)-A and CCK-B/gastrin receptors in human tumors. *Cancer Res.* **1997**, *57*, 1377-1386.

183. Wank, S. A.; Pisegna, J. R.; de Weerth, A. Brain and gastrointestinal cholecystokinin receptor family: structure and functional expression. *Proc. Natl. Acad. Sci. U. S. A.* **1992**, *89*, 8691-8695.

184. Wank, S. A. G protein-coupled receptors in gastrointestinal physiology. I. CCK receptors: an exemplary family. *Am. J. Physiol.* **1998**, *274*, G607-13.

185. Reubi, J. C.; Waser, B. Concomitant expression of several peptide receptors in neuroendocrine tumours: molecular basis for in vivo multireceptor tumour targeting. *Eur. J. Nucl. Med. Mol. Imaging* **2003**, *30*, 781-793.

186. Benedetti, E.; Morelli, G.; Accardo, A.; Mansi, R.; Tesauro, D.; Aloj, L. Criteria for the design and biological characterization of radiolabeled peptide-based pharmaceuticals. *BioDrugs* **2004**, *18*, 279-295.

187. Vaccaro, M.; Mangiapia, G.; Paduano, L.; Gianolio, E.; Accardo, A.; Tesauro, D.; Morelli, G. Structural and relaxometric characterization of peptide aggregates containing gadolinium complexes as potential selective contrast agents in MRI. *Chemphyschem* **2007**, *8*, 2526-2538.

188. Zhang, S.; Lovejoy, K. S.; Shima, J. E.; Lagpacan, L. L.; Shu, Y.; Lapuk, A.; Chen, Y.; Komori, T.; Gray, J. W.; Chen, X.; Lippard, S. J.; Giacomini, K. M. Organic cation transporters are determinants of oxaliplatin cytotoxicity. *Cancer Res.* **2006**, *66*, 8847-8857.

189. Sharma, P. K.; Bhatia, S. R. Effect of anti-inflammatories on Pluronic F127: micellar assembly, gelation and partitioning. *Int. J. Pharm.* **2004**, *278*, 361-377.

190. Basak, R.; Bandyopadhyay, R. Encapsulation of hydrophobic drugs in Pluronic F127 micelles: effects of drug hydrophobicity, solution temperature, and pH. *Langmuir* **2013**, *29*, 4350-4356.

191. Messori, L.; Abbate, F.; Marcon, G.; Orioli, P.; Fontani, M.; Mini, E.; Mazzei, T.; Carotti, S.; O'Connell, T.; Zanello, P. Gold(III) complexes as potential antitumor agents: solution chemistry and cytotoxic properties of some selected gold(III) compounds. *J. Med. Chem.* **2000**, *43*, 3541-3548.

192. Franchini, G. C.; Giusti, A.; Preti, C.; Tassi, L.; Zannini, P. Coordinating ability of methylpiperidine dithiocarbamates towards platinum group metals. *Polyhedron* **1985**, *4*, 1553-1558.

193. Hadjikostas, C. C.; Katsoulos, G. A.; Shakhatreh, S. K. Synthesis and spectral studies of some new palladium(II) and platinum(II) dithiocarbimato complexes. Reactions of bases with the corresponding N-alkyldithiocarbamates. *Inorg. Chim. Acta* **1987**, *133*, 129-132.

194. Zhang, X.; Jackson, J. K.; Burt, H. M. Determination of surfactant critical micelle concentration by a novel fluorescence depolarization technique. *J. Biochem. Biophys. Methods* **1996**, *31*, 145-150.

195. Kelland, L. The resurgence of platinum-based cancer chemotherapy. *Nature reviews.Cancer* **2007**, *7*, 573-584.

196. Ronconi, L.; Marzano, C.; Zanello, P.; Corsini, M.; Miolo, G.; Macca, C.; Trevisan, A.; Fregona, D. Gold(III) dithiocarbamate derivatives for the treatment of cancer: Solution chemistry, DNA binding, and hemolytic properties. *J. Med. Chem.* **2006**, *49*, 1648-1657.

197. Bindoli, A.; Rigobello, M. P.; Scutari, G.; Gabbiani, C.; Casini, A.; Messori, L. Thioredoxin reductase: A target for gold compounds acting as potential anticancer drugs. *Coord. Chem. Rev.* **2009**, *253*, 1692-1707.

198. Lincoln, D. T.; Ali Emadi, E. M.; Tonissen, K. F.; Clarke, F. M. The thioredoxin-thioredoxin reductase system: over-expression in human cancer. *Anticancer Res.* **2003**, *23*, 2425-2433.

199. Sun, Y.; Rigas, B. The thioredoxin system mediates redox-induced cell death in human colon cancer cells: implications for the mechanism of action of anticancer agents. *Cancer Res.* **2008**, *68*, 8269-8277.

200. Singh, S. S.; Li, Y.; Ford, O. H.; Wrzosek, C. S.; Mehedint, D. C.; Titus, M. A.; Mohler, J. L. Thioredoxin Reductase 1 Expression and Castration-recurrent Growth of Prostate Cancer. *Transl. Oncol.* **2008**, *1*, 153-157.

201. Yamada, M.; Tomida, A.; Yoshikawa, H.; Taketani, Y.; Tsuruo, T. Increased expression of thioredoxin/adult T-cell leukemia-derived factor in cisplatin-resistant human cancer cell lines. *Clin. Cancer Res.* **1996**, *2*, 427-432.

202. Kim, S. J.; Miyoshi, Y.; Taguchi, T.; Tamaki, Y.; Nakamura, H.; Yodoi, J.; Kato, K.; Noguchi, S. High thioredoxin expression is associated with resistance to docetaxel in primary breast cancer. *Clin. Cancer Res.* **2005**, *11*, 8425-8430.

203. Milacic, V.; Dou, Q. P. The tumor proteasome as a novel target for gold(III) complexes: implications for breast cancer therapy. *Coord. Chem. Rev.* **2009**, *253*, 1649-1660.

204. Loda, M.; Cukor, B.; Tam, S. W.; Lavin, P.; Fiorentino, M.; Draetta, G. F.; Jessup, J. M.; Pagano, M. Increased proteasome-dependent degradation of the cyclin-dependent kinase inhibitor p27 in aggressive colorectal carcinomas. *Nat. Med.* **1997**, *3*, 231-234.

205. Li, B.; Dou, Q. P. Bax degradation by the ubiquitin/proteasome-dependent pathway: involvement in tumor survival and progression. *Proc. Natl. Acad. Sci. U. S. A.* **2000**, *97*, 3850-3855.

206. Landis-Piwowar, K. R.; Milacic, V.; Chen, D.; Yang, H.; Zhao, Y.; Chan, T. H.; Yan, B.; Dou, Q. P. The proteasome as a potential target for novel anticancer drugs and chemosensitizers RID B-7903-2009. *Drug Resist. Update* **2006**, *9*, 263-273.

207. Groll, M.; Ditzel, L.; Lowe, J.; Stock, D.; Bochtler, M.; Bartunik, H. D.; Huber, R. Structure of 20S proteasome from yeast at 2.4 A resolution. *Nature* **1997**, *386*, 463-471.

208. Lopes, U. G.; Erhardt, P.; Yao, R.; Cooper, G. M. P53-Dependent Induction of Apoptosis by Proteasome Inhibitors. *J. Biol. Chem.* **1997**, *272*, 12893-12896.

209. Milacic, V.; Chen, D.; Ronconi, L.; Landis-Piwowar, K. R.; Fregona, D.; Dou, Q. P. A novel anticancer gold(III) dithiocarbamate compound inhibits the activity of a purified 20S proteasome and 26S proteasome in human breast cancer cell cultures and xenografts. *Cancer Res.* **2006**, *66*, 10478-10486.

210. Mendes, F.; Groessl, M.; Nazarov, A. a.; Tsybin, Y. O.; Sava, G.; Santos, I.; Dyson, P. J.; Casini, A. Metal-based inhibition of poly(ADP-ribose) polymerase--the guardian angel of DNA. *J. Med. Chem.* **2011**, *54*, 2196-206.

211. Chambon, P.; Weill, J. D.; Mandel, P. Nicotinamide mononucleotide activation of new DNA-dependent polyadenylic acid synthesizing nuclear enzyme. *Biochem. Biophys. Res. Commun.* **1963**, *11*, 39-43.

212. Lord, C. J.; Ashworth, A. The DNA damage response and cancer therapy. *Nature* **2012**, *481*, 287-294.

213. Yelamos, J.; Farres, J.; Llacuna, L.; Ampurdanes, C.; Martin-Caballero, J. PARP-1 and PARP-2: New players in tumour development. *Am. J. Cancer. Res.* **2011**, *1*, 328-346.

214. Huambachano, O.; Herrera, F.; Rancourt, A.; Satoh, M. S. Double-stranded DNA binding domain of poly(ADP-ribose) polymerase-1 and molecular insight into the regulation of its activity. *The Journal of biological chemistry* **2011**, *286*, 7149-60.

215. Eustermann, S.; Brockmann, C.; Mehrotra, P. V.; Yang, J. C.; Loakes, D.; West, S. C.; Ahel, I.; Neuhaus, D. Solution structures of the two PBZ domains from human APLF and their interaction with poly(ADP-ribose). *Nat. Struct. Mol. Biol.* **2010**, *17*, 241-243.

216. Langelier, M.; Planck, J. L.; Roy, S.; Pascal, J. M. Structural basis for DNA damage-dependent poly(ADP-ribosyl)ation by human PARP-1. *Science (New York, N.Y.)* **2012**, *336*, 728-32.

217. Rojo, F.; Garcia-Parra, J.; Zazo, S.; Tusquets, I.; Ferrer-Lozano, J.; Menendez, S.; Eroles, P.; Chamizo, C.; Servitja, S.; Ramirez-Merino, N.; Lobo, F.; Bellosillo, B.; Corominas, J. M.; Yelamos, J.; Serrano, S.; Lluch, A.; Rovira, A.; Albanell, J. Nuclear PARP-1 protein overexpression is associated with poor overall survival in early breast cancer. *Ann. Oncol.* **2012**, *23*, 1156-1164.

218. Rayet, B.; Gelinas, C. Aberrant rel/nfkb genes and activity in human cancer. *Oncogene* **1999**, *18*, 6938-6947.

219. Annunziata, C. M.; Stavnes, H. T.; Kleinberg, L.; Berner, A.; Hernandez, L. F.; Birrer, M. J.; Steinberg, S. M.; Davidson, B.; Kohn, E. C. Nuclear factor kappaB transcription factors are coexpressed and convey a poor outcome in ovarian cancer. *Cancer* **2010**, *116*, 3276-3284.

220. Hassa, P. O.; Hottiger, M. O. A role of poly (ADP-ribose) polymerase in NF-kappaB transcriptional activation. *Biol. Chem.* **1999**, *380*, 953-959.

221. Oliver, F. J.; Menissier-de Murcia, J.; Nacci, C.; Decker, P.; Andriantsitohaina, R.; Muller, S.; de la Rubia, G.; Stoclet, J. C.; de Murcia, G. Resistance to endotoxic shock as a consequence of defective NF-kappaB activation in poly (ADP-ribose) polymerase-1 deficient mice. *EMBO J.* **1999**, *18*, 4446-4454.

222. Tentori, L.; Lacal, P. M.; Muzi, A.; Dorio, A. S.; Leonetti, C.; Scarsella, M.; Ruffini, F.; Xu, W.; Min, W.; Stoppacciaro, A.; Colarossi, C.; Wang, Z. Q.; Zhang, J.; Graziani, G. Poly(ADP-ribose) polymerase (PARP) inhibition or PARP-1 gene deletion reduces angiogenesis. *Eur. J. Cancer* **2007**, *43*, 2124-2133.

223. Ferraris, D. V. Evolution of poly(ADP-ribose) polymerase-1 (PARP-1) inhibitors. From concept to clinic. *J. Med. Chem.* **2010**, *53*, 4561-4584.

224. Kummar, S.; Chen, A.; Parchment, R. E.; Kinders, R. J.; Ji, J.; Tomaszewski, J. E.; Doroshow, J. H. Advances in using PARP inhibitors to treat cancer. *BMC medicine* **2012**, *10*, 25-25.

225. Menear, K. A.; Adcock, C.; Boulter, R.; Cockcroft, X.; Copsey, L.; Cranston, A.; Dillon, K. J.; Drzewiecki, J.; Garman, S.; Gomez, S.; Javaid, H.; Kerrigan, F.; Knights, C.; Lau, A.; Loh, V. M.; Matthews, I. T. W.; Moore, S.; Connor, M. J. O.; Smith, G. C. M.; Martin, N. M. B. Novel Bioavailable Inhibitor of Poly (ADP-ribose) Polymerase-1. **2008**, 6581-6591.

226. Narendja, F. M.; Sauermann, G. The Use of Biotinylated Poly(ADP-Ribose) for Studies on Poly(ADP-Ribose)-Protein Interaction. *Anal. Biochem.* **1994**, *220*, 415-419.

227. Xia, M.; Huang, R.; Witt, K. L.; Southall, N.; Fostel, J.; Cho, M. H.; Jadhav, A.; Smith, C. S.; Inglese, J.; Portier, C. J.; Tice, R. R.; Austin, C. P. Compound cytotoxicity profiling using quantitative high-throughput screening. *Environ. Health Perspect.* **2008**, *116*, 284-291.